Focused Ultrasound-mediated Blood-Brain Barrier Opening for Diffuse Midline Glioma Radiosensitisation

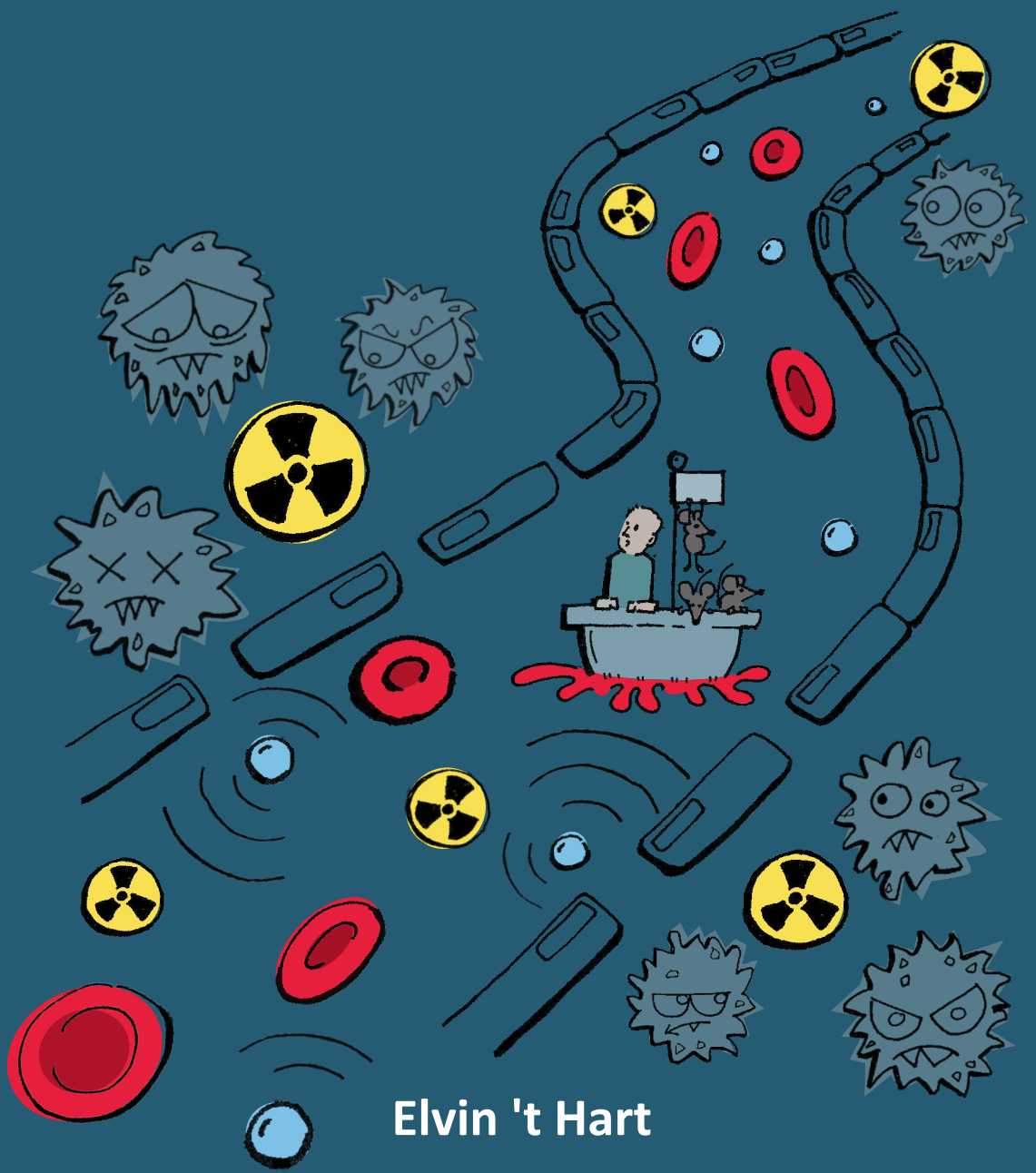

Elvin 't Hart

Focused Ultrasound-mediated Blood-Brain Barrier Opening for Diffuse Midline Glioma Radiosensitisation

Elvin ‘t Hart

ISBN: 978-94-6483-839-8

DOI: https://doi.org/10.33540/2174

Lay-out: Elvin ‘t Hart & Elvira ‘t Hart

Printing: RidderPrint I Ridderprint.nl

The work described in this thesis was performed at the Princess Máxima Center for pediatric oncology, within the framework of the Cancer, Stem cells and Development Biology (CSnD) graduate program of Utrecht University.

Focused Ultrasound-mediated Blood-Brain Barrier Opening for Diffuse Midline Glioma Radiosensitisation

Gefocust Ultrageluid bemiddelde Bloed-hersenbarrière Opening voor Radiosensitisatie van Difuus Midlijn Gliomen

(met een samenvatting in het Nederlands)

Proefschrift

ter verkrijging van de graad van doctor aan de
Universiteit Utrecht
op gezag van de
rector magnificus, prof. dr. H.R.B.M. Kummeling,
ingevolge het besluit van het college voor promoties
in het openbaar te verdedigen op

dinsdag 19 maart 2024 des middags te 12.15 uur

door

Elvin 't Hart

geboren op 12 april 1991
te Bemmel

Promotor:
Prof. dr. E.W. Hoving

Copromotoren:
Dr. M.G. Ries
Dr. D.G. van Vuurden

Beoordelingscommissie:
Prof. dr. A.D.R. Huitema
Prof. dr. C.T.W. Moonen
Dr. S.L.A. Plasschaert
Prof. dr. B.W. Raaymakers
Prof. dr. H.E. de Vries

Dit proefschrift werd mede mogelijk gemaakt met financiële steun van de KWF Young Investigator Grant (KWF 10911, Dr. D.G. van Vuurden)

Miauw Miauw Prrr Prrr…

Yaquina, Zaya & Zarro

Het is klaar…

Papa

Table of contents

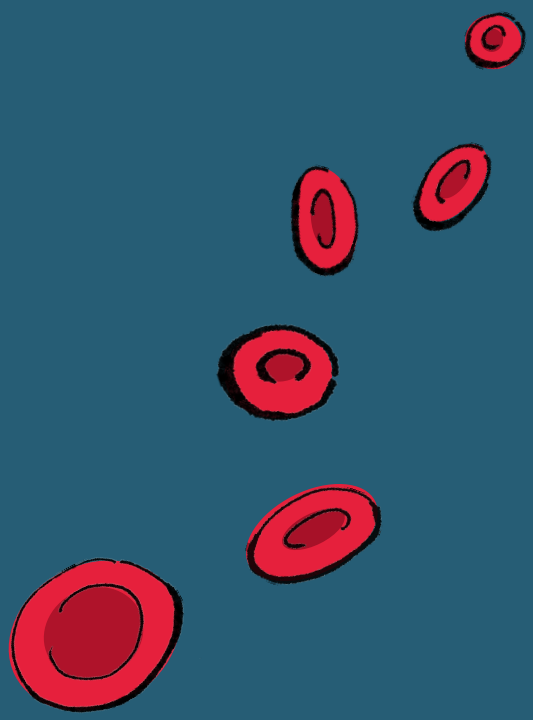

Chapter 1

General introduction and outline of the thesis

Elvin ’t Hart[1]

1. Princess Máxima Center for Pediatric Oncology, Heidelberglaan 25, 3584 CS, Utrecht, The Netherlands

General introduction

Paediatric cancer

Cancer is a disease characterized by abnormal and uncontrolled cell growth with the capacity to invade or expand to other organs of the body [1]. These invasive growth properties make the difference between a malignant or benign growth of a tumour. Benign tumours are in essence not life-threatening, but pressure by growth can cause reduced blood flow and/or tissue damage. Genetic alterations can even trigger benign tumours to express malignant growth properties in the end [2]. In 2020, there were 19.3 million new cases of cancer with almost ten million deaths, causing it to be one of the major health problems worldwide. The most common diagnosed cancers are breast (11.7%), lung (11.4%), colorectal (10%), prostate (7.3%) and stomach (5.6%), with lung being the most fatal variant (Figure 1) [3]. In 90-95% of all cancer cases, somatic mutations are caused by external factors (e.g. infection diseases or radiation) and lifestyle (e.g. smoking or diet), while the other 5-10% are caused by genetic defects [4].

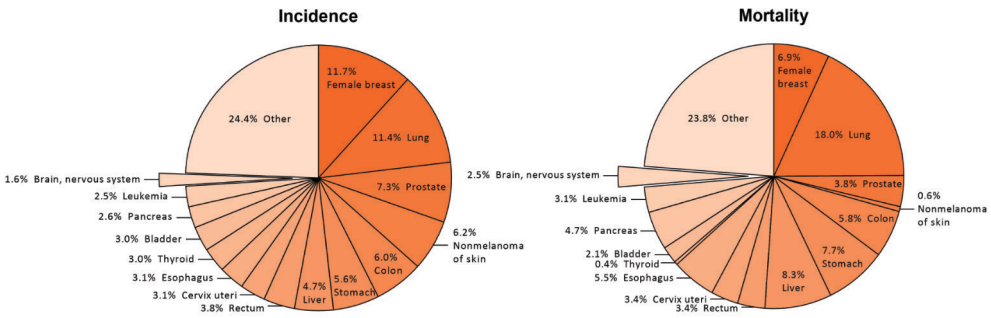

Figure 1: Occurrence of cancer types in 2020 based on incidence and mortality. Female breast cancer (11.7%) is the most diagnosed type and lung (18.0%) is the most fatal one based on the total amount of cancer deaths. Brain and nervous system cancer were diagnosed in 1.6% of all cases, while accounting for 2.5% of all cancer-related fatalities [3].

Of all the cancer cases, adult cancer is 40 times more frequent than paediatric cancer [5]. Adult cancer is primarily driven by external caused mutations, while paediatric cancer is instigated by inherent or spontaneously occurring genetic abnormalities [6]. Despite the relative lower occurrence, paediatric cancer is one of the leading mortality causes in children [7]. It is estimated that there are approximately 400.000 paediatric cancers cases worldwide every year [8]. Because of intensive research and chemotherapy in combination with surgery and radiation, survival of children with cancer has increased since the 1960s from 20-30% up to 83% [5,9]. The most common forms or paediatric cancers between 0-19 years of age are leukaemia and central nervous system (CNS) tumours [10].

Central nervous system tumour classifications

CNS tumours occur in the spine or brain and can be divided into two cell type categories, non-glial and glial. Glial cells are the non-neuronal cells of the CNS, including

oligodendrocytes, astrocytes, ependymal cells, and microglia. These cells are each responsible for either neuronal support, nutrient and oxygen supply, insulation, protection or removal of dead neurons [11]. Glial cell based gliomas account for 25-30% of all paediatric CNS tumours [12]. Glioma varieties are categorised based on their cell type, grade-score, and location, according to the World Health Organisation (WHO) classification system for CNS tumours [13]. Based on cell features, the main glial tumour types are ependymomas, astrocytomas, oligodendrogliomas, brainstem, and optic nerve glioma. The grade-score system distinguishes the extent of cancer development and growth. Low grade gliomas (grade I-II) are characterised by healthy looking cells, slow growth and little invasion, while high grade gliomas (HGG, grade III-IV) display atypical cell morphology, increased proliferation, angiogenesis and invasion [13]. Glioma location classification is based on the presence of the tumour in the infratentorial (brainstem and cerebellum) or supratentorial (cerebrum, optic nerve, and pineal gland) region.

Paediatric high-grade and diffuse midline gliomas

Paediatric HGGs (pHGG) compromise 10% of paediatric CNS tumours, but account for 40% of the mortality cases [14]. DNA and RNA sequencing, proteomics and methylation analysis has allowed for the subcategorization of four HGG types (1) diffuse midline glioma (DMG) H3K27-altered, (2) diffuse hemispheric glioma H3 G34-mutant, (3) diffuse paediatric-type high-grade glioma H3- and IDH-wildtype and (4) Infant-type hemispheric glioma. DMG, formerly when located in the pons known as diffuse intrinsic pontine glioma (DIPG), is a very aggressive pHGG and is mostly diagnosed between 6-9 years of age [15]. After diagnosis, children with DMG have a dismal prognosis with a median survival of 11 months and a 95% fatality rate within two years [16,17]. DMGs occur in the midline structures of the CNS (thalamus, pons, spinal cord), but are mostly found in the pons [13]. The pons is a vital part of the brainstem and is essential for various vital functions such as breathing, motoric coordination and sleep [18]. DMG expresses a diffuse and infiltrative growth pattern, intertwining with the neural tissue. Symptoms include facial asymmetry, speaking and swallowing difficulties, squinting, cranial nerve deficits, ataxia, and long tract signs [19].

DMG is characterized by H3K27 alterations concerning two point mutations at the histone H3 protein, occurring at the H3F3A gene coding into the H3.3 variant and to a lesser extent at the HIST1H3B/C gene coding into the H3.1 variant [20]. The mutation of the histone H3 protein causes the loss of trimethylation of the chromatin. This loss of trimethylation causes that the chromatin is no longer repressed, with distorted expression of oncogenes and tumour suppressor genes [21]. Other commonly found mutations in DMG include apoptosis regulation proteins such TP53, PPM1D and MAPK1. TP53 mutations are identified in 60% of all DMG cases, while PPM1D is found in 60% of TP53-wildtype patients [22]. Besides apoptosis deregulation also cell proliferation genes have been found to be mutated such as ACVR1, PDGFRA, PICK3CA and MYC [23–25]. While MYC is responsible for the genetic expression as a transcription factor, overexpression of PDGFRA stimulates cellular growth and differentiation and PICK3CA stimulates transformation [25–27].

Diffuse midline glioma treatment modalities

Based on the cancer type, location and disease progression, the most appropriate type of

treatment is chosen. The most commonly used and classical cancer treatment options are surgery, chemotherapy, and radiotherapy, while other novel methods include hormonal- , anti-angiogenic- , stem cell- and immunotherapy [28]. Treatment options for DMG have thus far been limited. DMG is mainly diagnosed based on the patients' symptoms and MRI scans. If possible, biopsies are taken for analysis and diagnosis conformation. However despite intensive research in the last decades, limited therapeutic efficacy has been established for children suffering from DMG [29].

Surgical resection

Maximal safe surgical resection is in general a preferable method for cancer treatment, with inflicting as little damage as possible to the healthy surrounding tissue. In case of DMG, surgery is limited due to the location and invasive growth of the tumour. As mentioned before, DMG can be found in the thalamus, spinal cord, cerebellum, and brainstem of the patient. The pons, which is part of the brainstem, is the most common affected structure which is located at the base of the brain and harbours essential neuronal structures such as cranial nerves and their nuclei and corticospinal tracts. Removal by surgery would bear a considerable risk of damage to these structures. Due to the intrusive growth of DMG cells in the midst of healthy pontine cells, the DMG tumour cannot be completely removed without also the removal of healthy tissue [30]. Any remaining tumour cells would continue to divide and grow, leading to tumour reoccurrence.

Chemotherapy

Since the introduction of chemotherapy in the 1940s, many cancer types have been successfully treated with improved survival and cure rates. The principle of chemotherapy is to disrupt the growth and multiplication capacities of cells forcing them into apoptosis. As a result, that cancerous cells, which have a high cell proliferation and growth are also more susceptible to cytostatic and cytotoxic agents than slow proliferating and growing healthy cells [31]. In case of DMG treatment, the therapeutic efficacy of chemotherapeutic agents has been limited at best, partly due to the presence of the blood-brain barrier (BBB) isolating the brain from the rest of the body [32]. Although as a prediction model for drugs crossing biological barriers such as the BBB, the Lipinski rule of five can be applied, which determines agents passing based on molecular weight, lipophilicity, polarity, hydrogen binding and charge [33]. However, this model does not include the role of drug efflux transporters [34]. Possibilities for BBB evasion are the usage of small molecules, viral vectors, nanoparticles, and exomes, but up-to-date did not significantly impact DMG treatment [35,36].

Radiotherapy

After the discovery of X-ray by Wilhelm Conrad Röntgen in 1895, the use of ionizing radiation has since established itself as an indispensable method for cancer treatment, treating 50% of all patients [37,38]. Radiotherapy is mainly used when surgery is not applicable and is based on the use of the ionizing radiation in which damage and destruction of cancerous cells is directly applied to predetermined areas with the least possible harmful effects on healthy tissue [39]. Because of the location, invasive growth and BBB, the current

standard of care for DMG consists of fractionated radiotherapy with 1.8-2 Gray (Gy) daily for 6 weeks, with a total dose of 54-60 Gy and adjuvant administration of temozolomide [40]. Whereas the usage of temozolomide for effective DMG treatment is debatable [41–43]. Studies involving lower cumulative doses of radiotherapy (<50 Gy) showed inferior survival rates whereas hyper-fractionated radiation schemes (66-78 Gy) did not improve survival compared to standardised radiation protocols. [44]. Hypo-fractionated radiotherapy did improve the quality of life for patients with equal survival rates [45,46].

Immunotherapy

As an alternative immunotherapy is an emerging treatment modality in the field of cancer, whereby the immune system is manipulated and educated against potential antigens. Subsequently, these antigens are promoted by the so-called antigen-presenting cells, like dendritic cells, stimulating the regulation of T and B lymphocytes [47]. Several studies have identified DMG-specific antigens for vaccine production such as the B7-H3 glycoprotein [48]. Following this research, multiple clinical trials have started to determine the feasibility, toxicity and preliminary efficacy of antigen-presenting by dendritic cells [49]. In addition, passive immunotherapy by the administration of humanized antibodies against PD-1 are in clinical evaluation for DMG treatment [50].

Radiotherapy induces DNA damage and upregulate repair mechanisms

Where radiotherapy is the only treatment option for DMG that currently provides relief and survival, it is important to understand its effects and consequences. Radiotherapy means the use of conventional high energy photon radiation involving X-rays and gamma-rays, with maximizing the given dose in cancerous cells and minimizing it in healthy cells. Cellular death by radiation is caused by unrepaired DNA damage, with fractionated radiation as optimal clinical treatment [51]. Because of the high proliferation of the cancer cells, there is less repair time available, making these more prone to die or go into apoptosis after multiple radiation doses [52].

DNA damage can occur due to both indirect and direct effects of radiation. Indirect effects are caused by the creation of free radicals upon radiation which can damage the DNA, while direct effects are quantified by on average 10,000 base damages, 1000 single-strand breaks (SSB) and 40 double strand breaks (DSB) of the DNA per cell [53,54]. DNA damage can consequently trigger specific SSB and DSB DNA repair pathways (Figure 2) [51]. SSBs are repaired through base excision repair (BER) by removal of the damaged base and phosphodiester bond, whereas PARP1 recruits the XRCC1 scaffolding protein which in turn recruit proteins responsible for mediate end-processing, gap synthesis, and DNA ligation. If not successfully repaired through BER SSBs can turn into DSBs [55]. In case of DSB repair two different mechanisms can be involved, namely non-homologous end-joining (NHEJ) (fast repair) and homologous recombination repair (HRR) (slow repair). NHEJ involves stabilization of the DNA ends by KU70 and KU80 mediation and DNA-PKcs recruitment. DNA-PKcs attracts XRCC4, LIG4, XLF, and PAXX for alignment and ligation of DNA ends fixing the DSB [56]. HRR occurs during the S and G2 phase of the cell cycle through the presence of a sister chromatid. HRR involves the resection of 5’ DNA ends followed by binding to a homologous DNA strand with subsequent DNA synthesis [57]. Secondary to the activation

of the DNA damage repair pathways is the inhibition of the cell cycle. Blockage of the cell cycle prevents pre-production of cells with impaired DNA with the main checkpoints at G1, S and G2 [58].

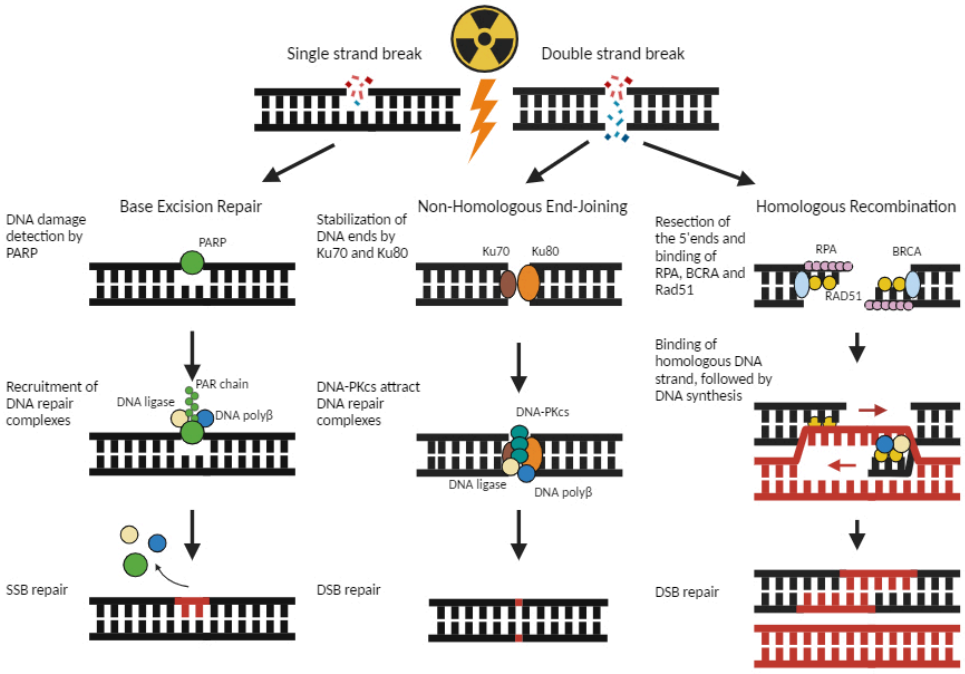

Figure 2: SSB and DSB DNA repair pathways, either by BER, NHEJ or HRR.

Radiosensitizers for targeted diffuse midline glioma treatment

Knowing that DNA repair pathways and cell cycle inhibition are important for the cancer cell survival upon radiation, is it also an important focus for new targeted treatment development for DMG. Besides the fact that these repairs systems are upregulated after radiation, several CNS tumours have a naturally increased PARP1 expression [59]. In addition, DMG is characterised by specific overexpression of DNA repair-associated genes, whereby it is suggested that targeted inhibition of selected proteins could be effective for DMG treatment [60]. To elapse the effect of radiotherapy, treatment combinations with an amplified effect seem to be a promising option. Drugs enhancing the radiosensitivity of cancer cells by counteracting its resistance mechanisms or expression are the so-called radiosensitizers. The following synergetic effects of radiosensitizers allow for lower drug concentration with reduced toxicity while maintaining the treatment efficacy [61]. Radiosensitizer targets can be roughly divided in seven subtypes: (1) tyrosine kinases and proliferation, (2) cell cycle and differentiation, (3) cell stabilization, (4) apoptosis, (5) epigenome, (6) immune system and (7) DNA damage repair pathways. Studies investigating the effects of radiosensitizers in DMG have observed effective treatment in vitro and in vivo by the inhibition of tyrosine kinases and proliferation [62,63], cell cycle and differentiation

[64–70], apoptosis [71], epigenome [72] and repair pathways [73,74]. While various radiosensitizers have been investigated and are in phase 2 clinical trials, no clinical improvement for DMG has been established yet [75].

Reduced brain permeability by the blood-brain barrier

The response to radiosensitizers, likechemotherapeutic drugs in general, is limited in DMG patients due to the presence of the BBB. The key function of the BBB is to ensure homeostasis of the CNS by protecting brain tissue from pathogens or toxic circulating substances, while regulating the transport of essential nutrients into and waste products out of the brain [76]. The BBB is a tightly regulated neurovascular unit, composed of endothelial cells, pericytes, a basal membrane and astrocytic endfeet [77]. This biological barrier displays restricted permeability due to the presence of a physical and functional barrier [78]. The physical barrier is formed by tight junctions to maintain endothelial cell-cell adhesion. These connections close the paracellular pathways, preventing unregulated transport of molecules between blood and brain [79]. The functional barrier is formed by the presence of solute carriers and ATP-binding cassette (ABC) transporters, responsible for the transport of conjugates, peptides, and drugs [80,81]. Medication uptake in the brain is particularly inhibited by P-glycoprotein (P-gp), besides breast cancer resistance protein (Bcrp) and other multi resistance related proteins of the ABC transporter family. Research has indicated that P-gp and Bcrp also play an important role of multidrug resistance in tumour cells , which actively transport drugs from the brain parenchyma back into the vascular system [82]. Because of these obstacles, it is difficult for molecules with a mass of >400 Da and low lipid solubility to pass the BBB. Subsequently, all large-molecule drugs and more than 98% of small-molecule drugs due to presence of these ABC transporters cannot penetrate the brain tissue [34], compromising the overall treatment efficacy in brain diseases [83] necessitating the development of alternative drug delivery strategies.

Focused ultrasound for drug delivery passed the blood-brain barrier

To enable the delivery of drugs to the brain by overcoming the BBB, various techniques have been developed, including nanoparticles, intranasal delivery, intra-arterial delivery, convection enhanced delivery, and focused ultrasound BBB opening (FUS-BBBO) [84]. FUS-BBBO is a promising therapeutic modality, using intravenously injected microbubbles in combination with locally applied ultrasound. These acoustic soundwaves cause the expansion and contraction of the microbubbles, also known as cavitation. The cavitation of these microbubbles cause stress on the endothelial cells of the BBB and by mechanical force pushes the cells apart [85]. During this process, the intracellular connections by tight junctions are disrupted, enhancing the paracellular but also transcellular transport of drugs (Figure 3) [86,87]. Successful drug delivery following FUS-BBBO depends on the properties of microbubbles, the mechanical index (MI), and molecular properties of the drug. Since the discovery of their ultrasonic properties, microbubbles have been used for diagnostic ultrasound imaging and proven useful for targeted drug delivery [88,89]. Microbubbles are 1-8µm wide bubbles filled with high molecular weight gasses and a lipid, polymer, or protein material coating which determines the lifespan in the circulatory system and degree of stretching [90,91][91]. The acoustic pressure and frequency of the applied ultrasound waves determine the MI and its extent of microbubble oscillation. Microbubbles exposed to a MI

of 0.1-0.3 experience stable cavitation, meaning its extension and compression with the backscatter of harmonics, sub-harmonics, and ultra-harmonics. Instead a MI of 0.3-06 cause inertial cavitation with a high energetic collapse of the microbubble with possible damaging effects on the blood vessel wall [90].

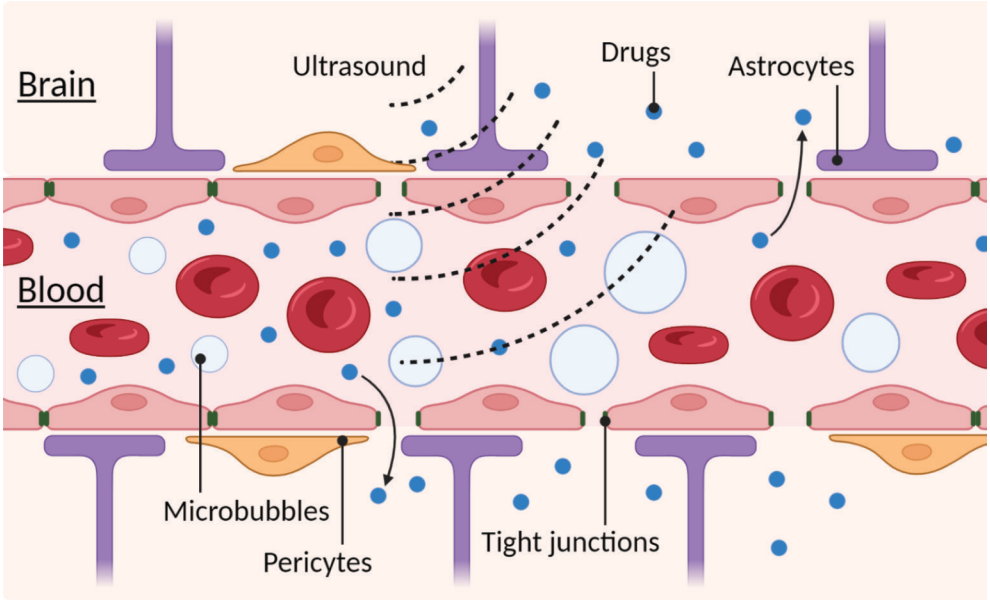

Figure 3: The BBB consists of pericytes, astrocyte endfeet and endothelial cells, with tight junctions in between. Under the influence of applied ultrasound, injected microbubbles expand and push the endothelial cells apart by disrupting the tight junctions in between. The resulting permeability of the BBB opens the possibility for drugs to extravasate into the brain parenchyma with possible brain tumour treatment.

Within the limits of safe practice, FUS-BBBO gives the option for temporal drug extravasation with permeability observed up to 24 hours after treatment, with tight junctions repair as size-time limited factor [92]. Large molecule-extravasation need a high MI to push the endothelial cells sufficient apart and have even a smaller window of opening [93]. ABC-transporters expression upon FUS-BBBO might be downregulated up to 48 hours with possible enhanced drug delivery [94,95], but they still seem to be sufficient effective [96]. FUS-BBBO has shown to be a safe treatment option in preclinical settings with temporal increased drug delivery into the brain parenchyma of gold nanoclusters, doxorubicin, etoposide, temozolomide and bevacizumab [97–101]. Enhanced drug delivery by FUS-BBBO has also demonstrated to be effective as shown through increased survival of preclinical brain tumour animal models [101,102]. Clinically, FUS-BBBO has proven to be a safe treatment option, is well tolerated in patients, is without adverse effects, and is already in use for the treatment of Alzheimer's disease and amyotrophic lateral sclerosis [103–106]. Additionally, no neuro-toxicity effects have been observed after FUS-BBBO with drug delivery of doxorubicin, temozolomide and carboplatin [106,107].

Outline of the thesis

Despite decades of research, little to no improvement of survival benefit for DMG patients has been achieved. The treatment options now available are mainly palliative with no curable prospects. Therefore, the aim of the work described in this thesis is to investigate new therapeutic options by radiosensitization of DMG combined with FUS-BBBO. In **chapter 2**, we present a systematic overview combined with a meta-analysis of the effects of radiotherapy on the permeabilization of the BBB in clinical and preclinical studies. It was unknown what the impact of various radiotherapy protocols were on BBB integrity over time. In this study we open the discussion for incorporating the influence of radiotherapy on the BBB for future adjuvant therapies with better patient care. Even though radiotherapy is still the cornerstone treatment for DMG, **chapter 3** discusses the possibilities of safe and temporal FUS-BBBO for drug delivery into the brain parenchyma in a preclinical setting. Based on commercially available components, an in-house stereotactic neuronavigation FUS system was developed for high throughput drug screening. **Chapter 4** examines the specifications of the frequently used HSJD-DIPG-007 patient-derived xenograft (PDX) DMG mouse model. This PDX DMG mouse model was assessed based on growth monitoring, metastases formation and two different intracranial cell injection substrates. In previous chapters, radiotherapy on BBB permeability, FUS-BBBO possibilities in rodents and a suitable DMG PDX model were discussed, subsequently **chapter 5** discusses the extravasation of the PARP1 inhibitor, olaparib, upon FUS-BBBO for radiosensitization treatment of a PDX DMG mouse model. Chapter 6 comprises a general discussion of the research presented in this thesis and future challenges in FUS-BBBO research for DIPG radiosensitization treatment.

Summaries of the thesis (English and Dutch) are supplied in the **addendum**.

References

[1] Cifone MA. In vitro growth characteristics associated with benign and metastatic variants of tumor cells. Cancer Metastasis Rev 1982;1:335–47. https://doi.org/10.1007/BF00124216.

[2] Kabalar ME, Karaman A, Aylu B, Ozmen SA, Erdem I. Genetic alterations in benign, preneoplastic and malignant breast lesions. Indian J Pathol Microbiol 2012;55:319–25. https://doi.org/10.4103/0377-4929.101737.

[3] Sung H, Ferlay J, Siegel RL, Laversanne M, Soerjomataram I, Jemal A, et al. Global Cancer Statistics 2020: GLOBOCAN Estimates of Incidence and Mortality Worldwide for 36 Cancers in 185 Countries. CA Cancer J Clin 2021;71:209–49. https://doi.org/10.3322/caac.21660.

[4] Anand P, Kunnumakkara AB, Sundaram C, Harikumar KB, Tharakan ST, Lai OS, et al. Cancer is a preventable disease that requires major lifestyle changes. Pharm Res 2008;25:2097–116. https://doi.org/10.1007/s11095-008-9661-9.

[5] Saletta F, Seng MS, Lau LMS. Advances in paediatric cancer treatment. Transl Pediatr 2014;3:156–82. https://doi.org/10.3978/j.issn.2224-4336.2014.02.01.

[6] Kattner P, Strobel H, Khoshnevis N, Grunert M, Bartholomae S, Pruss M, et al. Compare and contrast: pediatric cancer versus adult malignancies. Cancer Metastasis Rev 2019;38:673–82. https://doi.org/10.1007/s10555-019-09836-y.

[7] Siegel DA, Richardson LC, Henley SJ, Wilson RJ, Dowling NF, Weir HK, et al. Pediatric cancer mortality and survival in the United States, 2001-2016. Cancer 2020;126:4379–89. https://doi.org/10.1002/cncr.33080.

[8] Ward ZJ, Yeh JM, Bhakta N, Frazier AL, Atun R. Estimating the total incidence of global childhood cancer: a simulation-based analysis. Lancet Oncol 2019;20:483–93. https://doi.org/10.1016/S1470-2045(18)30909-4.

[9] Birch JM, Marsden HB, Jones PH, Pearson D, Blair V. Improvements in survival from childhood cancer: results of a population based survey over 30 years. Br Med J (Clin Res Ed) 1988;296:1372–6. https://doi.org/10.1136/bmj.296.6633.1372.

[10] Steliarova-Foucher E, Colombet M, Ries LAG, Moreno F, Dolya A, Bray F, et al. International incidence of childhood cancer, 2001-10: a population-based registry study. Lancet Oncol 2017;18:719–31. https://doi.org/10.1016/S1470-2045(17)30186-9.

[11] Jäkel S, Dimou L. Glial Cells and Their Function in the Adult Brain: A Journey through the History of Their Ablation. Front Cell Neurosci 2017;11:24. https://doi.org/10.3389/fncel.2017.00024.

[12] Qaddoumi I, Sultan I, Gajjar A. Outcome and prognostic features in pediatric gliomas: a review of 6212 cases from the Surveillance, Epidemiology, and End Results database. Cancer 2009;115:5761–70. https://doi.org/10.1002/cncr.24663.

[13] Louis DN, Perry A, Wesseling P, Brat DJ, Cree IA, Figarella-Branger D, et al. The 2021 WHO Classification of Tumors of the Central Nervous System: a summary. Neuro Oncol 2021;23:1231–51. https://doi.org/10.1093/neuonc/noab106.

[14] Ostrom QT, de Blank PM, Kruchko C, Petersen CM, Liao P, Finlay JL, et al. Alex's Lemonade Stand Foundation Infant and Childhood Primary Brain and Central Nervous System Tumors Diagnosed in the United States in 2007-2011. Neuro Oncol 2015;16 Suppl 1:x1–36. https://doi.org/10.1093/neuonc/nou327.

[15] Louis DN, Perry A, Reifenberger G, von Deimling A, Figarella-Branger D, Cavenee WK, et al.

The 2016 World Health Organization Classification of Tumors of the Central Nervous System: a summary. Acta Neuropathol 2016;131:803–20. https://doi.org/10.1007/s00401-016-1545-1.

[16] Hoffman LM, Veldhuijzen van Zanten SEM, Colditz N, Baugh J, Chaney B, Hoffmann M, et al. Clinical, Radiologic, Pathologic, and Molecular Characteristics of Long-Term Survivors of Diffuse Intrinsic Pontine Glioma (DIPG): A Collaborative Report From the International and European Society for Pediatric Oncology DIPG Registries. J Clin Oncol Off J Am Soc Clin Oncol 2018;36:1963–72. https://doi.org/10.1200/JCO.2017.75.9308.

[17] Jansen MH, Veldhuijzen van Zanten SE, Sanchez Aliaga E, Heymans MW, Warmuth-Metz M, Hargrave D, et al. Survival prediction model of children with diffuse intrinsic pontine glioma based on clinical and radiological criteria. Neuro Oncol 2015;17:160–6. https://doi.org/10.1093/neuonc/nou104.

[18] Tate MC, Lindquist RA, Nguyen T, Sanai N, Barkovich AJ, Huang EJ, et al. Postnatal growth of the human pons: a morphometric and immunohistochemical analysis. J Comp Neurol 2015;523:449–62. https://doi.org/10.1002/cne.23690.

[19] Donaldson SS, Laningham F, Fisher PG. Advances toward an understanding of brainstem gliomas. J Clin Oncol Off J Am Soc Clin Oncol 2006;24:1266–72. https://doi.org/10.1200/JCO.2005.04.6599.

[20] Khuong-Quang D-A, Buczkowicz P, Rakopoulos P, Liu X-Y, Fontebasso AM, Bouffet E, et al. K27M mutation in histone H3.3 defines clinically and biologically distinct subgroups of pediatric diffuse intrinsic pontine gliomas. Acta Neuropathol 2012;124:439–47. https://doi.org/10.1007/s00401-012-0998-0.

[21] Chan K-M, Fang D, Gan H, Hashizume R, Yu C, Schroeder M, et al. The histone H3.3K27M mutation in pediatric glioma reprograms H3K27 methylation and gene expression. Genes Dev 2013;27:985–90. https://doi.org/10.1101/gad.217778.113.

[22] Xu C, Liu H, Pirozzi CJ, Chen LH, Greer PK, Diplas BH, et al. TP53 wild-type/PPM1D mutant diffuse intrinsic pontine gliomas are sensitive to a MDM2 antagonist. Acta Neuropathol Commun 2021;9:178. https://doi.org/10.1186/s40478-021-01270-y.

[23] Hoffman LM, DeWire M, Ryall S, Buczkowicz P, Leach J, Miles L, et al. Spatial genomic heterogeneity in diffuse intrinsic pontine and midline high-grade glioma: implications for diagnostic biopsy and targeted therapeutics. Acta Neuropathol Commun 2016;4:1. https://doi.org/10.1186/s40478-015-0269-0.

[24] Grill J, Puget S, Andreiuolo F, Philippe C, MacConaill L, Kieran MW. Critical oncogenic mutations in newly diagnosed pediatric diffuse intrinsic pontine glioma. Pediatr Blood Cancer 2012;58:489–91. https://doi.org/10.1002/pbc.24060.

[25] Buczkowicz P, Hoeman C, Rakopoulos P, Pajovic S, Letourneau L, Dzamba M, et al. Genomic analysis of diffuse intrinsic pontine gliomas identifies three molecular subgroups and recurrent activating ACVR1 mutations. Nat Genet 2014;46:451–6. https://doi.org/10.1038/ng.2936.

[26] Zhang X, Zhang Z. Oncohistone Mutations in Diffuse Intrinsic Pontine Glioma. Trends in Cancer 2019;5:799–808. https://doi.org/10.1016/j.trecan.2019.10.009.

[27] Taylor KR, Vinci M, Bullock AN, Jones C. ACVR1 mutations in DIPG: lessons learned from FOP. Cancer Res 2014;74:4565–70. https://doi.org/10.1158/0008-5472.CAN-14-1298.

[28] Abbas Z, Rehman S. An Overview of Cancer Treatment Modalities. In: Shahzad HN, editor., Rijeka: IntechOpen; 2018, p. Ch. 6. https://doi.org/10.5772/intechopen.76558.

[29] Hargrave D, Bartels U, Bouffet E. Diffuse brainstem glioma in children: critical review of

clinical trials. Lancet Oncol 2006;7:241–8. https://doi.org/10.1016/S1470-2045(06)70615-5.

[30] Warren KE. Diffuse intrinsic pontine glioma: poised for progress. Front Oncol 2012;2:205. https://doi.org/10.3389/fonc.2012.00205.

[31] DeVita VTJ, Chu E. A history of cancer chemotherapy. Cancer Res 2008;68:8643–53. https://doi.org/10.1158/0008-5472.CAN-07-6611.

[32] Lapin DH, Tsoli M, Ziegler DS. Genomic Insights into Diffuse Intrinsic Pontine Glioma. Front Oncol 2017;7:57. https://doi.org/10.3389/fonc.2017.00057.

[33] Lipinski CA, Lombardo F, Dominy BW, Feeney PJ. Experimental and computational approaches to estimate solubility and permeability in drug discovery and development settings. Adv Drug Deliv Rev 1997;23:3–25.

[34] Pardridge WM. The blood-brain barrier: Bottleneck in brain drug development. NeuroRx 2005;2:3–14. https://doi.org/10.1602/neurorx.2.1.3.

[35] Dong X. Current Strategies for Brain Drug Delivery. Theranostics 2018;8:1481–93. https://doi.org/10.7150/thno.21254.

[36] Pardridge WM. Drug transport across the blood-brain barrier. J Cereb Blood Flow Metab Off J Int Soc Cereb Blood Flow Metab 2012;32:1959–72. https://doi.org/10.1038/jcbfm.2012.126.

[37] Baskar R, Lee KA, Yeo R, Yeoh K-W. Cancer and radiation therapy: current advances and future directions. Int J Med Sci 2012;9:193–9. https://doi.org/10.7150/ijms.3635.

[38] Delaney G, Jacob S, Featherstone C, Barton M. The role of radiotherapy in cancer treatment: estimating optimal utilization from a review of evidence-based clinical guidelines. Cancer 2005;104:1129–37. https://doi.org/10.1002/cncr.21324.

[39] Kano H, Flickinger JC, Tonetti D, Hsu A, Yang H-C, Flannery TJ, et al. Estimating the Risks of Adverse Radiation Effects After Gamma Knife Radiosurgery for Arteriovenous Malformations. Stroke 2017;48:84–90. https://doi.org/10.1161/STROKEAHA.116.014825.

[40] Stupp R, Mason WP, van den Bent MJ, Weller M, Fisher B, Taphoorn MJB, et al. Radiotherapy plus concomitant and adjuvant temozolomide for glioblastoma. N Engl J Med 2005;352:987–96. https://doi.org/10.1056/NEJMoa043330.

[41] Bailey S, Howman A, Wheatley K, Wherton D, Boota N, Pizer B, et al. Diffuse intrinsic pontine glioma treated with prolonged temozolomide and radiotherapy--results of a United Kingdom phase II trial (CNS 2007 04). Eur J Cancer 2013;49:3856–62. https://doi.org/10.1016/j.ejca.2013.08.006.

[42] Crotty EE, Leary SES, Geyer JR, Olson JM, Millard NE, Sato AA, et al. Children with DIPG and high-grade glioma treated with temozolomide, irinotecan, and bevacizumab: the Seattle Children's Hospital experience. J Neurooncol 2020;148:607–17. https://doi.org/10.1007/s11060-020-03558-w.

[43] Sirachainan N, Pakakasama S, Visudithbhan A, Chiamchanya S, Tuntiyatorn L, Dhanachai M, et al. Concurrent radiotherapy with temozolomide followed by adjuvant temozolomide and cis-retinoic acid in children with diffuse intrinsic pontine glioma. Neuro Oncol 2008;10:577–82. https://doi.org/10.1215/15228517-2008-025.

[44] Vanan MI, Eisenstat DD. DIPG in Children - What Can We Learn from the Past? Front Oncol 2015;5:237. https://doi.org/10.3389/fonc.2015.00237.

[45] Park J, Yea JW, Park JW. Hypofractionated radiotherapy versus conventional radiotherapy for diffuse intrinsic pontine glioma: A systematic review and meta-analysis. Medicine (Baltimore)

2020;99:e22721. https://doi.org/10.1097/MD.0000000000022721.

[46] Zaghloul MS, Eldebawy E, Ahmed S, Mousa AG, Amin A, Refaat A, et al. Hypofractionated conformal radiotherapy for pediatric diffuse intrinsic pontine glioma (DIPG): A randomized controlled trial. Radiother Oncol 2014;111:35–40. https://doi.org/https://doi.org/10.1016/j.radonc.2014.01.013.

[47] Waldmann TA. Immunotherapy: past, present and future. Nat Med 2003;9:269–77. https://doi.org/10.1038/nm0303-269.

[48] Zhou Z, Luther N, Ibrahim GM, Hawkins C, Vibhakar R, Handler MH, et al. B7-H3, a potential therapeutic target, is expressed in diffuse intrinsic pontine glioma. J Neurooncol 2013;111:257–64. https://doi.org/10.1007/s11060-012-1021-2.

[49] Van Gool SW, Makalowski J, Bonner ER, Feyen O, Domogalla MP, Prix L, et al. Addition of Multimodal Immunotherapy to Combination Treatment Strategies for Children with DIPG: A Single Institution Experience. Med (Basel, Switzerland) 2020;7. https://doi.org/10.3390/medicines7050029.

[50] Long W, Yi Y, Chen S, Cao Q, Zhao W, Liu Q. Potential New Therapies for Pediatric Diffuse Intrinsic Pontine Glioma. Front Pharmacol 2017;8:495. https://doi.org/10.3389/fphar.2017.00495.

[51] Jackson SP, Bartek J. The DNA-damage response in human biology and disease. Nature 2009;461:1071–8. https://doi.org/10.1038/nature08467.

[52] Begg AC, Stewart FA, Vens C. Strategies to improve radiotherapy with targeted drugs. Nat Rev Cancer 2011;11:239–53. https://doi.org/10.1038/nrc3007.

[53] Cannan WJ, Pederson DS. Mechanisms and Consequences of Double-Strand DNA Break Formation in Chromatin. J Cell Physiol 2016;231:3–14. https://doi.org/10.1002/jcp.25048.

[54] Foray N, Bourguignon M, Hamada N. Individual response to ionizing radiation. Mutat Res Rev Mutat Res 2016;770:369–86. https://doi.org/10.1016/j.mrrev.2016.09.001.

[55] Vens C, Begg AC. Targeting base excision repair as a sensitization strategy in radiotherapy. Semin Radiat Oncol 2010;20:241–9. https://doi.org/10.1016/j.semradonc.2010.05.005.

[56] Pannunzio NR, Watanabe G, Lieber MR. Nonhomologous DNA end-joining for repair of DNA double-strand breaks. J Biol Chem 2018;293:10512–23. https://doi.org/10.1074/jbc.TM117.000374.

[57] Morgan MA, Lawrence TS. Molecular Pathways: Overcoming Radiation Resistance by Targeting DNA Damage Response Pathways. Clin Cancer Res an Off J Am Assoc Cancer Res 2015;21:2898–904. https://doi.org/10.1158/1078-0432.CCR-13-3229.

[58] Biau J, Chautard E, Verrelle P, Dutreix M. Altering DNA Repair to Improve Radiation Therapy: Specific and Multiple Pathway Targeting. Front Oncol 2019;9:1009. https://doi.org/10.3389/fonc.2019.01009.

[59] Barton VN, Donson AM, Kleinschmidt-DeMasters BK, Gore L, Liu AK, Foreman NK. PARP1 expression in pediatric central nervous system tumors. Pediatr Blood Cancer 2009;53:1227–30. https://doi.org/10.1002/pbc.22141.

[60] Paugh BS, Broniscer A, Qu C, Miller CP, Zhang J, Tatevossian RG, et al. Genome-wide analyses identify recurrent amplifications of receptor tyrosine kinases and cell-cycle regulatory genes in diffuse intrinsic pontine glioma. J Clin Oncol Off J Am Soc Clin Oncol 2011;29:3999–4006. https://doi.org/10.1200/JCO.2011.35.5677.

[61] Farhood B, Goradel NH, Mortezaee K, Khanlarkhani N, Salehi E, Nashtaei MS, et al.

Melatonin as an adjuvant in radiotherapy for radioprotection and radiosensitization. Clin Transl Oncol Off Publ Fed Spanish Oncol Soc Natl Cancer Inst Mex 2019;21:268–79. https://doi.org/10.1007/s12094-018-1934-0.

[62] Miyahara H, Yadavilli S, Natsumeda M, Rubens JA, Rodgers L, Kambhampati M, et al. The dual mTOR kinase inhibitor TAK228 inhibits tumorigenicity and enhances radiosensitization in diffuse intrinsic pontine glioma. Cancer Lett 2017;400:110–6. https://doi.org/10.1016/j.canlet.2017.04.019.

[63] Flannery PC, DeSisto JA, Amani V, Venkataraman S, Lemma RT, Prince EW, et al. Preclinical analysis of MTOR complex 1/2 inhibition in diffuse intrinsic pontine glioma. Oncol Rep 2018;39:455–64. https://doi.org/10.3892/or.2017.6122.

[64] Werbrouck C, Evangelista CCS, Lobón-Iglesias M-J, Barret E, Le Teuff G, Merlevede J, et al. TP53 Pathway Alterations Drive Radioresistance in Diffuse Intrinsic Pontine Gliomas (DIPG). Clin Cancer Res an Off J Am Assoc Cancer Res 2019;25:6788–800. https://doi.org/10.1158/1078-0432.CCR-19-0126.

[65] Caretti V, Hiddingh L, Lagerweij T, Schellen P, Koken PW, Hulleman E, et al. WEE1 kinase inhibition enhances the radiation response of diffuse intrinsic pontine gliomas. Mol Cancer Ther 2013;12:141–50. https://doi.org/10.1158/1535-7163.MCT-12-0735.

[66] Mueller S, Hashizume R, Yang X, Kolkowitz I, Olow AK, Phillips J, et al. Targeting Wee1 for the treatment of pediatric high-grade gliomas. Neuro Oncol 2014;16:352–60. https://doi.org/10.1093/neuonc/not220.

[67] Amani V, Prince EW, Alimova I, Balakrishnan I, Birks D, Donson AM, et al. Polo-like Kinase 1 as a potential therapeutic target in Diffuse Intrinsic Pontine Glioma. BMC Cancer 2016;16:647. https://doi.org/10.1186/s12885-016-2690-6.

[68] Barton KL, Misuraca K, Cordero F, Dobrikova E, Min HD, Gromeier M, et al. PD-0332991, a CDK4/6 inhibitor, significantly prolongs survival in a genetically engineered mouse model of brainstem glioma. PLoS One 2013;8:e77639. https://doi.org/10.1371/journal.pone.0077639.

[69] Taylor IC, Hütt-Cabezas M, Brandt WD, Kambhampati M, Nazarian J, Chang HT, et al. Disrupting NOTCH Slows Diffuse Intrinsic Pontine Glioma Growth, Enhances Radiation Sensitivity, and Shows Combinatorial Efficacy With Bromodomain Inhibition. J Neuropathol Exp Neurol 2015;74:778–90. https://doi.org/10.1097/NEN.0000000000000216.

[70] Katagi H, Louis N, Unruh D, Sasaki T, He X, Zhang A, et al. Radiosensitization by Histone H3 Demethylase Inhibition in Diffuse Intrinsic Pontine Glioma. Clin Cancer Res an Off J Am Assoc Cancer Res 2019;25:5572–83. https://doi.org/10.1158/1078-0432.CCR-18-3890.

[71] Akamandisa MP, Nie K, Nahta R, Hambardzumyan D, Castellino RC. Inhibition of mutant PPM1D enhances DNA damage response and growth suppressive effects of ionizing radiation in diffuse intrinsic pontine glioma. Neuro Oncol 2019;21:786–99. https://doi.org/10.1093/neuonc/noz053.

[72] Meel MH, de Gooijer MC, Metselaar DS, Sewing ACP, Zwaan K, Waranecki P, et al. Combined Therapy of AXL and HDAC Inhibition Reverses Mesenchymal Transition in Diffuse Intrinsic Pontine Glioma. Clin Cancer Res an Off J Am Assoc Cancer Res 2020;26:3319–32. https://doi.org/10.1158/1078-0432.CCR-19-3538.

[73] Deland K, Starr BF, Mercer JS, Byemerwa J, Crabtree DM, Williams NT, et al. Tumor genotype dictates radiosensitization after Atm deletion in primary brainstem glioma models. J Clin Invest 2021;131. https://doi.org/10.1172/JCI142158.

[74] Chornenkyy Y, Agnihotri S, Yu M, Buczkowicz P, Rakopoulos P, Golbourn B, et al. Poly-ADP-Ribose Polymerase as a Therapeutic Target in Pediatric Diffuse Intrinsic Pontine Glioma and Pediatric

High-Grade Astrocytoma. Mol Cancer Ther 2015;14:2560–8. https://doi.org/10.1158/1535-7163.MCT-15-0282.

[75] Metselaar DS, du Chatinier A, Stuiver I, Kaspers GJL, Hulleman E. Radiosensitization in Pediatric High-Grade Glioma: Targets, Resistance and Developments. Front Oncol 2021;11:662209. https://doi.org/10.3389/fonc.2021.662209.

[76] Obermeier B, Daneman R, Ransohoff RM. Development, maintenance and disruption of the blood-brain barrier. Nat Med 2013;19:1584–96. https://doi.org/10.1038/nm.3407.

[77] Kadry H, Noorani B, Cucullo L. A blood-brain barrier overview on structure, function, impairment, and biomarkers of integrity. Fluids Barriers CNS 2020;17:69. https://doi.org/10.1186/s12987-020-00230-3.

[78] Abbott NJ, Patabendige AAK, Dolman DEM, Yusof SR, Begley DJ. Structure and function of the blood-brain barrier. Neurobiol Dis 2010;37:13–25. https://doi.org/10.1016/j.nbd.2009.07.030.

[79] Luissint A-C, Artus C, Glacial F, Ganeshamoorthy K, Couraud P-O. Tight junctions at the blood brain barrier: physiological architecture and disease-associated dysregulation. Fluids Barriers CNS 2012;9:23. https://doi.org/10.1186/2045-8118-9-23.

[80] Kusuhara H, Sugiyama Y. Active efflux across the blood-brain barrier: role of the solute carrier family. NeuroRx 2005;2:73–85. https://doi.org/10.1602/neurorx.2.1.73.

[81] Shen S, Zhang W. ABC transporters and drug efflux at the blood-brain barrier. Rev Neurosci 2010;21:29–53. https://doi.org/10.1515/revneuro.2010.21.1.29.

[82] Mahringer A, Ott M, Reimold I, Reichel V, Fricker G. The ABC of the blood-brain barrier - regulation of drug efflux pumps. Curr Pharm Des 2011;17:2762–70. https://doi.org/10.2174/138161211797440221.

[83] Van Tellingen O, Yetkin-Arik B, De Gooijer MC, Wesseling P, Wurdinger T, De Vries HE. Overcoming the blood-brain tumor barrier for effective glioblastoma treatment. Drug Resist Updat 2015;19:1–12. https://doi.org/10.1016/j.drup.2015.02.002.

[84] Haumann R, Videira JC, Kaspers GJL, van Vuurden DG, Hulleman E. Overview of Current Drug Delivery Methods Across the Blood-Brain Barrier for the Treatment of Primary Brain Tumors. CNS Drugs 2020;34:1121–31. https://doi.org/10.1007/s40263-020-00766-w.

[85] Burgess A, Shah K, Hough O, Hynynen K. Focused ultrasound-mediated drug delivery through the blood-brain barrier. Expert Rev Neurother 2015;15:477–91. https://doi.org/10.1586/14737175.2015.1028369.

[86] Sheikov N, McDannold N, Vykhodtseva N, Jolesz F, Hynynen K. Cellular mechanisms of the blood-brain barrier opening induced by ultrasound in presence of microbubbles. Ultrasound Med Biol 2004;30:979–89. https://doi.org/10.1016/j.ultrasmedbio.2004.04.010.

[87] Sheikov N, McDannold N, Sharma S, Hynynen K. Effect of focused ultrasound applied with an ultrasound contrast agent on the tight junctional integrity of the brain microvascular endothelium. Ultrasound Med Biol 2008;34:1093–104. https://doi.org/10.1016/j.ultrasmedbio.2007.12.015.

[88] Gramiak R, Shah PM. Echocardiography of the Aortic Root. Invest Radiol 1968;3.

[89] Tsutsui JM, Xie F, Porter RT. The use of microbubbles to target drug delivery. Cardiovasc Ultrasound 2004;2:23. https://doi.org/10.1186/1476-7120-2-23.

[90] Hernot S, Klibanov AL. Microbubbles in ultrasound-triggered drug and gene delivery. Adv

Drug Deliv Rev 2008;60:1153–66. https://doi.org/https://doi.org/10.1016/j.addr.2008.03.005.

[91] Kooiman K, Vos HJ, Versluis M, de Jong N. Acoustic behavior of microbubbles and implications for drug delivery. Adv Drug Deliv Rev 2014;72:28–48. https://doi.org/10.1016/j.addr.2014.03.003.

[92] Chu P-C, Chai W-Y, Tsai C-H, Kang S-T, Yeh C-K, Liu H-L. Focused Ultrasound-Induced Blood-Brain Barrier Opening: Association with Mechanical Index and Cavitation Index Analyzed by Dynamic Contrast-Enhanced Magnetic-Resonance Imaging. Sci Rep 2016;6:33264. https://doi.org/10.1038/srep33264.

[93] Chen H, Konofagou EE. The size of blood-brain barrier opening induced by focused ultrasound is dictated by the acoustic pressure. J Cereb Blood Flow Metab Off J Int Soc Cereb Blood Flow Metab 2014;34:1197–204. https://doi.org/10.1038/jcbfm.2014.71.

[94] Cho H, Lee H-Y, Han M, Choi J-R, Ahn S, Lee T, et al. Localized Down-regulation of P-glycoprotein by Focused Ultrasound and Microbubbles induced Blood-Brain Barrier Disruption in Rat Brain. Sci Rep 2016;6:31201. https://doi.org/10.1038/srep31201.

[95] Aryal M, Fischer K, Gentile C, Gitto S, Zhang Y-Z, McDannold N. Effects on P-Glycoprotein Expression after Blood-Brain Barrier Disruption Using Focused Ultrasound and Microbubbles. PLoS One 2017;12:e0166061. https://doi.org/10.1371/journal.pone.0166061.

[96] Wanek T, Römermann K, Mairinger S, Stanek J, Sauberer M, Filip T, et al. Factors Governing P-Glycoprotein-Mediated Drug-Drug Interactions at the Blood-Brain Barrier Measured with Positron Emission Tomography. Mol Pharm 2015;12:3214–25. https://doi.org/10.1021/acs.molpharmaceut.5b00168.

[97] Ye D, Zhang X, Yue Y, Raliya R, Biswas P, Taylor S, et al. Focused ultrasound combined with microbubble-mediated intranasal delivery of gold nanoclusters to the brain. J Control Release 2018;286:145–53. https://doi.org/10.1016/j.jconrel.2018.07.020.

[98] Alli S, Figueiredo CA, Golbourn B, Sabha N, Wu MY, Bondoc A, et al. Brainstem blood brain barrier disruption using focused ultrasound: A demonstration of feasibility and enhanced doxorubicin delivery. J Control Release 2018;281:29–41. https://doi.org/10.1016/j.jconrel.2018.05.005.

[99] Ishida J, Alli S, Bondoc A, Golbourn B, Sabha N, Mikloska K, et al. MRI-guided focused ultrasound enhances drug delivery in experimental diffuse intrinsic pontine glioma. J Control Release 2021;330:1034–45. https://doi.org/10.1016/j.jconrel.2020.11.010.

[100] Englander ZK, Wei H-J, Pouliopoulos AN, Bendau E, Upadhyayula P, Jan C-I, et al. Focused ultrasound mediated blood-brain barrier opening is safe and feasible in a murine pontine glioma model. Sci Rep 2021;11:6521. https://doi.org/10.1038/s41598-021-85180-y.

[101] Liu H-L, Hsu P-H, Lin C-Y, Huang C-W, Chai W-Y, Chu P-C, et al. Focused Ultrasound Enhances Central Nervous System Delivery of Bevacizumab for Malignant Glioma Treatment. Radiology 2016;281:99–108. https://doi.org/10.1148/radiol.2016152444.

[102] Liu H-L, Huang C-Y, Chen J-Y, Wang H-YJ, Chen P-Y, Wei K-C. Pharmacodynamic and therapeutic investigation of focused ultrasound-induced blood-brain barrier opening for enhanced temozolomide delivery in glioma treatment. PLoS One 2014;9:e114311. https://doi.org/10.1371/journal.pone.0114311.

[103] Dréan A, Lemaire N, Bouchoux G, Goldwirt L, Canney M, Goli L, et al. Temporary blood-brain barrier disruption by low intensity pulsed ultrasound increases carboplatin delivery and efficacy in preclinical models of glioblastoma. J Neurooncol 2019;144:33–41. https://doi.org/10.1007/s11060-019-03204-0.

[104] Mainprize T, Lipsman N, Huang Y, Meng Y, Bethune A, Ironside S, et al. Blood-Brain Barrier Opening in Primary Brain Tumors with Non-invasive MR-Guided Focused Ultrasound: A Clinical Safety and Feasibility Study. Sci Rep 2019;9:321. https://doi.org/10.1038/s41598-018-36340-0.

[105] Lipsman N, Meng Y, Bethune AJ, Huang Y, Lam B, Masellis M, et al. Blood-brain barrier opening in Alzheimer's disease using MR-guided focused ultrasound. Nat Commun 2018;9:2336. https://doi.org/10.1038/s41467-018-04529-6.

[106] Abrahao A, Meng Y, Llinas M, Huang Y, Hamani C, Mainprize T, et al. First-in-human trial of blood-brain barrier opening in amyotrophic lateral sclerosis using MR-guided focused ultrasound. Nat Commun 2019;10:4373. https://doi.org/10.1038/s41467-019-12426-9.

[107] Idbaih A, Canney M, Belin L, Desseaux C, Vignot A, Bouchoux G, et al. Safety and Feasibility of Repeated and Transient Blood-Brain Barrier Disruption by Pulsed Ultrasound in Patients with Recurrent Glioblastoma. Clin Cancer Res an Off J Am Assoc Cancer Res 2019;25:3793–801. https://doi.org/10.1158/1078-0432.CCR-18-3643.

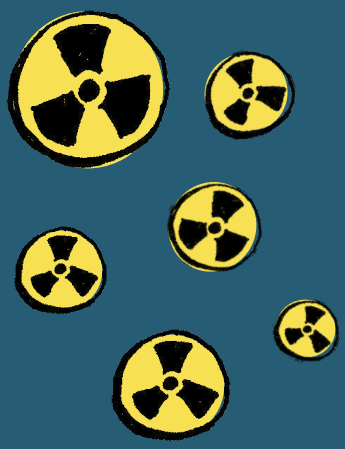

Chapter 2

Blood-brain barrier permeability following conventional photon radiotherapy - a systematic review and meta-analysis of clinical and preclinical studies

Elvin 't Hart[1]*, Zelda Odé[1]*, Marc Derieppe[1], Lucianne Groenink[2], Martijn Heymans[3], René Otten[4], Maarten Lequin[5], Geert Janssens[6], Eelco Hoving[1], Dannis van Vuurden[1]

1. Princess Máxima Center for Pediatric Oncology, Heidelberglaan 25, 3584 CS, Utrecht, The Netherlands
2. Division of Pharmacology, Utrecht Institute for Pharmaceutical Sciences, Utrecht University, The UMC Utrecht Brain Center, Utrecht, Universiteitsweg 99, 3584 CG, Utrecht, The Netherlands
3. Department of Epidemiology and Data Science, Amsterdam University Medical Center, De Boelelaan 1089a, 1081 HV, Amsterdam, The Netherlands
4. University Library, Vrije Universiteit Amsterdam, De Boelelaan 1105, 1081 HV, Amsterdam, The Netherlands
5. Department of Radiology, University Medical Center Utrecht, Heidelberglaan 100, 3584 CX, Utrecht, The Netherlands
6. Department of Radiotherapy, University Medical Center Utrecht, Heidelberglaan 100, 3584 CX, Utrecht, The Netherlands

Published in: Clinical and Translational Radiation Oncology; May 2022; 4;35:44-55. doi: 10.1016/j.ctro.2022.04.013Abstract

Abstract

Radiotherapy (RT) is a cornerstone treatment strategy for brain tumours. Besides cytotoxicity, RT can cause disruption of the blood-brain barrier (BBB) resulting in an increased permeability into the surrounding brain parenchyma. Although this effect is generally acknowledged, it remains unclear how and to what extent different radiation schemes affect BBB integrity. The aim of this systematic review and meta-analysis is to investigate the effect of photon RT regimens on BBB permeability, including reversibility in clinical and preclinical studies. We systematically reviewed relevant clinical and preclinical literature in PubMed, Embase, and Cochrane search engines. A total of 69 included studies (20 clinical, 49 preclinical) were qualitatively and quantitatively analysed by meta-analysis and evaluated on key determinants of RT-induced BBB permeability in different disease types and RT protocols. Qualitative data synthesis showed that 35% of the included clinical studies reported BBB disruption following RT, whereas 30% were inconclusive. Interestingly, no compelling differences were observed between studies with different calculated biological effective doses based on the fractionation schemes and cumulative doses; however increased BBB disruption was noted during patient follow-up after treatment. Qualitative analysis of preclinical studies showed RT BBB disruption in 78% of the included studies, which was significantly confirmed by meta-analysis ($p<0.01$). Of note, a high risk of bias, a publication bias and a high heterogeneity across the studies was observed. This systematic review and meta-analysis sheds light on the impact of RT protocols on BBB integrity and opens the discussion for integrating this factor in the decision-making process of future RT, with better study of its occurrence and influence on concomitant or adjuvant therapies.

Keywords

Blood-brain barrier, Radiotherapy, Permeability, Dose Fractionation, Radiotherapy Dosage

Introduction

Homeostasis of the central nervous system is sustained by the blood-brain barrier (BBB), also known as the neurovascular unit, that protects the brain tissue from potential harmful pathogens or substances. The BBB has a restricted permeability due to being both (1) a physical barrier formed by tight junctions between the endothelial cells that are surrounded by pericytes and a basal membrane and (2) a functional barrier where ATP-binding cassette efflux transporters have the potential to pump a large spectrum of molecules from the extravascular interstitium back into the blood stream [1]. These anatomical and functional features result in the exclusion of large substances (greater than 500 Da) [2] and over 98% of all small molecules from the brain, amongst which are chemotherapeutics and targeted therapies [3]. Hence, the BBB limits the overall treatment efficacy in brain malignancies because of the reduced, if not absent, drug delivery into the brain parenchyma [4,5].

Meanwhile, radiotherapy (RT), after maximal safe surgery, is still a cornerstone for the treatment of brain tumours such as high-grade gliomas and diffuse midline gliomas. While

conventional photon radiation therapy has been applied as a treatment modality for roughly 50% of all cancer patients [6], technological advances, like image-guided RT or different particle radiations (electron, proton, neutron beams) have improved the specificity of the treatment modality and enabled better and precise radiation treatment of the tumours while sparing the healthy tissue [7]. Despite this technical progress large volumes of the functioning brain issue has to be radiated due to the highly infiltrative nature of most primary brain tumours [8]. Due to low radio-sensitivity of certain tumours [9], often high dosages are needed to achieve the maximal anti-tumour effect, which also cause damage to the surrounding normal tissue. Vascular endothelial cells are one of the most radiosensitive cells and consequently the brain vasculature is prone to be affected by radiation [10].

There is evidence that BBB integrity is altered after the application of RT leading to both reversible and irreversible tissue damage for the patient. Whereas early brain damage caused by radiation is mostly reversible, later more chronic injuries, manifesting at the earliest three months after treatment, can cause (sometimes severe) problems for the patient [11]. It is assumed that cellular and vascular responses of the BBB upon RT is mediated by astrogliosis and endothelial ultrastructural changes [12]. These changes to the BBB can eventually lead to seizures, brain inflammation and leaky vessels causing haemorrhages and/or a stroke [13–15]. Furthermore, it has been postulated that mostly RT with cumulative doses between 20 and 30 Gy increases BBB permeability [16], however the actual impact of RT protocols (fractions, frequency) on BBB integrity remains to be elucidated, in order to support decision-making with regard to the prevention of toxicity and the use of concomitant chemotherapeutic therapies. To the best of our knowledge, there is no clear consensus on to what extent radiation doses and fractionation schemes to affect BBB integrity. Subsequently, it is unknown to what extent confounding factors such as the patients' clinical picture, interplay in the evaluation of RT-induced effects on BBB permeability. In addition, ascertainment of the kinetics of BBB opening can be helpful to decide on dosing and timing for drugs that are not expected to cross an intact BBB.

The aim of this study is therefore to provide a thorough review of clinical and preclinical studies that have ascertained the effect of conventional photon RT on BBB permeability and its reversibility following different RT regimens. A systematic review of all available clinical and preclinical literature was performed, in three different search engines. Data were processed by qualitative analysis and meta-analysis to statistically assess the extent of BBB disruption following photon radiation in comparison to a non-irradiated control group.

Methodology

Data sources and literature search

A literature search was performed based on the Preferred Reporting Items for Systematic Reviews and Meta-Analysis (PRISMA)-statement [17]. To identify all relevant publications, systematic searches in the bibliographic databases PubMed, Embase, and The Cochrane Library (via Wiley) were performed on April 24th, 2020, without any restrictions on publication date. Search terms were based on two key words; "Radiotherapy" and "Blood-brain barrier" and included controlled terms (MeSH in PubMed and Emtree in Embase), as

well as free text terms. The full search strategies for all databases can be found in the supplementary data, table S1, S2, and S3.

Study selection and in- and exclusion criteria

All abstracts from the search were screened and assessed for their relevance in this study. Upon inclusion and abstract screening, full articles were examined based on the in- and exclusion criteria, see table S4. To emphasize, the articles were screened for conventional photon RT, indicated as "RT" in the rest of the article. For both screening levels all studies were evaluated by two independent investigators.

Risk of bias of individual studies and publication bias assessment

Risk of bias was determined by the Cochrane Risk of Bias tool for the clinical studies [18] and by the SYRCLE Risk of Bias tool for the preclinical studies [19]. Parameters chosen were based on the objectives of this review and the characteristics of all included studies. "Other bias" includes all other potential sources of bias, not included in the predefined parameters. Scoring of the studies was performed by two independent investigators until a unanimous result was achieved. Risk of bias graphs were established by Review Manager 5.3 (The Cochrane Community) [20]. To estimate publication bias, a funnel plot was created in Rstudios[21] with the Metaviz package [22] and an Eggers test was performed [23]. Possible missing studies were imputed using the "trim and fill" method [24].

Data collection

For the qualitative and quantitative analyses, studies were classified based on 1) the disease type of the subjects (clinical only), 2) the preclinical model (preclinical only), 3) the type of radiation used, 4) the biological effective dose (BED) (≤50 Gy, 50-100 Gy and ≤100 Gy), 5) the readout technique that measured BBB disruption, and 6) the timepoint(s) which BBB disruption was measured (follow-up time). To allow for better interstudy comparison and analysis, per study both the RT fractionation scheme and cumulative radiation dose were used to calculate the biological effective dose (BED) based on the linear-quadratic formula by Fowler et al (1989) [25] with an α-β of 3 (patients with solid tumours and animals) or 10 (patients with AVM and leukaemia). The timing of the occurrence of BBB disruption by RT, described in the clinical studies was classified based on the radiation injury classification of Greene-Schloesser et al (2012) [26], as follows: 1) acute effects (within one month), 2) early delayed effects (within 1-6 months), and 3) late delayed effects (after 6 months of radiation)[26]. For preclinical studies the classification of Wei et al (2016) and Collins et al (2017) was used: 1) acute effects (within 4 weeks), 2) early delayed effects (within 4-12 weeks), and (3) late delayed effects (after 12 weeks) [27,28]. For the quantitative analyses, data was extracted from the studies either directly or using ImageJ [29] as a digital ruler for the figures.

Statistical analysis

Analyses were conducted using Review Manager 5.3 software (The Cochrane Community,

the Nordic Cochrane Centre: Copenhagen, 2014) [20]. The effect of RT on BBB permeability was assessed based on continuous variables found in the included studies, as described in table S4. Only studies containing a treatment and control group were eligible for meta-analysis. In the meta-analysis, random-effect models were applied because of anticipated heterogeneity [30] between studies with inverse-variance weighting to obtain the summary effect size. The summary effect measurement was calculated as the standard mean difference (SMD) with the corresponding 95% confidence interval (CI). Because most studies were composed of multiple experimental groups, the effect measurement was calculated at group level (instead of study level). Forest plots were generated based on the following parameters: 1) animal model, 2) BED, 3) read-out technique of BBB disruption and 4) follow-up time after radiation for all included quantitative preclinical studies. Subgroup analysis was applied if groups contained at least five studies or more. Heterogeneity was calculated by means of the dispersion index of effect sizes I2. Publication bias was studied using Funnel plots, the Egger method and trim and fill analysis.

Results

Search results

A total of 4883 unique studies were screened, of which 215 studies deemed eligible (figure 1). After full text assessment, 20 clinical studies and 49 preclinical studies could be included for qualitative analysis. The meta-analysis encompassed 29 preclinical studies. The remaining 20 preclinical studies were excluded because of missing information regarding the effect size, group size, or any procedural information. None of the clinical studies could be included in the meta-analysis, since none of these studies included randomized control groups.

Description of the Included Studies

The 20 relevant clinical studies were published between 1979 and 2018 (table 1). Of these 20 studies, four included patients diagnosed with arteriovenous malformations (AVM) [31–34], four described patients suffering from haematological cancers [35–38], one focused on nasopharyngeal cancer [39], six included primary brain tumour patients [40–46] and four studies included patients diagnosed with brain metastases of other cancer types [47–50]. The 49 preclinical studies were published between 1964 and 2019, consisting of different animal models (table 2). The majority of the studies, i.e., 27 (55%), investigate BBB disruption in rats [51–77]. In addition, eleven (22%) studies use mice [12,78–87], five involve rabbits [88–92], two include dogs [93,94] , two describe monkeys [95,96], one article studied the effects of RT on the BBB in sharks [97] and one in pigs [98].

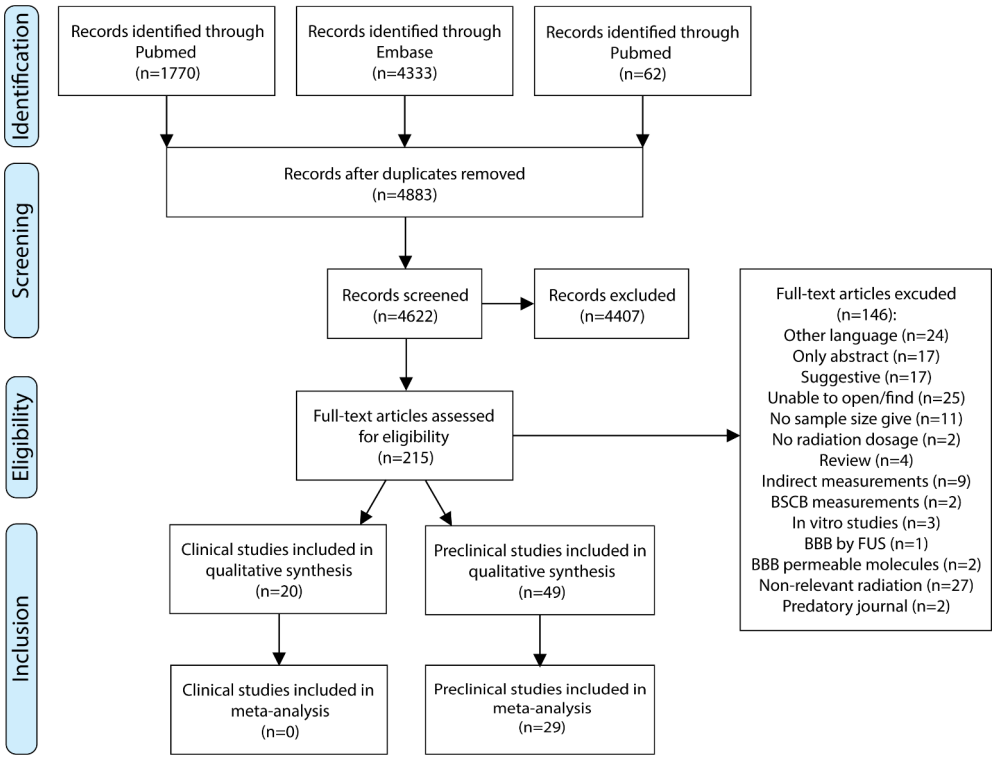

Figure 4: PRISM flow chart of study selection. After selection and filtering of a total of 4883 studies, 215 studies were included in this study, of which 20 clinical studies were evaluated for inclusion in the subsequent qualitative analysis and no clinical study was suited for meta-analysis. 49 preclinical studies were qualitatively analysed, of which 29 studies were included in the meta-analysis.

Table 1. Clinical studies included in the qualitative synthesis and the key parameters of interest in this review article.

	Author, year	*Disease type*	*Type of radiotherapy*	*Number of fractions*	*Fraction dose*	*Total dose*	*Biological Effective Dose*	*Readout technique*	*Age*	*Time*	*BBB disruption*
1	Lim et al, 2018	Supratentorial glioblastoma	RT	?	?	45 or 61.1 Gy	?	MRI	Adults	4.2 months	Yes
2	Okawa et al, 2018	Brain metastases (NSCLC)	WBRT	?	?	30 Gy	?	LC-MS	Adults	3 weeks	Yes
3	Teng et al, 2017	Brain metastases	WBRT/SRS	Single, 10 or 15	3 or 2.5 Gy	15, 18, 24, 30, or 37.5 Gy	37.5, 39, 46.9, 50.4 or 81.6	MRI	Adults	1 month	Yes
4	Fang et al, 2015	Brain metastases (NSCLC)	WBRT	10	3 Gy	30 Gy	39 Gy	LC-MS	Adults	29 days	No
5	Farjam et al, 2015	Low-grade glioma	Conformal or intensity-modulated RT	28 – 33	1.8 Gy	50.4-59.4 Gy	59.5-70.1 Gy	MRI	Adults	18 months	Yes
6	Moraes et al, 2015	AVM	RT/SRS	?	?	10-22.5 Gy	?	MRI/CT	Adults	>6 months	Unclear
7	Parkhutik et al, 2012	AVM	SRS	Single dose	-	24 Gy	216 Gy	MRI	Adults	63 months	Unclear
8	Cao et al, 2009	Low-grade glioma	Conformal RT	28 – 33	1.8 Gy	50.4-59.4 Gy	59.5-70.1 Gy	MRI	Adults	6 months	Unclear
9	Matulewicz et al, 2006	Glioma (high and low grade)	RT	30	2 Gy	60 Gy	72 Gy	NMR spectroscopy	Adults	24 months	Unclear
10	Tu et al, 2006	AVM	SRS	Single dose	-	18-20 Gy	126-153.3 Gy	Electron microscopy	Adults/children	64 months	Yes
11	Wu et al, 2006	Glioblastoma	RT	28	1.6 Gy	45 Gy	52.2 Gy	MRI/CT	-	5-10 days	No
12	Cao et al, 2005	High grade glioma	Conformal RT	35	2 Gy	70 Gy	84 Gy	MRI	Adults	6 months	Unclear
13	Levegrün et al, 2004	AVM	SRS	Single dose	-	19 Gy	139.3 Gy	MRI	Adults/children	26.8 months	Yes
14	Chan et al, 1999	Nasopharyngeal carcinoma	RT	?	?	66-71.2 Gy	?	MRI	Adults	4.4 years	Yes
15	Riccardi et al, 1998	Acute leukemia	RT	10 or 12	1.8 Gy	18 or 24 Gy	28.8 or 38.4 Gy	LC-MS	Children	24 hours	No
16	Ott et al, 1991	Intracranial lymphoma	RT	?	?	30 or 40 Gy	?	PET	Adults	21 weeks	No
17	Riccardi et al, 1991	Acute leukemia	RT	?	?	18 or 24 Gy	?	LC-MS	Children	1 year	No
18	Qin et al, 1990	Intracranial tumours	RT	15 or 20	2 Gy	30 or 40 Gy	36 or 48 Gy	CT	?	8 months	Unclear
19	Jarden et al, 1985	Brain metastases	WBRT	6 or 10	2, 3, or 4/6 Gy	20, or 30 Gy	24, 34 or 44.4 Gy	PET	Adults	72 hours	No
20	Seshadri et al, 1979	Acute leukemia/ non-hodgkin's lymphoma	RT	12 or 16	1.5 or 2 Gy	24 Gy	36 or 40 Gy	LC-MS	Adults/children	48 hours	No

Abbreviations: NSCLC, non-small cell lung cancer; AVM, arteriovenous malformations; RT, radiotherapy; WBRT, whole-brain RT; SRS, stereotactic radiosurgery; MRI, magnetic resonance imaging; LC-MS, liquid chromatography mass spectrometry; NMR, nuclear magnetic resonance; CT, computed tomography; PET, positron emission tomography

Table 2 Preclinical studies included in the qualitative synthesis and the key parameters of interest in this review article.

	Author, year	*Preclinical model*	*Type of radiotherapy*	*Number of fractions*	*Fraction dose*	*Total dose*	*Biological Effective Dose*	*Readout technique*	*Time*	*BBB disruption*	*Meta-analysis*
1	Jost et al, 2019	Rats	RT	6 fractions	5 Gy	30 Gy	45 Gy	MRI	2 days	Yes	Yes
2	Yoshida et al, 2018	Mice	RT	Single dose	-	60 Gy	420 Gy	EB extravasation	1 week	Unclear	Yes
3	Constanzo et al, 2017	Rats	Gamma knife RT	Single dose	-	10, 37, or 100 Gy	20, 173.9, 1100 Gy	MRI	140 days	Yes	Yes
4	Kalm et al, 2017	Mice	RT	Single dose	-	8 Gy	14.4 Gy	Radioactive brain uptake	72 hours	Yes	Yes
5	Zhou et al, 2017	Rats	RT	Single dose	-	6 Gy	9.6 Gy	Immunocytochemistry	24 hours	Yes	Yes
6	Murrell et al, 2016	Mice	WBRT	2	10 Gy	20 Gy	40 Gy	MRI	36 days	No	Yes
7	Ngen et al, 2016	Mice	RT	Single dose	-	80 Gy	720 Gy	MRI	2 weeks	Yes	Yes
8	Tamborini et al, 2016	Mice	WBRT	Single dose	-	2 Gy	2.4 Gy	immunohistochemistry	48 hours	Yes	Yes
9	Tong et al, 2016	Mice	RT	Single dose	-	10 Gy	20 Gy	EB extravasation	48 hours	Yes	yes
10	Fan et al, 2015	Rats	WBRT	Single dose	-	22 Gy	70.4 Gy	MRI or EB extravasation	2 hours	Yes	Yes
11	Zhang et al, 2015	Mice	RT	Single dose	-	20 Gy	60 Gy	EB extravasation	4 weeks	Yes	Yes
12	Cheng et al, 2014	Rats	Gamma knife RT	Single dose	-	60 Gy	420 Gy	EB extravasation	24 weeks	Yes	Yes
13	Jin et al, 2014	Rats	RT	2	3 Gy	6 Gy	7.8 Gy	EB extravasation	28 days	Yes	Yes
14	Lampron et al, 2012	Mice	WBRT	Single dose	-	10 Gy	20 Gy	immunohistochemistry	7 days	No	No
15	Guan et al, 2011	Rats	X-knife RT	Single dose	-	20 Gy	60 Gy	CT perfusion imaging	5 days	Yes	Yes
16	Khatri et al, 201	Rats	RT	Single dose	-	10 or 20 Gy	20 or 60 Gy	LC-MS	6 hours	Yes	No
17	Zhou et al, 2011	Rats	RT	4 or 8	5 Gy	20 or 40 Gy	30 or 60 Gy	EB extravasation	12 weeks	Yes	Yes
18	Liu et al, 2010	Rats	WBRT	Single dose	-	15 Gy	37.5 Gy	EB extravasation	24 hours	Yes	Yes
19	Wilson et al, 2009	Mice	RT	Single dose	-	20 Gy	60 Gy	Intravital microscopy	48 hours	Yes	Yes
20	Ernst-Stecken et al, 2007	Rats	SRS	2 - 4	10 Gy	20, 30, or 40 Gy	40, 60 or 80 Gy	MRI/CT	16 weeks	Yes	No
21	Yuan et al, 2006	Mice	RT	20	2 Gy	40 Gy	48 Gy	Intravital microscopy	180 days	Yes	Yes
22	Kaya et al, 2004	Rats	WBRT	Single dose	-	18 Gy	50.4 Gy	EB extravasation	24 hours	Yes	Yes
23	Yuan et al, 2003	Rats	RT	Single dose	-	20 Gy	60 Gy	Intravital microscopy	96 hours	Yes	Yes
24	Mima et al 1999	Rats	RT	Single dose	-	25 Gy	87.5 Gy	immunohistochemistry	5 days	Yes	No
25	Fike et al, 1998	Dogs	Interstitial RT	Single dose	-	20 Gy	60 Gy	CT	2-8 weeks	Yes	No
26	Karger et al, 1997	Rats	SRS	Single dose	-	20, 30, 40, 50, or 100 Gy	60, 120, 200, 300, 1100 Gy	MRI	19 months	Unclear	No
27	Kamiryo et al, 1996	Rats	Gamma knife RT	Single dose	-	50, 75, or 125 Gy	300, 637.5, 1687.5 Gy	EB extravasation	12 months	Unclear	No
28	Miot et al, 1995	Pigs	RT	Single dose	-	40 or 60 Gy	200, 420 Gy	MRI/EB extravasation	180 days	Yes	No
29	Nakata et al, 1995	Rats	RT	Single dose	-	20, 40, or 80 Gy	60, 200, 720 Gy	immunohistochemistry	30 days	Unclear	No
30	Omary et al, 1995	Rats	Gamma knife RT	Single dose	-	120 Gy	1560 Gy	MRI	4 weeks	Yes	No
31	Krueck et al, 1994	Rats	WBRT	Single dose	-	15 or 25 Gy	37.5 or 87.5 Gy	MRI	48 hours	Yes	Yes
32	Rubin et al, 1994	Rats	RT	Single dose	-	60 Gy	420 Gy	MRI	24 weeks	Yes	Yes
33	d'Avella et al, 1992	Rats	WBRT	20	2 Gy	40 Gy	48 Gy	Radioactive brain uptake	3 weeks	Yes	Yes

34	Lo et al, 1992	Rabbits	RT	Single dose	-	60 Gy	420 Gy	MRI	10 weeks	Unclear	Yes
35	Gobbel et al, 1991	Dogs	Interstitial RT	Single dose	-	20 Gy	60 Gy	CT	6 weeks	Yes	No
36	Lo et al, 1991	Rabbits	RT	Single dose	-	15 or 30 Gy	37.5 or 120 Gy	MRI	8 months	Yes	No
37	Bezek et al, 1990	Rats	RT	Single dose	-	25 Gy	87.5 Gy	Radioactive brain uptake	7 days	Unclear	No
38	Delattre et al, 1989	Rats	RT	Single dose	-	3 Gy	3.9 Gy	Radioactive brain uptake	3 hours	Yes	yes
39	Spence et al, 1987	Rats	Whole body RT	Single dose	-	20 Gy	60 Gy	Radioactive brain uptake	2 days	No	Yes
40	Kourtopouios et al, 1983	Rabbits	RT	Single dose	-	10 Gy	20 Gy	Chemical brain uptake	90 min	Yes	yes
41	Levin et al, 1979	Rats	RT	Single dose, 3, 5, 10, or 25	2 or 4 Gy	2, 4, 7, 10, 12, 20, 25, 30 Gy	2.4, 5.6, 11.9, 12, 16.8, 20, 24, 36 or 87.5 Gy,	Radioactive brain uptake	24 hours	Unclear	No
42	O'neill et al, 1977	Monkeys	RT	Single dose	-	35 Gy	157.5 Gy	EB extravasation	22 weeks	Yes	No
43	Blomstrand et al, 1975 (1)	Rabbits	RT	Single dose	-	30 Gy	120 Gy	EB extravasation	4 months	Yes	No
44	Blomstrand et al, 1975 (2)	Rabbits	RT	Single dose	-	30 Gy	120 Gy	EB extravasation	1 week	Yes	No
45	Olsson et al, 1975	Rats	RT	Single dose	-	300 Gy	9300 Gy	EB extravasation	9 days	Yes	No
46	Tanaka et al, 1975	Monkeys	RT	Single dose	-	35 Gy	157.5 Gy	Radioactive brain uptake	40 weeks	Yes	Yes
47	Olsson et al, 1972	Sharks	RT	Single dose	-	10, 35, 50, 107, 200, 250 or 300 Gy	20, 157.5, 300, 1251.9, 4200, 6500, 9300 Gy	EB extravasation	28 months	No	No
48	Bulat et al, 1966	Rats	WBRT	Single dose	-	9 or 80 Gy	17.1, 720 Gy	Chemical brain uptake	24 hours	No	Yes
49	Nair and Roth, 1964	Mice	RT	Single dose	-	80 or 115 Gy	720, 1437.5 Gy	Radioactive brain uptake	120 hours	Yes	No

Abbreviations: EB, Evan's Blue.

Risk of Bias and Reported Quality

The risk of bias for individual studies was assessed separately for clinical and preclinical studies. For clinical studies, a high or unclear risk of bias was found for seven of the twelve scoring criteria (figure S1). Conversely, a low risk of 75%, 75%, 60% and 55% was scored for the categories “Incomplete outcome data”, “Selective reporting”, “Reliability of outcome measurements” and “Timing similarity of outcome assessment” respectively, while no other bias is found. Preclinical studies were assessed with a high or unclear risk of bias for six of the ten scoring criteria (figure S2). A low risk of bias was assigned in 63%, 63% and 67% of the studies for the scoring criteria: “Baseline characteristics”, “incomplete outcome data” and “selective outcome reporting”, respectively. Three studies were found to have a high risk of “other bias” for the following reasons: 1) “missing statistics”, 2) “missing group sizes”, and 3) “fluctuating follow-up times”.

Effect of RT on BBB Permeability

Clinical data - Qualitative analysis

Of the 20 clinical studies that investigated BBB integrity after RT, Fifteen (75%) were performed in adults, three [32,33,38] (15%) in both adult and paediatric patients, and two [35,36] (10%) studied the effect of RT on the BBB in children only (table 1). Seven out of the 20 studies (35%) reported alterations of BBB permeability [32,33,39–41,47,50], six studies (30%) observed a shallow but unclear effect[31,34,42–44,46], whereas seven (35%) do not detect any effect [35–38,45,48,49] (figure 2A).

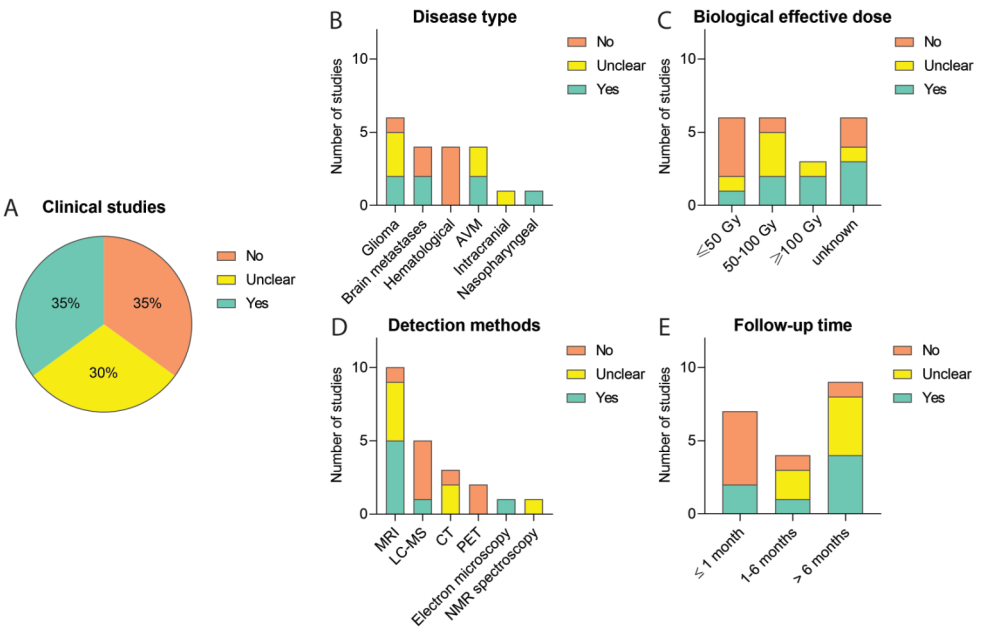

Figure 2: Effect of RT on BBB permeability in clinical studies - qualitative analysis. Analysing clinical studies, the absence or presence of RT-induced BBB permeability was evaluated (A) and subgrouped by disease type (B), Biological effective dose (C), BBB disruption detection method D), and duration of patient follow-up (E), showing differential effects.

Disease type

Two of the six studies including glioma and two of the four studies with patients suffering brain metastases observed BBB permeability after treatment (Figure 2B). None of the studies in which patients were treated with RT for a haematological disease reported any alteration of BBB integrity after treatment. Causal links between the application of radiation and the impact on the BBB in brain tumours and exposed non-tumour tissue, could not be established because of the design of the clinical studies.

Biological effective dose

In only one of the six studies [47], in which patients were treated with a BED of ≤50 Gy [47], and two of the six studies [41,47] with a BED of 50-100 Gy, an increase in BBB permeability was observed (figure 2C). Two of these studies, Farjam et al (2015) [41] (yes) and Cao et al (2009) [44] (unclear), noticed a peak in permeability at 1-1.5 months, which was reversed over time. Interestingly, in both studies patients with low-grade glioma were irradiated, with the same fractionation scheme, cumulative dose, BED, and the same read-out technique was applied. The three studies with a BED of ≥100 Gy used a single-dose radiation in patients suffering from AVM where RT is used for stereotactic radiosurgery; Tu et al (2006) [32] and Levegrün et al (2004)[33] reported a clear BBB disruption, while Parkhutik et al (2012) [31] only observed this in part of the patients. For the remaining six studies [34,35,37,39,40,50] no BED could be calculated, because details on the fractionation scheme applied were not reported. Of these six studies, three did observe an increased BBB permeability. Two of these studies, Chan et al (1999) [39] and Lim et al (2018) [40] used a cumulative dose between 61 and 80 Gy observed increased BBB breakdown after radiation. Looking at the fractionation scheme Farjam et al (2015) [41] was the only one of five studies with a fraction dose below 2 Gy that observed a significant increase in BBB permeability after 1 month of radiation, while Cao et al (2009) [44] reported temporal changes in the vascular volumes and Gd-DTPA signal in the cerebral tissue. One of the six studies with a 2Gy fraction scheme observed a clear increase BBB permeability after RT, in contrast to Cao et al (2005) [43] who noticed only a BBB permeability difference close to the tumour. Qin et al (1990) [46] noted a change but also observed recovery 8 months after radiation; the authors indicated that acute effects can be reversible and do not necessarily result in permanent damage. Remarkably Jarden et al (1985) described 6 Gy per fraction without any BBB alterations, albeit in combination with dexamethasone [49].

Detection method

Five [33,39–41,47] of the ten studies using Magnetic resonance imaging (MRI) measuring the enhancement/extravasation of gadolinium-DTPA observed a clear change in BBB permeability. Other studies used a more indirect technique to detect BBB disruption. One

[50] of the five studies using Liquid chromatography–mass spectrometry (LC-MS) to detect drugs in cerebrospinal fluid as a surrogate marker of BBB disruption noticed a change (figure 2D). Fang et al (2015) [48] treated patients with Gefitinib but did not observe an effect despite a high cumulative radiation dose (40 Gy vs 30 Gy). Tu et al (2006) [32] detected an alteration in BBB integrity by electron microscopy, while studies using computed tomography (CT) or Positron emission tomography (PET) imaging did not detect any effect. Even with a high cumulative dose of 60 Gy, Matulewicz et al (2006) [42], who used nuclear magnetic resonance (NMR) spectroscopy, could not draw any clear conclusion but observed oscillations of choline-containing compounds over time, which might be indicative of BBB disruption and repair processes.

Follow-up time

Two of the seven clinical studies (29%) investigating an acute effect in BBB permeability after radiotherapy (figure 2E) reported changes after three and four weeks [47,50]. Of the four studies studying early delayed effects, only Lim et al (2018) observed a clear increase in BBB permeability [40], while Cao et al (2009) [44] and Cao et al (2005) [43]were unclear In their conclusion but both documented a peak of BBB permeability for radiation doses greater than 40 and in the range 20 to 40 Gy respectively. Late delayed effects of radiation on the BBB is found in four of nine studies [32,33,39,41].

Preclinical data – qualitative analysis

With respect to the qualitative analysis of the 49 preclinical studies, 38 (78%) reported a clear difference in BBB permeability after RT, six (12%) detect an unclear effect, and five (10%) did not observe an effect (figure 3A).

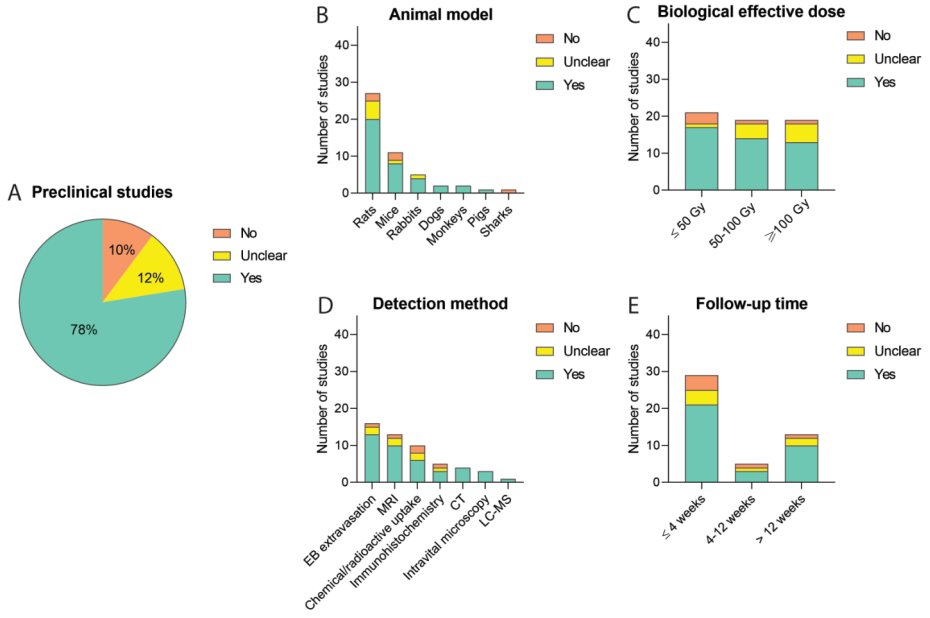

Figure 3: Effect of RT on BBB permeability in preclinical studies - qualitative analysis. Analysing preclinical studies, the absence or presence of RT-induced BBB permeability was evaluated (A), and subgrouped by animal model used (B), Biological effective dose (C), BBB disruption detection method (D), and duration of follow-up (E), showing differential effects.

Animal model

In 55% of the preclinical studies, rats were examined as animal model. Of these rat studies 74% reported that radiotherapy influenced the BBB permeability (Figure 3B). Other animal species were less frequently used, but permeability changes were also observed in mice, rabbits, dogs, monkeys, and pigs, but not for sharks. Olsson et al (1972) concluded that the shark brain is not a suitable model because of its radio-resistant properties [97]. Of note, Spence et al (1987) [66] and Bulat (1966) [67] reported an absence of effect on BBB integrity disturbances in rats after a short follow-up time of 24 and 48 hours. In addition, in two mouse studies, no changes were observed in BBB permeability; Murrell et al (2016) [83] and Lampron et al (2012) [78] noticed no changes in BBB permeability with a cumulative dose of 20 and 10 Gy respectively.

Biological effective dose

Most of the preclinical studies (81%) with a BED of ≤50 Gy reported an increase of BBB permeability. Comparable effects were observed in studies using a BED of 50-100 Gy (74%) and ≥100 Gy (68%), see figure 3C. Although an overall comparable BED was used, clinical studies relatively used a higher cumulative dose compared to preclinical studies, whereas in clinical studies BBB permeability was observed to lesser extent than in preclinical studies (35% vs 78%). Additionally, the bulk of the preclinical studies (84%) used a single dose fraction for the irradiation of the animals, with 76% of these studies observing an enhanced BBB permeability. When multiple fractionations were applied, the animals received 2 or up to 10 Gy per fraction, with a cumulative dose of 6 or up to 40 Gy. Levin et al (1979) [75], applied fractions of 2 or 4 Gy with a cumulative dose up to 30 Gy and detected some permeability changes, whereas Murrell et al (2016) [83] did not observe any change after two fractions of 10 Gy with a cumulative dose of 20 Gy.

Detection method

Unlike clinical studies, animal research more easily allowed for post-mortem observations and the usage of multiple detection methods (figure 3D). Interestingly, two of the five studies that did not observe a BBB integrity issue were analysed by Evans Blue extravasation or Immunohistochemistry [78,97], in which brain surgery and processing was necessary to acquire the results. When comparing clinical and preclinical studies that use MRI, the results are relatively similar.

Follow-up time

For each follow-up time (acute, early delayed, and late delayed) most preclinical studies observed a relatively equal occurrence of increased BBB permeability: 72%, 60% and 77%,

respectively (figure 3E). In contrast, in clinical studies an increase in BBB permeability was predominantly reported as late delayed effect.

Preclinical data – Meta-analysis

The 29 preclinical studies included in the meta-analysis showed a significant effect of radiation on BBB permeability between irradiated animals (radiotherapy group) and non-irradiated animals (control group): -9.92 [-11.89, -7.95] (n=29, p<0.01) (figure S3). However, heterogeneity was high (I2 = 98%).

Preclinical model

In the studies included in the meta-analysis, in both mice (34%) and rats (55%), RT significantly increased BBB permeability (mice SMD -10.97 [-15.77, -6.18], n=10, p<0.01; rats- SMD 8.79 [-11.24, -6.70], n=16, p<0.01) (figure S4). Subgroup analysis did not show any significant difference between effect estimates in mice and rats (p=0.26). Heterogeneity in both subgroups was high (I2=98% and I2=98%) in mice and rats, respectively. Moreover, the studies using monkeys and rabbits were excluded from the meta-analysis because data was insufficient to create a subgroup, i.e., group size lower than five.

Biological effective dose

A significant effect of radiation on BBB permeability was found in all the three subgroups of the BED, ≤50 Gy, 50-100 Gy and ≥100 Gy: -8.14 [-10.60, -5.69] (n=15, p<0.01), -11.66 [-15.97, -7.35] (n=11, p<0.01), and -6.63 [-9.53, -3.74] (n=8, p<0.01) (figure S5). No significant difference of these effects is found between the three subgroups (Chi2, p=0.16). In addition, a substantial heterogeneity was found in all three subgroups: I2=98%, I2=99%, and I2=97%, indicating a low similarity between studies with similar BEDs.

Detection method

Subgroup analysis of the detection methods: Evans Blue extravasation, MRI (gadolinium-DTPA) and extravasation of radioactive tracers (figure S6), showed a significant increase in BBB permeability after radiation: -23.75 [-34.82, -12.69] (n=7, p<0.01), -6.77 [-9.44, -4.10] (n=8, p<0.01) and -8.81 [-14.36, -3.26] (n=5, p<0.01), respectively. Comparison of the effect estimates between subgroups showed a significant difference in BBB permeability (p=0.01), which could be ascribed to a difference between the sensitivity of Evans Blue extravasation and MRI (ΔSMD= 16.98, 95% CI -25.38, -8.59) as a detection method. Heterogeneity was high in each subgroup: I2=98 %, I2=97% and I2=98% for Evans Blue, MRI, or radioactive tracers, respectively.

Follow-up time

The onset of BBB permeability after radiation therapy was explored with acute, early delayed, and late delayed categories and a significant increase in BBB permeability is observed in all follow-up time categories: -7.75 [-9.65, -5.85] (n=25, p<0.01), -6.06 [-8.83, -3.29] (n=7, p<0.01) and -5.79 [-9.07, -2.52] (n=5, p<0.01), respectively (figure S7). For each

category, a high heterogeneity was found: I2=98% (, I2=97%, and I2=94%, respectively. No significant difference between these follow-up time categories was found (p=0.46).

Publication bias

Potential publication bias was assessed for the outcome of BBB permeability upon RT in the 29 preclinical studies included in the meta-analysis (figure S8). Asymmetry observed in the funnel plot suggests the presence of publication bias, which was confirmed by Egger's regression line. The funnel plot indicates that studies with small cohorts favouring negative results were missing in the publication record. Trim and fill analysis resulted in the addition of 13 extra predicted studies (black dots), with a new total calculated effect), indicating an overestimation of the effect size. Despite this overestimation, the effect of radiation on BBB permeability remains significant.

Discussion

Conventional photon RT is a therapeutic cornerstone in brain cancer and it is commonly postulated that this treatment modality alters BBB permeability [16], a key protective component to maintain brain tissue homeostasis. The downside of a dysfunctional BBB is that the brain tissue is more exposed to blood-borne proteins, waste products and pathogens, potentially resulting in a variation of neurological disorders such as neuroinflammatory reactions and neurodegenerative diseases [99–101]. On the other hand, in the context of neurological diseases and brain cancer, an increased BBB permeability can have therapeutic advantages, whereby drugs that normally have limited access to the brain parenchyma are able to better reach the diseased brain [4]. To illustrate, new upcoming techniques such as focused ultrasound, aim to increase the BBB permeability locally and transiently for the extravasation of drugs into the brain parenchyma for the treatment of neurodegenerative diseases such as Alzheimer's Diseases and primary brain tumours as well as brain metastases [102–104]. In scope of the safety of patients and their (concomitant and adjuvant) treatment, it is crucial to monitor, evaluate and control the extent of BBB permeability caused by RT. However, the factors leading to BBB alteration remain to be better understood and a thorough analysis of the evidence on RT-induced BBB disruption thus far has been lacking. This systematic review and meta-analysis therefore explored the contribution of these determinants in the state-of-the-art literature. Based on a qualitative analysis of relevant literature and by performing a meta-analysis, we conclude from preclinical and clinical studies that photon radiotherapy indeed enhances the permeability of the BBB, although the low level of data-reporting and likely occurrence of publication bias of the included studies, limits the strength of these conclusions.

For better comparison between studies the BED was calculated, whereas clinical studies mostly observed BBB permeability upon RT at ≥100 Gy, preclinical studies display an overall effect in each of the BED categories. Most of the preclinical studies used a single dose instead of a multiple fractionation scheme which is mainly used in the clinical studies. The three included clinical studies using a single dose (18-24 Gy) observed an increase in BBB permeability, while this effect was observed in only 20% of the preclinical studies applying fractionation protocols at a respectively equal cumulative dose. Another point of interest,

laboratory animals are generally given a higher BED given compared to the patients in the clinical studies. Recently, the use of proton therapy as an alternative to conventional photon therapy is gaining popularity. Proton beam RT may possibly overcome the effects of RT at the BBB to some extent, as proton therapy is characterized by the highest energy deposition at the point of interest without an exit dose, hereby lowering the dose in the surrounding healthy tissue [105]. Now an emerging option for paediatric patients it may herewith reduce long term side effects at the developing brain. However, to our knowledge, there is still a limited data on the effects of proton therapy on BBB permeability, we were unable to analyse this in this systematic review and meta-analysis. Concerning the follow-up time, in clinical studies, increased BBB permeability was often observed after six-months, which could be explained by radio-necrosis [106]. In meantime a significant effect was reported in all post-RT time subcategories in the pre-clinical studies. Both clinical and preclinical studies mentioned a peak in permeability a few months after radiation, followed by BBB restoration afterwards [41,56]. Furthermore, a correlation between longer permeability effects and increased radiation doses was observed [44,58,72]. Over the years, the techniques to measure BBB permeability have improved and are more refined in their measurements. Older clinical studies mostly did not detect any BBB permeability change while over the years MRI became more the standard and studies using this technique found the opposite effect. Older preclinical studies mostly relied only on the extravasation of Evans Blue for visible conformation of increase permeability and reported mostly negative results, but on the other hand more recent studies using Evans Blue measured that BBB permeability is increased after RT.

The disease type, stage and/or use of different pharmacological agents are also thought to cause alterations of the BBB and are therefore likely to be confounding factors in the assessment of RT-induced BBB alteration. For instance, glioblastoma often exhibits areas of increased BBB permeability at diagnosis, which is progressive in advanced stages of the disease [107]. This permeability not only occurs along the disease course, but is also often characterized, at a specific disease stage, by a spatial intra-patient heterogeneity owing to the anarchic formation of a blood-tumour barrier in the case of certain brain cancers [108]. Noteworthy, also inter-patient heterogeneity induces a significant variability in the interpretation of permeability data in BBB studies. For example, clinical studies exploring haematological malignancies did not observe any permeability indicating the fact that underlying diseases may influence the extent of BBB permeability, confounded that the cumulative dose of RT in these studies was lower. Moreover, most of the patients in the included clinical studies were treated with additional medication, which could have further compromised or restored BBB integrity [37,38]. There is evidence that certain pharmacological agents exert an effect on BBB functioning and structure, for example inducing BBB permeability by efflux transporter inhibition [109], or by reinforcement, as reported in studies including dexamethasone [49]. Dexamethasone is often prescribed to reduce cerebral oedema [110] in brain malignancies by initiating the glucocorticoid receptor-mediated signalling, ultimately leading to strengthening and restoration of BBB integrity [111]. It is often assumed that the juvenile brain (especially that of infants) is more permeable than the adult brain, even though animal and clinical studies [112–114] observed well-developed tight junctions and similar activity of transporters. As the juvenile brain is still in development, it can be hypothesized that it is more prone to damage and

collateral effects [115]. Of the five clinical studies included, three enrolled paediatric patients but observed no effect on BBB permeability after radiation [35,36,38].

Our systematic review indicated that preclinical studies reported more RT-induced BBB permeability than clinical studies: 78% vs 35%, respectively. Besides the parameters investigated in this review several more other reasons can explain more the discrepancy: first, pre-clinical studies are designed and performed in a more controlled fashion, thus potentially reducing group variability and, in turn, increasing statistical power and ultimately finding significant differences. Second, preclinical studies give access to more readout modalities, which allows for multiparametric ascertainment and cross-validation of disease hallmarks, e.g., albumin extravasation into the brain parenchyma. In contrast, clinical studies mostly use MRI and/or LC-MS of CSF. However, preclinical protocols often require animal anaesthesia using agents that induce hemodynamic changes, e.g., isoflurane-induced vasodilation and increase in blood flow, which is directly sensed by the endothelial barrier, and may activate pathways that potentially modify BBB integrity likely to generate experimental biases [116]. Nonetheless, clinical modalities, such as MRI, CT, and PET, can be performed in patients without resorting to the administration of anaesthetics. The ascertainment of BBB leakiness in clinical MRI protocols mainly uses gadolinium chelates whose extravasation, according to their high molecular weights, is mediated by tight junctions at a specific disease stage, thus only reflecting the status of the physical BBB; however, BBB leakiness for smaller sized molecules is also mediated by its functional counterpart, mainly including transcytosis, which may be upregulated in the course of specific diseases but cannot be measured by conventional MRI protocols. Drug-PET imaging after RT, using radioisotopes such as 11C or 18F for small molecule drugs and 89Zr for monoclonal antibodies allows for visualization of enhanced brain uptake of these compounds. Based on subgroup analysis of the pre-clinical studies, Evans Blue extravasation shows a significant increase in BBB permeability compared to MRI and radioactive compounds, which have a similar effect size and seem to be more related. Conversely, in case of Evans Blue extravasation the results are obtained from post-mortem tissues, while MRI and radioactive compounds are acquired in real-time, explaining this discrepancy. The (pre)clinical studies using MRI show similar results, which might indicate that this technique is more reliable to determine BBB disruption in both humans and animals. More preclinical research is therefore needed to study the effect of RT on BBB disruption for small to large sized molecules.

In our meta-analysis, no clinical subgroup was eligible for further processing owing to the absence of non-irradiated control groups. All the eligible subgroups, i.e., including at least five studies, showed a significant RT-induced BBB permeability. One of the excluded subgroups concerns monkeys, which are particularly interesting due to their intracranial vessel structure close to humans [117]. However, the only non-human primate study exploring RT-induced BBB permeability reported non-significant differences in BBB permeability. The allocation of the follow-up time for the animal models was solely based on rats [27,28], which might have influenced the outcome of all the other models and was not specifically established for radiation effects.

Importantly, the majority of the clinical and preclinical studies scored either a high or

unclear risk of bias, affecting the reliability of the data, but also can cause an over- or underestimation of the results [118]. In case of the clinical data, bias can be caused by certain ethical considerations, for example patients can be excluded due to deviant baselines characteristics, which can cause an overestimation of the results. Last, a potential publication bias was detected, and may also explain the difference found between clinical and preclinical studies in our qualitative analyses where the percentage of studies reporting an effect of RT on BBB permeability was higher for the preclinical studies. Nevertheless, the "trim and fill" analysis confirmed RT-induced BBB disruption.

Conclusion and future perspectives

This systematic review and meta-analysis of the literature demonstrate that RT influences BBB permeability, although our findings show that suboptimal study designs and a publication bias in the selected studies may be the source of an overestimation of the extent of BBB permeability induced by RT. Worth mentioning, the robust comparison of the variables between the studies for qualitative and quantitative analysis makes it even more difficult for any hard conclusions.

Future preclinical and clinical studies using novel readout modalities should therefore be focused on fully elucidating the extent and timing of BBB opening induced by RT. These considerations will be key to adjust and guide treatment planning in treatment regimens that include RT to the brain. The effect of RT on the BBB in patients can be studied in more detail and longitudinally during and after radiotherapy, using advanced MRI and PET studies. Drug imaging with PET after RT, will provide more insight on possible RT-induced enhancement of drug delivery to the brain, avoiding toxicity and optimizing concomitant and adjuvant treatment strategies for an optimal therapeutic index [119].

References

[1] Abbott NJ, Patabendige AAK, Dolman DEM, Yusof SR, Begley DJ. Structure and function of the blood-brain barrier. Neurobiol Dis 2010;37:13–25. https://doi.org/10.1016/j.nbd.2009.07.030.

[2] Lipinski CA, Lombardo F, Dominy BW, Feeney PJ. Experimental and computational approaches to estimate solubility and permeability in drug discovery and development settings. Adv Drug Deliv Rev 1997;23:3–25.

[3] Pardridge WM. The blood-brain barrier: Bottleneck in brain drug development. NeuroRx 2005;2:3–14. https://doi.org/10.1602/neurorx.2.1.3.

[4] Van Tellingen O, Yetkin-Arik B, De Gooijer MC, Wesseling P, Wurdinger T, De Vries HE. Overcoming the blood-brain tumor barrier for effective glioblastoma treatment. Drug Resist Updat 2015;19:1–12. https://doi.org/10.1016/j.drup.2015.02.002.

[5] De Vries NA, Beijnen JH, Boogerd W, Van Tellingen O. Blood-brain barrier and chemotherapeutic treatment of brain tumors. Expert Rev Neurother 2006;6:1199–209. https://doi.org/10.1586/14737175.6.8.1199.

[6] Delaney G, Jacob S, Featherstone C, Barton M. The role of radiotherapy in cancer treatment: estimating optimal utilization from a review of evidence-based clinical guidelines. Cancer 2005;104:1129–37. https://doi.org/10.1002/cncr.21324.

[7] Baskar R, Lee KA, Yeo R, Yeoh K-W. Cancer and radiation therapy: current advances and future directions. Int J Med Sci 2012;9:193–9. https://doi.org/10.7150/ijms.3635.

[8] Claes A, Idema AJ, Wesseling P. Diffuse glioma growth: a guerilla war. Acta Neuropathol 2007;114:443–58. https://doi.org/10.1007/s00401-007-0293-7.

[9] Cohen-Jonathan-Moyal É, Vendrely V, Motte L, Balosso J, Thariat J. Radioresistant tumours: From identification to targeting. Cancer Radiother 2020;24:699–705. https://doi.org/10.1016/j.canrad.2020.05.005.

[10] O'Connor MM, Mayberg MR. Effects of radiation on cerebral vasculature: A review. Neurosurgery 2000;46:138–51. https://doi.org/10.1093/neurosurgery/46.1.138.

[11] Bentzen SM. Preventing or reducing late side effects of radiation therapy: radiobiology meets molecular pathology. Nat Rev Cancer 2006;6:702.

[12] Yuan H, Gaber MW, Boyd K, Wilson CM, Kiani MF, Merchant TE. Effects of fractionated radiation on the brain vasculature in a murine model: Blood-brain barrier permeability, astrocyte proliferation, and ultrastructural changes. Int J Radiat Oncol Biol Phys 2006;66:860–6. https://doi.org/10.1016/j.ijrobp.2006.06.043.

[13] Marchi N, Angelov L, Masaryk T, Fazio V, Granata T, Hernandez N, et al. Seizure-promoting effect of blood-brain barrier disruption. Epilepsia 2007;48:732–42. https://doi.org/10.1111/j.1528-1167.2007.00988.x.

[14] Obermeier B, Daneman R, Ransohoff RM. Development, maintenance and disruption of the blood-brain barrier. Nat Med 2013;19:1584–96. https://doi.org/10.1038/nm.3407.

[15] Cheng KM, Chan CM, Fu YT, Ho LC, Cheung FC, Law CK. Acute hemorrhage in late radiation necrosis of the temporal lobe: report of five cases and review of the literature. J Neurooncol 2001;51:143–50. https://doi.org/10.1023/a:1010631112015.

[16] Van Vulpen M, Kal HB, Taphoorn MJB, El Sharouni SY. Changes in blood-brain barrier

permeability induced by radiotherapy: Implications for timing of chemotherapy? (Review). Oncol Rep 2002;9:683–8. https://doi.org/10.3892/or.9.4.683.

[17] Moher D, Liberati A, Tetzlaff J, Altman DG. Preferred reporting items for systematic reviews and meta-analyses: the PRISMA statement. J Clin Epidemiol 2009;62:1006–12. https://doi.org/10.1016/j.jclinepi.2009.06.005.

[18] Higgins JPT, Altman DG, Gøtzsche PC, Jüni P, Moher D, Oxman AD, et al. The Cochrane Collaboration's tool for assessing risk of bias in randomised trials. BMJ 2011;343:1–9. https://doi.org/10.1136/bmj.d5928.

[19] Hooijmans CR, Rovers MM, Vries RBM De, Leenaars M, Ritskes-hoitinga M, Langendam MW. SYRCLE ' s risk of bias tool for animal studies. BMC Med Res Methodol 2014;14:1–9. https://doi.org/10.1186/1471-2288-14-43.

[20] The Nordic Cochrane Centre, The Cochrane Collaboration. Review Manager (RevMan). Version 5.3. Copenhagen: The Nordic Cochrane Centre, The Cochrane Collaboration, 2014. n.d.

[21] RStudio Team. RStudio: Integrated Development for R. RStudio 2020.

[22] Kossmeier, M., Tran, U. S., & Voracek M. Visualizing Meta-Analytic Data with R Package Metaviz. R Package Version 0.3, 1. 2020.

[23] Egger M, Davey Smith G, Schneider M, Minder C. Bias in meta-analysis detected by a simple, graphical test. BMJ 1997;315:629–34. https://doi.org/10.1136/bmj.315.7109.629.

[24] Duval S, Tweedie R. Trim and fill: A simple funnel-plot-based method of testing and adjusting for publication bias in meta-analysis. Biometrics 2000;56:455–63. https://doi.org/10.1111/j.0006-341x.2000.00455.x.

[25] Fowler JF. The linear-quadratic formula and progress in fractionated radiotherapy. Br J Radiol 1989;62:679–94. https://doi.org/10.1259/0007-1285-62-740-679.

[26] Greene-Schloesser D, Robbins ME, Peiffer AM, Shaw EG, Wheeler KT, Chan MD. Radiation-induced brain injury: A review. Front Oncol 2012;2:1–18. https://doi.org/10.3389/fonc.2012.00073.

[27] Wei T, Guo TZ, Li WW, Kingery WS, Clark JD. Acute versus chronic phase mechanisms in a rat model of CRPS. J Neuroinflammation 2016;13:1–15. https://doi.org/10.1186/s12974-015-0472-8.

[28] Collins KH, Hart DA, Smith IC, Issler AM, Reimer RA, Seerattan RA, et al. Acute and chronic changes in rat soleus muscle after high-fat high-sucrose diet. Physiol Rep 2017;5:1–10. https://doi.org/10.14814/phy2.13270.

[29] Rasband, W.S., ImageJ, U. S. National Institutes of Health, Bethesda, Maryland, USA, https://imagej.nih.gov/ij/, 1997-2018. n.d.

[30] DerSimonian R, Laird N. Meta-analysis in clinical trials revisited. Contemp Clin Trials 2015;45:139–45. https://doi.org/10.1016/j.cct.2015.09.002.

[31] Parkhutik V. Late clinical and radiological complications of stereotactical radiosurgery of arteriovenous malformations of the brain. Neuroradiology 2012;55:405–12. https://doi.org/10.1007/s00234-012-1115-8.

[32] Tu J, Stoodley MA, Morgan MK, Storer KP. Responses of arteriovenous malformations to radiosurgery: Ultrastructural changes. Neurosurgery 2006;58:749–57. https://doi.org/10.1227/01.NEU.0000192360.87083.90.

[33] Levegrün S, Hof H, Essig M, Schlegel W, Debus J. Radiation-induced changes of brain tissue after radiosurgery in patients with arteriovenous malformations: Correlation with dose distribution parameters. Int J Radiat Oncol Biol Phys 2004;59:796–808. https://doi.org/10.1016/j.ijrobp.2003.11.033.

[34] Moraes PL, Dias RS, Weltman E, Giordani AJ, Benabou S, Segreto HRC, et al. Outcome of cerebral arteriovenous malformations after linear accelerator reirradiation. Surg Neurol Int 2015;6:96. https://doi.org/10.4103/2152-7806.158205.

[35] Riccardi R. CRANIAL IRRADIATION AND CEREBROSPINAL FLUID LEVELS OF 6-MERCAPTOPURINE IN CHILDREN WITH ACUTE LEUKEMIA RICCARDO 1991:95–8.

[36] Riccardi R, Riccardi A, Lasorella A, Servidei T, Mastrangelo S. Cranial irradiation and permeability of blood-brain barrier to cytosine arabinoside in children with acute leukemia. Clin Cancer Res 1998;4:69–73.

[37] Ott RJ, Brada M, Flower MA, Babich JW, Cherry SR, Deehan BJ. Measurements of blood-brain barrier permeability in patients undergoing radiotherapy and chemotherapy for primary cerebral lymphoma. Eur J Cancer Clin Oncol 1991;27:1356–61. https://doi.org/10.1016/0277-5379(91)90009-3.

[38] Seshadri RS, Ryall RG, Rice MS, Leahy M, Ellis R. The Effect of Cranial Irradiation on Blood-Brain Barrier Permeability to Methotrexate. J Paediatr Child Health 1979;15:184–6. https://doi.org/10.1111/j.1440-1754.1979.tb01223.x.

[39] Chan YL, Leung SF, King a D, Choi PH, Metreweli C. Late radiation injury to the temporal lobes: morphologic evaluation at MR imaging. Radiology 1999;213:800–7. https://doi.org/10.1148/radiology.213.3.r99dc07800.

[40] Lim WH, Choi SH, Yoo R-E, Kang KM, Yun TJ, Kim J-H, et al. Does radiation therapy increase gadolinium accumulation in the brain?: Quantitative analysis of T1 shortening using R1 relaxometry in glioblastoma multiforme patients. PLoS One 2018;13:e0192838. https://doi.org/10.1371/journal.pone.0192838.

[41] Farjam R, Pramanik P, Aryal MP, Srinivasan A, Chapman CH, Tsien CI, et al. A radiation-induced hippocampal vascular injury surrogate marker predicts late neurocognitive dysfunction 2015;93:908–15. https://doi.org/10.1016/j.ijrobp.2015.08.014.A.

[42] Matulewicz łukasz, Sokół M, Michnik A, Wydmański J. Long-term normal-appearing brain tissue monitoring after irradiation using proton magnetic resonance spectroscopy in vivo: Statistical analysis of a large group of patients. Int J Radiat Oncol Biol Phys 2006;66:825–32. https://doi.org/10.1016/j.ijrobp.2006.06.001.

[43] Cao Y, Tsien CI, Shen Z, Tatro DS, Ten Haken R, Kessler ML, et al. Use of magnetic resonance imaging to assess blood-brain/blood-glioma barrier opening during conformal radiotherapy. J Clin Oncol 2005;23:4127–36. https://doi.org/10.1200/JCO.2005.07.144.

[44] Cao Y, Tsien CI, Sundgren PC, Nagesh V, Normolle D, Buchtel H, et al. Dynamic contrast-enhanced magnetic resonance imaging as a biomarker for prediction of radiation-induced neurocognitive dysfunction. Clin Cancer Res 2009;15:1747–54. https://doi.org/10.1158/1078-0432.CCR-08-1420.

[45] Wu GN, Ford JM, Alger JR. MRI measurement of the uptake and retention of motexafin gadolinium in glioblastoma multiforme and uninvolved normal human brain. J Neurooncol 2006;77:95–103. https://doi.org/10.1007/s11060-005-9101-1.

[46] Qin D, Zheng R, Tang J, Li J-X, Hu Y-H. Influence of Radiation on the Blood-Brain Barrier and Optimum Time of Chemotherapy. Radiat Oncol 1990;19:1507–10.

[47] Teng F, Tsien CI, Lawrence TS, Cao Y. Blood–tumor barrier opening changes in brain metastases from pre to one-month post radiation therapy. Radiother Oncol 2017;125:89–93. https://doi.org/10.1016/j.radonc.2017.08.006.

[48] Fang L, Sun X, Song Y, Zhang Y, Li F, Xu Y, et al. Whole-brain radiation fails to boost intracerebral gefitinib concentration in patients with brain metastatic non-small cell lung cancer: A self-controlled, pilot study. Cancer Chemother Pharmacol 2015;76:873–7. https://doi.org/10.1007/s00280-015-2847-z.

[49] Jarden JO, Dhawan V, Poltorak A, Posner JB, Rottenberg DA. Positron emission tomographic measurement of blood-to-brain and blood-to-tumor transport of 82Rb: The effect of dexamethasone and whole-brain radiation therapy. Ann Neurol 1985;18:636–46. https://doi.org/10.1002/ana.410180603.

[50] Okawa S, Shibayama T, Shimonishi A, Nishimura J, Ozeki T, Takada K, et al. Success of Crizotinib Combined with Whole-Brain Radiotherapy for Brain Metastases in a Patient with Anaplastic Lymphoma Kinase Rearrangement-Positive Non-Small-Cell Lung Cancer. Case Rep Oncol 2018;11:777–83. https://doi.org/10.1159/000492150.

[51] Khatri A, Gaber W, Brundage RC, Naimark MD, Hanna SK, Stewart CF, et al. Effect of radiation on the penetration of irinotecan in rat cerebrospinal fluid. Cancer Chemother Pharmacol 2011;68:721–31. https://doi.org/10.1007/s00280-010-1542-3.

[52] Ernst-Stecken A, Jeske I, Hess A, Rödel F, Ganslandt O, Grabenbauer G, et al. Hypofractionated stereotactic radiotherapy to the rat hippocampus: Determination of dose response and tolerance. Strahlentherapie Und Onkol 2007;183:440–6. https://doi.org/10.1007/s00066-007-1715-0.

[53] Zhou K, Boström M, Joakim Ek C, Li T, Xie C, Xu Y, et al. Radiation induces progenitor cell death, microglia activation, and blood-brain barrier damage in the juvenile rat cerebellum. Sci Rep 2017;7:1–14. https://doi.org/10.1038/srep46181.

[54] Fan XW, Chen F, Chen Y, Chen GH, Liu HH, Guan SK, et al. Electroacupuncture prevents cognitive impairments by regulating the early changes after brain irradiation in rats. PLoS One 2015;10:1–17. https://doi.org/10.1371/journal.pone.0122087.

[55] Cheng L, Ma L, Ren H, Zhao H, Pang Y, Wang Y, et al. Alterations in the expression of vascular endothelial growth factor in the rat brain following gamma knife surgery. Mol Med Rep 2014;10:2263–70. https://doi.org/10.3892/mmr.2014.2520.

[56] Jin X, Liang B, Chen Z, Liu X, Zhang Z. The dynamic changes of capillary permeability and upregulation of VEGF in rats following radiation-induced brain injury. Microcirculation 2014;21:171–7. https://doi.org/10.1111/micc.12103.

[57] Guan L, Xia B, Qi X-X, Xu K, Li Z, Zhao Y. Early changes measured by CT perfusion imaging in tumor microcirculation following radiosurgery in rat C6 brain gliomas. J Neurosurg 2011;114:1672–80. https://doi.org/10.3171/2011.1.jns101513.

[58] Zhou H, Liu Z, Liu J, Wang J, Zhou D, Zhao Z, et al. Fractionated radiation-induced acute encephalopathy in a young rat model: Cognitive dysfunction and histologic findings. Am J Neuroradiol 2011;32:1795–800. https://doi.org/10.3174/ajnr.A2643 LK - http://vu.on.worldcat.org/atoztitles/link?sid=EMBASE&issn=01956108&id=doi:10.3174%2Fajnr.A2643&atitle=Fractionated+radiation-induced+acute+encephalopathy+in+a+young+rat+model%3A+Cognitive+dysfunction+and+histologic+findings&stitle=Am.+J.+Neuroradiol.&title=American+Journal+of+Neuroradiology&volume=32&issue=10&spage=1795&epage=1800&aulast=Zhou&aufirst=&auinit=H.&aufull=Zhou+H.&coden=AAJND&isbn=&pages=1795-1800&date=2011&auinit1=H&auinitm=.

[59] Liu J-L, Tian D-S, Wu G, Li Z-W, Wang W, Xie M-J, et al. Tamoxifen alleviates irradiation-induced brain injury by attenuating microglial inflammatory response in vitro and in vivo. Brain Res

2010;1316:101–11. https://doi.org/10.1016/j.brainres.2009.12.055.

[60] Kaya M, Palanduz A, Kalayci R, Kemikler G, Simsek G, Bilgic B, et al. Effects of lipopolysaccharide on the radiation-induced changes in the blood-brain barrier and the astrocytes. Brain Res 2004;1019:105–12. https://doi.org/10.1016/j.brainres.2004.05.102.

[61] Yuan H, Gaber MW, McColgan T, Naimark MD, Kiani MF, Merchant TE. Radiation-induced permeability and leukocyte adhesion in the rat blood-brain barrier: Modulation with anti-ICAM-1 antibodies. Brain Res 2003;969:59–69. https://doi.org/10.1016/S0006-8993(03)02278-9.

[62] Krueck WG, Schmiedl UP, Maravilla KR, Spence AM, Starr FL, Kenney J. MR assessment of radiation-induced blood-brain barrier permeability changes in a rat glioma model. Am J Neuroradiol 1994;15:625–32.

[63] Mima T, Ogawa Y, Taniguchi T, Toyonaga S, Mori K. Early decrease of P-glycoprotein in the endothelium of the rat brain capillaries after moderate dose of irradiation. Neurol Res 1999;21:209–15. https://doi.org/10.1080/01616412.1999.11740920.

[64] Rubin P, Gash DM, Hansen JT, Nelson DF, Williams JP. Disruption of the blood-brain barrier as the primary effect of CNS irradiation. Radiother Oncol 1994;31:51–60. https://doi.org/10.1016/0167-8140(94)90413-8.

[65] D'Avella D, Cicciarello R, Albiero F, Mesiti M, Gagliardi ME, Russi E, et al. Quantitative Study of Blood-Brain Barrier Permeability Changes after Experimental Whole- Brain Radiation Experimental 1992;30:1992–8.

[66] Spence AM, Lewellen TK, Abbott GL, Graham MM, O'Gorman LA. Regional Blood-to-Tissue Transport in an Irradiated Rat Glioma Model. Radiat Res 1987;111:225. https://doi.org/10.2307/3576981.

[67] Bulat M, Supek Z, Deanović Ž. Effect of x-irradiation on the permeability of the blood-brain barrier for 5-hydroxytryptamine in normal and adrenalectomized rats. Int J Radiat Biol 1966;11:307–10. https://doi.org/10.1080/09553006614551141.

[68] Bezek S, Trnovec T, Ščasnár V, Ďurišová M, Kukan M, Kállay Z, et al. Irradiation of the head by60Co opens the blood-brain barrier for drugs in rats. Experientia 1990;46:1017–20. https://doi.org/10.1007/BF01940660.

[69] Jost G, Frenzel T, Boyken J, Pietsch H. Impact of brain tumors and radiotherapy on the presence of gadolinium in the brain after repeated administration of gadolinium-based contrast agents: an experimental study in rats. Neuroradiology 2019;61:1273–80. https://doi.org/10.1007/s00234-019-02256-3.

[70] Delattre JY, Shapiro WR, Posner JB. Acute effects of low-dose cranial irradiation on regional capillary permeability in experimental brain tumors. J Neurol Sci 1989;90:147–53. https://doi.org/10.1016/0022-510x(89)90097-x.

[71] Karger CP, Hartmann GH, Peschke P, Debus J, Hoffmann U, Brix G, et al. Dose-response relationship for late functional changes in the rat brain after radiosurgery evaluated by magnetic resonance imaging. Int J Radiat Oncol Biol Phys 1997;39:1163–72. https://doi.org/10.1016/S0360-3016(97)00387-8.

[72] Kamiryo T, Kassell NF, Thai QA, Lopes MBS, Lee KS, Steiner L. Histological changes in the normal rat brain after gamma irradiation. Acta Neurochir (Wien) 1996;138:451–9. https://doi.org/10.1007/BF01420308.

[73] Nakata H, Yoshimine T, Murasawa A, Kumura E, Harada K, Ushio Y, et al. Early blood-brain barrier disruption after high-dose single-fraction irradiation in rats. Acta Neurochir (Wien)

1995;136:82–7. https://doi.org/10.1007/BF01411440.

[74] Omary RA, Berr SS, Kamiryo T, Lanzino G, Kassell NF, Lee KS, et al. Gamma knife irradition-Induced changes in the normal rat brain studied with 1H magnetic resonance spectroscopy and imaging. Acad Radiol 1995;2:1043–51. https://doi.org/10.1016/S1076-6332(05)80511-2.

[75] Levin VA, Edwards MS, Byrd A. Quantitative Observations of the Acute Effects of X-Irradiation on Brain Capillary Permeability: Part 1. Radiat Oncol 1979;5:1627–31.

[76] Olsson Y, Klatzo I, Carsten A. The effect of acute radiation injury on the permeability and ultrastructure of intracerebral capillaries. Neuropathol Appl Neurobiol 1975;1:59–68.

[77] Constanzo J, Masson-Côté L, Tremblay L, Fouquet JP, Sarret P, Geha S, et al. Understanding the continuum of radionecrosis and vascular disorders in the brain following gamma knife irradiation: An MRI study. Magn Reson Med 2017;78:1420–31. https://doi.org/10.1002/mrm.26546.

[78] Lampron A, Lessard M, Rivest S. Effects of Myeloablation, Peripheral Chimerism, and Whole-Body Irradiation on the Entry of Bone Marrow-Derived Cells into the Brain. Cell Transplant 2012;21:1149–59. https://doi.org/10.3727/096368911X593154.

[79] Wilson CM, Gaber MW, Sabek OM, Zawaski JA, Merchant TE. Radiation-Induced Astrogliosis and Blood-Brain Barrier Damage Can Be Abrogated Using Anti-TNF Treatment. Int J Radiat Oncol Biol Phys 2009;74:934–41. https://doi.org/10.1016/j.ijrobp.2009.02.035.

[80] Nair V, Roth LJ. Effect of X-Irradiation and Certain Other Treatments on Blood Brain Barrier Permeability. Radiat Res 1964;23:249–64. https://doi.org/10.2307/3571606.

[81] Yoshida Y, Sejimo Y, Kurachi M, Ishizaki Y, Nakano T, Takahashi A. X-ray irradiation induces disruption of the blood–brain barrier with localized changes in claudin-5 and activation of microglia in the mouse brain. Neurochem Int 2018;119:199–206. https://doi.org/10.1016/j.neuint.2018.03.002 LK - http://vu.on.worldcat.org/atoztitles/link?sid=EMBASE&issn=18729754&id=doi:10.1016%2Fj.neuint.2018.03.002&atitle=X-ray+irradiation+induces+disruption+of+the+blood%E2%80%93brain+barrier+with+localized+changes+in+claudin-5+and+activation+of+microglia+in+the+mouse+brain&stitle=Neurochem.+Int.&title=Neurochemistry+International&volume=119&issue=&spage=199&epage=206&aulast=Yoshida&aufirst=Yukari&auinit=Y.&aufull=Yoshida+Y.&coden=NEUID&isbn=&pages=199-206&date=2018&au.

[82] Kalm M, Boström M, Sandelius Å, Eriksson Y, Ek CJ, Blennow K, et al. Serum concentrations of the axonal injury marker neurofilament light protein are not influenced by blood-brain barrier permeability. Brain Res 2017;1668:12–9. https://doi.org/10.1016/j.brainres.2017.05.011.

[83] Murrell DH, Wong E, Jensen MD, Zarghami N, Foster PJ, Chambers AF. Evaluating Changes to Blood-Brain Barrier Integrity in Brain Metastasis over Time and after Radiation Treatment. Transl Oncol 2016;9:219–27. https://doi.org/10.1016/j.tranon.2016.04.006.

[84] Ngen EJ, Wang L, Wong J, Armour M, Gandhi N, Gabrielson KL, et al. A preclinical murine model for the early detection of radiation-induced brain injury using magnetic resonance imaging and behavioral tests for learning and memory: with applications for the evaluation of possible stem cell imaging agents and therapies. J Neurooncol 2016;128:225–33. https://doi.org/10.1007/s11060-016-2111-3.

[85] Tamborini M, Locatelli E, Rasile M, Monaco I, Rodighiero S, Corradini I, et al. A Combined Approach Employing Chlorotoxin-Nanovectors and Low Dose Radiation to Reach Infiltrating Tumor Niches in Glioblastoma. ACS Nano 2016;10:2509–20. https://doi.org/10.1021/acsnano.5b07375.

[86] Tong F, Zhang J, Liu L, Gao X, Cai Q, Wei C, et al. Corilagin Attenuates Radiation-Induced Brain Injury in Mice. Mol Neurobiol 2016;53:6982–96. https://doi.org/10.1007/s12035-015-9591-6.

[87] Zhang J, Tong F, Cai Q, Chen LJ, Dong JH, Wu G, et al. Shenqi Fuzheng Injection attenuates irradiation-induced brain injury in mice via inhibition of the NF-κB signaling pathway and microglial activation. Acta Pharmacol Sin 2015;36:1288–99. https://doi.org/10.1038/aps.2015.69.

[88] Lo EH, Frankel KA, Steinberg GK, Delapaz RL, Fabrikant JI. High-dose Single-Fraction Brain Irradiation: MRI, Cerebral Blood Flow, Electrophysiological, and Histological Studies 1992;22:47–55.

[89] Lo EH, Delapaz RL, Frankel KA, Poljak A, Phillips MH, Brennan KM, et al. MRI and PET of Delayed Heavy-Ion Radiation Injury in the Rabbit Brain. Radiat Oncol 1991;20:689–96.

[90] Blomstrand C. Dexamethasone effect on blood-brain barrier damage caused by acute hypertension in x-irradiated rabbits 1975:331–4.

[91] Blomstrand C, Johansson B, Rosengren B. Blood-brain barrier lesions in acute hypertension in rabbits after unilateral X-ray exposure of brain. Acta Neuropathol 1975;31:97–102. https://doi.org/10.1007/BF00688143.

[92] Kourtópouios H, Holm SE, Norrby SR. The effects or irradiation and probenecid on cerebrospinal fluid transport of penicillin. J Antimicrob Chemother 1983;11:251–5. https://doi.org/10.1093/jac/11.3.251.

[93] Fike JR, Gobbel GT, Mesiwala AH, Shin HJ, Nakagawa M, Lamborn KR, et al. Cerebrovascular effects of the bradykinin analog RMP-7 in normal and irradiated dog brain. J Neurooncol 1998;37:199–215. https://doi.org/10.1023/a:1005874206814.

[94] Gobbel GT, Marton LJ, Lamborn K, Seilhan TM, Fike JR. Modification of Radiation-Induced Brain Injury by a-Difluoromethylornithine. Radiat Re 1991;128:306–15.

[95] Tanaka A, Ueno H, Yamashita Y, Caveness WF. Regional Cerebral Blood Flow in Delayed Brain Swelling Following X-Irradiation of the Right Occipital Lobe in the Monkey. Brain Res 1975;96:233–46.

[96] O'Neill RR, Wakisaka S, Malamut BL. Computer Assisted Tomography of Focal Cerebral Radiation Necrosis in the Monkey. J Neuropathol Exp Neurol 1977;36:950–955.

[97] Olsson Y, Carsten AL, Klatzo I. Effects of Gamma Radiation on the Shark Brain. Acta Neuropathol 1972;21:1–10. https://doi.org/10.1007/978-3-319-23162-4_2.

[98] Miot E, Hoffschir D, Pontvert D, Gaboriaud G, Alapetite C, Masse R, et al. Quantitative Magnetic Resonance and Isotopic Imaging: Early Evaluation of Radiation Injury to the Braini. Radiat Oncol 1995;32:121–8.

[99] Takata F, Nakagawa S, Matsumoto J, Dohgu S. Blood-Brain Barrier Dysfunction Amplifies the Development of Neuroinflammation: Understanding of Cellular Events in Brain Microvascular Endothelial Cells for Prevention and Treatment of BBB Dysfunction. Front Cell Neurosci 2021;15:661838. https://doi.org/10.3389/fncel.2021.661838.

[100] Erickson MA, Banks WA. Blood-brain barrier dysfunction as a cause and consequence of Alzheimer's disease. J Cereb Blood Flow Metab Off J Int Soc Cereb Blood Flow Metab 2013;33:1500–13. https://doi.org/10.1038/jcbfm.2013.135.

[101] Sweeney MD, Kisler K, Montagne A, Toga AW, Zlokovic B V. The role of brain vasculature in neurodegenerative disorders. Nat Neurosci 2018;21:1318–31. https://doi.org/10.1038/s41593-018-0234-x.

[102] Lipsman N, Meng Y, Bethune AJ, Huang Y, Lam B, Masellis M, et al. Blood-brain barrier opening in Alzheimer's disease using MR-guided focused ultrasound. Nat Commun 2018;9:2336. https://doi.org/10.1038/s41467-018-04529-6.

[103] Ishida J, Alli S, Bondoc A, Golbourn B, Sabha N, Mikloska K, et al. MRI-guided focused ultrasound enhances drug delivery in experimental diffuse intrinsic pontine glioma. J Control Release 2021;330:1034–45. https://doi.org/10.1016/j.jconrel.2020.11.010.

[104] Englander ZK, Wei H-J, Pouliopoulos AN, Bendau E, Upadhyayula P, Jan C-I, et al. Focused ultrasound mediated blood-brain barrier opening is safe and feasible in a murine pontine glioma model. Sci Rep 2021;11:6521. https://doi.org/10.1038/s41598-021-85180-y.

[105] Kirsch DG, Tarbell NJ. New technologies in radiation therapy for pediatric brain tumors: the rationale for proton radiation therapy. Pediatr Blood Cancer 2004;42:461–4. https://doi.org/10.1002/pbc.10471.

[106] Walker AJ, Ruzevick J, Malayeri AA, Rigamonti D, Lim M, Redmond KJ, et al. Postradiation imaging changes in the CNS: how can we differentiate between treatment effect and disease progression? Future Oncol 2014;10:1277–97. https://doi.org/10.2217/fon.13.271.

[107] Sarkaria JN, Hu LS, Parney IF, Pafundi DH, Brinkmann DH, Laack NN, et al. Is the blood-brain barrier really disrupted in all glioblastomas? A critical assessment of existing clinical data. Neuro Oncol 2018;20:184–91. https://doi.org/10.1093/neuonc/nox175.

[108] Arvanitis CD, Ferraro GB, Jain RK. The blood-brain barrier and blood-tumour barrier in brain tumours and metastases. Nat Rev Cancer 2020;20:26–41. https://doi.org/10.1038/s41568-019-0205-x.

[109] Wagner CC, Bauer M, Karch R, Feurstein T, Kopp S, Chiba P, et al. A pilot study to assess the efficacy of tariquidar to inhibit P-glycoprotein at the human blood-brain barrier with (R)-11C-verapamil and PET. J Nucl Med 2009;50:1954–61. https://doi.org/10.2967/jnumed.109.063289.

[110] Kostaras X, Cusano F, Kline GA, Roa W, Easaw J. Use of dexamethasone in patients with high-grade glioma: a clinical practice guideline. Curr Oncol 2014;21:e493-503. https://doi.org/10.3747/co.21.1769.

[111] Hue CD, Cho FS, Cao S, Dale Bass CR, Meaney DF, Morrison B 3rd. Dexamethasone potentiates in vitro blood-brain barrier recovery after primary blast injury by glucocorticoid receptor-mediated upregulation of ZO-1 tight junction protein. J Cereb Blood Flow Metab Off J Int Soc Cereb Blood Flow Metab 2015;35:1191–8. https://doi.org/10.1038/jcbfm.2015.38.

[112] Nitta T, Hata M, Gotoh S, Seo Y, Sasaki H, Hashimoto N, et al. Size-selective loosening of the blood-brain barrier in claudin-5-deficient mice. J Cell Biol 2003;161:653–60. https://doi.org/10.1083/jcb.200302070.

[113] Johansson PA, Dziegielewska KM, Ek CJ, Habgood MD, Liddelow SA, Potter AM, et al. Blood-CSF barrier function in the rat embryo. Eur J Neurosci 2006;24:65–76. https://doi.org/10.1111/j.1460-9568.2006.04904.x.

[114] Møllgård K, Dziegielewska KM, Holst CB, Habgood MD, Saunders NR. Brain barriers and functional interfaces with sequential appearance of ABC efflux transporters during human development. Sci Rep 2017;7:11603. https://doi.org/10.1038/s41598-017-11596-0.

[115] Saunders NR, Liddelow SA, Dziegielewska KM. Barrier mechanisms in the developing brain. Front Pharmacol 2012;3:46. https://doi.org/10.3389/fphar.2012.00046.

[116] Yang S, Gu C, Mandeville ET, Dong Y, Esposito E, Zhang Y, et al. Anesthesia and surgery impair blood–brain barrier and cognitive function in mice. Front Immunol 2017;8. https://doi.org/10.3389/fimmu.2017.00902.

[117] Casals JB, Pieri NC, Feitosa ML, Ercolin AC, Roballo KC, Barreto RS, et al. The Use of Animal Models for Stroke Research: A Review. Comp Med 2011;61:305–13. https://doi.org/10.1109/

TAES.1968.5408692.

[118] Wood L, Egger M, Gluud LL, Schulz KF, Jüni P, Altman DG, et al. Empirical evidence of bias in treatment effect estimates in controlled trials with different interventions and outcomes: meta-epidemiological study. BMJ 2008;336:601–5. https://doi.org/10.1136/bmj.39465.451748.AD.

[119] Ghosh KK, Padmanabhan P, Yang C-T, Ng DCE, Palanivel M, Mishra S, et al. Positron emission tomographic imaging in drug discovery. Drug Discov Today 2021. https://doi.org/10.1016/j.drudis.2021.07.025.

Supplementary data

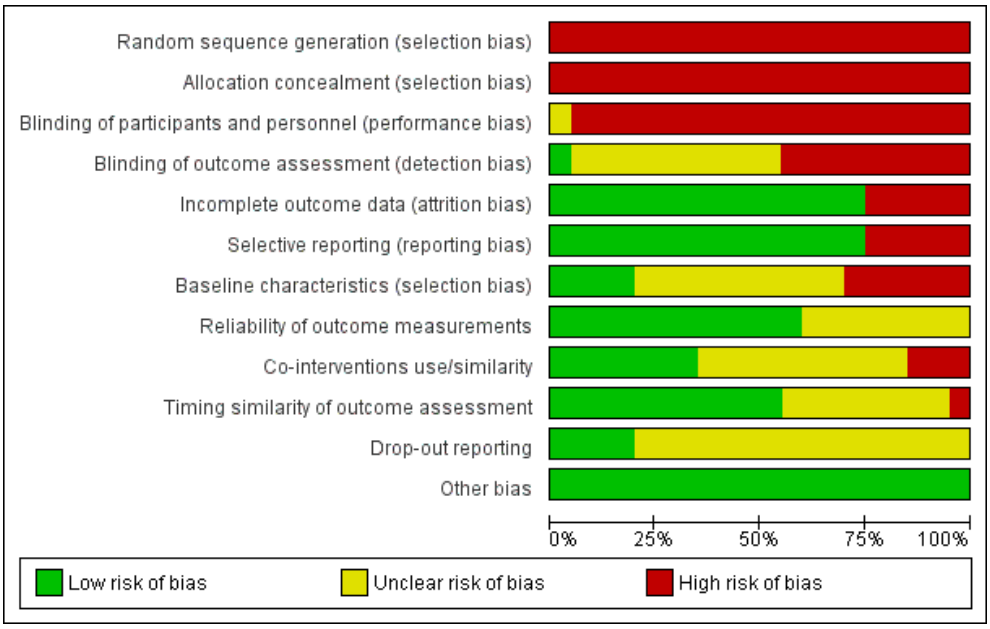

Figure S1. Risk of bias assessment of clinical studies qualitatively analysed. Risk of bias assessment of the clinical studies based on the twelve scoring criteria displayed. Data is presented as the percentage of studies with a low, unclear, or high risk of bias for each of the scoring criteria. Whereas (1) incomplete outcome data, (2) selective reporting, (3) reliability of outcome measurements, and (4) timing similarity of outcome assessment has mostly studies with a low risk of bias.

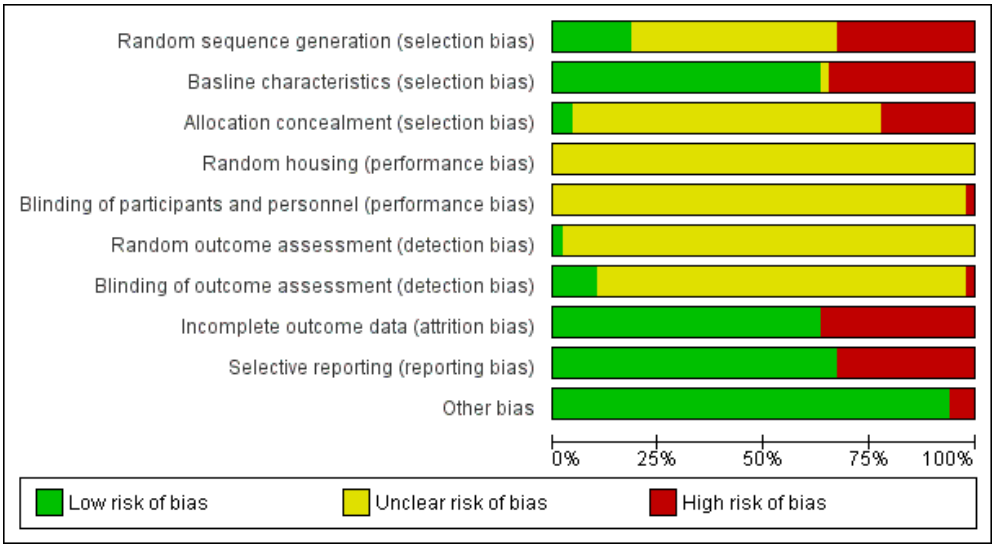

Figure S2. Risk of bias assessment of preclinical studies qualitatively analysed. Risk of bias assessment of the preclinical studies based on the 10 scoring criteria displayed. Data is presented as the percentage of studies with a low, unclear, or high risk of bias for each of the scoring criteria. Whereas (1) baseline characteristics, (2) incomplete outcome data, and (3) selective has mostly studies with a low risk of bias.

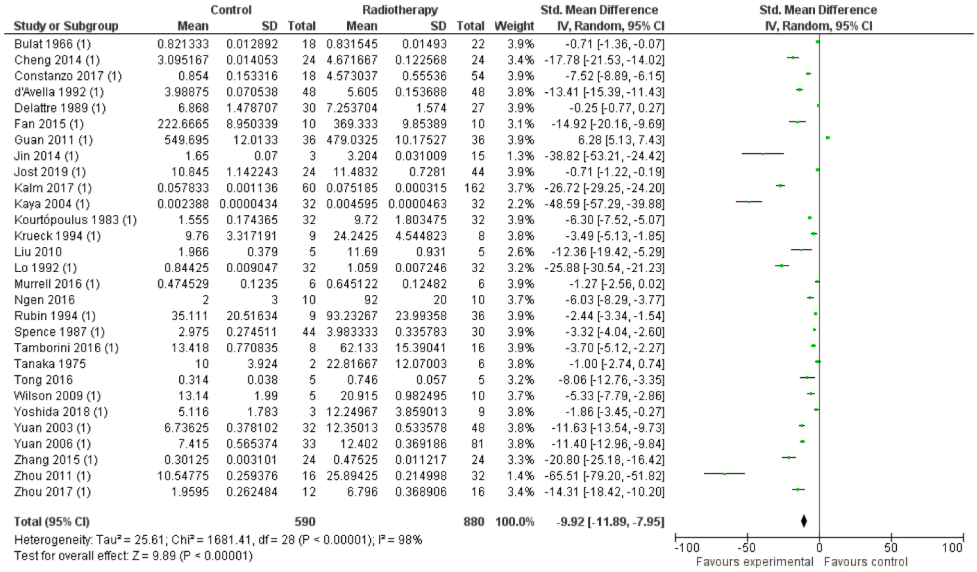

Figure S3. Meta-analysis of all included preclinical studies. Meta-analysis was performed on all the included preclinical studies, with a total of 590 irradiated subjects and 880 control subjects. A standard mean difference of -9.92 [-1.89, -7.95] was calculated for all selected studies, indicating BBB disruption by RT. Random effects model of SMD: p<0.00001. Abbreviations: CI, confidence interval; SD, standard deviation; SMD, standard mean difference.

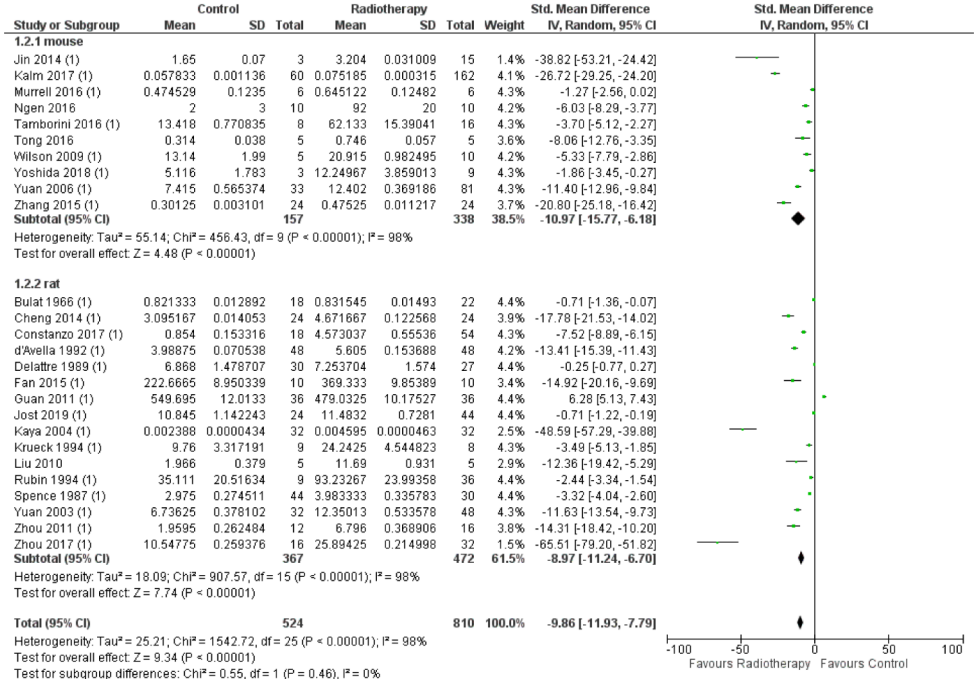

Figure S4. Meta-analysis of different subgroups based on preclinical models used in included preclinical studies. Meta-analysis was performed on subgroups using different animal models in the detection of BBB permeability following radiotherapy. Subgroups containing ≥5 studies are included in the analysis. The different animal models

analysed were mice (338 irradiated subjects and 157 control subjects) and rats (472 irradiated subjects and 367 control subjects). A standard mean difference of -10.97 [-15.77, -6.18] and -8.97 [11.24, -6,70] was calculated between the mouse model and the rat model indicating BBB disruption by RT. No significant difference was found within each subgroup (p=0.46). Random effects model of SMD: p<0.00001.

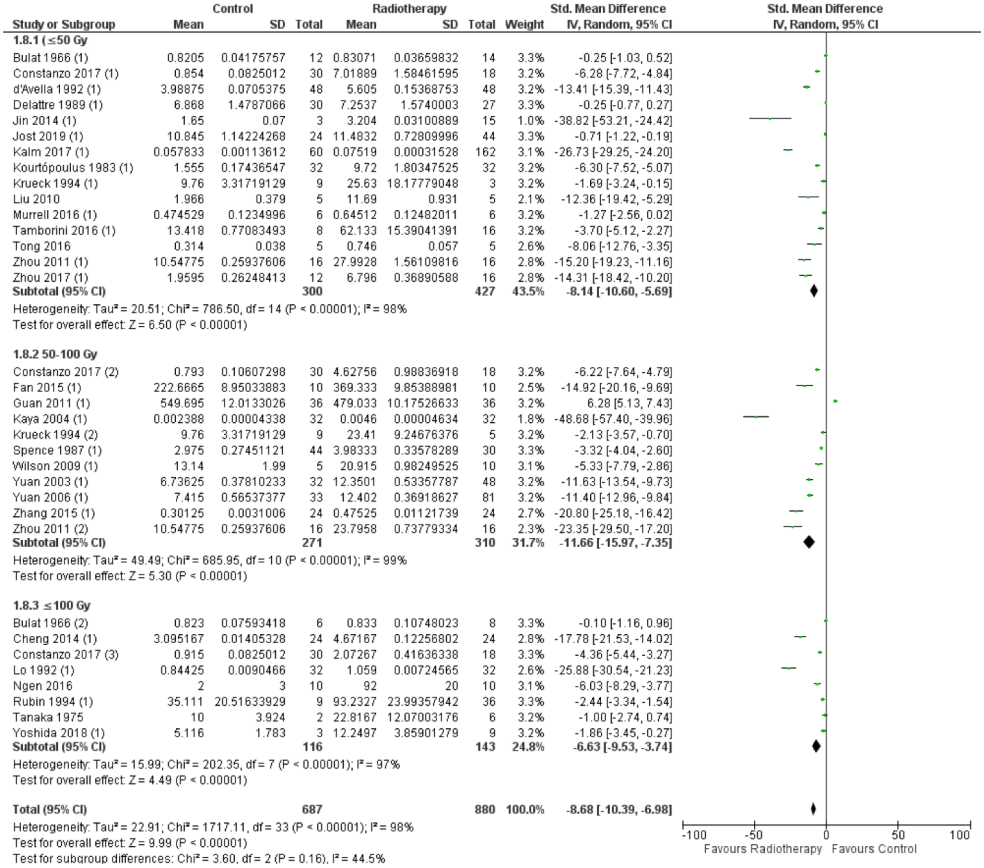

Figure S5. Meta-analysis of different subgroups based on the calculated biological effective dose used in included preclinical studies. Meta-analysis was performed on subgroups using different BED of radiotherapy. Subgroups for BED analysed were, ≤50 Gy (15 studies, 427 irradiated subjects and 300 control subjects), 50-100 Gy (11 studies, 310 irradiated subjects and 310 control subjects), and ≥100 Gy (8 studies, 143 irradiated subjects and 116 control subjects). A standard mean difference of -8.14 [-10.60, -5.69], -11.66 [-15.97, -7.35], and -6.63 [-9.53, -3.74] was calculated at ≤50 Gy, 50-100 Gy and ≥100 Gy indicating BBB disruption by RT. No significant RT effect was found between each of these subgroups (p=0.16). Random effects model of SMD: p<0.00001.

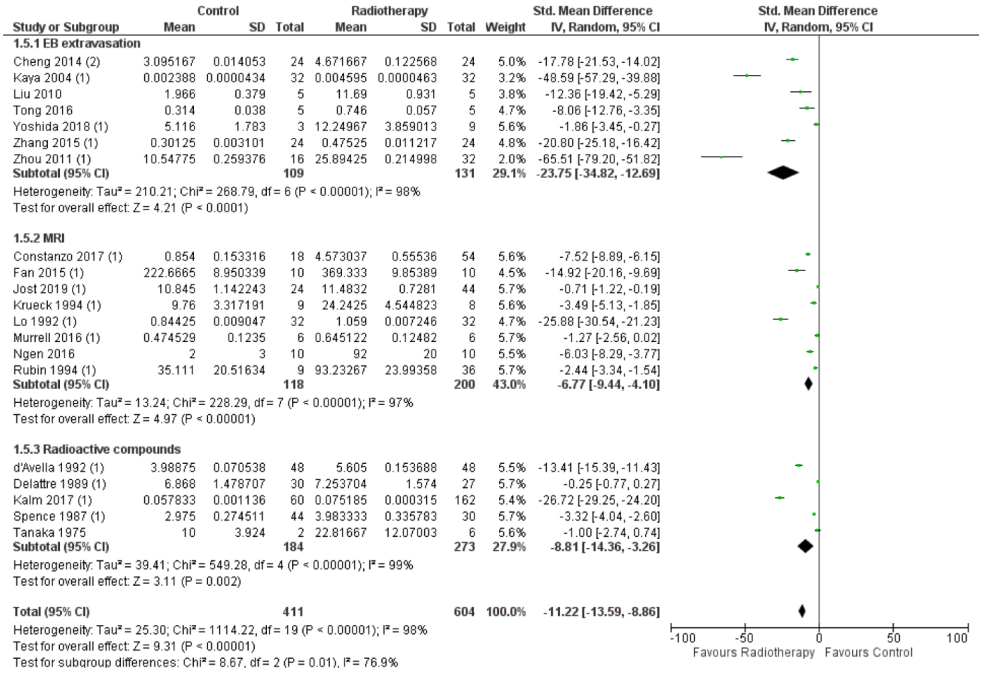

Figure S6. Meta-analysis of different subgroups based on detection method for BBB disruption used in included preclinical studies. Meta-analysis was performed on subgroups using different read-out techniques for BBB disruption following radiotherapy. Subgroups containing ≥5 studies are included in the analysis. The different detection methods analysed were EB extravasation (7 studies, 131 irradiated subjects and 109 control subjects), MRI (8 studies, 200 irradiated subjects and 118 control subjects), and brain uptake of radioactive compounds (5 studies, 273 irradiated subjects and 184 control subjects). A standard mean difference of -23.75 [-34.82, -12.69], -6.77 [-9.44, -4,10] and -8.81 [-14.36, -3.26] was calculated in these groups, indicating BBB disruption by RT. Significant difference was found between these subgroups (p=0.01). Random effects model of SMD: p<0.00001.

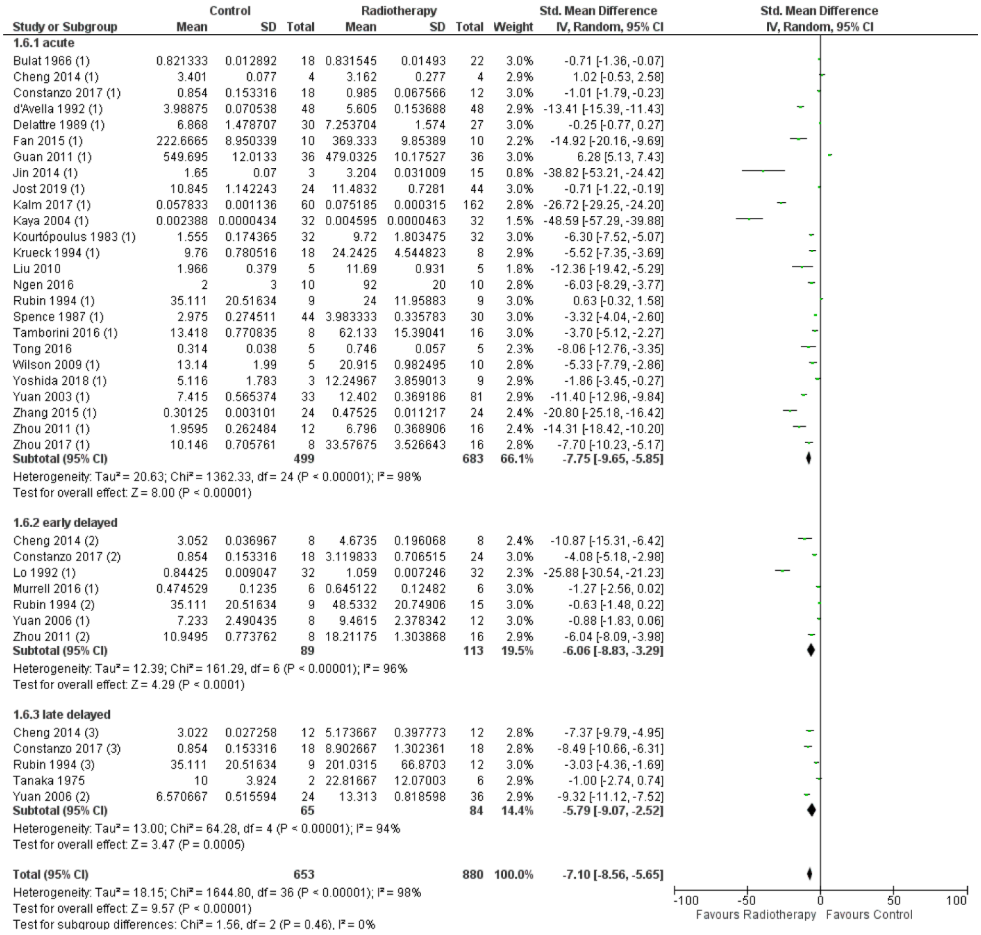

Figure S7. Meta-analysis of different subgroups based on follow-up time used in included preclinical studies. Meta-analysis was performed on subgroups using different follow-up times for BBB disruption measurement following radiotherapy. Subgroups containing ≥5 studies are included in the analysis. Different follow-up times analysed were acute (25 studies, 683 irradiated subjects and 499 control subjects), early delayed (7 studies, 113 irradiated subjects and 89 control subjects), and late delayed (5 studies, 84 irradiated subjects and 65 control subjects). A standard mean difference of -7.757 [-9.65, -5.85], -6.06 [-8.83, -3,29] and -5.79 [-9.07, -2.52] was calculated for acute, early delayed and late delayed, indicating BBB disruption by RT. No significant difference was found between each of these subgroups (p=0.46). Random effects model of SMD: p<0.00001.

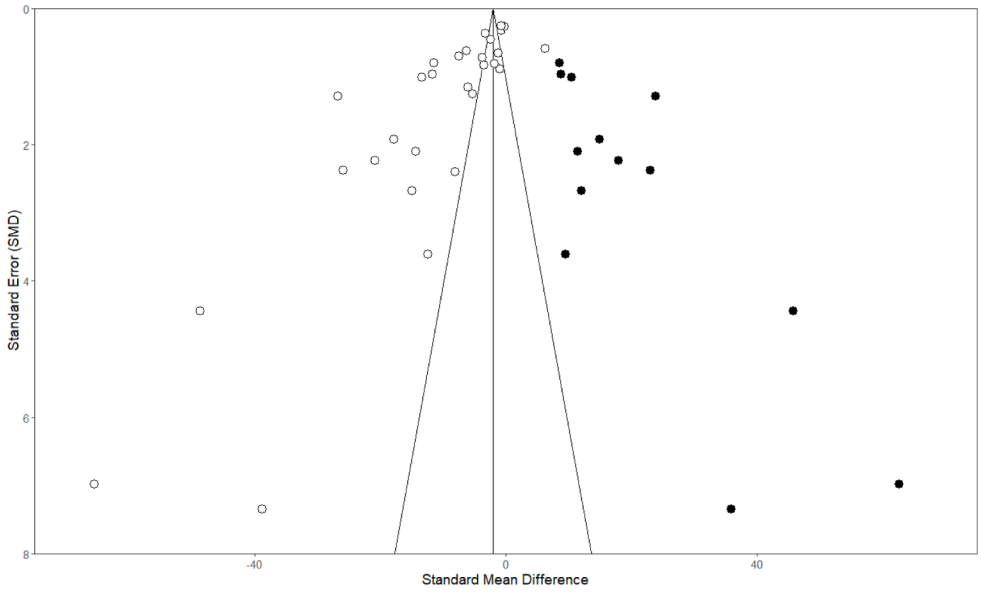

Figure S8. Funnel plot for publication bias assessment for included preclinical studies in meta-analysis. The SMD value of each study is plotted against the SE. The asymmetry of the funnel plot suggests the presence of publication bias, with an underrepresentation of studies reporting absence of effect or reduced permeability of the BBB following radiotherapy. Despite the "trim and fill" analysis (black dots), the calculated estimate effect still significantly favoured BBB permeability caused by RT.

Table S1. Search strategy PubMed based on search terms for (1) BBB, (2) radiotherapy, (3) capillary permeability and (4) brain.

	Query	*Results*
#6	#3 OR #5	1770
#5	#2 AND #4	111
#4	("Capillary Permeability"[Mesh]) AND "Brain"[Mesh]	2731
#3	#1 AND #2	1753
#2	"Radiotherapy"[Mesh] OR "Radiation"[Mesh] OR "radiotherapy" [Subheading] OR radiotherap*[tiab] OR radiation*[tiab] OR irradiation*[tiab]	990471
#1	"Blood-Brain Barrier"[Mesh] OR blood brain barrier*[tiab] OR bloodbrain barrier*[tiab] OR blood liquor barrier*[tiab] OR brain blood barrier*[tiab] OR hemato encephalic barrier*[tiab] OR hematoencephalic barrier*[tiab] OR hemoencephalic barrier*[tiab]	48363

Table S2. Search strategy Embase based on search terms for (1) BBB, (2) radiotherapy, (3) capillary permeability and (4) brain.

	Query	*Results*
#6	#3 OR #5	4333
#5	#2 AND #4	199
#4	'blood vessel permeability'/exp AND 'brain'/exp	2373
#3	#1 AND #2	4204
#2	'radiotherapy'/exp OR 'radiation'/exp OR 'irradiation'/exp OR radiotherapy:lnk OR radiotherap*:ti,ab,kw OR radiation*:ti,ab,kw OR irradiation*:ti,ab,kw	1331647
#1	'blood brain barrier'/exp OR 'blood brain barrier disruption'/exp OR 'blood brain barrier dysfunction'/exp OR 'blood brain barrier leakage'/exp OR 'blood brain barrier damage'/exp OR 'blood brain barrier permeability'/exp OR 'blood brain barrier*':ti,ab,kw OR 'bloodbrain barrier*':ti,ab,kw OR 'blood liquor barrier*':ti,ab,kw OR 'bloodliquor barrier*':ti,ab,kw OR 'brain blood barrier*':ti,ab,kw OR 'brainblood barrier*':ti,ab,kw OR 'hemato encephalic barrier*':ti,ab,kw OR 'hematoencephalic barrier*':ti,ab,kw OR 'hemo encephalic barrier*':ti,ab,kw OR 'hemoencephalic barrier*':ti,ab,kw	75692

Table S3. Search strategy Cochrane Library based on search terms for (1) BBB, (2) and radiotherapy.

	Query	*Results*
#3	#1 and #2	62
#2	radiotherap*:ti,ab,kw OR radiation*:ti,ab,kw OR irradiation*:ti,ab,kw	47292
#1	(blood NEXT brain NEXT barrier*):ti,ab,kw OR (bloodbrain NEXT barrier*):ti,ab,kw OR (blood NEXT liquor NEXT barrier*):ti,ab,kw OR (bloodliquor NEXT barrier*):ti,ab,kw OR (brain NEXT blood NEXT barrier*):ti,ab,kw OR (brainblood NEXT barrier*):ti,ab,kw OR (hemato NEXT encephalic NEXT barrier*):ti,ab,kw OR (hematoencephalic NEXT barrier*):ti,ab,kw OR (hemo NEXT encephalic NEXT barrier*):ti,ab,kw OR (hemoencephalic NEXT barrier*):ti,ab,kw	979

Table S4. Study inclusion and exclusion criteria

	Inclusion	*Exclusion*
1	Preclinical and clinical studies	Reviews and in vitro studies
2	Study written in English	Indication of blood-spinal cord disruption, suggestive evidence that BBB was disrupted
3	Full study available	Usage of radiotherapy in combination with other medication, boron neutron capture therapy, laser radiation, microwave radiation, GSM radiation, thermal radiation, microbeam radiation therapy, proton beam radiation, alpha particle radiation, or indirect radiation
4	Indication of radiotherapy type used	BBB disruption induced by other mechanisms (e.g. HIFU/osmotic disruption)
5	Indication of radiotherapy dosage used	Study assessing BBB disruption only in irradiated subjects
6	Indication of follow-up time used	
7	Indication whether the BBB was disrupted	
8	Indication of compound (or size of molecule) used for extravasation	
9	Indication of the method used for BBB disruption measurement	
10	Detection of radiotherapy induced BBB disruption	
11	Study assessing BBB disruption in irradiated vs non-irradiated subjects	

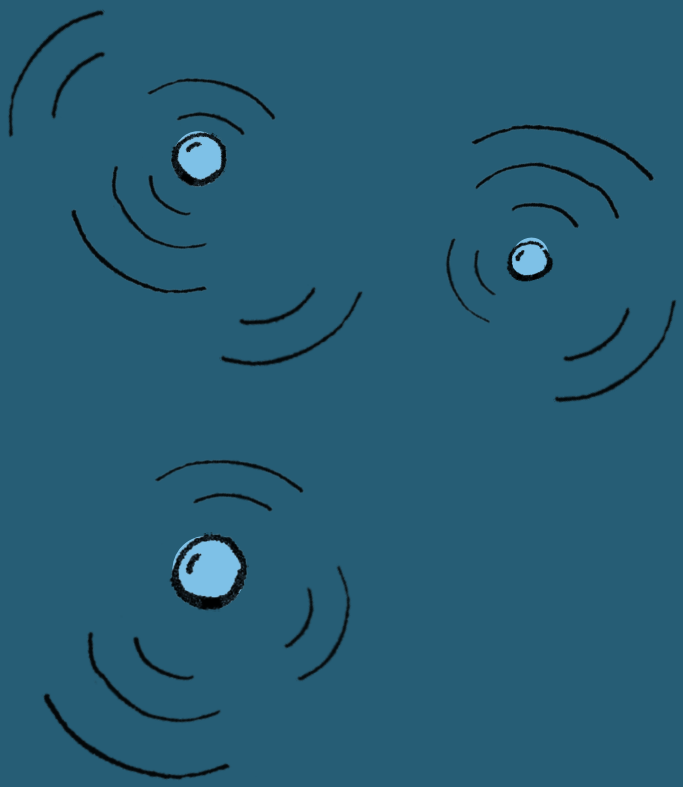

Chapter 3

A high-throughput image-guided stereotactic neuronavigation and focused ultrasound system for blood-brain barrier opening in rodents

Rianne Haumann[1,2]*, Elvin 't Hart[2]*, Marc Derieppe[2], Helena Besse[3], Gertjan Kaspers[1,2], Eelco Hoving[2], Dannis van Vuurden[1,2], Esther Hulleman[1,2], Mario Ries[3]

1. Amsterdam UMC, Vrije Universiteit Amsterdam, Pediatric Oncology, Cancer Center Amsterdam, The Netherlands
2. Princess Máxima Center for Pediatric Oncology, Utrecht, The Netherlands
3. Imaging Division, Utrecht University, Utrecht, The Netherlands

Published in: Journal of Visualized Experiments: JoVE; July 2020; 16;(161). doi: 10.3791/61269

Abstract

The blood-brain barrier (BBB) has been a major hurdle for the treatment of various brain diseases. Endothelial cells, connected by tight junctions, form a physiological barrier preventing large molecules (>500 Da) from entering the brain tissue. Microbubble-mediated focused ultrasound (FUS) can be used to induce a transient local BBB opening, allowing larger drugs to enter the brain parenchyma. In addition to large-scale clinical devices for clinical translation, preclinical research for therapy response assessment of drug candidates requires dedicated small animal ultrasound setups for targeted BBB opening. Preferably, these systems allow high-throughput workflows with both high-spatial precision as well as integrated cavitation monitoring, while still being cost effective in both initial investment and running costs. Here, we present a bioluminescence and X-ray guided stereotactic small animal FUS system that is based on commercially available components and fulfills the aforementioned requirements. A particular emphasis has been placed on a high degree of automation facilitating the challenges typically encountered in high-volume preclinical drug evaluation studies. Examples of these challenges are the need for standardization in order to ensure data reproducibility, reduce intra-group variability, reduce sample size and thus comply with ethical requirements and decrease unnecessary workload. The proposed BBB system has been validated in the scope of BBB opening facilitated drug delivery trials on patient-derived xenograft models of glioblastoma multiforme and diffuse midline glioma.

Introduction

The blood-brain barrier (BBB) is a major obstacle for drug delivery into the brain parenchyma. Most therapeutic drugs that have been developed do not cross the BBB due to their physicochemical parameters (e.g., lipophilicity, molecular weight, hydrogen bond acceptors and donors) or are not retained due to their affinity for efflux transporters in the brain [1,2]. The small group of drugs that can cross the BBB are typically small lipophilic molecules, which are only effective in a limited number of brain diseases [1,2]. As a consequence, for the majority of brain diseases, pharmacological treatment options are limited and new drug delivery strategies are needed [3,4].

Therapeutic ultrasound is an emerging technique that can be used for different neurological applications such as BBB disruption (BBBD), neuromodulation, and ablation [4–7]. In order to achieve a BBB opening with an extracorporeal ultrasound emitter through the cranium, focused ultrasound (FUS) is combined with microbubbles. Microbubble-mediated FUS results in increased bioavailability of drugs in the brain parenchyma [5,8,9]. In the presence of sound waves, microbubbles start to oscillate initiating transcytosis and disruption of the tight junctions between the endothelial cells of the BBB, enabling paracellular transport of larger molecules [10]. Previous studies confirmed the correlation between the intensity of the acoustic emission and the biological impact on the BBB opening [11–14]. FUS in combination with microbubbles has already been used in clinical trials for the treatment of glioblastoma using temozolomide or liposomal doxorubicin as the chemotherapeutic agent, or for therapy of Alzheimer's disease and amyotrophic lateral sclerosis [5,9,15,16].

Since ultrasound mediated BBB opening results in entirely new possibilities for pharmacotherapy, preclinical research for clinical translation is needed to assess the

therapy response of selected drug candidates. This typically requires a high-throughput workflow with both high-spatial precision and preferably an integrated cavitation detection for monitoring of targeted BBB opening with a high reproducibility. If possible, these systems need to be cost effective in both initial investment and running costs in order to be scalable according to the study size. Most preclinical FUS systems are combined with MRI for image-guidance and treatment planning [15,17–19]. Although MRI gives detailed information about the tumor anatomy and volume, it is an expensive technique, which is generally performed by trained/skilled operators. In addition, high-resolution MRI may not always be available for researchers in preclinical facilities and requires long scanning times per animal, making it less suitable for high-throughput pharmacological studies. Noteworthy is that, for preclinical research in the field of neuro-oncology, in particular infiltrative tumor models, the possibility to visualize and target the tumor is essential for treatment success [20]. Currently, this requirement is only fulfilled by MRI or by tumors transduced with a photoprotein, enabling visualization with bioluminescence imaging (BLI) in combination with administration of the photoprotein substrate.

MRI-guided FUS systems often use a water bath to ensure ultrasound wave propagation for transcranial applications, whereby the head of the animal is partly submerged in the water, the so called ''bottom-up'' systems [15,17,18]. While these designs work generally well in smaller animal studies, they are a compromise between animal preparation times, portability and realistically maintainable hygienic standards during usage. As an alternative to MRI, other guidance methods for stereotactic navigation encompass the use of a rodent anatomical atlas [21–23], laser pointer assisted visual sighting [24], pinhole-assisted mechanical scanning device [25], or BLI [26]. Most of these designs are “top-down” systems in which the transducer is placed on top of the animal’s head, with the animal in a natural position. The ''topdown'' workflow consists either of a water bath [22,25,26] or a water-filled cone [21,24]. The benefit of using a transducer inside a closed cone is the more compact footprint, shorter setup time and straight-forward decontamination possibilities simplifying the entire workflow.

The interaction of the acoustic field with the microbubbles is pressure dependent and ranges from low-amplitude oscillations (referred to as stable cavitation) to transient bubble collapse (referred to as inertial cavitation) [27,28]. There is an established consensus that ultrasound-BBBD requires an acoustic pressure well above the stable cavitation threshold to achieve successful BBBD, but below the inertial cavitation threshold, which is generally associated with vascular/neuronal damage [29]. The most common form of monitoring and control is the analysis of the (back-)scattered acoustic signal using passive cavitation detection (PCD), as suggested by McDannold et al. [12]. PCD relies on the analysis of the Fourier spectra of microbubble emission signals, in which the strength and appearance of stable cavitation hallmarks (harmonics, subharmonics, and ultraharmonics) and inertial cavitation markers (broadband response) can be measured in real-time.

A “one size fits all” PCD-analysis for precise pressure control is complicated due to the polydispersity of the microbubble formulation (the oscillation amplitude depends strongly on the bubble diameter), the differences in bubble shell properties between brands, and the acoustic oscillation, which depends strongly on frequency and pressure [30–32]. As a

consequence, many different PCD detection protocols have been suggested, which have been adapted to particular combinations of all these parameters and have been used in various application scenarios (ranging from in vitro experimentation over small animal protocols to PCD for clinical usage) for robust cavitation detection and even for retroactive feedback control of the pressure [11,14,30–35]. The PCD protocol employed in the scope of this study is derived directly from McDannold et al. [12] and monitors the harmonic emission for the presence of stable cavitation and broadband noise for inertial cavitation detection.

We have developed an image-guided neuronavigation FUS system for transient opening of the BBB to increase drug delivery into the brain parenchyma. The system is based on commercially available components and can be easily adapted to several different imaging modalities, depending on the available imaging techniques in the animal facility. Since we require a high-throughput workflow, we have opted to use X-ray and BLI for image-guidance and treatment planning. Tumor cells transduced with a photoprotein (e.g., luciferase) are suitable for BLI imaging [20]. After administration of the photoprotein substrate, tumor cells can be monitored in vivo and tumor growth and location can be determined [20,36]. BLI is a low-cost imaging modality, it enables to follow the tumor growth over time, it has fast scanning times and it correlates well with tumor growth measured with MRI [36,37]. We have opted to replace the water bath with a water-filled cone attached to the transducer to enable flexibility to freely move the platform on which the rodent is mounted [8,24]. The design is based on a detachable platform equipped with integration of (I) small-animal stereotactic platform (II) fiducial markers with both X-ray and opticalimage compatibility (III) rapid-detachable anesthesia mask, and (IV) integrated temperature regulated animal heating system. After the initial induction of anesthesia, the animal is mounted in a precise position on the platform where it remains during the entire procedure. Consequently, the entire platform passes all stations of the workflow of the entire intervention, while maintaining an accurate and reproducible positioning and sustained anesthesia. The control software allows the automatic detection of the fiducial markers and automatically registers all types of images and image modalities (i.e., micro-CT, X-ray, BLI and fluorescence imaging) into the frame of reference of the stereotactic platform. With help of an automatic calibration procedure, the focal length of the ultrasound transducer is precisely known within, which enables the automatic fusion of interventional planning, acoustic delivery and follow-up imaging analysis. As shown in Figure 1 and Figure 2, this setup provides a high degree of flexibility to design dedicated experimental workflows and allows interleaved handling of the animal at different stations, which in-turn facilitates high-throughput experiments. We have used this technique for successful drug delivery in mouse xenografts of high-grade glioma such as diffuse midline glioma.

Protocol

All in vivo experiments were approved by the Dutch ethical committee (license permit number AVD114002017841) and the Animal Welfare Body of the Vrije Universiteit Amsterdam, the Netherlands. The investigators were trained in the basics of the FUS system in order to minimize the discomfort of the animals.

1. Focused ultrasound system

NOTE: The described setup is an inhouse built BBB disruption system based on commercially available components and includes a 3D-printed custom-made cone and detachable stereotactic platform. The system is designed modular, which facilitates modifications according to available equipment and specific use. The protocol describes the procedure for the sonoporation of a larger area in the pontine region of the mouse brain. By adjusting the target location, different parts of the brain could be targeted. In this study a 1 MHz monoelement transducer with a focal length of 75 mm, an aperture of 60 mm and a focal area of 1.5 x 1.5 x 5 mm (FWHM of peak pressure) was used. The focal plane of the transducer is positioned through the cranium of the animal in the horizontal plane intersecting with the ear bars.

1. Select an appropriate transducer for BBB opening in rodents.

NOTE: Based on the properties of the microbubbles and the employed frequency, the acoustic settings, in particular the mechanical index (MI), are subject to change [13,38].

2. Place the transducer in the 3D-printed cone.

3. Employ an acoustically transparent mylar membrane at the bottom-end of the cone to achieve acoustic coupling of the beam propagation path, and fill the cone with degassed water.

4. Mount the transducer above the animal on a motorized linear stage as shown in Figure 1 allowing automatic vertical positioning of the transducer.

5. Design a detachable stereotactic platform based on the requirements of the study, which includes temperature regulated heating, bite and ear bars, anesthesia and multi-modality fiducial markers, as shown in Figure 1 and Figure 2. The mounting of the stereotactic platform consists of a 2D linear stage system, which allows precise automatic positioning (< 0.1 mm) of the animal under the beam.

6. Connect the transducer to the acoustic emission chain shown in Figure 1 consisting of a transducer, a function generator and a power amplifier.

7. Devise an image-processing pipeline to detect the multimodality fiducial markers that allows precise sonoporation targeting of the brain area of interest and collection of the cavitation data detected by the needle hydrophone.

8. Calibrate the system and determine the focus point of the transducer in correspondence to vertical positioning of the animal on the stereotactic platform.

2. Animal preparation

NOTE: The following protocol is specified for mice but can be adapted for rats. For these experiments female athymic nude Foxn1-/- mice (6-8 week old) were used.

1. Allow the animal to acclimatize for at least one week in the animal facility and weigh the animal regularly.

2. Administer buprenorphine (0.05 mg/kg) via subcutaneous (s.c.) injection 30 min prior to FUS treatment to start analgesic treatment.

3. Anesthetize the animal with 3% isoflurane, 2 L/min O2 and verify that the animal is deeply anesthetized. Keep the animals anesthetized during the whole procedure and monitor the breathing frequency and heart rate to adjust the concentration of isoflurane as required.

4. Apply eye ointment to prevent dry eyes and avoid possible injury.

5. Remove hair on the top of the head with a razor and depilatory cream and wash afterwards with water to remove any residues to avoid irritation to the skin.

6. For experiments with BLI tumor models, inject 150 µL of D-luciferin (30 mg/mL) intraperitoneal (i.p.) with a 29 G insulin syringe for BLI image-guidance.

7. Insert a 26-30 G tail vein catheter and flush the catheter and vein with a small volume of heparin solution (5 UI/ mL). Fill the catheter with heparin solution to avoid blood clotting.

NOTE: Good catheterization is seen when there is a reflux of blood into the catheter. Avoid air bubbles in the catheter to prevent emboli. To avoid excessive injection pressure, make sure the length of the catheter is as short as possible.

8. Place the animal on the temperature regulated stereotactic platform to avoid hypothermia.

NOTE: Hypothermia reduces blood circulation, which can affect the injection/circulation of microbubbles and the pharmacokinetics of the drugs [39].

9. Immobilize and fix the head of the animal on the stereotactic platform using ear bars and a bite bar. Fixate the body with a strap and tape the tail of the animal to the platform.

3. In vivo image-guided focused ultrasound

NOTE: For this protocol a 1 MHz mono-element transducer with a tone-burst pulse with a 10 ms duration, a MI of 0.4 and a pulse repetition frequency of 1.6 Hz with 40 cycles for 240 s was used. The protocol is optimized for microbubbles stabilized by phospholipids containing sulphur hexafluoride (SF6) as an innocuous gas, whereby the mean bubble diameter is 2.5 µm and more than 90% of the bubbles are smaller than 8 µm.

1. Place the stereotactic platform with the mounted animal in the imaging modality (e.g., BLI or X-ray) and take image(s) of the animal.

2. Use the multi-modality fiducial markers in combination with the image-processing pipeline to mark the position of the animal according to the focus point of the transducer.

3. Determine the target area by placing a brain outline over the acquired X-ray image or using BLI images to determine the center of the tumor (Figure 2). The position of specific parts of the brain are specified in the Paxinos Brain Atlas [40] using the skull markings bregma and lambda as reference points. For example the pons is located x=-1.0, y=-0.8 and z=-4.5 from lambda.

4. Shield the animal's nostrils and mouth with adhesive tape to prevent ultrasound gel interfering with breathing.

5. Apply ultrasound gel on top of the animal's head.

6. Retract the skin of the animals' neck, lubricate the needle hydrophone with ultrasound gel and place the needle hydrophone in the direct vicinity of the occipital bone.

7. Guide the transducer to the correct position using the image-processing pipeline and the focus point.

8. Apply the preconfigured settings to all attached devices and target the brain region of interest.

NOTE: Depending on the research question, tumor or brain regions can be sonoporated as a single focal point or as volumetric shape, as shown in Figure 2.

9. Activate microbubbles as described by the manufacturer. Inject one bolus of 120 µL (5.4 µg) of microbubbles.

10. Flush the tail vein catheter with saline to check the opening of the catheter.

11. Inject the microbubbles and start the insonation.

12. Record microbubble cavitation with the needle hydrophone.

13. Administer an intravascular contrast agent or drug after sonoporation. The dose, timing and planning are dependent on the purpose of the study and the drug.

NOTE: Evans blue is a common color agent to assess BBB opening [41].

14. Monitor the animal until the predetermined time point or before the humane endpoint.

4. Analysis of microbubble cavitation

NOTE: Here the applied procedure is described, which is suitable for in vivo experimentation for SF6-phospholipid microbubbles with an average diameter of 2.5 µm (80% of the bubbles below 8 µm) excited with a burst-tone pulse of 10 ms duration at a frequency of 1 MHz, as originally suggested by McDannold et al. [12].

1. Fourier-transform the recorded PCD signal from the timedomain into the frequency domain.

2. Integrate the resulting spectral power for stable cavitation detection around the 2nd and 3rd harmonic (± 50 kHz), as shown in Figure 3 (green box at 2 and 3 MHz).

3. Integrate the spectral power for inertial cavitation detection, between principal frequency, the 2nd , 3rd harmonic, the 1st and 2nd ultraharmonic and the first subharmonic (± 150 kHz), as shown in Figure 3 (red boxes).

4. Integrate the spectral power around the principle frequency (1 MHz ± 50 kHz) for the normalization of both previously obtained PCD signals. NOTE: The PCD signal, for SF6-phospholipid microbubbles in vivo experiments at 1 MHz, does not display ultraharmonics or subharmonics before inertial cavitation sets in, as shown in Figure 3.

Representative Results

The described FUS system (Figure 1 and Figure 2) and the associated workflow have been used in over a 100 animals and produced reproducible data on both healthy and tumor bearing mice. Based on the recorded cavitation and the spectral density at the harmonics at the peak moment of the microbubble bolus injection, the spectral power of each frequency can be calculated using the Fourier analysis as explained in step 4 of the Protocol. Based on the acoustic protocol (1 MHz, 10 ms pulse duration) with a MI of 0.4 in combination with microbubbles, the normalized integrated power spectrum at the 2nd and 3rd harmonics normalized the integrated power spectrum of the excitation frequency observed in Figure 3. This provided a very sensitive and reliable means of stable cavitation detection, in comparison to no detection of subharmonics when no microbubbles were injected or the observation of inertial cavitation when a MI of 0.6 was applied. In case of inertial cavitation, an increased broad-band noise floor of up to 25 dB was detected as well as the appearance of ultra-harmonics and subharmonics. Although an acoustic pressure of an MI of 0.4 and 0.6 resulted in no macroscopic damage, microscopic damage was evidenced histologically at a MI of 0.6, as shown in Figure 4. A further increase of the pressure amplitude up to a MI of 0.8 resulted in a macroscopic brain hemorrhage of larger vessels and wide-spread tissue lysis with the extravasation of erythrocytes. The histological findings corresponded to the acoustic data from the passive cavitation sensor, as shown in Figure 3, confirming the damaging properties of inertial cavitation of the brain tissue. As a consequence, a MI of 0.4 was chosen as the safe pressure amplitude that provided very reproducible BBB-opening, while providing a safe margin to the inertial cavitation regime, as observed before [11].

Intravenous Evans blue was injected to validate the opening of the BBB in the pontine region. The strong albumin binding of Evans blue leads to a large molecule of more than 66

kDa [42] . At the level of the pons and partly the cerebellum, extravasation of Evans blue-conjugated albumin was observed in the mouse treated with FUS and microbubbles in contrast to the mouse without microbubbles (Figure 5). This emphasizes the precise targeting of the region of interest based on image-guided stereotactic navigation with the in-house build FUS system and the described protocol.

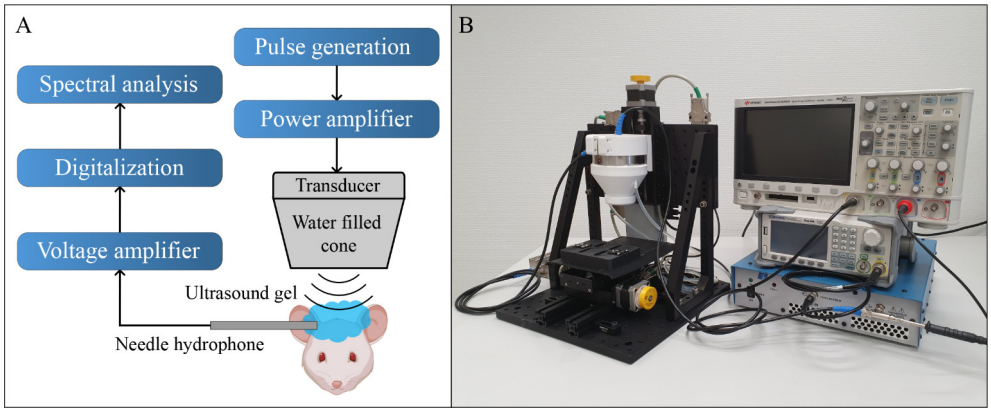

Figure 1: Focused ultrasound setup. (A) Schematic representation of the focused ultrasound set up. (B) Picture of the focused ultrasound setup. The system consists of a top-down mounted transducer on a 1D linear stage over a second 2D stage for automatic 3D positioning. The transducer is built in a water filled beam-cone, closed at the bottom with an acoustically transparent mylar membrane, which conducts the sound to the cranium of the animal. The transducer is connected to a power amplifier, which is inturn connected to an arbitrary waveform generator (AWG) for signal generation. For cavitation detection a detachable hydrophone in combination with a low-noise voltage amplifier is used. The hydrophone is placed in the direct vicinity of the occipital bone. The external hydrophone has a 2 mm active surface and is acoustically coupled with ultrasound gel. Both the standard 200 MHz oscilloscope and relayed to a control computer (not shown) for on-the-fly processing and real-time control.

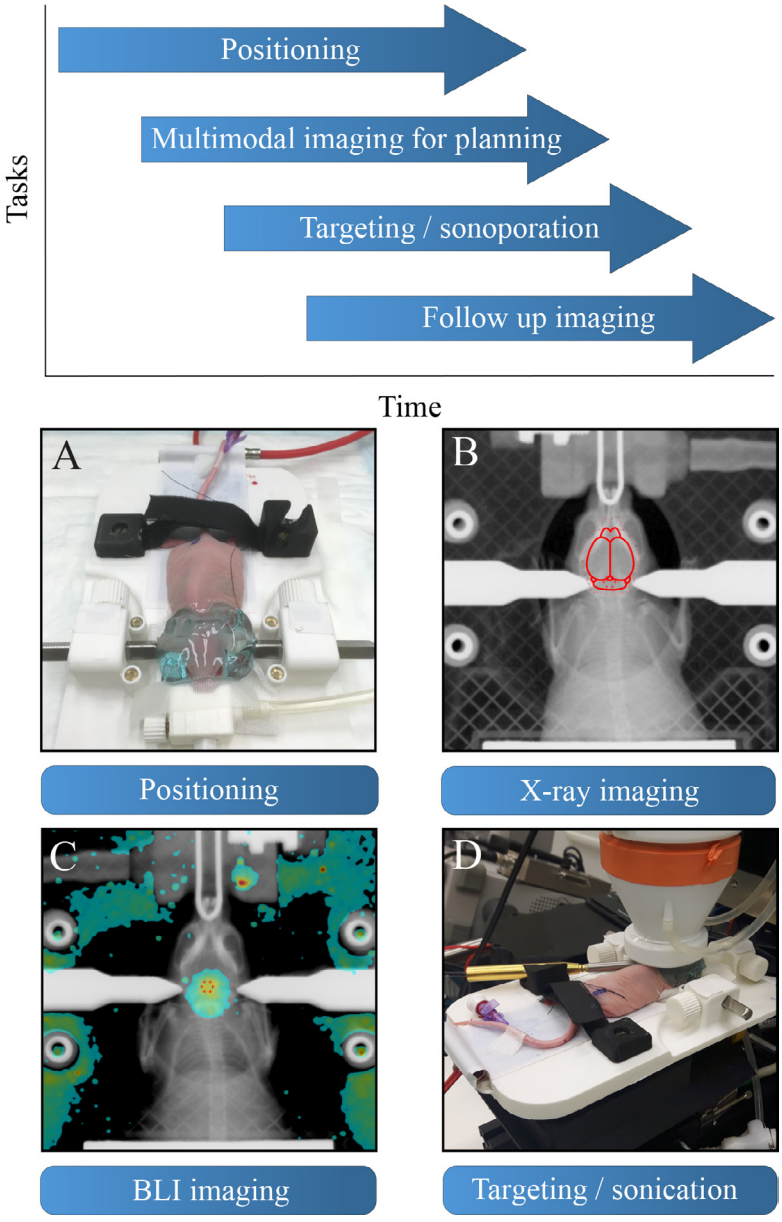

Figure 2: Focused ultrasound workflow. The proposed workflow of the focused ultrasound system starts with (A) the initial positioning of animal on a detachable stereotactic platform, note the application of the acoustic coupling gel (applied post BLI/X-ray). Simultaneously multimodal imaging can be conducted for targeting. (B) At first X-ray imaging is a possibility, whereas a region of interest can be targeted with the help of an outline of the brain (which in turn is referenced to the mouse brain atlas [40], adapted to the size and posture of the skull). (C) Alternatively, a BLI image of a luciferase transfected diffuse midline glioma tumor overlaid on an X-ray maximum intensity projection can be applied for targeting. (D) Subsequently, the stereotactic platform is mounted with the animal in therapy position with both hydrophone and transducer attached. The transducer automatically drives in therapy position and sonicates the chosen trajectory post bolus injection. The system is optimized for high-throughput experiments, whereby multiple platforms allow interleaved work, as shown on top

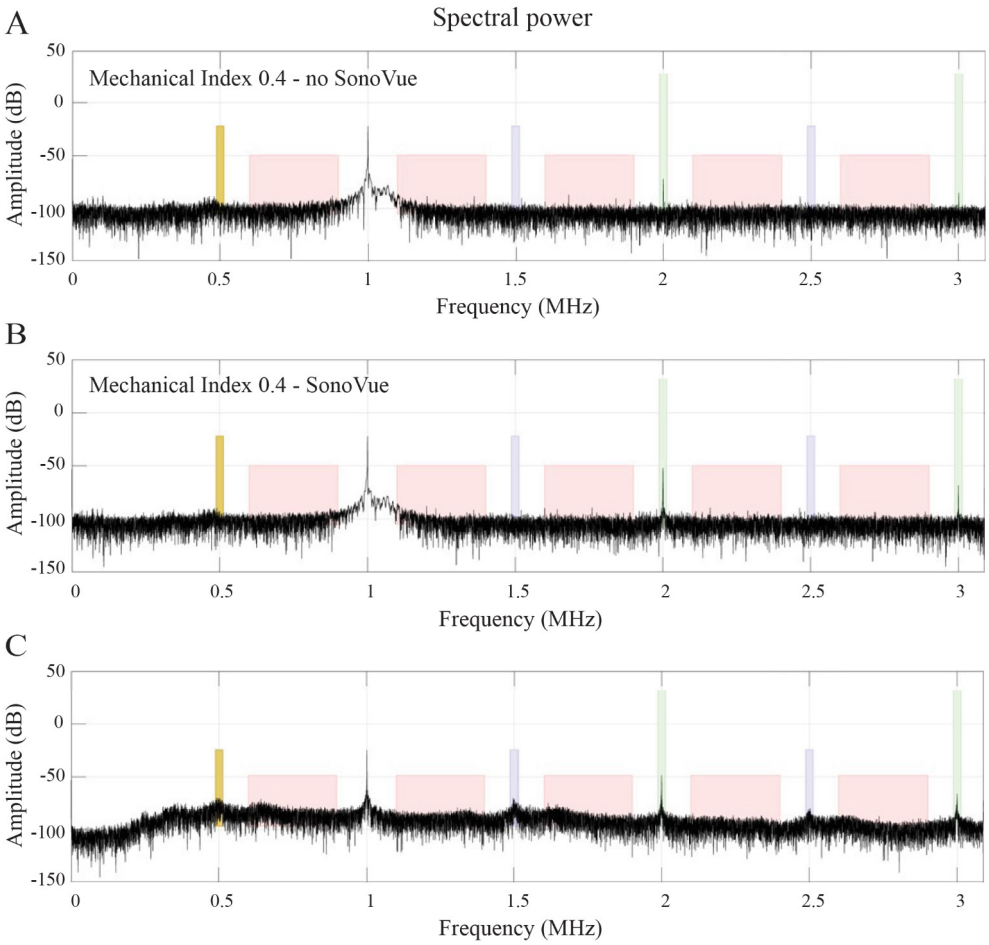

Figure 3: Cavitation monitoring. (A) Frequency spectrum of an in vivo experiment in the absence of microbubble administation at a MI of 0.4 at 1 MHz. (B) Shown is the corresponding spectrum at peak-bolus after injection of microbubbles. Note the increase of the higher harmonics, which is indicative for stable cavitation of the microbubbles. (C) Corresponding spectrum observed at a higher MI of 0.6 in combination with microbubble injection, within the transition band to the onset of inertial cavitation, leading to an increase in noise floor up to 25 dB and the appearance of ultraharmonics and subharmonics.

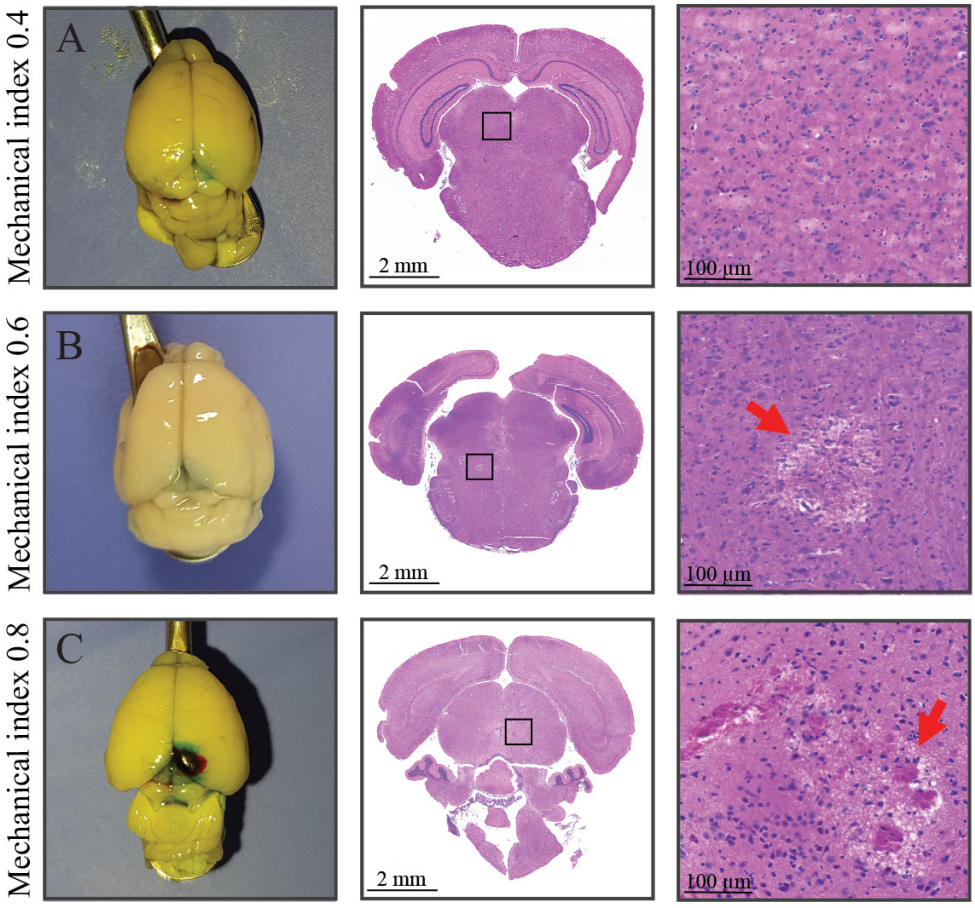

Figure 4: BBB opening and associated histology. (A) Stable cavitation using an MI of 0.4 evidenced an intact brain parenchyma in both white light macroscopy and HE stained microscopy. (B) After a MI of 0.6 first signs of local irreversible tissue damage of the brain parenchyma is becoming apparent in the HE stained histological data. (C) For even higher mechanical pressure of MI 0.8, macroscopic hemorrhaging is apparent as well as wide-spread tissue lysis of the brain parenchyma and the extravasation of erythrocytes due to microhemorrhaging. The blue hue in the white light macroscopy is indicative for the extravasation of the co-injected intra-vascular contrast agent Evans blue indicating BBB opening (see Figure 5 for a sagittal view).

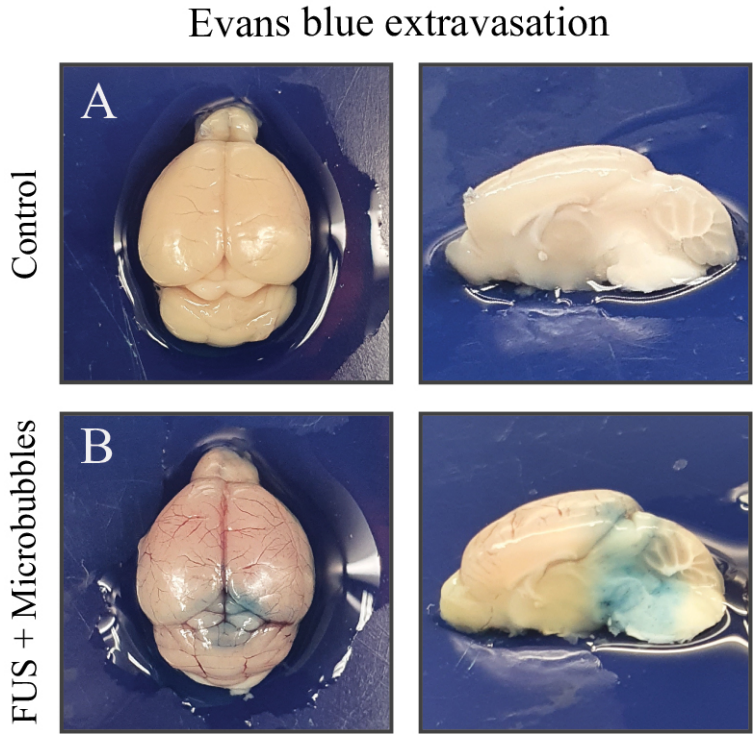

Figure 5: Validation of BBB opening. Demonstration of successful BBB opening in the stable cavitation regime (B) compared to the control (A), no microbubbles injected. In this case Evans blue has been used as an intravascular contrast agent. The strong albumin-binding of Evans blue leads to a large molecule of more than 66 kDa. As a consequence, evidence of the Evans blue extravasation is indicative for paracellular transport across the BBB due to a (partial) opening of the tight junctions.

Discussion

In this study, we developed a cost-effective image guided based FUS system for transient BBB disruption for increased drug delivery into the brain parenchyma. The system was largely built with commercially available components and in conjunction with X-ray and BLI. The modularity of the proposed design allows the use of several imaging modalities for planning and assessment in high-throughput workflows. The system can be combined with more comprehensive highresolution 3D imaging modalities, for example high-resolution MRI or micro-CT, while for the bulk of the study 2D imaging modalities such as 2D X-ray and/or BLI are used. 2D Xray and/or BLI are both considerably more cost effective as well as ideal for high-volume studies due to their respective short acquisition times. The transducer described here is well suited to produce BBBD in larger areas (on the scale of a mouse brain) in deeper parts of the brain (f number of 1.25). We have used the system for diffusely growing tumors in the pontine region [43,44]. For these regions a larger volume needs to be sonoporated that encompasses the entire tumor region in the pons. The modular system can easily be adjusted for other types of brain tumors in more supratentorial parts of the brain. In order to decide on the transducer type one should hold into account the f-number,

focal length and frequency.

The overall design proposes thereby two refinements compared to previously suggested designs. (I) Frequently a water bath is used for ultrasound wave transmission of therapeutic systems. For transcranial applications in small animals this type of design reslts in larger and inverted setups, whereby the animal is partially submerged [11,22,25]. While these designs work generally very well in the scope of smaller animal studies, they are a compromise with respect to setup times, portability and realistically maintainable hygienic standards during usage. In particular the latter is of considerable importance in the scope studies encompassing immunocompromised animals and thus strict hygienic standards. As a consequence, in order to design a system with a more compact footprint, shorter setup time, easy decontamination possibilities and a natural position of the animal during the entire workflow, a “topdown” design was chosen. (II) The second design choice that differs from several previously described designs was to omit the direct integration of the acoustic delivery system into a medical imaging system such as anMRI or a micro-CT [15,17–19,45]. While fully integrated systems are ideal for longitudinal pharmacokinetic studies or explorative research on a limited number of animals, such setups are generally less suitable for high-volume pharmacological studies due to considerably increased complexity, high running-costs and need for trained/skilled operators. Furthermore, such systems are generally limited to only one imaging modality. As a consequence, the proposed design here relies on a modular detachable stereotactic platform, which is compatible with several imaging modalities (micro-CT, small animal MRI, a variety of BLI/fluorescence cameras, these with or without integrated X-ray imaging) and provides also multi-modality fiducial markers for automatic fusion of all image data in a common frame of reference for both interventional planning and the follow-up post BBB opening.

With respect to practical considerations, the most critical point of failure in the procedure is the stability of the microbubbles due to their limited lifetime and their fragile nature. We would like to emphasize that the following discussion concerns microbubbles stabilized by phospholipids and containing sulphur hexafluoride (SF6) as an innocuous gas [46,47], while other microbubble formulations will generally display different properties.

Timing before microbubble injection: The advertised lifespan of commercially available microbubbles after rehydration is between as 3 and 4 hours. While this is suitable for diagnostic ultrasound applications, it should be noted that during this entire period the microbubbles continuously lose gas and consequently the mean bubble diameter is subject to a continuous downward-drift from the initial average size of 2.5 µm. For therapeutic applications such as ultrasoundmediated BBBD this implies much stricter timing-imperatives, since the oscillation amplitude of stable cavitation (at a given frequency and pressure) and the onset-threshold of inertial cavitation are as a direct consequence also subject to a continuous drift. In our experience, we have observed that microbubbles are best used within 30 minutes after rehydration in order to obtain reproducible results, similar to previous reportings [48].

Timing after microbubble injection: In larger primates, commercially available SF6-phospholipid microbubbles display a blood-plasma elimination half-life of about 6 minutes

and more than 80% of the administered gas is exhaled via the lungs after only 11 minutes [48]. In small mammals such as mice and rats the blood-plasma elimination halflife of this type of microbubbles in vivo is with 90-120 seconds considerably shorter due to the higher heart rate [20]. As a consequence, the rapid dynamic of the microbubble concentration directly after bolus injection and the fast subsequent plasma elimination combined with the continuous gas volume loss of the bubbles imposes strict timing requirements on the sonication/injection protocol in order to obtain reproducible results within the short duration of 3-4 minutes post-injection. Longer procedures or more extensive volumes of BBBD require preferably a continuous administration of microbubbles. However, such an approach is complicated by the buoyancy of the bubbles in both the syringe and the feeding-system and also introduces a considerably increased dead volume by the required infusion tubing. In our experience the simpler solution of splitting the total injection volume into 2 to 3 smaller sub-doses provided a robust and reproducible results.

In addition, microbubbles are very pressure sensitive and high hydrostatic pressures during injection are therefore not recommended. Large needles (>19 G) are recommended for the transfer of microbubbles into a plastic tube or to draw up microbubbles with a syringe [49]. For i.v. injection in mice 26-30 G needles are recommended; since larger needles are more difficult to insert into the tail vein. The 26 G needle is recommended since the hydrostatic pressure is lower with this needle. However, in case of difficult venous access the 30 G needle is recommended.

The cranium of the mouse is an important attenuator of the pressure amplitude that significantly lowers the pressure amplitude at the focus. Attenuation is determined by the frequency of the transducer and the density of the medium the ultrasound wave propagates. Higher ultrasound frequencies and high tissue densities, like bone results in high attenuation. The pressure amplitude is partially absorbed by bone and some pressure amplitude is lost by reflection and scattering [50]. In our experiments we have determined in mouse cadavers that the attenuation at 1 MHz is 14.5 ± 1.3 dB/cm with an average skull thickness of 0.9 mm as shown before [21,50]. Cavitation monitoring is highly recommended since microbubbles reflect distinct acoustic emissions during stable cavitation and inertial cavitation. Wideband emission is a distinct acoustic emission for inertial cavitation [12]. Realtime monitoring makes it possible to detect inertial cavitation and lower the pressure amplitude accordingly to avoid tissue damage.

Previous reports described the influence of the type of anesthesia on the achieved BBB permeability [11,31]. For isoflurane based anesthesia, a vasodilation occurs shortly after anesthesia initiation, which is associated with a slight reduction of the cerebral blood flow. Furthermore, anesthesia over extended durations, in particular in absence of a temperature stabilization, leads to a reduced heart rate. Since both factors can potentially lead to a larger variance of the cerebral concentration of both microbubbles or coadministered drugs, a strict anesthesia protocol is advisable to achieve reproducible results [51]. Anesthesia with 1.5% v/v isoflurane in 2 L/min oxygen for 35 to 45 minutes was not problematic, as advised by Constantinides et al. [51]. In contrast to McDannold et al. who showed that this gas mixture in combination with the specific type of their microbubbles was problematic [52], we have not observed noteworthy problems with this type of microbubbles. Alternatively,

the animals can be anesthetized with a mix of ketamine/xylazine, which has no known vasoactive effects [53].

In summary, the imaging-guided BBB-opening technique described here has been used for high-volume preclinical drug evaluation studies that demonstrated the efficiency of the suggested workflow. The system could thereby be operated by non-technical personnel after a short training due to the high degree of automation. This in combination with the simplicity of the setup resulted in a high degree of standardization, which in turn ensures experimental reproducibility, reduced intra-group variability and thus allows to reduce the required sample size.

Acknowledgments

This project was funded by the KWF-STW (Drug Delivery by Sonoporation in Childhood Diffuse Intrinsic Pontine Glioma and High-grade Glioma). We thank Ilya Skachkov and Charles Mougenot for their input in the development of the system.

References

[1] Lipinski CA. Lead- and drug-like compounds: the rule-of-five revolution. Drug Discov Today Technol 2004;1:337–41. https://doi.org/10.1016/j.ddtec.2004.11.007.

[2] Pardridge WM. Blood-brain barrier delivery. Drug Discov Today 2007;12:54–61. https://doi.org/10.1016/j.drudis.2006.10.013.

[3] Alli S, Figueiredo CA, Golbourn B, Sabha N, Wu MY, Bondoc A, et al. Brainstem blood brain barrier disruption using focused ultrasound: A demonstration of feasibility and enhanced doxorubicin delivery. J Control Release 2018;281:29–41. https://doi.org/10.1016/j.jconrel.2018.05.005.

[4] Burgess A, Hynynen K. Noninvasive and targeted drug delivery to the brain using focused ultrasound. ACS Chem Neurosci 2013;4:519–26. https://doi.org/10.1021/cn300191b.

[5] Meng Y, Pople CB, Lea-Banks H, Abrahao A, Davidson B, Suppiah S, et al. Safety and efficacy of focused ultrasound induced blood-brain barrier opening, an integrative review of animal and human studies. J Control Release Off J Control Release Soc 2019;309:25–36. https://doi.org/10.1016/j.jconrel.2019.07.023.

[6] Darrow DP. Focused Ultrasound for Neuromodulation. Neurother J Am Soc Exp Neurother 2019;16:88–99. https://doi.org/10.1007/s13311-018-00691-3.

[7] Zhou Y-F. High intensity focused ultrasound in clinical tumor ablation. World J Clin Oncol 2011;2:8–27. https://doi.org/10.5306/wjco.v2.i1.8.

[8] O'Reilly MA, Hough O, Hynynen K. Blood-Brain Barrier Closure Time After Controlled Ultrasound-Induced Opening Is Independent of Opening Volume. J Ultrasound Med Off J Am Inst Ultrasound Med 2017;36:475–83. https://doi.org/10.7863/ultra.16.02005.

[9] Mainprize T, Lipsman N, Huang Y, Meng Y, Bethune A, Ironside S, et al. Blood-Brain Barrier Opening in Primary Brain Tumors with Non-invasive MR-Guided Focused Ultrasound: A Clinical Safety and Feasibility Study. Sci Rep 2019;9:321. https://doi.org/10.1038/s41598-018-36340-0.

[10] Dasgupta A, Liu M, Ojha T, Storm G, Kiessling F, Lammers T. Ultrasound-mediated drug delivery to the brain: principles, progress and prospects. Drug Discov Today Technol 2016;20:41–8. https://doi.org/10.1016/j.ddtec.2016.07.007.

[11] O'Reilly MA, Waspe AC, Chopra R, Hynynen K. MRI-guided disruption of the blood-brain barrier using transcranial focused ultrasound in a rat model. J Vis Exp 2012. https://doi.org/10.3791/3555.

[12] McDannold N, Vykhodtseva N, Hynynen K. Targeted disruption of the blood-brain barrier with focused ultrasound: association with cavitation activity. Phys Med Biol 2006;51:793–807. https://doi.org/10.1088/0031-9155/51/4/003.

[13] McDannold N, Vykhodtseva N, Hynynen K. Blood-brain barrier disruption induced by focused ultrasound and circulating preformed microbubbles appears to be characterized by the mechanical index. Ultrasound Med Biol 2008;34:834–40. https://doi.org/10.1016/j.ultrasmedbio.2007.10.016.

[14] Sun T, Zhang Y, Power C, Alexander PM, Sutton JT, Aryal M, et al. Closed-loop control of targeted ultrasound drug delivery across the blood-brain/tumor barriers in a rat glioma model. Proc Natl Acad Sci U S A 2017;114:E10281–90. https://doi.org/10.1073/pnas.1713328114.

[15] Lipsman N, Meng Y, Bethune AJ, Huang Y, Lam B, Masellis M, et al. Blood-brain barrier opening in Alzheimer's disease using MR-guided focused ultrasound. Nat Commun 2018;9:2336.

https://doi.org/10.1038/s41467-018-04529-6.

[16] Carpentier A, Canney M, Vignot A, Reina V, Beccaria K, Horodyckid C, et al. Clinical trial of blood-brain barrier disruption by pulsed ultrasound. Sci Transl Med 2016;8:343re2. https://doi.org/10.1126/scitranslmed.aaf6086.

[17] Chopra R, Curiel L, Staruch R, Morrison L, Hynynen K. An MRI-compatible system for focused ultrasound experiments in small animal models. Med Phys 2009;36:1867–74. https://doi.org/10.1118/1.3115680.

[18] Kinoshita M, McDannold N, Jolesz FA, Hynynen K. Targeted delivery of antibodies through the blood-brain barrier by MRI-guided focused ultrasound. Biochem Biophys Res Commun 2006;340:1085–90. https://doi.org/10.1016/j.bbrc.2005.12.112.

[19] Larrat B, Pernot M, Aubry J-F, Dervishi E, Sinkus R, Seilhean D, et al. MR-guided transcranial brain HIFU in small animal models. Phys Med Biol 2010;55:365–88. https://doi.org/10.1088/0031-9155/55/2/003.

[20] Contag CH, Jenkins D, Contag PR, Negrin RS. Use of reporter genes for optical measurements of neoplastic disease in vivo. Neoplasia 2000;2:41–52. https://doi.org/10.1038/sj.neo.7900079.

[21] Choi JJ, Pernot M, Small SA, Konofagou EE. Noninvasive, transcranial and localized opening of the blood-brain barrier using focused ultrasound in mice. Ultrasound Med Biol 2007;33:95–104. https://doi.org/10.1016/j.ultrasmedbio.2006.07.018.

[22] Bing C, Ladouceur-Wodzak M, Wanner CR, Shelton JM, Richardson JA, Chopra R. Transcranial opening of the blood-brain barrier in targeted regions using a stereotaxic brain atlas and focused ultrasound energy. J Ther Ultrasound 2014;2:13. https://doi.org/10.1186/2050-5736-2-13.

[23] Marquet F, Teichert T, Wu S-Y, Tung Y-S, Downs M, Wang S, et al. Real-time, transcranial monitoring of safe blood-brain barrier opening in non-human primates. PLoS One 2014;9:e84310. https://doi.org/10.1371/journal.pone.0084310.

[24] Anastasiadis P, Mohammadabadi A, Fishman MJ, Smith JA, Nguyen BA, Hersh DS, et al. Design, characterization and evaluation of a laser-guided focused ultrasound system for preclinical investigations. Biomed Eng Online 2019;18:36. https://doi.org/10.1186/s12938-019-0656-z.

[25] Liu H-L, Pan C-H, Ting C-Y, Hsiao M-J. Opening of the blood-brain barrier by low-frequency (28-kHz) ultrasound: a novel pinhole-assisted mechanical scanning device. Ultrasound Med Biol 2010;36:325–35. https://doi.org/10.1016/j.ultrasmedbio.2009.10.004.

[26] Zhu L, Cheng G, Ye D, Nazeri A, Yue Y, Liu W, et al. Focused Ultrasound-enabled Brain Tumor Liquid Biopsy. Sci Rep 2018;8:6553. https://doi.org/10.1038/s41598-018-24516-7.

[27] Bader KB, Holland CK. Gauging the likelihood of stable cavitation from ultrasound contrast agents. Phys Med Biol 2013;58:127–44. https://doi.org/10.1088/0031-9155/58/1/127.

[28] Neppiras EA. Acoustic cavitation series: part one: Acoustic cavitation: an introduction. Ultrasonics 1984;22:25–8. https://doi.org/https://doi.org/10.1016/0041-624X(84)90057-X.

[29] Aryal M, Arvanitis CD, Alexander PM, McDannold N. Ultrasound-mediated blood-brain barrier disruption for targeted drug delivery in the central nervous system. Adv Drug Deliv Rev 2014;72:94–109. https://doi.org/10.1016/j.addr.2014.01.008.

[30] Tung Y-S, Choi JJ, Baseri B, Konofagou EE. Identifying the inertial cavitation threshold and skull effects in a vessel phantom using focused ultrasound and microbubbles. Ultrasound Med Biol 2010;36:840–52. https://doi.org/10.1016/j.ultrasmedbio.2010.02.009.

[31] Arvanitis CD, Livingstone MS, Vykhodtseva N, McDannold N. Controlled ultrasound-induced blood-brain barrier disruption using passive acoustic emissions monitoring. PLoS One 2012;7:e45783. https://doi.org/10.1371/journal.pone.0045783.

[32] Tsai C-H, Zhang J-W, Liao Y-Y, Liu H-L. Real-time monitoring of focused ultrasound blood-brain barrier opening via subharmonic acoustic emission detection: implementation of confocal dual-frequency piezoelectric transducers. Phys Med Biol 2016;61:2926–46. https://doi.org/10.1088/0031-9155/61/7/2926.

[33] Chen W-S, Brayman AA, Matula TJ, Crum LA. Inertial cavitation dose and hemolysis produced in vitro with or without Optison. Ultrasound Med Biol 2003;29:725–37. https://doi.org/10.1016/s0301-5629(03)00013-9.

[34] Qiu Y, Luo Y, Zhang Y, Cui W, Zhang D, Wu J, et al. The correlation between acoustic cavitation and sonoporation involved in ultrasound-mediated DNA transfection with polyethylenimine (PEI) in vitro. J Control Release Off J Control Release Soc 2010;145:40–8. https://doi.org/10.1016/j.jconrel.2010.04.010.

[35] Sun T, Jia N, Zhang D, Xu D. Ambient pressure dependence of the ultra-harmonic response from contrast microbubbles. J Acoust Soc Am 2012;131:4358–64. https://doi.org/10.1121/1.4707512.

[36] Rehemtulla A, Stegman LD, Cardozo SJ, Gupta S, Hall DE, Contag CH, et al. Rapid and quantitative assessment of cancer treatment response using in vivo bioluminescence imaging. Neoplasia 2000;2:491–5. https://doi.org/10.1038/sj.neo.7900121.

[37] Puaux A-L, Ong LC, Jin Y, Teh I, Hong M, Chow PKH, et al. A comparison of imaging techniques to monitor tumor growth and cancer progression in living animals. Int J Mol Imaging 2011;2011:321538. https://doi.org/10.1155/2011/321538.

[38] Wu S-K, Chu P-C, Chai W-Y, Kang S-T, Tsai C-H, Fan C-H, et al. Characterization of Different Microbubbles in Assisting Focused Ultrasound-Induced Blood-Brain Barrier Opening. Sci Rep 2017;7:46689. https://doi.org/10.1038/srep46689.

[39] van den Broek MPH, Groenendaal F, Egberts ACG, Rademaker CMA. Effects of hypothermia on pharmacokinetics and pharmacodynamics: a systematic review of preclinical and clinical studies. Clin Pharmacokinet 2010;49:277–94. https://doi.org/10.2165/11319360-000000000-00000.

[40] Paxinos, G., Franklin KB. Paxinos and Franklin's the mouse brain in stereotaxic coordinates. Academic press; 2019.

[41] Saunders NR, Dziegielewska KM, Møllgård K, Habgood MD. Markers for blood-brain barrier integrity: how appropriate is Evans blue in the twenty-first century and what are the alternatives? Front Neurosci 2015;9:385. https://doi.org/10.3389/fnins.2015.00385.

[42] Yao L, Xue X, Yu P, Ni Y, Chen F. Evans Blue Dye: A Revisit of Its Applications in Biomedicine. Contrast Media Mol Imaging 2018;2018:7628037. https://doi.org/10.1155/2018/7628037.

[43] Caretti V, Zondervan I, Meijer DH, Idema S, Vos W, Hamans B, et al. Monitoring of tumor growth and post-irradiation recurrence in a diffuse intrinsic pontine glioma mouse model. Brain Pathol 2011;21:441–51. https://doi.org/10.1111/j.1750-3639.2010.00468.x.

[44] Yoshimura J, Onda K, Tanaka R, Takahashi H. Clinicopathological study of diffuse type brainstem gliomas: analysis of 40 autopsy cases. Neurol Med Chir (Tokyo) 2003;43:375–82; discussion 382. https://doi.org/10.2176/nmc.43.375.

[45] Yang F-Y, Wang H-E, Lin G-L, Teng M-C, Lin H-H, Wong T-T, et al. Micro-SPECT/CT-based pharmacokinetic analysis of 99mTc-diethylenetriaminepentaacetic acid in rats with blood-brain

barrier disruption induced by focused ultrasound. J Nucl Med 2011;52:478–84. https://doi.org/10.2967/jnumed.110.083071.

[46] Sirsi S, Borden M. Microbubble Compositions, Properties and Biomedical Applications. Bubble Sci Eng Technol 2009;1:3–17. https://doi.org/10.1179/175889709X446507.

[47] Greis C. Technology overview: SonoVue (Bracco, Milan). Eur Radiol 2004;14 Suppl 8:P11-5.

[48] Schneider M. Characteristics of SonoVuetrade mark. Echocardiography 1999;16:743–6. https://doi.org/10.1111/j.1540-8175.1999.tb00144.x.

[49] Talu E, Powell RL, Longo ML, Dayton PA. Needle size and injection rate impact microbubble contrast agent population. Ultrasound Med Biol 2008;34:1182–5. https://doi.org/10.1016/j.ultrasmedbio.2007.12.018.

[50] Pinton G, Aubry J-F, Bossy E, Muller M, Pernot M, Tanter M. Attenuation, scattering, and absorption of ultrasound in the skull bone. Med Phys 2012;39:299–307. https://doi.org/10.1118/1.3668316.

[51] Constantinides C, Mean R, Janssen BJ. Effects of isoflurane anesthesia on the cardiovascular function of the C57BL/6 mouse. ILAR J 2011;52:e21-31.

[52] McDannold N, Zhang Y, Vykhodtseva N. The Effects of Oxygen on Ultrasound-Induced Blood-Brain Barrier Disruption in Mice. Ultrasound Med Biol 2017;43:469–75. https://doi.org/10.1016/j.ultrasmedbio.2016.09.019.

[53] McDannold N, Zhang Y, Vykhodtseva N. Blood-brain barrier disruption and vascular damage induced by ultrasound bursts combined with microbubbles can be influenced by choice of anesthesia protocol. Ultrasound Med Biol 2011;37:1259–70. https://doi.org/10.1016/j.ultrasmedbio.2011.04.019.

Materials

Name	Company	Catalog Number	Comments
1 mL luer-lock syringe	Becton Dickinson	309628	Plastipak
19 G needle	Terumo Agani	8AN1938R1	
23 G needle	Terumo Agani	8AN2316R1	
3M Transpore surgical tape	Science applied to life	7000032707	or similar
Arbitrary waveform generator	Siglent	n.a.	SDG1025, 25 MHz, 125 Msa/s
Automated stereotact	in-house built	n.a.	Stereotact with all elements were inhouse built
Bruker In-Vivo Xtreme	Bruker	n.a.	Includes software
Buffered NaCl solution	B. Braun Melsungen AG	220/12257974/110	
Buprenorphine hydrochloride	Indivior UK limitd	n.a.	0.324 mg
Cage enrichment: paper-pulp smart home	Bio services	n.a.	
Carbon filter	Bickford	NC0111395	Omnicon f/air
Ceramic spoon	n.a.	n.a.	
Cotton swabs	n.a.	n.a.	
D-luciferin, potassium salt	Gold Biotechnology	LUCK-1	
Ethanol	VUmc pharmacy	n.a.	70%
Evans Blue	Sigma Aldrich	E2129	
Fresenius NaCl 0.9%	Fresenius Kabi	n.a.	NaCl 0.9 %, 1000 mL
Histoacryl	Braun Surgical	n.a.	Histoacryl 0.5 mL
Hydrophone	Precision Acoustics	n.a.	
Insulin syringe	Becton Dickinson	324825/324826	0.5 mL and 0.3 mL
Isoflurane	TEVA Pharmachemie BV	8711218013196	250 mL
Ketamine	Alfasan	n.a.	10 %, 10 mL
Mouse food: Teklad global 18% protein rodent diet	Envigo	2918-11416M	
Neoflon catheter	Becton Dickinson	391349	26 GA 0.6 x 19 mm
Oscilloscope	Keysight technologies	n.a.	InfiniiVision DSOX024A
Plastic tubes	Greiner bio-one	210261	50 mL
Power amplifier	Electronics & Innovation Ltd	210L	Model 210L
Preamplifier DC Coupler	Precision Acoustics	n.a.	Serial number: DCPS94
Scissors	Sigma Aldrich	S3146-1EA	or similar
Sedazine	AST Farma	n.a.	2%
SonoVue microbubbles	Bracco	n.a.	8 µl/ml
Sterile water	Fresenius Kabi	n.a.	1000 mL
Syringe	n.a.	n.a.	various syringes can be used
Temgesic	Indivior UK limitd	n.a.	0.3 mg/ml
Transducer	Precision Acoustics	n.a.	1 MHz
Tweezers	Sigma Aldrich	F4142-1EA	or similar
Ultrasound gel	Parker Laboratories Inc.	01-02	Aquasonic 100
Vidisic gel	Bausch + Lomb	n.a.	10 g

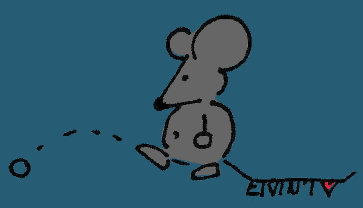

Chapter 4

Towards standardisation of a diffuse midline glioma patient-derived xenograft mouse model based on suspension matrices for preclinical research

Elvin 't Hart[1], John Bianco[1], Helena Besse[2], Lois Chin Joe Kie[1], Lesley Cornet[1], Kimberly Eikelenboom[1], Thijs van den Broek[1], Marc Derieppe[1], Yan Su[1], Eelco Hoving[1], Mario Ries[2,#], Dannis van Vuurden[1,#]

1. Princess Máxima Center for Pediatric Oncology, Heidelberglaan 25, 3584 CS, Utrecht, the Netherlands

2. Center for Imaging Sciences, University Medical Center Utrecht, Heidelberglaan 100, 3584 CX Utrecht, the Netherlands

Published in: Biomedicines; February 2023; 11;11(2):527; doi: 10.3390/biomedicines11020527

Abstract

Diffuse midline glioma (DMG) is an aggressive brain tumour with high mortality and limited clinical therapeutic options. Although in vitro research has shown effectiveness of medication, successful translation to the clinic remains elusive. A literature search highlighted the high variability and lack of standardisation in protocols applied for establishing the commonly used HSJD-DIPG-007 patient-derived xenograft (PDX) model, based on animal host, injection location, number of cells inoculated, volume, and suspension matrices. This study evaluated the HSJD-DIPG-007 PDX model with respect to its ability to mimic human disease progression for therapeutic testing in vivo. Mice received intracranial injections of HSJD-DIPG-007 cells suspended in either PBS or Matrigel. Survival, tumour growth and metastases were assessed to evaluate differences in suspension matrix used. After cell implantation no severe side effects were observed. Additionally, no differences were detected in terms of survival or tumour growth between the two suspension groups. We observed delayed metastases in the Matrigel group, with a significant difference compared to mice with PBS suspended cells. In conclusion, using Matrigel as suspension matrix is a reliable method for establishing a DMG PDX mouse model, with delayed metastases formation and is a step forward to obtaining a standardised in vivo PDX model.

Graphical abstract

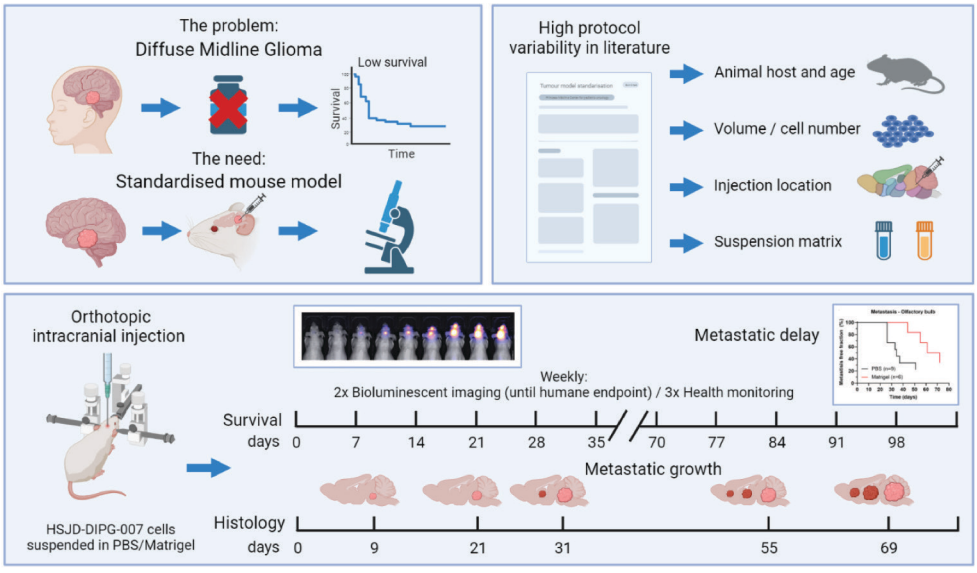

Keywords

HSJD-DIPG-007, Diffuse Midline Glioma, PDX model, Matrigel, Metastases

Introduction

Paediatric high-grade gliomas (pHGG) are malignant brain tumours found in the hemispheres and midline structures of the brain and account for 10% of all central nervous system (CNS) tumours in children, while being responsible for 40% of all fatal cases. Diffuse intrinsic pontine glioma (DIPG) is a particularly aggressive and invasive pHGG subtype arising in the brainstem (pons) and has been recognised as a distinct type within the paediatric diffuse high-grade glioma family in the 5th edition of the WHO Classification of Tumours of the Central Nervous System [1], and as such these tumours have been reclassified to 'diffuse midline glioma, H3K27-altered' (DMG). Alterations in H3K27 in DMG include point mutations at the histone H3K27M, predominantly with H3.3 expression and to a lesser degree H3.1 with up to 80% of tumours harbouring one of these mutations [2]. H3.3 mutations cause trimethylation loss of the chromatin with altered manifestation of oncogenes and tumour suppressor genes [3]. Loss of H3K27 trimethylation by overexpression of EZHIP has been observed in H3K27 wildtype DMG [4]. In addition, DMGs are also commonly associated with mutations in the TP53 gene (up to 60%), and to a lesser extent mutations in PPM1D (up to 30%) [5]. Combined, these mutations increase the aggressiveness of DMGs, and are associated with a poor overall prognosis. Genomic analyses have revealed that DMGs are molecularly complex, also harbouring mutations in ACVR1, ATRX, H3F3A, HIST1H3B/c, MYC, PDGFRA, PIK3CA, PTEN and RB1 that can cooperate with mutated TP53 and PPM1D to promote tumour formation [2,6–9]. In addition to pontine localization, DMGs can occur in other midline structures, such as the thalamus and spinal cord.

Pontine DMGs are mainly diagnosed in children between 6-9 years of age. Rapid progression of this disease results in a median survival of 11 months and a 95% fatality rate within 2 years after diagnosis [10,11]. DMG is commonly found in the brainstem, a delicate brain region responsible for the execution of vital functions [1,12]. Clinical symptoms are caused by pressure of the tumour and dysfunction of the brainstem, resulting in cranial nerve deficits such as facial and abducens nerve palsy, multiple cranial neuropathies, long tract, and cerebellar signs such as paresis and ataxia [13]. Because of the deli-cate location and invasive nature of DMG, radical surgery is impossible while chemotherapy is complicated by the presence of the blood-brain barrier (BBB), preventing 98% and 100% of small and large molecules to enter the brain [14,15]. While tumour progression can cause BBB disruption and subsequently increased BBB-permeability, most of the BBB in DMG remains intact over the course of the disease. Even when BBB disruption is observed, this occurs mostly at the core of the tumour lesion after onset of local tissue necrosis [16]. Therefore, the current standard of care of DMG is fractionated radiotherapy of 1.8-2Gy daily cumulating to a total dose of 54-60Gy, with concurrent temozolomide causing temporal tumour growth delay, but also inevitable recurrence [17]. Metastasis along the neuroaxis is rarely seen at diagnosis (2%) but can increase to up to 17.3% at disease progression [10,18], where an under-recognised pattern of subventricular spread was observed in the majority of investigated cases, with infiltration of the subventricular zone as well as tumour nodules in the frontal horns of the lateral ventricles [19].

Although intensive research has been conducted for the treatment of DMG, little clinical

progress has been made to date [20]. Even though in vitro drug screening has evidenced several promising chemotherapeutic candidates for DMG treatment, the successful translation to preclinical in vivo studies has demonstrated to be challenging [20–25]. Additionally, therapeutic translational complexity is added due to the biological differences between patients and animal models of the disease [26]. Although small animals do not develop DMG spontaneously, in vivo studies are made possible by establishing genetically engineered mouse models (GEMM) or patient-derived xenografts (PDX) [27]. GEMM models have an altered genomic profile to mimic the human disease allowing genet-ic/fundamental research to be conducted, while PDX models use orthotopic injection of human primary DMG cells in (partially) immune deficient animals. The role of these models in preclinical research is to facilitate recapitulation of human malignancies and the associated disease progression, allowing validation of therapeutic agents or interventional techniques before clinical trials [28,29].

HSJD-DIPG-007 is an established DMG cell line from the Sant Joan de Déu Hospital in Barcelona, derived from the autopsy of a radiotherapy-naive, 6-year-old male that died one month after diagnosis and received one course of chemotherapy (cisplatin and irinotecan). These HSJD-DIPG-007 tumour cells harbour mutations in H3F3A K27M, ACVR1 R206H, PPM1Dp.P428fs and PIK3CAp.H1047R [5,30]. In recent years, HSJD-DIPG-007 has increasingly been used as a cell line for DMG PDX mouse models [31]. This model displays an intact BBB as well as an invasive growth pattern that mimics human pathology for a large part of disease progression, rendering it appealing for evaluating therapeutic response and efficiency [32]. However, a standardised method in establishing ortho-topic in vivo models using HSJD-DIPG-007 cells has not yet been developed. Current protocols using this cell type vary between studies on several levels, such as use of cell sus-pension matrix, site of implantation and volume/number of tumour cells inoculated. A lack of a standardised approach also complicates comparison while potentiating different experimental outcomes. Finally, the development time and extent of diffuse, infiltrative growth and metastasis make these models difficult to compare to human disease progression. Since metastases at diagnosis is a relatively rare occurrence in DMG patients, optimising the cell implantation procedure in a standardised manner could better mimic tumour growth progression in vivo, with greater correlation with human disease progression.

We postulated that using Matrigel instead of phosphate buffered saline (PBS) as a cell suspension matrix for tumour cell inoculation in preclinical models would prevent premature cell dissemination. Local confinement of the tumour is particularly relevant for locoregional treatment paradigms such as convection-enhanced and focused ultra-sound-mediated drug delivery to the brainstem in preclinical research. The aim of this study is to provide a literature overview of the HSJD-DIPG-007 DMG PDX model, to ex-tract common features and to investigate the impact of dissimilarities. For the later, the presented work focuses on the comparison of the extent of infiltrative and metastatic growth patterns of the model with cells inoculated with either PBS or Matrigel as suspension substrate in athymic nude mice, and the relevance of the time delay between inoculation and onset of therapy.

Materials and methods

Literature search

A literature search was performed to identify publications using the HSJD-DIPG-007 cell line to create an overview of preclinical DMG tumour models using this cell line without any exclusion criteria. Upon study inclusion, data was classified based on (1) animal host and age, (2) location of injection, (3) injected volume and cell concentration, (4) cells suspension matrix and (5) treatment and follow-up. The age of the mice is categorised based on their postnatal (≤3 weeks), adolescent (3-9 weeks) and adult (>9 weeks) phase [33].

Animals

All experiments were conducted on 6–8-week-old male athymic nude Foxn1-/- mice (Code 069, Envigo, Netherlands) in accordance with guidelines of the Dutch ethical committee and the Animal Welfare Body of Utrecht University (AVD3990020209445). A total of 34 mice were used for the study, consisting of 15 for DMG PDX tumour growth and survival validation, and 19 that were sacrificed at designated timepoints for histological analysis. Mice were housed under specific pathogen-free conditions in separately ventilated cages, at up to four animals/cage, and allowed to acclimatise for 2 weeks before experimental procedures. Mice were kept on regular laboratory food and water ad libitum, with a fixed 12-hour (h) light/dark cycle in accordance with ARRIVE guidelines [2]. Measurable outcomes in PDX models of DMG are not influenced by gender, and as such gender dimension was not relevant for this study [34]. A detailed description of housing conditions of animals is available as Supplementary Material.

Cells

HSJD-DIPG-007 cells were grown and maintained in 1:1 Neurobasal-A and Advanced DMEM/F-12 medium containing 10mM HEPES buffer, 1x MEM non-essential amino acids, 1% GlutaMAX, 1mM Sodium pyruvate, 1x B-27 minus vitamin-A (ThermoFisher, USA), 10ng/ml PDGF-AA, 10ng/ml PDGF-BB, 20ng/ml bFGF, 20ng/ml EGF (Peprotech, UK), 2µg/ml heparin (Leo Pharmaceuticals, Netherlands) and 1mg/ml primocin (InvivoGen, USA). Medium was refreshed every 3-4 days. Single cell suspensions were obtained using Accutase (ThermoFisher). Cells were cultured at 37°C, 5% CO2 and 95% humidity. For in vivo tumour growth monitoring by bioluminescence imaging (BLI), HSJD-DIPG-007 cells were transduced to express firefly luciferase as previously described [35]. Following infection, eGFP-lucF gene positive HSJD-DIPG-007 cells were selected using a Sony SH800 Cell Sorter (Sony, Japan). Before cell implantation, HSJD-DIPG-007 cells were suspended in 1X PBS (pH 7.4) or Matrigel (50% v/v, in PBS, Corning, USA) and kept on ice until used.

Drugs

Pre- and post-surgical analgesia was managed with 67µg/ml carprofen (Faculty of Veterinary Medicine pharmacy, Netherlands) per os (p.o.) in drinking water with an additional sub-cutaneous (s.c.) injection of 5mg/kg before surgery. Further pain suppression

was performed by s.c. injection of 0.5% lidocaine (B. Braun, Germany) during surgery. Anaesthesia was maintained with isoflurane mixed with air (3% induction, 1.8% maintenance, Zoetis, Netherlands). BLI signal of engrafted cells was monitored by intra-peritoneal (i.p.) injection of 150mg/kg D-luciferin (Cayman Chemical, Netherlands) in PBS. Euthanasia was performed via i.p. injection of a mix of 7.14mg/ml ketamine (Alfasan, Netherlands) and 0.714mg/ml sedazine (AST Farma, Netherlands) in PBS.

Tumour cell implantation

Twenty-four hours before and after orthotopic intracranial injection with eGFP-lucF-gene positive HSJD-DIPG-007 cells, mice received carprofen p.o. in drinking water. Thirty minutes before surgery carprofen was administrated s.c. for local pain management. After anaesthesia with isoflurane, mice were fixed on a stereotactic frame with bite and ear bars. Eye cream was applied to prevent eye damage, while the mice were kept warm during the procedure. After incision of the skin, a drop of lidocaine was added before removal of the facia on the skull. Using a high-speed drill, a burr hole was made in the skull 0.8mm posterior and 1.0mm lateral to the lambda. At a depth of 4.5mm in the pontine region, a total of 5x105 HSJD-DIPG-007 cells suspended in 4.3µl of PBS or Matrigel were injected at a rate of 2µl/min using a 5µl Hamilton syringe fitted with a 26-gauge needle. After injection, the needle remained in place for 7min before being slowly retracted to prevent cell accumulation in the needle tract. Wound closure was performed by applying topical skin adhesive (Histoacryl, B. Brand, Germany) before placing the mice under a heating lamp until awake. Possible signs of stress and post-operative complications (lack of food/water intake, anti-social behaviour, motor deficits) were carefully monitored.

Tumour growth assessment with bioluminescence

Mice were weighed three times a week while their tumour growth was monitored twice a week by measuring the BLI signal of engrafted eGFP-lucF-gene positive HSJD-DIPG-007 cells using the MILABS U-OI camera (Houten, Netherlands). For signal measurement, mice were anaesthetised with isoflurane and injected 5 minutes later with D-luciferin before positioning in the camera. BLI images were taken under anaesthesia from 5 to 30 min after D-luciferin injection with a 60 second exposure. Signal intensity was quantified within the region of interest (ROI) of the whole animals' head by using ImageJ software [36]. Mice were sacrificed with ketamine/sedazine after reaching their scientific or humane endpoints. Humane endpoints were defined based on 20% weight loss from cell implantation, 15% weight loss within two days, or development of neuro-logical deficiencies such as circling, hyperexcitability, convulsions, or ataxia.

Histological analysis

Histopathological elements, tumour size, location and proliferation were determined by human vimentin and haematoxylin and eosin (H&E) staining. After euthanasia, mice were transcranial perfused with PBS followed by 10% formalin, after which the brain was excised and post-fixed in 10% formalin for 48h before paraffin embedding. Sagittal sections of 4µm were made using a microtome (Leica Biosystems) and mounted on Superfrost® Plus microscope slides. Before staining, sections were deparaffinized and subjected to antigen

retrieval with sodium citrate buffer (10mM, pH6, 95-100°C, 30min). Endogenous peroxidase activity was reduced by incubation in 3% hydrogen peroxidase for 20min, after which sections were washed twice with deionized water and once with 1X Tris-buffered saline containing 0.1% Tween (TBST). Sections were blocked for 1h at room temperature with antibody diluent clear (VWRKBD09-125, VWR, USA) before overnight incubation at 4oC with rabbit anti-human vimentin [SP20] (1:5 – 1:8, ab27608, Abcam, UK) followed by washing with TBST. Sections were then incubated for 2h at room temperature with biotinylated affinity-purified goat anti-rabbit secondary antibody (1:500, BA-1000, IgG (H+L), Vector Laboratories, USA) before washing with TBST. VECTASTAIN® Elite ABC-HRP Peroxidase (PK-6100, Vector Laboratories) was applied for 1h at room temperature followed by a 3 – 4 min incubation in 3,3'-diaminobenzidine (DAB, K346711-2, Agilent Dako, Netherlands) before counterstaining with haematoxylin (Epredia, Nether-lands).

Data and statistical analysis

Weight and tumour growth measured by BLI signal was analysed using an independent t-test. Survival was analysed using a Kaplan-Meier plot and Log-rank test. Metastases formation in olfactory bulb and spinal cord were analysed by a non-parametric Kolmogorov-Smirnov test to compare cumulative distributions. A p-value of ≤0.05 was considered statistically significant. Statistical analyses were performed using GraphPad Prism (v9, GraphPad Software, LLC, USA). Photographic and electronic images were obtained on a Leica DMi8 and processed using Adobe Photoshop 21 (Adobe Inc, USA).

Results

HSJD-DIPG-007 PDX model in literature

A total of 20 articles have been published between 2016 and 2022 using the HSJD-DIPG-007 cell line for establishing a DMG PDX mouse model [5,25,31,32,37–52]. An overview of these studies is given in Table 1. For the orthotopic generation of DMG, 65% of the studies described injection in the pontine/brainstem region, 20% in the 4th ventricle, and 15% in a combination of both 4th ventricle/pons. In 75% of the studies adolescent mice were used for establishing the tumour model, 15% used early postnatal mice, and 10% did not define the age. Athymic nude, nude BALB/c, NOD-SCID and NOD-SCID gamma (NSG) nude mice were used as host animals in 30%, 20%, 30% and 15% of the cases respectively, with one study (representing 5%) using an athymic nude rat. Injection volume ranged between 1µl and 5µl, with 45% of the cases injecting 5x105 HSJD-DIPG-007 cells. Only one study used 7.5x105 cells suspended in 7.5µl for establishing the PDX model using athymic nude rat as host. PBS, Matrigel or medium were used as suspension matrices in 20%, 40% and 10% of the studies reported, respectively. In 20% of the studies an undefined suspension matrix was used, while the remaining 10% used combinations or other matrices. Treatment application ranged from day 0 up to day 80 after cell inoculation. Despite the high variety of treatments performed in these studies, prolonged survival or delayed tumour growth was observed in 82% of cases reporting treatment outcomes.

Table 1: Summary of studies using HSJD-DIPG-007 for establishing a DMG PDX model from 2016 to 2022

Animal Host	Age (weeks)	Location	Total cells inoculated	Volume	Suspension matrix	Days before treatment	Treatment Strategy	Treatment efficiency	Reference
Athymic nude	n.d.	Brainstem	5×10^5	n.d.	n.d.	21	RG7388	Enhanced survival	[5]
NOD-SCID	7	Pons	$3x10^5$	2 µl	Matrigel	28	Panobinostat	No	[25]
NOD-SCID	5	Pons	2×10^5	5 µl	Matrigel	None	None	Not assessed	[31]
Athymic nude	6	Pons	5×10^5	5 µl	PBS	37	Doxorubicin & FUS	No	[32]
Athymic nude	n.d.	Pons	5×10^5	5 µl	n.d.	14	BGB324, Panobinostat & CED	Enhanced survival combined with CED	[47]
NOD-SCID	6–8	4th Ventricle	5×10^5	4 µl	Matrigel	28	OKN-007 and LDN-193189	Reduced cellular activity	[48]
NOD-SCID gamma (NSG)	8-10	Pons	4×10^5	2 µl	Medium:Matrigel (1:1)	21	2-DG & IDH1 inhibitor	Enhanced survival & decreased growth	[49]
Athymic nude rat	4	4th Ventricle	$7{,}5\times10^5$	7.5 µl	n.d.	28	SN-38	Not assessed	[50]
Nude BALB/c	8	4th Ventricle/Pons	2×10^5	3 µl	n.d.	21	DCA, Metformin & RT	Enhanced survival combined with RT	[51]
NOD-SCID	7-8	4th Ventricle/Pons	2×10^5	2 µl	Matrigel	28	CBL0137 & Panobinostat	Enhanced survival in combination	[52]
Nude BALB/c	6	Pons	1×10^4	1 µl	HBSS	21	CRAd.S.pK7	Enhanced survival	[37]
NOD-SCID gamma (NSG)	5-7	Pons	1×10^5	2 µl	Serum free media	80	ALDH+/- & GDC-0084	Enhanced survival	[38]
Nude BALB/c	5-7	Brainstem	2×10^5	2 µl	Matrigel	30	DMFO & AMXT	Enhanced survival & decreased growth	[39]
Athymic nude	3	4th Ventricle	5×10^5	5 µl	Matrigel	25	Vandetanib & Everolimus	Enhanced survival in combination	[40]
Athymic nude	7-9	Striatum/Pons	$5x10^5$	5 µl	PBS	75	Bevacizumab	Not assessed	[41]
Athymic nude	6–8	Pons	5×10^5	5 µl	PBS	7-8	Doxorubicin & CED	No	[42]
NOD-SCID	4-5	4th Ventricle	5×10^5	2 µl	PBS	0	HSV1716	Reduced cellular growth	[43]
Nude BALB/c	5–6	4th Ventricle/Pons	2×10^5	2 µl	Matrigel	28-35	Temozolomide & RT	RT enhance survival	[44]
NOD-SCID gamma (NSG)	0-2 days	Brainstem	$1x10^3$	n.d.	Tumour stem medium	0	GSK2830371	Enhanced survival	[45]
NOD-SCID	3	Pons	5×10^5	5 µl	Matrigel	21–28	LDN-193189 & LDN-214117	Enhanced survival	[46]

n.d.: not defined.

Well-being and weight profiles upon implantation procedure

Orthotopic injections of HSJD-DIPG-007 cells suspended in PBS (n=9) or Matrigel (n=6) did not give rise to deleterious neurological complications following implantation. Time frame of the surgery and anaesthesia affected the wakefulness of the mice after-wards, where extended procedures resulted in lengthier recovery times until the mice were fully active and mobile (observation), even though mouse core temperature was monitored and maintained throughout the procedure. Following cell implantation, mice initially lost weight, but gained on average 16% of their initial weight by day 37 for PBS and 15% by day 30 for Matrigel injected mice. No significant differences in overall weight gain or loss were measured between the PBS and Matrigel group (Figure 1). An early and aggressive tumour onset can explain the severe weight loss in one PBS mouse (Supplementary Figure 1).

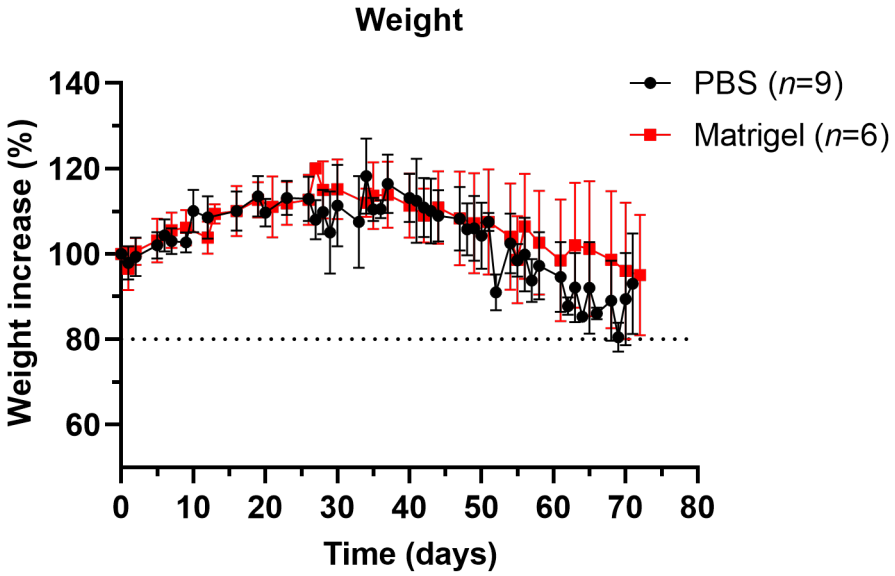

Figure 1. Weight profiles of mice inoculated with HSJD-DIPG-007 cells suspended either in PBS or Matrigel. Changes in weight after intracranial implantation of HSJD-DIPG-007 cells suspended in either PBS or Matrigel were monitored. Weight increased consistently up to day 37 for PBS and day 30 for Matrigel groups, after which weight loss set-in, lasting until terminal endpoint. No significant differences between PBS or Matrigel groups were observed. Dotted line represents the weight threshold of the humane endpoint. Data points are expressed as mean weight ± SD.

Survival and tumour growth using PBS or Matrigel as suspension matrices

Despite different suspension matrices being used, no significant differences in survival between PBS and Matrigel groups were observed. Mice with PBS or Matrigel survived up to 90 and 100 days, and with a median overall survival of 70 and 75 days respectively (Figure 2A). PBS mice were sacrificed in 2/9 cases based on neurological symptoms of motor functions like tremors and paralysis, 6/9 based on weight loss, and 1/9 for both conditions. Matrigel mice were sacrificed in 2/6 cases based on neurological symptoms, 3/6 based on

weight loss, and in 1/6 case, the animal passed away during BLI. BLI signal confirmed successful cell implantation in all animals of both treatment groups. Steady exponential tumour growth was observed up to day 30 post implantation, after which the growth increase exceeded around day 40 1.8 AU/day for both (Figure 2B, C and Supplementary Figure 2). The increased exponential growth could be indicative of locoregional metastasis formation with tumour spreading outside the injection location of the pons. No significant differences in tumour growth were observed between the PBS and Matrigel groups.

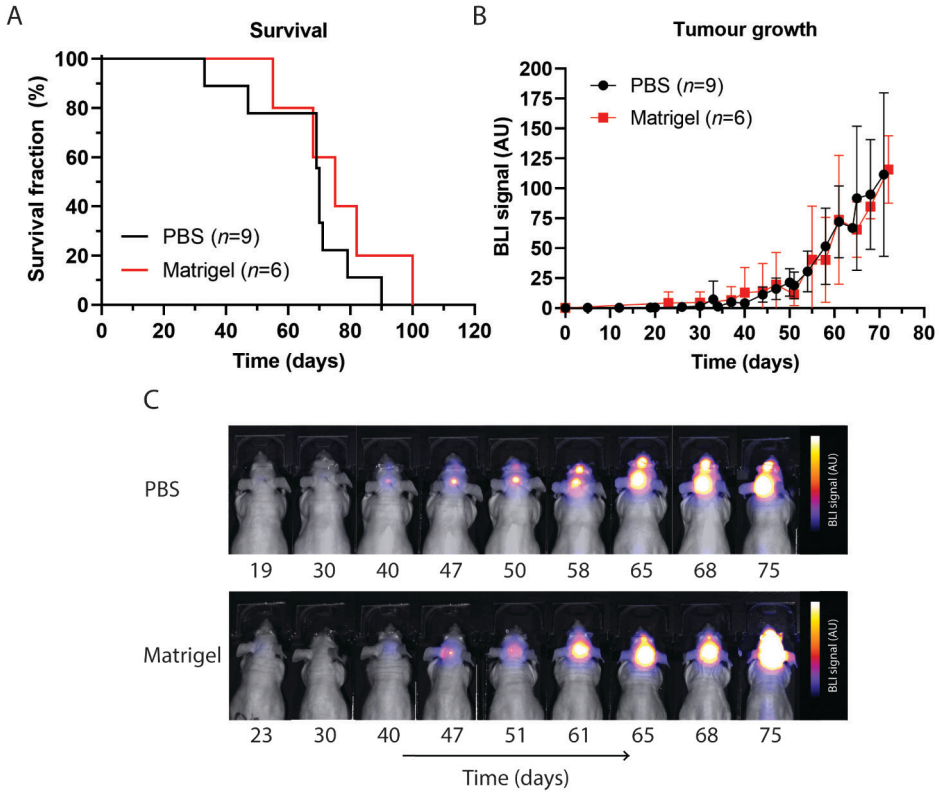

Figure 2. Survival and tumour growth following inoculation with HSJD-DIPG-007 cells sus-pended in PBS or Matrigel. (A) Kaplan-Meier curve showing survival following cell inoculation and tumour progression. No significant difference between PBS and Matrigel suspension groups was observed. (B) Tumour volume over time in both PBS and Matrigel suspension groups, showing that tumour growth was comparable up to 75 days. Data points are expressed as mean signal intensity ± SD. (C) BLI signal showing tumour growth over time. Tumour development within the pontine region, as well as metastatic development in the olfactory bulb region, can be seen in both PBS and Matrigel groups, progressing with time. AU = arbitrary unit.

Metastases occurrence in olfactory bulb and spinal cord

Because DMGs are tumours beginning in the pontine region and spreading on mid-disease in the majority of cases to adjacent areas, the HSJD-DIPG-007 PDX model should preferably recapitulate this growth pattern, in particular for the evaluation of locoregional treatment at the initial stage of disease [53]. Based on BLI signal, the first onset of metastases in the frontal lobe (olfactory bulb) was observed at day 26 after inoculation in the PBS group, and

day 44 after inoculation in the Matrigel group. A median metastasis-free survival (MMFS) in the olfactory bulb of 33 vs 58 days was found for PBS and Matrigel mice, with a significant difference between the groups (Figure 3A). Metastatic formations in the spinal cord were first observed at day 37 post inoculation in the PBS group and 44 post inoculation in the Matrigel group, with a MMFS of 47 and 68 days, respectively (Figure 3B). At time of death, two of the nine mice in the PBS group had not developed metastases, while only one had metastasis in the olfactory bulb. Of the six Matrigel mice, two did not develop metastases and one developed an olfactory bulb metastasis.

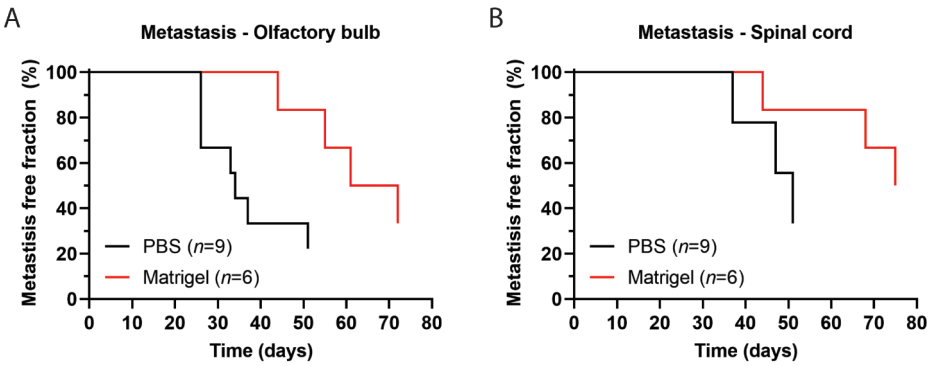

Figure 3. Distant metastatic formations over time monitored through BLI signal following HSJD-DIPG-007 cell inoculation into the pontine region. (A) Metastasis in the olfactory bulb in PBS and Matrigel suspension groups with a median onset of 33 and 53 days, respectively. A significant difference between the two groups was found ($p<0.05$). (B) Metastasis in the spinal cord in PBS and Matrigel suspension groups with a median onset of 47 and 68 days, respectively, but without a significant difference ($p>0.05$).

Mice with cells suspended in PBS showed local growth up to day 31, with subsequent locoregional progression as well as metastatic formations in the mid cerebrum/lateral ventricle, with eventual spreading into the cerebellum and olfactory bulb. Mice with cells suspended in Matrigel showed local growth up to day 31 and presence of tumour cells in the lateral ventricles, with delayed locoregional progression and distal striatal infiltration with inevitable invasion of the whole brain at day 55 (Figure 4). No histopathological or morphological differences were observed in the mice of both groups by H&E staining (Supplementary Figure 3). Anti-human vimentin staining confirmed local injection of HSJD-DIPG-007 in the pontine region of the mice and showcased that contamination of the cerebrospinal fluid (CSF) and dissemination to other brain structures in proximity to the injection site through the perivascular system (PVS) can occur (Figure 5).

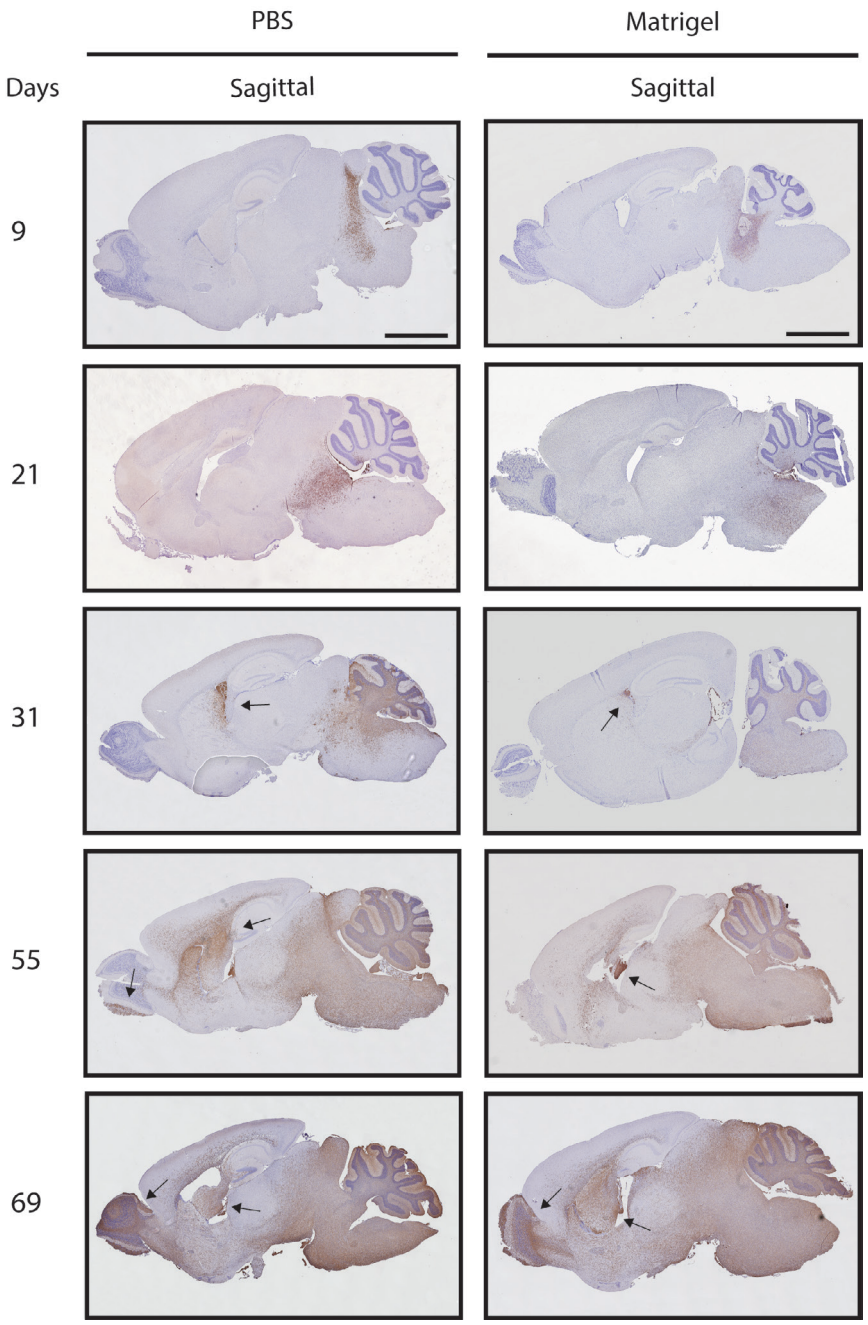

Figure 4. Anti-human vimentin staining of mouse brains showing tumour progression over time following inoculation with HSJD-DIPG-007 cells suspended in PBS or Matrigel. Tumour progression over time can be seen in both PBS and Matrigel groups through the accumulation and spread of human vimentin positive cells (brown staining) within the pons and other, more distant brain regions. Metastases can be observed from day 31 in both PBS and Matrigel suspension groups (black arrows). Whole brain invasion of tumour cells can be observed at day 55 in both groups. Mouse brains in both groups have been counterstained with haematoxylin. n = 9 for PBS group, n = 10 for Matrigel group. Scale bar = 2mm.

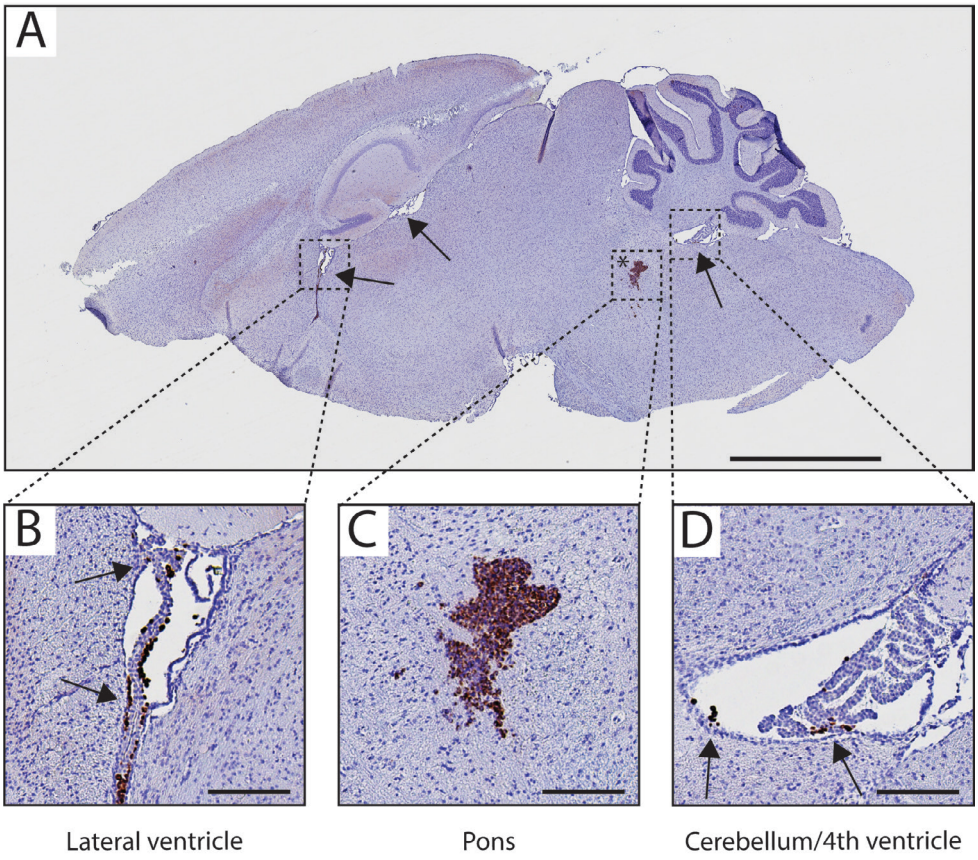

Figure 5. HSJD-DIPG-007 cells within the pons and disseminated throughout the brain immediately following inoculation. (A) Matrigel suspended HSJD-DIPG-007 cells within the pons area (asterisk) as well as in distant brain structures (arrows) at time zero, identified via anti-human vimentin staining. Magnification of HSJD-DIPG-007 cells present in the choroid plexus of the lateral ventricle (B), pons (C), and choroid plexus of the cerebellum/4th ventricle (D). Counter-staining is with haematoxylin. Scale bar = 2mm for A, 100 µm for B – D.

A comparative histopathological analysis of clinical autopsy derived DMG with the orthotopic E98 DIPG mouse model was previously performed by Caretti and colleagues [53]. To determine the clinical relevance of the HSJD-DIPG-007 PDX model, we used the histology panel of DMG patient tissue of Carreti et al. for a comparative assessment of disease progression (Figure 6). Perivascular tumour dissemination in the HSJD-DIPG-007 PDX model was seen to be like that observed in the DMG patient (Figure 6C, D). Similarities were also observed in brain parenchyma invasion in the HSJD-DIPG-007 model and clinical DMG (Figure 6G, H), as well as vascular proliferation (Figure 6K, L).

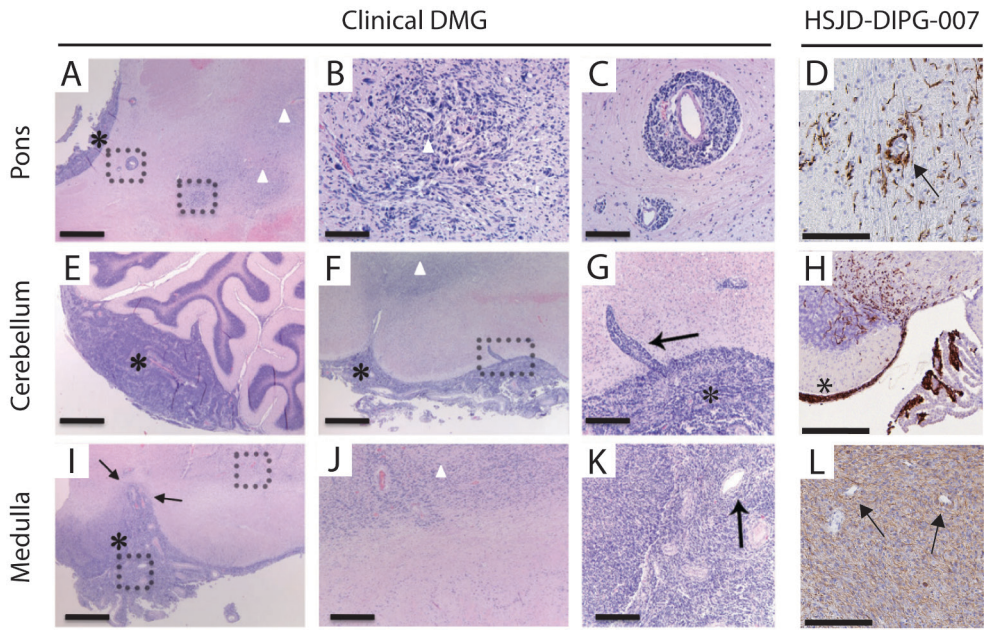

Figure 6. Comparative assessment of clinical DMG and HSJD-DIPG-007 PDX model histopathology. The comparative clinical DMG panel (panes A, B, C, E, F, G, I, J, K) has been adapted and reproduced with permission from Caretti et al [53]. (A, E, F, I) H&E staining of clinical DMG at the pons, cerebellum, and medulla. (B, C, G, J, K) Magnifications of H&E staining indicated by the dotted squares. (D, H, L) Anti-human vimentin staining of HSJD-DIPG-007 PDX model at the pons, cerebellum, and medulla. (A, E, F, G, H, I) Asterisks indicate leptomeningeal growth. (D, G) Arrows indicate perivascular growth and (I, K, L) blood vessels in dense tumour areas. Scale bars = 250 µm (A, F, I), 62.5 µm (B, C, G), 125 µm (J, K), 500 µm (E), 50 µm (D, H, L).

Discussion

DMG is an invasive paediatric brain tumour with a high mortality rate, and because of location and infiltrative nature of the disease, radiotherapy is the only effective palliative treatment option currently available [10,17]. As DMG rarely develops naturally in animals, PDX animal models are important for preclinical in vivo therapy efficacy validation. However, due to translational complexities between preclinical research and clinical applicability, there is a demand of PDX models emulating human disease progression. Metastases and immediate organ-specific proliferation infrequently occurs in patients in early stages of disease progression but can be seen in late/end stages of DMG [19]. Ideally DMG models would reproduce this form of early disease progression, which is observed in most of the patients as an initial diffuse local tumour proliferation in the pontine area, with subsequent expansion through the medulla, the cerebellum and the thalamic areas. Since DMG patients suffer from a rapid progression of disease in the vital pontine area leading to a poor prognosis, late-stage disease beyond this point is rarely observed.

The HSJD-DIPG-007 cell line, derived from the autopsy of a 6-year-old, is widely used for establishing DMG PDX models, but the high heterogeneity between protocols indicates that a universal procedure is yet to be developed. With the aim of facilitating a standardised

inoculation method, this study investigated and optimised the growth pattern of the HSJD-DIPG-007 PDX model for local or metastatic phenotype treatment based on two different suspension matrices.

Studies in other cancer models, such as pancreatic cancer, have shown the im-portance of suspension matrix when tumour cells are injected locally, and the issues such as leakage, low tumour formation and the development of metastases that can arise [54]. Local introduction of cells into the brain is a delicate matter, requiring precision in location, as well as in the injection procedure to avoid positive and negative pressure build-up that could dissipate the cells in an unfavourable manner. A possible alternative to common suspension matrices such as growth medium and PBS could be the basement membrane Matrigel, due to its composition resembling the extracellular matrix of many tissues, as well as its favourable viscoelastic properties where it remains liquid at low temperatures but polymerises to a dense matrix at temperatures above 10oC [55]. No standardised procedure in establishing the HSJD-DIPG-007 PDX model could be discerned from the studies outlined in Table 1. Protocols differed considerably in all reported parameters, as well as in the stated level of detail provided, with the most noteworthy differences being in the suspension matrix used, day at which treatment was initiated, and treatment modality or efficacy. In our study comparing PBS and Matrigel, we selected to use animals at 6–8 weeks of age for inoculation of the HSJD-DIPG-007 cell line, corresponding to the age range used by 50% of the studies reported in Table 1, and commonly used for in vivo studies. To ensure adequate cell grafting, we also opted for 5x105 total cell inoculation for both PBS and Matrigel suspension groups.

Initial observations made in comparing PBS and Matrigel groups was in weight stability following HSJD-DIPG-007 cell implantation. Substantial fluctuations, including rapid gains/losses in a short period of time are reliable indications of health in in vivo animal models. In our study no significant differences in weight were observed between the PBS and Matrigel group. The weight gained in the first 4 – 5 weeks after cell implantation could be due to the young 6 – 8-week age of the mice, in which they were still in their adolescent and body growth phase [33].

As DMG progresses quite rapidly in children, symptoms are typically not evident for 4 to 6 weeks before diagnosis [56]. Patients present to the clinic when disease progression is relatively advanced, with a triad of symptoms consisting of cranial neuropathy, long tract signs, and cerebellar signs [57]. By this stage, DMG may have been developing for 12 months or more. In our study, mice in both groups were asymptomatic and gained weight for 30 days, as seen in figure 1, after which tumour presence could be verified and followed by BLI, and weight loss began to occur. The subsequent weight loss could be at-tributed to progression of the tumour in the pontine region, the consequence of which could be diminished appetite. Figure 2 shows how BLI signal intensified rapidly post day 30, with strong signal being observed in brain regions outside the graft area, suggesting the presence of metastatic formations. However, this increase in BLI signal did not correspond with overall survival, as no significant differences were observed irrespective of whether cells were inoculated using PBS or Matrigel. Both groups also had comparable tumour growth rates during the steady growth phase of the first 4 weeks post inoculation as well as the

exponential growth phase, thereafter, further supporting the similar survival times observed and confirming that suspension matrix on its own does not influence local tumour growth or survival.

Strikingly, analysis of the BLI signal did show differences between PBS and Matrigel groups in terms of metastatic formations within the olfactory bulbs, as seen in figure 3, suggesting that Matrigel does significantly delay onset of metastases by an average of ap-proximately 3 weeks. Delays in spinal cord were also observed in the Matrigel group, and even though these were not found to be significant, the suggestion that Matrigel influences metastasis formation is present. The polymerisation of the cell loaded Matrigel upon injection into the pons could have contributed to reduced cellular leakage into the brain parenchyma or into the needle tract produced during the inoculation procedure, without altering tumour growth rate. The observation that the use of one suspension matrix significantly delays metastases when compared to another further emphasises the need for a standardised protocol in establishing DMG PDX models through orthotopic injection of cells into the pons. This was confirmed, as seen in figure 4, through anti-human vimentin staining of HSJD-DIPG-007 cell inoculated mouse brains at various stages of tumour development. The staining confirmed that the pons was accurately targeted and that the cells successfully engrafted and were able to induce local tumour formation. Tumour growth rapidly progressed with time, while advanced metastatic formations were observed by 31 days within the mid brain, and 55 days within the olfactory bulbs of the PBS suspension group, while not in the Matrigel group.

The PVS and cerebrospinal fluid hydrodynamics are important factors that must also be considered, especially when DMG PDX models are established. It has previously been shown that connections between the CSF and nasal lymphatic vessels in mammals, including humans and rodents, share common characteristics [58]. Metastases can initially be seen in the location of the lateral ventricle, followed by formations in the olfactory bulbs, which coincides with the direction of CSF flow in both humans and rodents. In humans, CFS circulates in a caudal-directed manner through the ventricles to the sub-arachnoid space, resulting in an exchange of various substances in a to-and-from manner between the CSF and interstitial compartments [59].

A proportion of the CSF drains into the cribriform place while the rest is recycled into the brain parenchyma through perivascular spaces surrounding blood vessels. Peri-vascular space connections penetrating deep into the brainstem and 4th ventricle have also been observed. New PVS connections between ventricles and different parts of the brain parenchyma have been revealed suggesting a possible role for the ventricles as a source or sink for solutes in the brain [60].

These observations further demonstrate that Matrigel, as a suspension matrix, is more favourable in supporting local tumour growth at the site of inoculation and delays the onset of metastases, especially to the olfactory bulbs, in a significant manner, further supporting its use as a more suitable suspension matrix than PBS. It may be that Matrigel supresses perivascular proliferation of inoculated cells, resulting in a model of disease progression that more closely resembles that seen in patients as described by Caretti and colleagues [19].

Although Matrigel delays metastases overall, the inoculation procedure itself is not infallible. When injecting a substance 4 – 5mm deep within the mouse brain, the needle passes through several structures and does cause a degree of disruption to adjacent tissues, while also disturbing the CSF present in the brain. As shown in figure 5, rogue cells can be seen already circulating within the brain outside the pontine region immediately following inoculation. The circulating CSF could potentially distribute these cells through the lateral ventricles and on to the olfactory bulbs, which also act as a CSF sink and out-flow to the nasal lymphatics [60], where they can give rise to metastatic formations developing very early following initial inoculation. Therefore, it is imperative that any residual cells that may remain on the outside of the needle while filling with cell-containing suspension matrix be removed thoroughly before injection into the brain.

When the observations of tumour volume and BLI signal of figure 3 are compared with the immunohistochemical images of the tumour progression in figure 4, we can see that although BLI signal is not detected before 40 days post inoculation of HSJD-DIPG-007 cells, tumour progression with extensive infiltration of the brain parenchyma by tumour cells is already present by day 21. This suggests that BLI signal alone is not reliable in determining early and local tumour formation, and thus should not be used as a measure to determine onset of treatment as tumour size and burden, including the presence of metastases could be underestimated. Such an underestimation could render treatment regimens unsuccessful because of a too large tumour burden rather than treatment inefficacy, leading to false negatives and ultimate rejection of suitable drug or treatment candidates. From the immunohistological data obtained, in addition to using Matrigel as a cell suspension, we would suggest that treatment initiation be performed between 7- and 14-days post cell inoculation. This timeframe would allow for cells to engraft and tumour formation to occur to a point where the burden is not too high to render treatment ineffective, and not too low to result in false positives. It is noteworthy that of the studies listed in Table 1, only 1/5 initiated treatment within this timeline, while the majority started therapy three or more weeks following cell implantation. For locoregional therapy approaches, treating within two weeks would also ensure that the entire tumour within the pons is targeted, and not later occurring metastatic formation within other brain regions which are missed, especially in the distant olfactory bulbs.

In summary, the HSJD-DIPG-007 PDX mouse model is one that has gained interest in DMG research as it does resemble human disease progression in a clinically relevant manner, as figure 6 shows. Vital elements, such as perivascular tumour dissemination, invasion of the parenchyma, as well as vascular proliferation are well emulated in the HSJD-DIPG-007 PDX model. As Caretti [53] showed in both the clinical and E98 DMG tumours, and observations in the HSJD-DIPG-007 model used in this study, perivascular migration appears to be a route by which invasion of the brain parenchyma can occur by tumour cells located in the subarachnoid space. However, for this model to be optimally utilised in preclinical research, standardisation of its establishment needs to be achieved.

Based on our results, we propose a standardised method of using Matrigel as a sus-pension matrix to inoculate cells within the pons to delay metastases to other brain regions. We also suggest treatment initiation be within 1-2 weeks of grafting to ensure an adequate but not

overbearing tumour burden for assessment of treatment strategies. Further standardisation of this model assessing animal host used, total cells inoculated, injection volume and graft location is needed so that a reliable and reproducible model that recapitulates the histological characteristics of DMG can be established.

Acknowledgements

This project was supported by KWF Young Investigator Award (KWF 10911, Dr. D.G. van Vuurden). The authors also thank Dr. Ángel Montero Carcaboso (Sant Joan de Déu Barcelona Hospital) for kindly providing the HSJD-DIPG-007 patient derived cell line used in this study. Graphical abstract created with BioRender.com

References

[1] Louis DN, Perry A, Wesseling P, Brat DJ, Cree IA, Figarella-Branger D, et al. The 2021 WHO Classification of tumors of the central nervous system: a summary. Neuro Oncol 2021;23:1231–51. https://doi.org/10.1093/neuonc/noab106.

[2] Khuong-Quang D-A, Buczkowicz P, Rakopoulos P, Liu X-Y, Fontebasso AM, Bouffet E, et al. K27M mutation in histone H3.3 defines clinically and biologically distinct subgroups of pediatric diffuse intrinsic pontine gliomas. Acta Neuropathol 2012;124:439–47. https://doi.org/10.1007/s00401-012-0998-0.

[3] Chan K-M, Fang D, Gan H, Hashizume R, Yu C, Schroeder M, et al. The histone H3.3K27M mutation in pediatric glioma reprograms H3K27 methylation and gene expression. Genes Dev 2013;27:985–90. https://doi.org/10.1101/gad.217778.113.

[4] Castel D, Kergrohen T, Tauziède-Espariat A, Mackay A, Ghermaoui S, Lechapt E, et al. Histone H3 wild-type DIPG/DMG overexpressing EZHIP extend the spectrum diffuse midline gliomas with PRC2 inhibition beyond H3-K27M mutation. Acta Neuropathol 2020;139:1109–13. https://doi.org/10.1007/s00401-020-02142-w.

[5] Xu C, Liu H, Pirozzi CJ, Chen LH, Greer PK, Diplas BH, et al. TP53 wild-type/PPM1D mutant diffuse intrinsic pontine gliomas are sensitive to a MDM2 antagonist. Acta Neuropathol Commun 2021;9:178. https://doi.org/10.1186/s40478-021-01270-y.

[6] Zarghooni M, Bartels U, Lee E, Buczkowicz P, Morrison A, Huang A, et al. Whole-genome profiling of pediatric diffuse intrinsic pontine gliomas highlights platelet-derived growth factor receptor alpha and poly (ADP-ribose) polymerase as potential therapeutic targets. J Clin Oncol Off J Am Soc Clin Oncol 2010;28:1337–44. https://doi.org/10.1200/JCO.2009.25.5463.

[7] Paugh BS, Broniscer A, Qu C, Miller CP, Zhang J, Tatevossian RG, et al. Genome-wide analyses identify recurrent amplifications of receptor tyrosine kinases and cell-cycle regulatory genes in diffuse intrinsic pontine glioma. J Clin Oncol 2011;29:3999–4006. https://doi.org/10.1200/JCO.2011.35.5677.

[8] Buczkowicz P, Hoeman C, Rakopoulos P, Pajovic S, Letourneau L, Dzamba M, et al. Genomic analysis of diffuse intrinsic pontine gliomas identifies three molecular subgroups and recurrent activating ACVR1 mutations. Nat Genet 2014;46:451–6. https://doi.org/10.1038/ng.2936.

[9] Zhang L, Chen LH, Wan H, Yang R, Wang Z, Feng J, et al. Exome sequencing identifies somatic gain-of-function PPM1D mutations in brainstem gliomas. Nat Genet 2014;46:726–30. https://doi.org/10.1038/ng.2995.

[10] Hoffman LM, Veldhuijzen van Zanten SEM, Colditz N, Baugh J, Chaney B, Hoffmann M, et al. Clinical, radiologic, pathologic, and molecular characteristics of long-term survivors of diffuse intrinsic pontine glioma (DIPG): a collaborative report from the international and european society for pediatric oncology DIPG registries. J Clin Oncol 2018;36:1963–72. https://doi.org/10.1200/JCO.2017.75.9308.

[11] Jansen MH, Veldhuijzen van Zanten SE, Sanchez Aliaga E, Heymans MW, Warmuth-Metz M, Hargrave D, et al. Survival prediction model of children with diffuse intrinsic pontine glioma based on clinical and radiological criteria. Neuro Oncol 2015;17:160–6. https://doi.org/10.1093/neuonc/nou104.

[12] Tate MC, Lindquist RA, Nguyen T, Sanai N, Barkovich AJ, Huang EJ, et al. Postnatal growth of the human pons: a morphometric and immunohistochemical analysis. J Comp Neurol 2015;523:449–62. https://doi.org/10.1002/cne.23690.

[13] Fisher PG, Breiter SN, Carson BS, Wharam MD, Williams JA, Weingart JD, et al. A clinicopathologic reappraisal of brain stem tumor classification. Identification of pilocystic

astrocytoma and fibrillary astrocytoma as distinct entities. Cancer 2000;89:1569–76. https://doi.org/10.1002/1097-0142(20001001)89:7<1569::aid-cncr22>3.0.co;2-0.

[14] Pardridge WM. Blood-brain barrier delivery. Drug Discov Today 2007;12:54–61. https://doi.org/10.1016/j.drudis.2006.10.013.

[15] Stupp R, Hegi ME, Mason WP, van den Bent MJ, Taphoorn MJB, Janzer RC, et al. Effects of radiotherapy with concomitant and adjuvant temozolomide versus radiotherapy alone on survival in glioblastoma in a randomised phase III study: 5-year analysis of the EORTC-NCIC trial. Lancet Oncol 2009;10:459–66. https://doi.org/10.1016/S1470-2045(09)70025-7.

[16] Warren KE. Beyond the blood-brain barrier: the importance of central nervous system (CNS) pharmacokinetics for the treatment of CNS tumors, including diffuse intrinsic pontine glioma. Front Oncol 2018;8:239. https://doi.org/10.3389/fonc.2018.00239.

[17] Stupp R, Mason WP, van den Bent MJ, Weller M, Fisher B, Taphoorn MJB, et al. Radiotherapy plus concomitant and adjuvant temozolomide for glioblastoma. N Engl J Med 2005;352:987–96. https://doi.org/10.1056/NEJMoa043330.

[18] Gururangan S, McLaughlin CA, Brashears J, Watral MA, Provenzale J, Coleman RE, et al. Incidence and patterns of neuraxis metastases in children with diffuse pontine glioma. J Neurooncol 2006;77:207–12. https://doi.org/10.1007/s11060-005-9029-5.

[19] Caretti V, Bugiani M, Freret M, Schellen P, Jansen M, van Vuurden D, et al. Subventricular spread of diffuse intrinsic pontine glioma. Acta Neuropathol 2014;128:605–7. https://doi.org/10.1007/s00401-014-1307-x.

[20] Hargrave D, Bartels U, Bouffet E. Diffuse brainstem glioma in children: critical review of clinical trials. Lancet Oncol 2006;7:241–8. https://doi.org/10.1016/S1470-2045(06)70615-5.

[21] Veringa SJE, Biesmans D, van Vuurden DG, Jansen MHA, Wedekind LE, Horsman I, et al. In vitro drug response and efflux transporters associated with drug resistance in pediatric high grade glioma and diffuse intrinsic pontine glioma. PLoS One 2013;8:e61512. https://doi.org/10.1371/journal.pone.0061512.

[22] Grasso CS, Tang Y, Truffaux N, Berlow NE, Liu L, Debily M-A, et al. Functionally defined therapeutic targets in diffuse intrinsic pontine glioma. Nat Med 2015;21:555–9. https://doi.org/10.1038/nm.3855.

[23] Mueller S, Hashizume R, Yang X, Kolkowitz I, Olow AK, Phillips J, et al. Targeting Wee1 for the treatment of pediatric high-grade gliomas. Neuro Oncol 2014;16:352–60. https://doi.org/10.1093/neuonc/not220.

[24] Caretti V, Hiddingh L, Lagerweij T, Schellen P, Koken PW, Hulleman E, et al. WEE1 kinase inhibition enhances the radiation response of diffuse intrinsic pontine gliomas. Mol Cancer Ther 2013;12:141–50. https://doi.org/10.1158/1535-7163.MCT-12-0735.

[25] Hennika T, Hu G, Olaciregui NG, Barton KL, Ehteda A, Chitranjan A, et al. Pre-clinical study of panobinostat in xenograft and genetically engineered murine diffuse intrinsic pontine glioma models. PLoS One 2017;12:e0169485. https://doi.org/10.1371/journal.pone.0169485.

[26] Perlman RL. Mouse models of human disease: an evolutionary perspective. Evol Med Public Heal 2016;2016:170–6. https://doi.org/10.1093/emph/eow014.

[27] Chen Z, Peng P, Zhang X, Mania-Farnell B, Xi G, Wan F. Advanced pediatric diffuse pontine glioma murine models pave the way towards precision medicine. Cancers (Basel) 2021;13. https://doi.org/10.3390/cancers13051114.

[28] Funato K, Major T, Lewis PW, Allis CD, Tabar V. Use of human embryonic stem cells to model pediatric gliomas with H3.3K27M histone mutation. Science 2014;346:1529–33. https://doi.org/10.1126/science.1253799.

[29] Monje M, Mitra SS, Freret ME, Raveh TB, Kim J, Masek M, et al. Hedgehog-responsive candidate cell of origin for diffuse intrinsic pontine glioma. Proc Natl Acad Sci U S A 2011;108:4453–8. https://doi.org/10.1073/pnas.1101657108.

[30] Taylor KR, Mackay A, Truffaux N, Butterfield Y, Morozova O, Philippe C, et al. Recurrent activating ACVR1 mutations in diffuse intrinsic pontine glioma. Nat Genet 2014;46:457–61. https://doi.org/10.1038/ng.2925.

[31] Vinci M, Burford A, Molinari V, Kessler K, Popov S, Clarke M, et al. Functional diversity and cooperativity between subclonal populations of pediatric glioblastoma and diffuse intrinsic pontine glioma cells. Nat Med 2018;24:1204–15. https://doi.org/10.1038/s41591-018-0086-7.

[32] Haumann R, Bianco JI, Waranecki PM, Gaillard PJ, Storm G, Ries M, et al. Imaged-guided focused ultrasound in combination with various formulations of doxorubicin for the treatment of diffuse intrinsic pontine glioma. Transl Med Commun 2022;7:8. https://doi.org/10.1186/s41231-022-00115-7.

[33] Brust V, Schindler PM, Lewejohann L. Lifetime development of behavioural phenotype in the house mouse (Mus musculus). Front Zool 2015;12:S17. https://doi.org/10.1186/1742-9994-12-S1-S17.

[34] Qi L, Kogiso M, Du Y, Zhang H, Braun FK, Huang Y, et al. Impact of SCID mouse gender on tumorigenicity, xenograft growth and drug-response in a large panel of orthotopic PDX models of pediatric brain tumors. Cancer Lett 2020;493:197–206. https://doi.org/https://doi.org/10.1016/j.canlet.2020.08.035.

[35] Kholosy WM, Derieppe M, Ham F Van Den, Ober K, Su Y, Custers L, et al. Neuroblastoma and DIPG Organoid Coculture System for Personalized Assessment of Novel Anticancer Immunotherapies 2021.

[36] Schneider CA, Rasband WS, Eliceiri KW. NIH Image to ImageJ: 25 years of image analysis. Nat Methods 2012;9:671–5. https://doi.org/10.1038/nmeth.2089.

[37] Chastkofsky MI, Pituch KC, Katagi H, Zannikou M, Ilut L, Xiao T, et al. Mesenchymal stem cells successfully deliver oncolytic virotherapy to diffuse intrinsic pontine glioma. Clin Cancer Res 2021;27:1766–77. https://doi.org/10.1158/1078-0432.CCR-20-1499.

[38] Surowiec RK, Ferris SF, Apfelbaum A, Espinoza C, Mehta RK, Monchamp K, et al. Transcriptomic analysis of diffuse intrinsic pontine glioma (DIPG) identifies a targetable ALDH-positive subset of highly tumorigenic cancer stem-like cells. Mol Cancer Res 2021;19:223–39. https://doi.org/10.1158/1541-7786.MCR-20-0464.

[39] Khan A, Gamble LD, Upton DH, Ung C, Yu DMT, Ehteda A, et al. Dual targeting of polyamine synthesis and uptake in diffuse intrinsic pontine gliomas. Nat Commun 2021;12:971. https://doi.org/10.1038/s41467-021-20896-z.

[40] Carvalho DM, Richardson PJ, Olaciregui N, Stankunaite R, Lavarino C, Molinari V, et al. Repurposing vandetanib plus everolimus for the treatment of ACVR1-mutant diffuse intrinsic pontine glioma. Cancer Discov 2022;12:416–31. https://doi.org/10.1158/2159-8290.CD-20-1201.

[41] Jansen MHA, Lagerweij T, Sewing ACP, Vugts DJ, van Vuurden DG, Molthoff CFM, et al. Bevacizumab targeting diffuse intrinsic pontine glioma: results of 89Zr-Bevacizumab PET imaging in brain tumor models. Mol Cancer Ther 2016;15:2166–74. https://doi.org/10.1158/1535-7163.MCT-15-0558.

[42] Sewing ACP, Lagerweij T, van Vuurden DG, Meel MH, Veringa SJE, Carcaboso AM, et al. Preclinical evaluation of convection-enhanced delivery of liposomal doxorubicin to treat pediatric diffuse intrinsic pontine glioma and thalamic high-grade glioma. J Neurosurg Pediatr 2017;19:518–30. https://doi.org/10.3171/2016.9.PEDS16152.

[43] Cockle J V, Brüning-Richardson A, Scott KJ, Thompson J, Kottke T, Morrison E, et al. Oncolytic herpes simplex virus inhibits pediatric brain tumor migration and invasion. Mol Ther Oncolytics 2017;5:75–86. https://doi.org/10.1016/j.omto.2017.04.002.

[44] Tsoli M, Shen H, Mayoh C, Franshaw L, Ehteda A, Upton D, et al. International experience in the development of patient-derived xenograft models of diffuse intrinsic pontine glioma. J Neurooncol 2019;141:253–63. https://doi.org/10.1007/s11060-018-03038-2.

[45] Akamandisa MP, Nie K, Nahta R, Hambardzumyan D, Castellino RC. Inhibition of mutant PPM1D enhances DNA damage response and growth suppressive effects of ionizing radiation in diffuse intrinsic pontine glioma. Neuro Oncol 2019;21:786–99. https://doi.org/10.1093/neuonc/noz053.

[46] Carvalho D, Taylor KR, Olaciregui NG, Molinari V, Clarke M, Mackay A, et al. ALK2 inhibitors display beneficial effects in preclinical models of ACVR1 mutant diffuse intrinsic pontine glioma. Commun Biol 2019;2:156. https://doi.org/10.1038/s42003-019-0420-8.

[47] Meel MH, de Gooijer MC, Metselaar DS, Sewing ACP, Zwaan K, Waranecki P, et al. Combined therapy of AXL and HDAC inhibition reverses mesenchymal transition in diffuse intrinsic pontine glioma. Clin Cancer Res 2020;26:3319–32. https://doi.org/10.1158/1078-0432.CCR-19-3538.

[48] Thomas L, Smith N, Saunders D, Zalles M, Gulej R, Lerner M, et al. OKlahoma Nitrone-007: novel treatment for diffuse intrinsic pontine glioma. J Transl Med 2020;18:424. https://doi.org/10.1186/s12967-020-02593-5.

[49] Chung C, Sweha SR, Pratt D, Tamrazi B, Panwalkar P, Banda A, et al. Integrated metabolic and epigenomic reprograming by H3K27M mutations in diffuse intrinsic pontine gliomas. Cancer Cell 2020;38:334-349.e9. https://doi.org/10.1016/j.ccell.2020.07.008.

[50] Chaves C, Declèves X, Taghi M, Menet M-C, Lacombe J, Varlet P, et al. Characterization of the blood-brain barrier integrity and the brain transport of SN-38 in an orthotopic xenograft rat model of diffuse intrinsic pontine glioma. Pharmaceutics 2020;12. https://doi.org/10.3390/pharmaceutics12050399.

[51] Shen H, Yu M, Tsoli M, Chang C, Joshi S, Liu J, et al. Targeting reduced mitochondrial DNA quantity as a therapeutic approach in pediatric high-grade gliomas. Neuro Oncol 2020;22:139–51. https://doi.org/10.1093/neuonc/noz140.

[52] Ehteda A, Simon S, Franshaw L, Giorgi FM, Liu J, Joshi S, et al. Dual targeting of the epigenome via FACT complex and histone deacetylase is a potent treatment strategy for DIPG. Cell Rep 2021;35:108994. https://doi.org/10.1016/j.celrep.2021.108994.

[53] Caretti V, Zondervan I, Meijer DH, Idema S, Vos W, Hamans B, et al. Monitoring of tumor growth and post-irradiation recurrence in a diffuse intrinsic pontine glioma mouse model. Brain Pathol 2011;21:441–51. https://doi.org/10.1111/j.1750-3639.2010.00468.x.

[54] Jiang Y-J, Lee C-L, Wang Q, Zhou Z-W, Yang F, Jin C, et al. Establishment of an orthotopic pancreatic cancer mouse model: cells suspended and injected in Matrigel. World J Gastroenterol 2014;20:9476–85. https://doi.org/10.3748/wjg.v20.i28.9476.

[55] Kleinman HK, McGarvey ML, Liotta LA, Robey PG, Tryggvason K, Martin GR. Isolation and characterization of type IV procollagen, laminin, and heparan sulfate proteoglycan from the EHS sarcoma. Biochemistry 1982;21:6188–93. https://doi.org/10.1021/bi00267a025.

[56] Johung TB, Monje M. Diffuse Intrinsic Pontine Glioma: New Pathophysiological Insights and Emerging Therapeutic Targets. Curr Neuropharmacol 2017;15:88–97. https://doi.org/10.2174/1570159x14666160509123229.

[57] Donaldson SS, Laningham F, Fisher PG. Advances toward an understanding of brainstem gliomas. J Clin Oncol Off J Am Soc Clin Oncol 2006;24:1266–72. https://doi.org/10.1200/JCO.2005.04.6599.

[58] Johnston M, Zakharov A, Papaiconomou C, Salmasi G, Armstrong D. Evidence of connections between cerebrospinal fluid and nasal lymphatic vessels in humans, non-human primates and other mammalian species. Cerebrospinal Fluid Res 2004;1:2. https://doi.org/10.1186/1743-8454-1-2.

[59] Orešković D, Klarica M. Development of hydrocephalus and classical hypothesis of cerebrospinal fluid hydrodynamics: facts and illusions. Prog Neurobiol 2011;94:238–58. https://doi.org/10.1016/j.pneurobio.2011.05.005.

[60] Magdoom KN, Brown A, Rey J, Mareci TH, King MA, Sarntinoranont M. MRI of Whole Rat Brain Perivascular Network Reveals Role for Ventricles in Brain Waste Clearance. Sci Rep 2019;9:11480. https://doi.org/10.1038/s41598-019-44938-1.

Supplementary data

Supplementary Table 1: List of conditions, materials, and manufacturers related to the in vivo experiments including living conditions, cage enrichments, food, water, and health monitoring of the animals by pathogen detection in the research facility.

Parameter	Condition/Material	Manufacturer
Temperature	21 ± 1°C	-
Relative Humidity	45 – 64%, TouchSLIM Plus™ AHU	Tecniplast S.p.A., Italy
Lighting	12h light/dark (7 a.m. – 7 p.m.)	-
Housing	Specific Pathogen Free	-
Caging	GM500 Mouse IVC (Green Line)	Tecniplast S.p.A., Italy
Mice/cage	Up to 4	-
Bedding	Wooden flakes	Aspen Animal Bedding, USA
Diet	ssniff® R/M-H (V153x), *ad libitum*	Ssniff Spezialdiäten GmbH, Netherlands
Water	Sterile, *ad libitum*	Aqua B. Braun, Germany
Enrichment	Tissue	WEPA Professional GmbH, Germany
	Mouse Tunnel	Bio-Serv, USA
Pathogen detection	Dirty-bedding sentinels	-

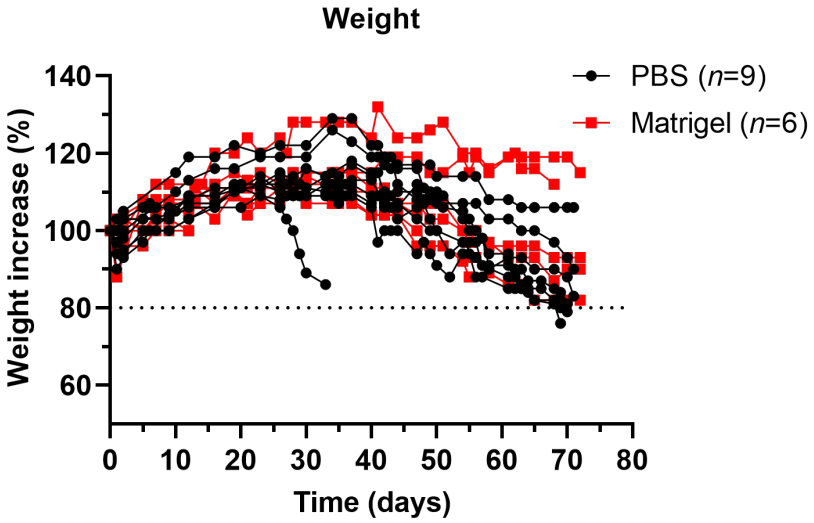

Supplementary Figure 1: Weight profiles of individual mice after inoculation with HSJD-DIPG-007 cells suspended in PBS or Matrigel. Weight was monitored until terminal endpoint. Dotted line represents humane endpoint threshold (representing 20% weight loss).

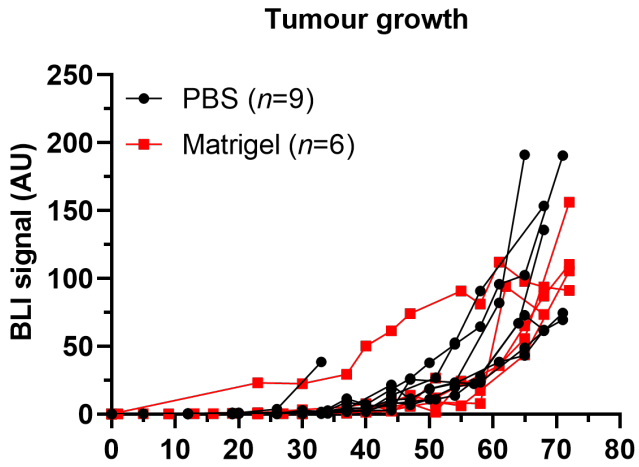

Supplementary Figure 2: Tumour growth profiles of individual mice following inoculation with HSJD-DIPG-007 cells suspended in PBS or Matrigel. Individual tumour volume over time in both PBS and Matrigel suspension groups shows comparable tumour growth up to 75 days.

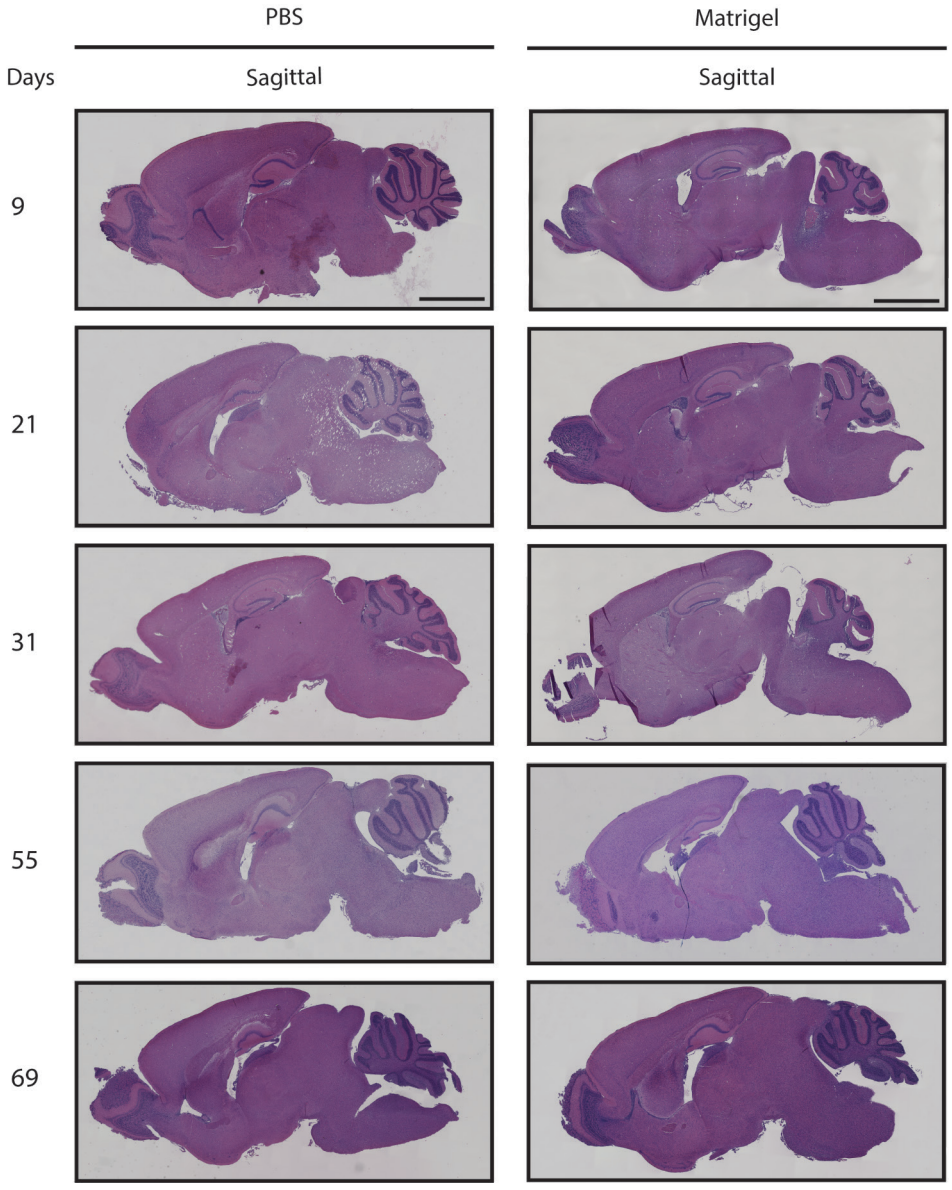

Supplementary Figure 3: Haematoxylin & Eosin staining of mouse brains with tumour progression over time following inoculation with HSJD-DIPG-007 cells suspended in PBS or Matrigel. No apparent histological changes were observed over time. Scale bar = 2mm.

Chapter 5

Radiosensitisation by olaparib through focused ultrasound delivery in a diffuse midline glioma model

Elvin ’t Hart[1], John Bianco[1], Maaike Bruin[2], Marc Derieppe[1], Helena Besse[3], Kjelle-Lars Berkhout[1], Lois Chin Joe Kie[1], Yan Su[1], Eelco Hoving[1], Alwin Huitema[1,2,4], Mario Ries[3#], Dannis van Vuurden[1#]

1. Princess Maxima Center for Pediatric Oncology, Heidelberglaan 25, 3584 CS, Utrecht, the Netherlands

2. Department of Pharmacy and Pharmacology, the Netherlands Cancer Institute, Antoni van Leeuwenhoek Hospital, Plesmanlaan 121, 1066CX, Amsterdam, the Netherlands

3. Center for Imaging Sciences, University Medical Center Utrecht, Heidelberglaan 100, 3584 CX Utrecht, the Netherlands

4. Department of Clinical Pharmacy, University Medical Center Utrecht, Utrecht University, Heidelberglaan 100, 3584 CX Utrecht, the Netherlands

Published in: Journal of Controlled Release; May 2023; 357:287-298. doi: 10.1016/j.jconrel.2023.03.058

Abstract

Background and purpose: Diffuse midline glioma H3K27-altered (DMG) is an aggressive, inoperable, predominantly paediatric brain tumour. Treatment strategies are limited, resulting in a median survival of only 11 months. Currently, radiotherapy (RT), often combined with temozolomide, is considered the standard of care but remains palliative, highlighting the urgency for new therapies. Radiosensitisation by olaparib, an inhibitor of PARP1 and subsequently PAR-synthesis, is a promising treatment option. We assessed whether PARP1 inhibition enhances radiosensitivity in vitro and in vivo following focused ultrasound mediated blood-brain barrier opening (FUS-BBBO).

Methods: Effects of PARP1 inhibition were evaluated in vitro using viability, clonogenic, and neurosphere assays. In vivo olaparib extravasation and pharmacokinetic profiling following FUS-BBBO was measured by LC-MS/MS. Survival benefit of FUS-BBBO combined with olaparib and RT was assessed using a patient-derived xenograft (PDX) DMG mouse model.

Results: Treatment with olaparib in combination with radiation delayed tumour cell proliferation in vitro through the reduction of PAR. Prolonged exposure of low olaparib concentration was more efficient in delaying cell growth than short exposure of high concentration. FUS-BBBO increased olaparib bioavailability in the pons by 5.36-fold without observable adverse effects. A Cmax of 54.09 µM in blood and 1.39 µM in the pontine region was achieved following administration of 100 mg/kg olaparib. Although RT combined with FUS-BBBO mediated olaparib extravasation delayed local tumour growth, survival benefits were not observed in an in vivo DMG PDX model.

Conclusions: Olaparib effectively radiosensitises DMG cells in vitro and reduces primary tumour growth in vivo when combined with RT. Further studies are needed to investigate the therapeutic benefit of olaparib in suitable preclinical PDX models.

Graphical abstract

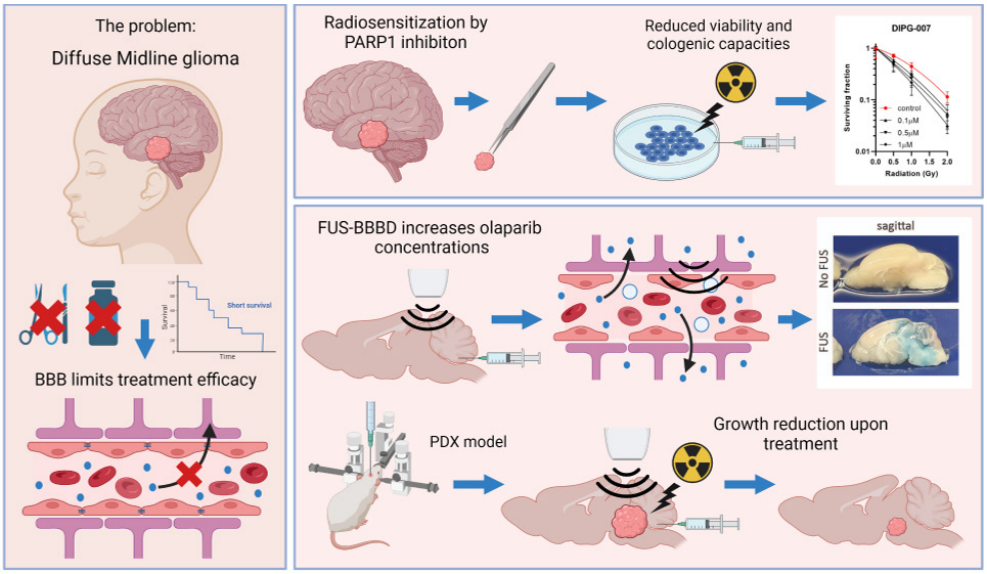

Keywords:

Diffuse midline glioma H3K27-altered; radiosensitisation; PARP1; blood-brain barrier; focused ultrasound

Introduction

Diffuse midline gliomas H3K27-altered (DMG) are WHO grade IV invasive, rapidly growing high-grade gliomas (HGG), occurring in the pons, thalamus, and spinal cord of children and young adults, and together with hemispheric HGG, account for 8-12% of all central nervous system tumours in children [1]. Despite years of intensive research, significant curative progress for pontine DMG, formally known as diffuse intrinsic pontine glioma (DIPG), has remained elusive [2]. As a consequence, the average survival of DMG patients is only 11 months, with a 95% fatality rate within 2 years of diagnosis [3,4]. Currently radiotherapy (RT), either as monotherapy or in combination with temozolomide is the standard of care. Radical surgery is impossible due to the intrinsic nature and infiltrative growth of the tumour [5]. Although RT is not curative, 80% of the children display symptom relief and benefit from an increased life expectancy of 6 months [6,7]. Chemotherapy efficacy is generally hampered by a largely intact blood-brain barrier (BBB), lack of therapeutic targets and chemoresistance [8].

DMG/DIPG tumours display a compromised ability to repair double-strand DNA breaks (DSBs) due to the occurrence of P53 mutations and defective homologous recombination repair (HRR), possibly by amplification of cyclin D2 (CCND2) and TOP3A, and heterozygous mutations in HRR-related genes such as ATM, BRCA2, BLM, ATR, PALB2, RAD50 and RAD51C,

and Fanconi anaemia related genes such as BRIP1, FANCM, FANCA, and FANCG [9,10]. DSB repair/HRR-deficient tumours are ideal candidates for poly(ADP-ribose) polymerase (PARP) inhibition therapy, as these tumours are more dependent on DNA single-strand break (SSB) repair, where PARP1 is an important player [11,12]. PARP1 is accountable for the detection and initiation of SSB repair through the synthesis of poly(ADP-ribose) (PAR) chains, which acts as a signal for other DNA-repair proteins [5,13,14]. If PAR-synthesis and subsequent DNA repair is impaired by PARP inhibition, SSBs are converted to DSBs that eventually lead to DSB repair by HRR, non-homologous end-joining or cell death in DSB repair deficient cells (synthetic lethality).

Pre-treatment with the PARP1 inhibitor olaparib, in combination with RT, has been shown to inhibit cell growth and DSB repair in several cell lines in vitro, including medulloblastoma, ependymoma, HGG, glioblastoma and DMG [15,16]. The potential radiosensitising effect has also been validated in in vivo models of lung, breast, glioblastoma, and pancreatic cancers [17–20]. Moreover, several clinical trials have been performed to validate this combined therapy effect [21–23]. To date, clinical trials involving PARP inhibition in combination with RT for primary brain tumours and metastases have not yet proven to be effective [24–27].

Delivery of radiosensitisers within the brain is complicated by the BBB, which prevents 98% of all small molecule and nearly 100% of the large molecules to cross and remain in the brain parenchyma [28–30]. To facilitate delivery of radiosensitisers across the BBB, focused ultrasound mediated blood-brain barrier opening (FUS-BBBO) has been suggested for local drug delivery. FUS-BBBO uses low frequency ultrasound waves to cause stable cavitation of intravenously injected microbubbles (MBs), resulting in BBB opening (BBBO) [31]. Mechanical interaction of MBs with the BBB temporarily cause the dislocation of tight junctions between endothelial cells and increased transcytosis, thereby enhancing permeability into the brain parenchyma [32,33]. Furthermore, BBB drug transporters are also thought to be affected by FUS-BBBO [34]. In vivo, FUS-BBBO has been shown to increase the concentration of molecules into the brain parenchyma by up to fifty-fold [35–37]. So far, FUS-BBBO with stable cavitation has displayed little to no side-effects and lasts for 4-24 hours (h), after which BBB function is restored [38,39].

The primary goal of this study was to investigate if FUS-BBBO enhances olaparib concentration in the brain, and when given in concert with RT inhibits tumour growth and prolongs survival of a xenograft DMG tumour model. In this study we therefore evaluated the radiosensitising effects of olaparib in two patient-derived DMG cell lines in vitro, as well as the extravasation of olaparib into the pons by FUS-BBBO in vivo. In vivo-like pharmacokinetic (pK) profiles were applied to DMG neurosphere cultures in vitro to assess radiosensitisation before potential benefit of this combination therapy was validated in a patient-derived xenograft (PDX) tumour model.

Materials and methods

Cell lines and culture

HSJD-DIPG-007 and HSJD-DIPG-011 DIPG cells were obtained from the University of

Barcelona and were grown as suspension cultures in 1:1 Neurobasal-A and Advanced DMEM/F-12 medium containing working concentrations of 10 mM HEPES buffer, 1 × MEM non-essential amino acids, 1% GlutaMAX, 1 mM Sodium pyruvate, 1 × B-27 minus vitamin-A, 10 ng/ml PDGF-AA, 10ng/ml PDGF-BB (all from ThermoFisher, USA), 20 ng/ml bFGF, 20 ng/ml EGF (Princess Maxima Center pharmacy), 2 µg/ml heparin (StemCell Technologies, Germany) and 1 mg/ml primocin (InvivoGen, USA). KNS42 glioma cells were obtained from Xenotech (IFO50356) and were grown as adherent cultures in DMEM/F-12 supplemented with 10% heat-inactivated foetal bovine serum (FBS, ThermoFisher) and penicillin/streptomycin. Cell lines were maintained at a constant temperature of 37 °C and 5% CO2 and a humidity of 95%, with media changes every 3-4 days. For in vivo PDX mouse models, HSJD-DIPG-007 cells were chosen for grafting into male hosts as they are a well characterised cell line derived from the brainstem/pons of a male paediatric patient (Accession: CVCL_VU70), whereas HSJD-DIPG-011 cells are derived from a female paediatric patient [40]. HSJD-DIPG-007 cells were transduced to express firefly luciferase following a previously described protocol [41], enabling in vivo tumour growth monitoring through bioluminescence imaging (BLI). Briefly, HEK293T cells were transfected with Polyethylenimine (PEI) using an envelope plasmid (pHDMG (ENV)), packing plasmids (pHDMG-Hgpm2, pRC/CMV-Rev1b, pHDM-Tat1b) and a transfer plasmid (eGFP-ffLuc_epHIV7) for lentiviral plasmid production. HSJD-DIPG-007 cells were then infected, and eGFP-lucF-gene positive cells were sorted using a Sony SH800 Cell Sorter (Sony, Japan).

Animals

For pharmacokinetic profiling and safety of the FUS-BBBO/olaparib combination, 6-12-week-old naïve female athymic nude Foxn1-/- mice (n=25, Charles River, France) were used. For PDX survival studies, 5–6-week-old male athymic nude Foxn1-/- mice (n=42, Envigo, France) were used. Mice were housed under pathogen-free conditions in individually ventilated cages in groups up to five and maintained on standard laboratory food and water ad libitum, with a fixed 12-hour (h) light/dark cycle in compliance with ARRIVE guidelines [42]. For the purposes of this study, gender dimension was considered to be partly relevant. Although a recent study assessing the effects of mouse gender on tumorigenicity, xenograft growth and drug response in a large panel of PDX models of paediatric brain tumours demonstrated that mouse gender did not significantly impact measurable outcomes [43], recent studies have shown that olaparib pharmacokinetics in rats is gender-dependent, with low clearance, long half-life, high plasma exposure and high viability seen in female rats compared to males. As our study wanted to show that olaparib extravasation can be achieved with FUS-BBBO, female animals were selected for the pharmacokinetic profiling phase [44,45]. For PDX studies, male hosts were used in order to sex-match donor cells, which were derived from the brainstem/pons of a male paediatric patient [40].

Drugs and contrast agents

For in vitro experiments, a 10 mM stock solution of olaparib (434.46 Da, AZD-2281, MedChemExpress, Sweden) was prepared in dymethylsulfoxide (DMSO). For in vivo studies, olaparib was prepared with 3% DMSO and 10% (2-Hydroxypropyl)-β-cyclodextrin in phosphate buffered saline (PBS) at 5 mg/ml before i.p. injection. Pre- and post-surgical pain

was managed with carprofen p.o. (67 µg/ml in drinking water, Faculty of Veterinary Medicine pharmacy, Utrecht, Netherlands) and s.c. injection (5 mg/kg), lidocaine (s.c., 0.5%, B. Braun, Germany) and buprenorphine hydrochloride (s.c., 0.05 mg/kg, Temgesic, Schering-Plough, Netherlands). Surgical anaesthesia was with Isoflurane mixed with air (3% for induction, 1.8% for maintenance, 2 L/min O2). Anaesthesia for irradiation was induced with dexmedetomidine (s.c., 50 µg/kg in 0.9% saline, Orion Pharma, UK) and reversed with atipamezole hydrochloride (s.c., 13.3 mg/kg, Alzane, Laboratorios Syva, Spain). D-luciferin Potassium Salt (i.p., 150 mg/kg, in PBS, Cayman Chemical, Netherlands) was used for monitoring engrafted cells. Blood coagulation was prevented with heparin (50 UI/kg, Leo Pharmaceuticals, Netherlands). A 4% v/v Evans blue solution (filtered, in PBS, Sigma Aldrich, Netherlands) was used to assess BBB integrity. Euthanasia was performed using 10:1 Ketamine:Sedazine (7.14 mg/ml and 0.714 mg/ml respectively, in PBS, Alfasan and AST Farma, Netherlands).

Cell viability

For viability analysis, HSJD-DIPG-007 and -011 cells were seeded in triplicate in black, clear bottom 96 well culture plates (Corning, USA) at a density of 2500 cells/well in normal culture conditions as described above. Cultures underwent a 30 minutes (min) exposure of vehicle or olaparib (0.01-3 µM concentration range) before irradiation with 0-4 Gy using a benchtop cell irradiator (1.66 Gy/min, 130 kV, 5.0 mA, Cellrad, Precision, USA), after which they were maintained with constant drug exposure for 72 h, in accordance with previous studies that have established 72 hours as optimal screening duration for in vitro oncolytic compounds in 3-dimensional cultures [46,47]. Cell viability was then determined using the CellTiter-Glo® 3D Cell Viability Assay (Promega, USA) according to the manufacturers' instructions, and the resulting luminescence signal was measured using a Spectramax iD3 plate reader (Molecular Devices, USA).

Clonogenic survival

To assess clonogenic survival, the soft agar method was used as previously described [4]. Briefly, a 0.33% agar suspension containing HSJD-DIPG-007 and -011 single cells was plated over a 0.5% agar underlay in 24 well plates, at a density of 800-6400 cells/well. Cells were pre-treated with vehicle or olaparib (0.1-1 µM) 30 min before irradiation (0-2 Gy) as described above. Cultures were maintained for 10-14 days with constant drug exposure under normal culture conditions after which colony growth was assessed using a Thiazolyl Blue Tetrazolium Blue (MTT) assay (Sigma-Aldrich). Surviving fractions were calculated based on the colonies times the plating efficacy. The plating efficacy was calculated by colonies divided by cell seeding as previously described [48].

Neurosphere growth

For neurosphere growth assays, HSJD-DIPG-007 and -011 were plated as single cells in low attachment, U-bottom 96 well culture plates (400 cells/well, BRANDplates®, Sigma-Aldrich) and neurospheres were allowed to form for 4 days before being exposed short-term (2h) to either 0.68 or 1.36 µM olaparib, or long-term (72 h) to either 0.018 or 0.036 µM olaparib, after which they were transferred to drug-free medium. At 30 min after initial exposure to

olaparib, neurospheres received 1.8 Gy radiation fractions/day for 5 consecutive days (9 Gy total). Non-irradiated exposed cells served as control, and cultures were maintained up to 28 days. Growth was monitored with a Leica DMi1 microscope (Leica Biosystems, Netherlands) and size was quantified by ImageJ [49].

Western blot

For western blot analysis of PARP1, PAR and β-actin protein expression, cells were plated in normal culture conditions as described above as single cells and allowed to acclimatise for 24 h, after which a 6 h treatment with olaparib ranging from 1 to 5 µM, with or without 1.8 Gy radiation was performed. Non-treated, irradiated cells were used as controls. Following treatment, HSJD-DIPG-007 and -011 cells were collected, pelleted, and lysed with ice cold RIPA lysis buffer (ThermoFisher) containing Halt protease and phosphatase inhibitors (1:100, Bio-Rad, USA). For adherent KNS42 cultures, cells were washed twice with PBS before ice cold RIPA buffer was directly added to the culture flasks, after which the cells were dislodged using a cell scraper. Cell suspensions were then transferred to pre-cooled microcentrifuge tubes and centrifuged at 4 oC for 30 min at maximum speed. The protein containing supernatant was transferred to a new tube and kept on ice. Protein concentrations were determined using a Pierce BCA Protein Assay Kit (ThermoFisher) as per manufacturers' instructions. Lysates of equal protein concentrations were separated using 10% SDS-PAGE, followed by electrotransfer to PVDF membranes using the Trans-Blot® Turbo™ transfer system (all from Bio-Rad). The membranes were then blocked with 5% non-fat dry milk (in 20 mM Tris, 137 mM NaCl, 0.1% Tween) for 1 h at room temperature before incubation overnight at 4 °C with either rabbit anti-PARP1 antibody (1:500, #9542, Cell Signaling Technology, USA), rabbit anti-PAR antibody (1:500, #4336-BPC-100, Trevigen, USA), or mouse anti-β-actin antibody (1:5000, #A5441, Sigma-Aldrich). Membranes were then washed and incubated with an appropriate swine anti-rabbit or rabbit anti-mouse horseradish peroxidase (HRP) conjugated secondary antibody (1:500, #P021702-2 or #P016102-2, IgG, Agilent Dako, USA) for 1 h at room temperature. Protein bands were detected using enhanced chemiluminescence (Bio-Rad) and expression was quantified using ImageJ [49].

BBBO by FUS and olaparib pK values

The procedure for image-guided MB mediated FUS-BBBO using an in-house stereotactic platform has been previously described in detail [50]. To manage acute perioperative pain, mice (n=25) were administered with 0.05 mg/kg buprenorphine via i.p. injection 15 min before anaesthesia with isoflurane. Once sedated, a 26-gauge catheter (Neoflon, Bectom Dickinson, Sweden) was placed in the lateral tail vein and flushed with heparin to prevent blood coagulation. Mice were then mounted on a custom-made platform and secured in place with ear bars. X-ray imaging for transducer guiding/targeting was performed with the In-Vivo Xtreme™ optical imaging system (Bruker, Germany). Mice were then placed onto the stereotactic platform and a hydrophone (Precision Acoustics, United Kingdom) was positioned behind the left ear of the animal to monitor scattered cavitation signal. A connection with an ultrasonic mono-element focused transducer was made with ultrasound gel. MBs (60 µl, SonoVue, Bracco, Amsterdam) [51] were administered through the tail vein

catheter, and FUS was initiated at 1 MHz, with 1.6 Hz pulse repetition frequency (PRF) and 400 kPa pressure, in a hexagonal pattern of 10 millisecond tone bursts, with a second boli of MBs administered at 60 seconds from the start of FUS-BBBO (total duration of 120 seconds).

Depending on group, mice underwent FUS-BBBO exposure as described above before receiving either 10 or 100 mg/kg olaparib immediately following the procedure via i.p. in 4 sub-injections at 5 min intervals. Mice were then sacrificed after 15, 30, 45 and 120 min after drug administration. Before sacrifice, Evans blue was injected i.p. to assess BBB permeability. Mice were then deeply sedated with ketamine/sedazine after which blood was collected via cardiac puncture after which animals were transcardially perfused with 50 ml saline. Brain tissue, organs, muscle, and blood/plasma were collected and stored at -80 °C for histological or liquid chromatography–mass spectrometry (LC-MS/MS) analysis. The experimental design is outlined in figure 1 A.

Survival analysis upon RT and olaparib extravasation in a PDX model

Inoculation of HSJD-DIPG-007 xenografts have been previously described [52]. In brief, 24 h before and after intracranial injection, mice received 0.067 mg/ml carprofen p.o. in drinking water. 30 min pre-surgery, mice also received a s.c. injection of 5 mg/kg carprofen for acute perioperative pain management. Mice were then anaesthetised with isoflurane and fixed in a stereotactic frame. Once immobile, a 5 mm long incision was made along the midline, after which a burr hole was drilled into the skull 0.8 mm posterior and 1.0 mm lateral to the lambda using a high-speed drill. A 5 µl Hamilton syringe fitted with a 26-gauge needle was then used to inject 5 µl of PBS containing 5 × 105 eGFP-lucF-HSJD-DIPG-007 cells at a depth of 4.5 mm, at a rate of 2 µl/min. After injection, the needle was kept in place for 7 min before being slowly extracted as a measure to prevent cells accumulating into the needle track. The wound was closed using topical skin adhesive (Histoacryl, B. Brand, Germany), and the animals were transferred under a heating lamp and allowed to awaken, while signs of distress and post-operative complications were closely monitored. Mouse weight was monitored 3 times/week, while tumour grafting was confirmed, and progression monitored, through BLI twice a week until humane euthanasia endpoints were reached. The human euthanasia endpoints were determined based on 20% weight loss from the beginning of the treatment, 15% weight loss in two days or showing symptoms related to neurological deficiencies. One animal in group 2 died prematurely before treatment, and one animal in group 6 died during FUS-BBBO procedure. Mice were anaesthetised with isoflurane and injected (i.p.) with 150 mg/kg D-luciferin before BLI signal detection using the MILABS U-OI system (MILABS, Netherlands). Three BLI scans were performed at 5, 10 and 15 min after D-luciferin injection (60 second exposure time). BLI data was analysed using customized software in MATLAB (MATLAB version R2020a) to determine BLI signal intensity by verification of the highest signal measured. After death/sacrifice, brains were extracted and fixed in 10% formalin (Sigma-Aldrich) for histological analysis.

Based on BLI signal, at 21 days after intracranial implantation, mice were evenly distributed in 6 groups (n=7): 1) control, 2) olaparib, 3) RT, 4) FUS-BBBO+olaparib, 5) FUS+RT, 6) FUS-BBBO+olaparib+RT. Group 1 (control) received 0.9% saline i.p. injections for 5 consecutive days. Groups 2, 4, 5, and 6 underwent MB mediated FUS treatment on days 1 and 4. Groups

3, 5, and 6 underwent daily cranial radiation of 1.8 Gy in a small-animal irradiator (whole head, 200 kV, 4.0 mA, Yxlon International AS, Denmark) for 5 consecutive days, following identically adjusted conditions used for in vitro radiation analyses. Groups 2, 4, and 6 received 100 mg/kg olaparib via i.p. injection for 5 consecutive days. When treatments were combined, olaparib was given immediately after FUS with 4 sub-injections at 5 min intervals (at time 0, 5, 10 and 15 min). Thirty minutes after FUS and/or 15 min after the last sub-injection of olaparib, RT was given. The experimental design is outlined in figure 1B.

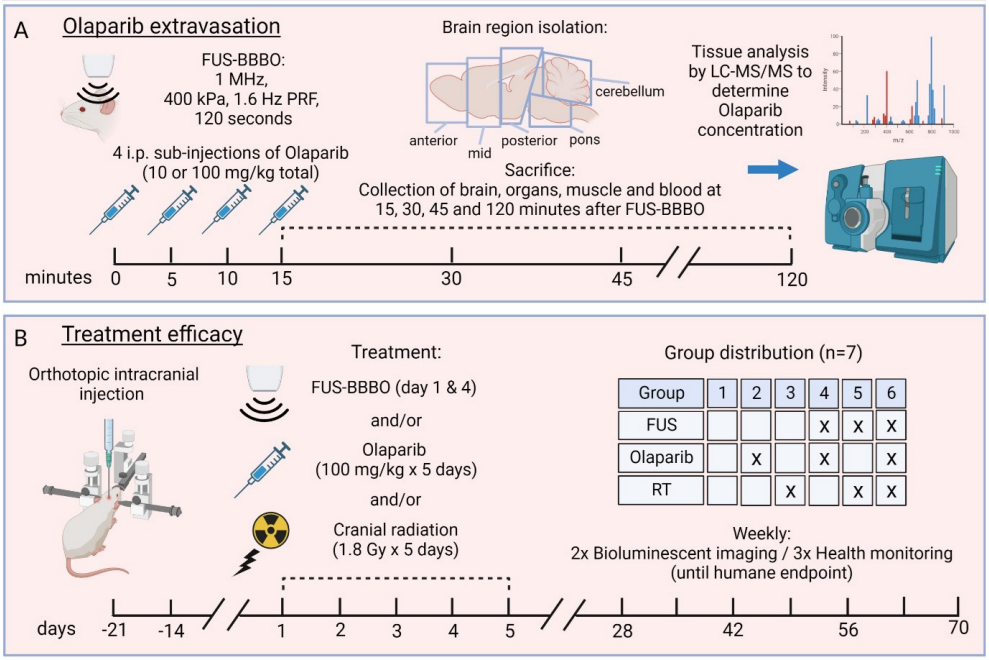

Figure 1: Experimental design of olaparib extravasation via FUS-BBBO and subsequent assessment of treatment efficacy in combination with radiotherapy. (A) Outline of pharmacokinetic profiling of olaparib following FUS-BBBO. A total of 10 or 100 mg/kg olaparib was administered within 15 min following FUS-BBBO, after which tissue samples (brain, organs, muscle, blood) were collected at 15-, 30-, 45-, and 120-min post administration to determine olaparib concentration by LC-MS/MS analysis. (B) Outline of treatment efficacy to determine radiosensitising effects of olaparib in combination with radiotherapy and FUS-BBBO in a DMG PDX mouse model using 100 mg/kg olaparib per day for 5 days. Tumour growth was monitored with bioluminescent imaging until humane endpoints were reached.

Liquid chromatography–mass spectrometry (LC-MS/MS)

Collected blood was centrifuged at 1500 g for 15 min at 4 oC, and the resulting plasma phase was stored at -20 oC until analysed. Following exsanguination, whole brain, heart, lung, liver, kidney, spleen and left hindleg muscle were rapidly removed, weighed, and stored at -80 oC until processed. Before analysis, tissues were homogenized in an appropriate volume of control human lithium heparin plasma (Bioreclamations LLC, USA) using a FastPrep-24TM 5G Grinder (MP Biomedicals, USA) and stored at -20 oC until analysed.

Olaparib concentrations in plasma and tissue homogenates were analysed using a

previously reported and validated liquid-chromatography mass spectrometry (LC-MS/MS) method [53]. Validation of the assay on mouse tissue was performed by spiking brain homogenate with olaparib at a final concentration of 400 ng/ml before analysis on a human lithium heparin plasma calibration curve. The intra-run accuracy and precision were -6.8% and 5.2% respectively, and within the required ±15% according to FDA and EMA guidelines [54,55]. For quantification, 10 µl mouse plasma was added to 90 µl lithium heparin plasma. The limit of detection was set to 0.3 ng/ml (limit of quantification range 1 ng/ml – 5000 ng/ml). Total concentration measured by LC-MS/MS are free and protein-bound fractions of olaparib.

Histological analysis

To determine histopathological elements, tumour size, location and proliferation, haematoxylin and eosin (H&E) and human vimentin staining was performed as previously described [56]. Following euthanasia and perfusion, brains were excised and fixed in 10% formalin before embedding in paraffin, after which 4µm sagittal sections were made using a microtome (Leica Biosystems) and mounted onto glass cover slides. Sections were deparaffinised before use and underwent antigen retrieval in sodium citrate buffer (10 mM, 95-100 °C, 30 min) before staining for human vimentin. Endogenous peroxidase activity was quenched by immersing the slides in 3% hydrogen peroxide (in PBS) for 20 min, followed by two rinses in deionised water and one rinse in PBS-Tween. Sections were then blocked using antibody diluent clear (VWRKBD09-125, VWR, USA) for 1 h at room temperature before incubation with rabbit anti-human vimentin [SP20] (1:5, ab27608, Abcam, England) overnight at 4 oC. Sections were then washed and incubated with a biotinylated affinity-purified goat anti-rabbit secondary antibody (1:500, BA-1000, IgG (H+L), Vector Laboratories, USA) for 2h at room temperature. Following secondary antibody incubation, VECTASTAIN® Elite ABC-HRP Peroxidase (PK-6100, Vector Laboratories) was applied for 2 h, followed by a 3 min incubation in 3,3'-diaminobenzidine (DAB, K346711-2, Agilent Dako). Sections were then counterstained with haematoxylin, dehydrated in a graded series of alcohol, immersed in xylene, and mounted using Permount™ mounting medium (ThermoFisher).

Data processing and statistical analysis

Western blots, cell viability and clonogenic assays were statistically verified using a two-way ANOVA. Extravasation of olaparib was analysed using the Mann-Whitney U test. Survival was analysed using a Kaplan-Meier and Log-rank test. A p-value of ≤ 0.05 was considered statistically significant. The statistical analyses were performed using GraphPad Prism (version 9, GraphPad Software, LLC, USA).

Results

***In vitro* radiosensitisation of DMG cells by PARP1 inhibition**

Western blot showed that HSJD-DIPG-007 and -011 (DMG) cells display higher PARP1, but lower PAR activity than KNS42 (glioma) cells (figure 2 A, C, E), which was further increased following 1.8 Gy radiation (figure 2 B, D, F). Radiation alone elevated PARP1 expression by

2.34- and 1.95-fold in HSJD-DIPG-007 and -011, respectively, and 2.55-fold in KNS42, and was not affected by the addition of olaparib (figure 2 C, D). Radiation alone elevated PAR expression by 7.42- and 6.42-fold the DMG and 3.04-fold in glioma cells but was significantly inhibited when combined with olaparib in all three cells lines (figure 2 E, F).

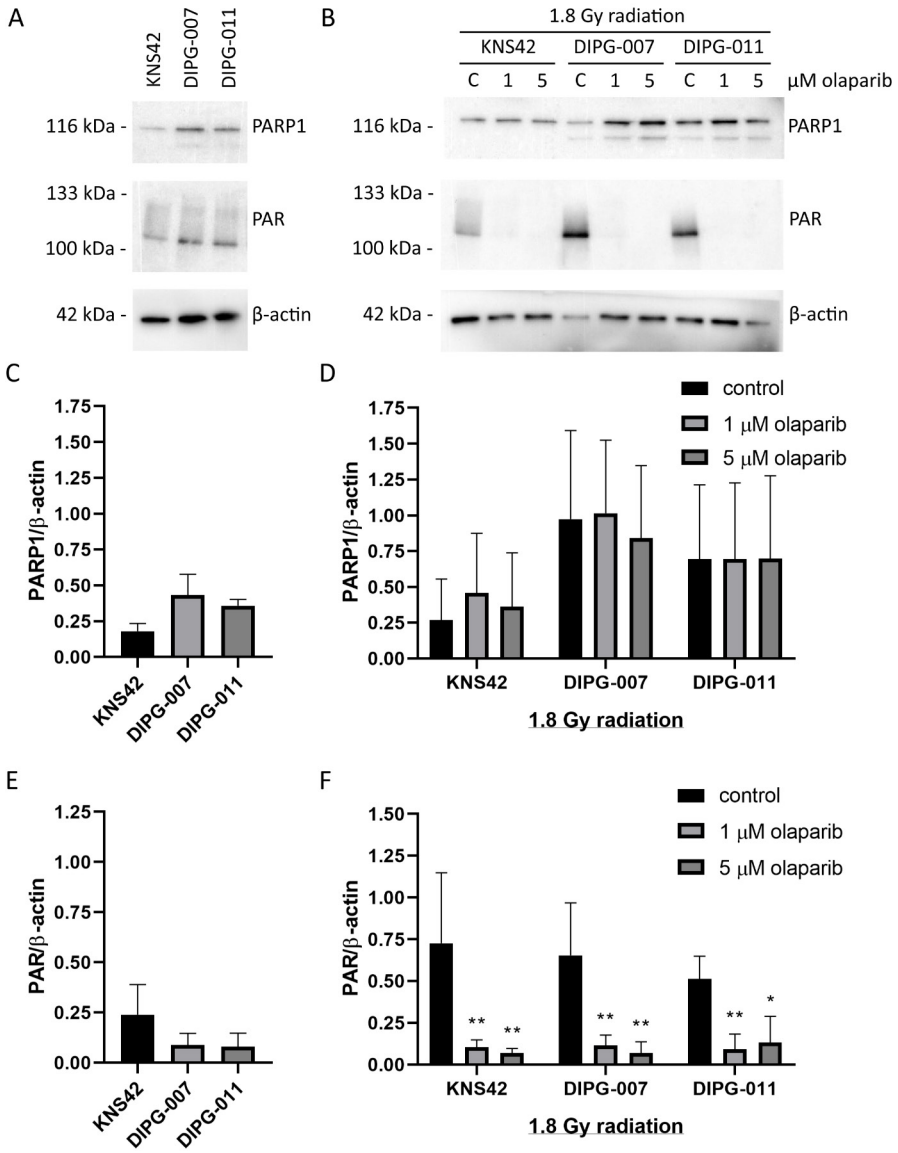

Figure 2: PARP1 and PAR expression in glioma and DIPG cell lines. Western blot analysis of KNS42, HSJD-DIPG-007 and HSJD-DIPG-011 cell lines showing intrinsic expression levels of PARP1 and PAR in untreated, non-irradiated cells (A) and after 6h treatment with or without 1 or 5 μM olaparib and 1.8 Gy radiation, showing inhibition of PAR-synthesis upon treatment with olaparib (B). Densitometry data of WB analysis showing PARP1 levels in untreated cells (C) and following olaparib/radiation treatment (D). Densitometry data of WB analysis showing PAR levels in untreated cells (E) and following olaparib/radiation treatment (F). Data points are expressed as mean ± SD (n=3), *p<0.05, **p<0.01.

Cell exposure to olaparib as a single treatment modality showed that HSJD-DIPG-007 and -011 have similar cell viability sensitivity to olaparib with a 50% inhibitory concentration (IC50) of 3.4 and 4.1 µM respectively (data not shown). Pre-treatment 30 min before 1.8 Gy radiation demonstrated radiosensitising effects of olaparib through a decrease in cell viability compared to control cells, where HSJD-DIPG-007 was more sensitive to the combination treatment, while HSJD-DIPG-011 was more affected by radiation alone (figure 3 A, B). Clonogenic capacities were also reduced with the combination treatment in both DIPG cell lines (figure 3 C, D).

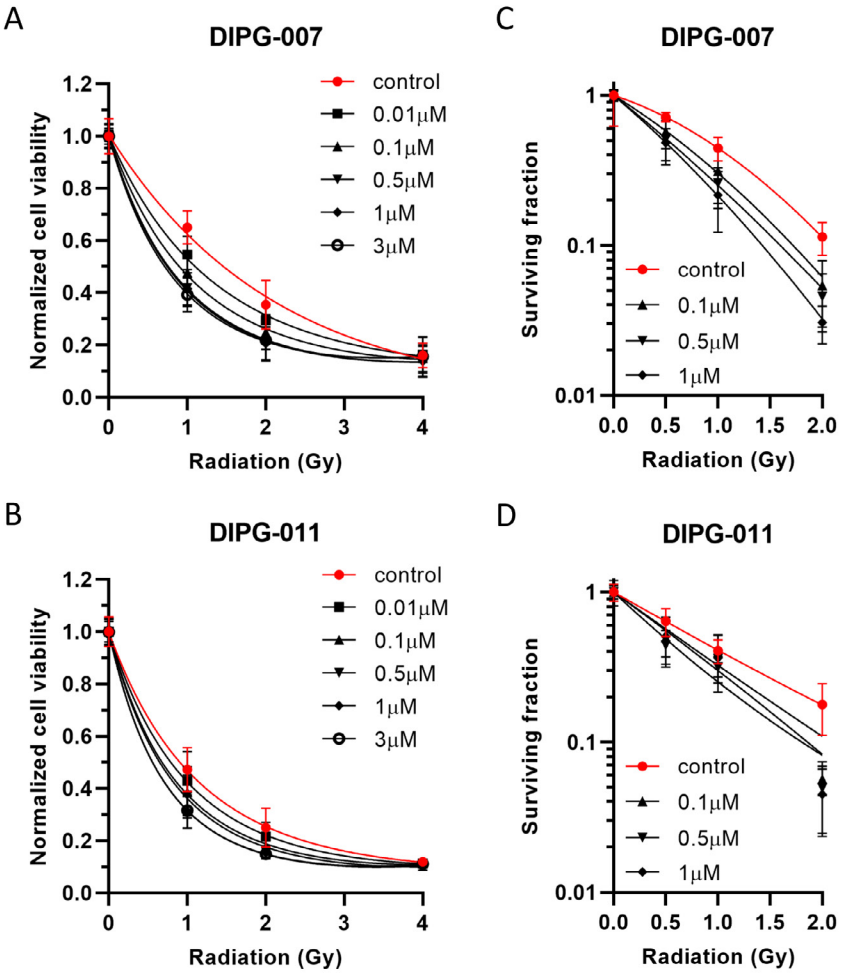

Figure 3: Cell viability and clonogenic survival of DIPG cell lines. Viability of HSJD-DIPG-007 (A) and HSJD-DIPG-011 (B) cells 72 h following 0-4 Gy radiation alone or in combination with a 30 min pre-treatment of 0.01-3 µM olaparib, showing a viability reduction in both cell lines. Significant differences were found in all treatment groups (except 0.01 µM) at 1.0 and 2.0 Gy ($p<0.05$). Clonogenic capacities were reduced in HSJD-DIPG-007 (C) and HSJD-DIPG-011 (D) cells 10-14 days after 0-2 Gy radiation alone or in combination with a 30 min pre-treatment of 0.1-1 µM olaparib. Significant differences were found at all treatments (except 0.1 µM) in at 0.5 and 1.0 Gy in HSJD-DIPG-007, and only at 0.5 Gy in HSJD-DIPG-011 ($p<0.05$). Normalised data points are expressed as mean ± SD (n=3).

FUS-BBBO and local olaparib extravasation in the pons

Based on radiosensitisation properties of olaparib in vitro, extravasation of 10 mg/kg olaparib after FUS-BBBO was investigated. Stable cavitation in the vicinity of the pons was monitored via passive cavitation detection (figure S1), with effective BBBO observed through extravasation of Evans blue (figure 4 A). A significant increase of olaparib was observed in the pons (5.36-fold) and cerebellum (3.18-fold) 30 min after injection combined with FUS-BBBO, while no elevation was observed in the posterior, middle and anterior cerebrum based on the blood/tissue ratio at that time point (figure 4 B). Based on total concentration, a significant difference in the pons and cerebellum after FUS-BBBO was observed, with no apparent increase in other brain regions or tissues examined (figure S2 A, B). Pharmacokinetic profiling of olaparib in blood, following administration of 10 mg/kg i.p., showed a Cmax of 1978±446.75 ng/mL (4.55 µM), a Tmax of 30 min, an area under the curve (AUC) of 1833.11 ng.g-1.h (4.22 µM.h), and a T1/2 of 15.05 min. Pharmacokinetic profiling of olaparib in the pons with FUS-BBBO showed a Cmax of 149.38±84.19 ng/g (0.34 µM) tissue, a Tmax of 30 min, an AUC of 151.64 ng.g-1.h (0.35 µM.h), and a T1/2 of 15.34 min (figure 4 C, D). When 100 mg/kg of olaparib was administered in combination with FUS-BBBO, compared to 10 mg/kg, an 11.88-fold (54.09 µM) increase in blood concentration was observed, with only a 4.04-fold increase in the pons (Cmax of 603.2±179.68 ng/g tissue, equating to 1.39 µM) (figure 4 E, F). Dose-related neurotoxicity of 100 mg/kg olaparib in combination with FUS-BBBO was not observed within 24 h of administration (data not shown).

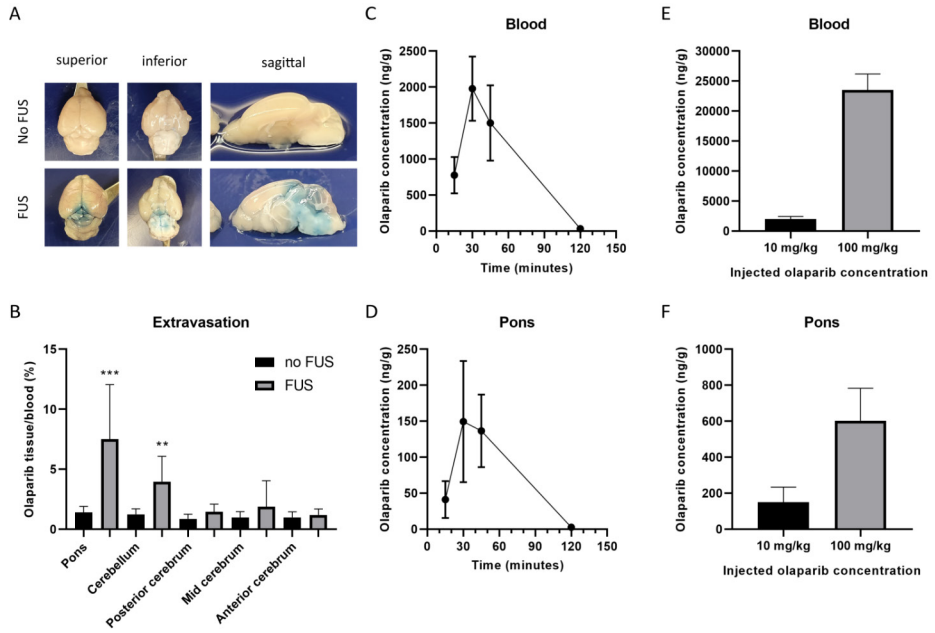

Figure 4: FUS-BBBO, local extravasation of olaparib and pK value determination. (A) Evans blue extravasation with or without FUS-BBBO in the pontine region. (B) Blood/tissue ratios of olaparib administered alone or 30 min after FUS-BBBO showed a significant increase in the pons (5.36-fold) and cerebellum (3.18-fold), while no significant elevations were observed in the posterior, middle and anterior cerebrum. Measurements at 15-, 30-, 45-, and 120

min post olaparib administration (10 mg/kg) following FUS-BBBO revealed a Cmax of 1978.75 ± 446.7 5ng/g (4.55 µM) olaparib in blood (C) and 149.38 ± 84.19 ng/g in the pons (0.34 µM) (D), and a Tmax of 30 min was found in both blood and pons. Following FUS-BBBO and administration of 10 mg/kg or 100 mg/kg of olaparib, an 11.88-fold increase (23500 ng/g ±2687, 54.09 µM) in Cmax was observed in blood (E), while a 4.04-fold increase (603 ng/g ±179.68, 1.39 µM) in Cmax was observed in the pons (F). Data points are expressed as mean ± SD. **p<0.01, ***p<0.001.

Pharmacokinetics parameters upon FUS-BBBO decreases in vitro neurosphere growth

The pK profiles of olaparib extravasation with FUS-BBBO were used to mimic conditions in vitro using a neurosphere growth assay. Based on pK profiling (100 mg/kg), a potential in vivo-tissue AUC of 1.41 µM.h olaparib (4.04-fold increase of 10 mg/kg AUC) was predicted. To test olaparib potency, AUCs of 1.3 and 2.6 µM.h were investigated at short (2 h) or prolonged (72 h) exposure times in combination with RT. Treatment with 9 Gy (5x1.8 Gy) radiation alone delayed HSJD-DIPG-007 and -011 neurosphere growth by 14-18 days (figure 5 A, B). While no differences were observed in HSJD-DIPG-007, radiation with prolonged exposure to low olaparib concentrations delayed neurosphere regrowth more efficiently than short exposure to high concentration in HSJD-DIPG-011, despite a comparable AUC (figure 5 C, D).

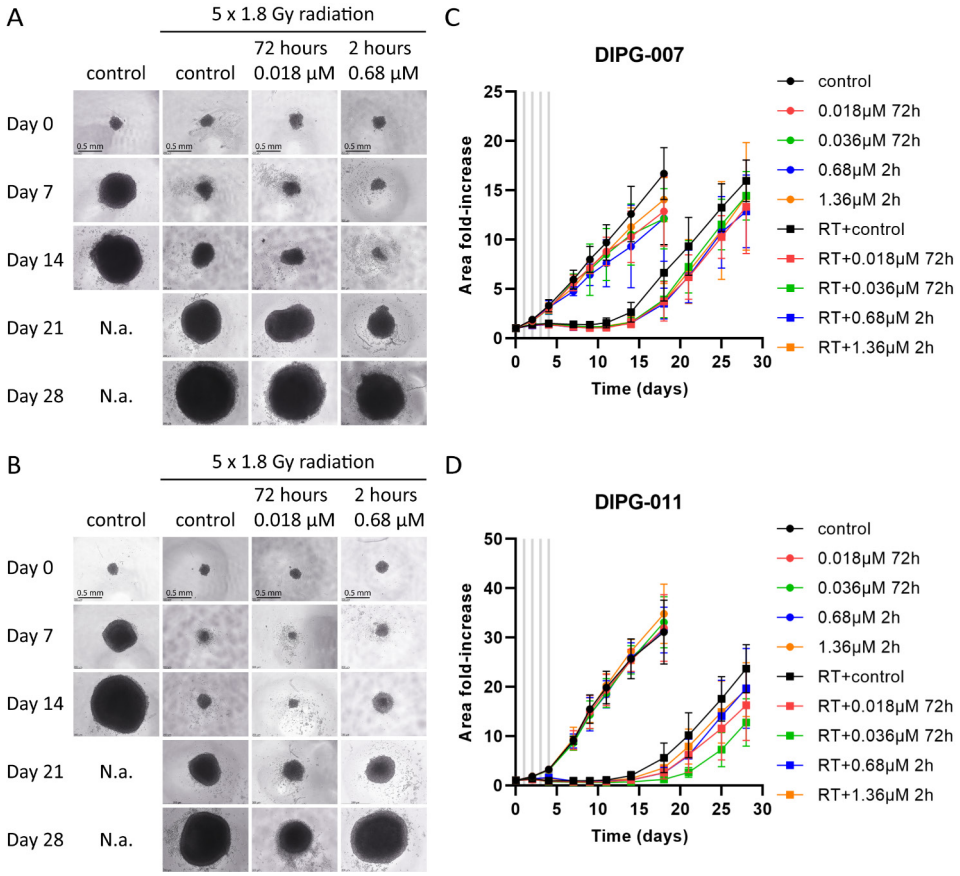

Figure 5: Neurosphere radiosensitisation based on in vivo pK values. Daily dose of 1.8 Gy fractionated radiation (9 Gy total) delayed neurosphere growth by 14 days in both HSJD-DIPG-07 (A) and HSJD-DIPG-011 (B). Both short (2 h) and prolonged exposure (72 h) of varying olaparib concentrations extended regrowth delay in HSJD-DIPG-007 (C) and HSJD-DIPG-011 (D) in a dose/time dependant manner. Neurosphere growth was monitored until 18- or 28-days post radiation/olaparib treatment until spheres outgrew the imaging field and were too large to assess. Significant differences were found in all treatment groups with RT and olaparib compared to RT alone after 18 days of treatment for HSJD-DIPG-007 (except for 0.036 µM on day 21, 25 and 28 and 1.36 µM on day 28) and HSJD-DIPG-011 (except for 0.018 µM on day 18, 0.68 µM on day 18, and 1.36 µM on day 18, 21 and 25) ($p<0.05$).

Treatment efficacy upon FUS-BBBO olaparib extravasation and RT in a PDX model

Next, efficacy of olaparib and radiation was assessed in vivo using a HSJD-DIPG-007 PDX mouse model, 21 days post intracranial injection. Although no survival benefit was observed between groups (figure 6 A), local BLI signal in the pons did indicate tumour growth delay in animals treated with RT, irrespective of any other treatment paradigm (figure 6 B, C). Vimentin staining showed observable differences between groups. Metastatic formations were present in the olfactory bulbs of 45% of all animals, while primary pontine tumour growth was delayed in RT, and interestingly more so in fully (FUS-BBBO/olaparib/RT) treated animals (figure 6 D). No visible histological differences between groups were observed in olfactory bulbs and pons, based on H&E staining (figure S3).

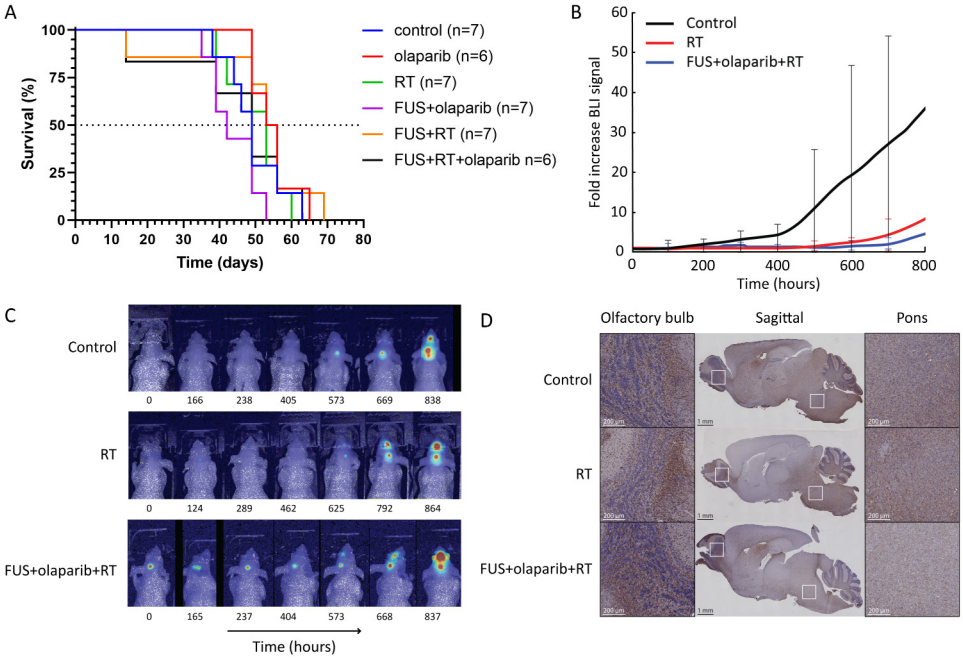

Figure 6: Survival and tumour growth efficacy upon FUS-BBBO, olaparib and RT. (A) Kaplan-Meier curve showing overall survival following therapy. No significant difference between groups was observed. (B) Tumour growth suppression was observed between control, RT only, and full combination (FUS-BBBO/olaparib/RT) groups at 33 days post treatment in the pons. (C) BLI monitoring of tumour development revealed disease dissemination in control, radiated, and olaparib treated animals. (D) Human vimentin positive cells within the pons and olfactory bulbs of animals showing extensive tumour progression. Fully treated mice (FUS-BBBO/olaparib/RT) had a lower tumour burden within the pons compared to all other groups.

Discussion

DMG remains one of the most lethal paediatric tumours, with no curative efficacy of current treatment options. Previous studies have shown that PARP inhibition, in combination with radiation, is efficacious both in vitro and in vivo [57], and that FUS-BBBO can effectively disrupt the BBB to facilitate drug delivery [58]. This study's main goal was to investigate if enhanced delivery of PARP inhibitors via FUS-BBBO can, when combined with RT, improve therapeutic response in a DMG PDX model. We investigated the hypotheses that (I) elevated PARP expression in DMG cells represents potential therapeutic targets, (II) FUS-BBBO qualitatively improves the transport of olaparib across the BBB into the brain parenchyma, (III) in vivo realistic pK values in combination with RT can be mimicked in vitro with a potential therapeutic benefit, and (IV) olaparib extravasation by FUS-BBBO is potentially beneficial in xenograft model when combined with RT.

Our in vitro findings in DMG cell lines confirm previously reported elevated levels of PARP expression [12,15,16], and showed that inhibition of PAR-synthesis by olaparib significantly enhances radiosensitisation. To assess tolerability, we used in vivo pK profiling to establish the bioavailability of olaparib in healthy brain parenchyma with and without enhanced delivery via FUS-BBBO. Our data indicates that 100mg/kg of olaparib is well tolerated in mice, and that FUS-BBBO promotes an influx of olaparib in the brain without deleterious side effects, as similarly reported [33,49]. Several research groups have previously shown that increased local bioavailability of drugs in the parenchyma can be achieved through FUS-BBBO [35,36,59,60]. In our study, local FUS-enhanced extravasation accomplished a 5.36-fold increase of olaparib in the pons, based on the blood/tissue ratio. In recent years, besides olaparib, multiple PARP inhibitors have been developed of which several have been approved for clinical use [57,61]. Compared to olaparib, niraparib and pamiparib have improved BBB penetration properties, while talazoparib has a better binding efficacy [62–64]. However, due to the lack of good comparative studies, it is unknown to what extent the effectiveness of each PARP inhibitor is. The advantage of FUS-BBBO is local drug delivery, while a BBB permeable drug extravasates into the whole brain, thus losing its regional specificity and potentially increasing neurotoxicity.

In vivo bioavailability results were translated for in vitro testing, where we found that inhibition of PAR-synthesis by olaparib in combination with RT lead to acute radiosensitisation as well as delayed proliferation post treatment, observed by limited neurosphere re-growth. Although the degree of PAR-synthesis inhibition can depend on the cell line, this effect was also observed with olaparib doses well below IC50 values in both DMG cell lines. From a therapeutic perspective, these results suggest that this treatment strategy could lead to both a reduction in required RT dose, as well as delay of tumour growth progression post therapy. The observation that neurosphere growth delay was similar after both 2 h and 72 h incubations with olaparib in the HSJD-DIPG-007 cell line could suggest that there is a therapeutic window of opportunity within the short period in which FUS-BBBO can be exploited to deliver drugs to the brain parenchyma.

To qualitatively validate if this observation could be exploited in vivo, we assessed this treatment combination in a PDX animal model. RT was applied 30 min after olaparib

administration, which corresponds to the Tmax and Cmax observed upon pK profiling. Although no survival benefit was observed following treatment, several insights into the potential of this treatment strategy were gained. In both groups where RT alone was applied, a significant reduction in local tumour growth was seen, confirming our in vitro observations. When RT was combined with FUS-BBBO and olaparib, a further reduction in local tumour growth, albeit non-significant, confirmed that the radiosensitisation effect we saw in vitro was reproducible in vivo. This shows that the approach of utilising FUS-BBBO to deliver drugs over a short period of time is feasible. Subsequently, multiple potential radiosensitizers proven to be effective in vitro for the treatment of DMG are now also eligible for in vivo testing.

Although some positive observations were made, several factors contributed to the lack of therapeutic efficacy in the study. For example, in the PDX model used, rapid disease progression was observed across all groups, with most animals surviving only 40 days post treatment due to severe weight loss, possibly arising from diminished appetite. Indeed, by 33 days post-treatment, widespread disease was observed throughout the brain, including formation of secondary foci. We found severe metastases formations in the olfactory bulbs of the animals, which could explain the equal survival times across all groups, despite substantially different overall local tumour burden, as a factor of anosmia induced fasting [65]. Olaparib has also been reported to suppress appetite [44], which could additionally contribute to reduced food intake in mice with anosmia. Treatment of animals was initiated 21 days post inoculation of tumour cells, which could be too late for a local therapeutic intervention such as FUS-BBBO to have an effect, due to the presence of locally invasive and metastatic disease [66]. Further studies to assess optimal treatment initiation time, with consideration of treating metastatic areas such as the olfactory bulbs using FUS-BBBO, as well as technical factors such as feasibility in continued FUS-BBBO application, need to be conducted to optimise therapeutic applications of FUS-BBBO in animal models of DMG.

In conclusion, this study has shown that PARP1 inhibition is a promising radiosensitisation strategy for DMG. FUS-BBBO could temporarily enhance olaparib delivery into the brain at clinically relevant values, supported by in vitro growth inhibition of DMG cells exposed to olaparib and radiation. Further preclinical studies are needed to determine optimal start of treatment and dosing regimen, as well as timing of FUS-BBBO with improved survival benefit.

Acknowledgements

This project was supported by KWF Young Investigator Award (KWF 10911, Dr. D.G. van Vuurden). The authors thank Dr. Angel Montero Carcaboso (Barcelona) for kindly providing the patient derived DMG cell lines. We also thank Dr. Wissam Beaino for hosting the experiments at the Radionuclide Center (Department of Radiology and Nuclear Medicine, Amsterdam University Medical Center, Amsterdam, Netherlands), Luc Lucas for his technical expertise in LC-MS/MS (Bioanalytical Laboratory of the Pharmacy, Netherlands Cancer Institute, Amsterdam, Netherlands) and Prof. Jan Molenaar for providing plasmids (Princes Máxima Center for Pediatric Oncology, Utrecht, Netherlands). Graphical abstract and figure 1 created with BioRender.com

References

[1] Louis DN, Perry A, Reifenberger G, von Deimling A, Figarella-Branger D, Cavenee WK, et al. The 2016 World Health Organization Classification of Tumors of the Central Nervous System: a summary. Acta Neuropathol 2016;131:803–20. https://doi.org/10.1007/s00401-016-1545-1.

[2] Hargrave D, Bartels U, Bouffet E. Diffuse brainstem glioma in children: critical review of clinical trials. Lancet Oncol 2006;7:241–8. https://doi.org/10.1016/S1470-2045(06)70615-5.

[3] Hoffman LM, Veldhuijzen van Zanten SEM, Colditz N, Baugh J, Chaney B, Hoffmann M, et al. Clinical, radiologic, pathologic, and molecular characteristics of long-term survivors of diffuse intrinsic pontine glioma (DIPG): a collaborative report from the international and european society for pediatric oncology DIPG registries. J Clin Oncol 2018;36:1963–72. https://doi.org/10.1200/JCO.2017.75.9308.

[4] Jansen MH, Veldhuijzen van Zanten SE, Sanchez Aliaga E, Heymans MW, Warmuth-Metz M, Hargrave D, et al. Survival prediction model of children with diffuse intrinsic pontine glioma based on clinical and radiological criteria. Neuro Oncol 2015;17:160–6. https://doi.org/10.1093/neuonc/nou104.

[5] Stupp R, Hegi ME, Mason WP, van den Bent MJ, Taphoorn MJB, Janzer RC, et al. Effects of radiotherapy with concomitant and adjuvant temozolomide versus radiotherapy alone on survival in glioblastoma in a randomised phase III study: 5-year analysis of the EORTC-NCIC trial. Lancet Oncol 2009;10:459–66. https://doi.org/10.1016/S1470-2045(09)70025-7.

[6] Lassman LP, Arjona VE. Pontine gliomas of childhood. Lancet (London, England) 1967;1:913–5. https://doi.org/10.1016/s0140-6736(67)91485-7.

[7] Ataç MS, Blaauw G. Radiotherapy in brain-stem gliomas in children. Clin Neurol Neurosurg 1979;81:281-IN11. https://doi.org/https://doi.org/10.1016/0303-8467(79)90032-5.

[8] Warren KE. Beyond the blood-brain barrier: the importance of central nervous system (CNS) pharmacokinetics for the treatment of CNS tumors, including diffuse intrinsic pontine glioma. Front Oncol 2018;8:239. https://doi.org/10.3389/fonc.2018.00239.

[9] Mackay A, Burford A, Carvalho D, Izquierdo E, Fazal-Salom J, Taylor KR, et al. Integrated Molecular Meta-Analysis of 1,000 Pediatric High-Grade and Diffuse Intrinsic Pontine Glioma. Cancer Cell 2017;32:520-537.e5. https://doi.org/10.1016/j.ccell.2017.08.017.

[10] Pedersen H, Schmiegelow K, Hamerlik P. Radio-Resistance and DNA Repair in Pediatric Diffuse Midline Gliomas. Cancers (Basel) 2020;12. https://doi.org/10.3390/cancers12102813.

[11] Ashworth A. A Synthetic Lethal Therapeutic Approach: Poly(ADP) Ribose Polymerase Inhibitors for the Treatment of Cancers Deficient in DNA Double-Strand Break Repair. J Clin Oncol 2008;26:3785–90. https://doi.org/10.1200/JCO.2008.16.0812.

[12] Zarghooni M, Bartels U, Lee E, Buczkowicz P, Morrison A, Huang A, et al. Whole-genome profiling of pediatric diffuse intrinsic pontine gliomas highlights platelet-derived growth factor receptor alpha and poly (ADP-ribose) polymerase as potential therapeutic targets. J Clin Oncol Off J Am Soc Clin Oncol 2010;28:1337–44. https://doi.org/10.1200/JCO.2009.25.5463.

[13] Ostrom QT, Gittleman H, Fulop J, Liu M, Blanda R, Kromer C, et al. CBTRUS Statistical Report: Primary Brain and Central Nervous System Tumors Diagnosed in the United States in 2008-2012. Neuro Oncol 2015;17 Suppl 4:iv1–62. https://doi.org/10.1093/neuonc/nov189.

[14] Ray Chaudhuri A, Nussenzweig A. The multifaceted roles of PARP1 in DNA repair and chromatin remodelling. Nat Rev Mol Cell Biol 2017;18:610–21. https://doi.org/10.1038/nrm.2017.53.

[15] van Vuurden DG, Hulleman E, Meijer OLM, Wedekind LE, Kool M, Witt H, et al. PARP inhibition sensitizes childhood high grade glioma, medulloblastoma and ependymoma to radiation. Oncotarget 2011;2:984–96. https://doi.org/10.18632/oncotarget.362.

[16] Chornenkyy Y, Agnihotri S, Yu M, Buczkowicz P, Rakopoulos P, Golbourn B, et al. Poly-ADP-Ribose Polymerase as a Therapeutic Target in Pediatric Diffuse Intrinsic Pontine Glioma and Pediatric High-Grade Astrocytoma. Mol Cancer Ther 2015;14:2560–8. https://doi.org/10.1158/1535-7163.MCT-15-0282.

[17] Senra JM, Telfer BA, Cherry KE, McCrudden CM, Hirst DG, O'Connor MJ, et al. Inhibition of PARP-1 by olaparib (AZD2281) increases the radiosensitivity of a lung tumor xenograft. Mol Cancer Ther 2011;10:1949–58. https://doi.org/10.1158/1535-7163.MCT-11-0278.

[18] Jannetti SA, Carlucci G, Carney B, Kossatz S, Shenker L, Carter LM, et al. PARP-1-Targeted Radiotherapy in Mouse Models of Glioblastoma. J Nucl Med 2018;59:1225–33. https://doi.org/10.2967/jnumed.117.205054.

[19] Waissi W, Nicol A, Jung M, Rousseau M, Jarnet D, Noel G, et al. Radiosensitizing Pancreatic Cancer with PARP Inhibitor and Gemcitabine: An In Vivo and a Whole-Transcriptome Analysis after Proton or Photon Irradiation. Cancers (Basel) 2021;13. https://doi.org/10.3390/cancers13030527.

[20] Michmerhuizen AR, Pesch AM, Moubadder L, Chandler BC, Wilder-Romans K, Cameron M, et al. PARP1 Inhibition Radiosensitizes Models of Inflammatory Breast Cancer to Ionizing Radiation. Mol Cancer Ther 2019;18:2063–73. https://doi.org/10.1158/1535-7163.MCT-19-0520.

[21] Robson M, Im S-A, Senkus E, Xu B, Domchek SM, Masuda N, et al. Olaparib for Metastatic Breast Cancer in Patients with a Germline BRCA Mutation. N Engl J Med 2017;377:523–33. https://doi.org/10.1056/NEJMoa1706450.

[22] de Haan R, van Werkhoven E, van den Heuvel MM, Peulen HMU, Sonke GS, Elkhuizen P, et al. Study protocols of three parallel phase 1 trials combining radical radiotherapy with the PARP inhibitor olaparib. BMC Cancer 2019;19:901. https://doi.org/10.1186/s12885-019-6121-3.

[23] Loap P, Loirat D, Berger F, Ricci F, Vincent-Salomon A, Ezzili C, et al. Combination of Olaparib and Radiation Therapy for Triple Negative Breast Cancer: Preliminary Results of the RADIOPARP Phase 1 Trial. Int J Radiat Oncol Biol Phys 2021;109:436–40. https://doi.org/10.1016/j.ijrobp.2020.09.032.

[24] Mehta MP, Curran WJ, Wang D, Wang F, Kleinberg L, Brade A, et al. Phase I Safety and Pharmacokinetic (PK) Study of Veliparib in Combination With Whole Brain Radiation Therapy (WBRT) in Patients (pts) With Brain Metastases. Int J Radiat Oncol 2012;84:S269–70. https://doi.org/https://doi.org/10.1016/j.ijrobp.2012.07.702.

[25] Chabot P, Hsia T-C, Ryu J-S, Gorbunova V, Belda-Iniesta C, Ball D, et al. Veliparib in combination with whole-brain radiation therapy for patients with brain metastases from non-small cell lung cancer: results of a randomized, global, placebo-controlled study. J Neurooncol 2017;131:105–15. https://doi.org/10.1007/s11060-016-2275-x.

[26] Baxter PA, Su JM, Onar-Thomas A, Billups CA, Li X-N, Poussaint TY, et al. A phase I/II study of veliparib (ABT-888) with radiation and temozolomide in newly diagnosed diffuse pontine glioma: a Pediatric Brain Tumor Consortium study. Neuro Oncol 2020;22:875–85. https://doi.org/10.1093/neuonc/noaa016.

[27] Sim H-W, McDonald KL, Lwin Z, Barnes EH, Rosenthal M, Foote MC, et al. A randomized phase II trial of veliparib, radiotherapy, and temozolomide in patients with unmethylated MGMT glioblastoma: the VERTU study. Neuro Oncol 2021;23:1736–49. https://doi.org/10.1093/neuonc/noab111.

[28] Sá-Pereira I, Brites D, Brito MA. Neurovascular unit: a focus on pericytes. Mol Neurobiol

2012;45:327–47. https://doi.org/10.1007/s12035-012-8244-2.

[29] Hawkins BT, Davis TP. The blood-brain barrier/neurovascular unit in health and disease. Pharmacol Rev 2005;57:173–85. https://doi.org/10.1124/pr.57.2.4.

[30] Pardridge WM. Blood-brain barrier delivery. Drug Discov Today 2007;12:54–61. https://doi.org/10.1016/j.drudis.2006.10.013.

[31] Burgess A, Shah K, Hough O, Hynynen K. Focused ultrasound-mediated drug delivery through the blood-brain barrier. Expert Rev Neurother 2015;15:477–91. https://doi.org/10.1586/14737175.2015.1028369.

[32] Sheikov N, McDannold N, Sharma S, Hynynen K. Effect of focused ultrasound applied with an ultrasound contrast agent on the tight junctional integrity of the brain microvascular endothelium. Ultrasound Med Biol 2008;34:1093–104. https://doi.org/10.1016/j.ultrasmedbio.2007.12.015.

[33] Sheikov N, McDannold N, Jolesz F, Zhang Y-Z, Tam K, Hynynen K. Brain arterioles show more active vesicular transport of blood-borne tracer molecules than capillaries and venules after focused ultrasound-evoked opening of the blood-brain barrier. Ultrasound Med Biol 2006;32:1399–409. https://doi.org/10.1016/j.ultrasmedbio.2006.05.015.

[34] Cho H, Lee H-Y, Han M, Choi J-R, Ahn S, Lee T, et al. Localized Down-regulation of P-glycoprotein by Focused Ultrasound and Microbubbles induced Blood-Brain Barrier Disruption in Rat Brain. Sci Rep 2016;6:31201. https://doi.org/10.1038/srep31201.

[35] Alli S, Figueiredo CA, Golbourn B, Sabha N, Wu MY, Bondoc A, et al. Brainstem blood brain barrier disruption using focused ultrasound: A demonstration of feasibility and enhanced doxorubicin delivery. J Control Release 2018;281:29–41. https://doi.org/10.1016/j.jconrel.2018.05.005.

[36] Sheikov N, McDannold N, Vykhodtseva N, Jolesz F, Hynynen K. Cellular mechanisms of the blood-brain barrier opening induced by ultrasound in presence of microbubbles. Ultrasound Med Biol 2004;30:979–89. https://doi.org/10.1016/j.ultrasmedbio.2004.04.010.

[37] Englander ZK, Wei H-J, Pouliopoulos AN, Bendau E, Upadhyayula P, Jan C-I, et al. Focused ultrasound mediated blood-brain barrier opening is safe and feasible in a murine pontine glioma model. Sci Rep 2021;11:6521. https://doi.org/10.1038/s41598-021-85180-y.

[38] Todd N, Zhang Y, Arcaro M, Becerra L, Borsook D, Livingstone M, et al. Focused ultrasound induced opening of the blood-brain barrier disrupts inter-hemispheric resting state functional connectivity in the rat brain. Neuroimage 2018;178:414–22. https://doi.org/10.1016/j.neuroimage.2018.05.063.

[39] Park J, Zhang Y, Vykhodtseva N, Jolesz FA, McDannold NJ. The kinetics of blood brain barrier permeability and targeted doxorubicin delivery into brain induced by focused ultrasound. J Control Release Off J Control Release Soc 2012;162:134–42. https://doi.org/10.1016/j.jconrel.2012.06.012.

[40] Bairoch A. The Cellosaurus, a Cell-Line Knowledge Resource. J Biomol Tech 2018;29:25–38. https://doi.org/10.7171/jbt.18-2902-002.

[41] Kholosy WM, Derieppe M, Ham F Van Den, Ober K, Su Y, Custers L, et al. Neuroblastoma and DIPG Organoid Coculture System for Personalized Assessment of Novel Anticancer Immunotherapies 2021.

[42] Kilkenny C, Browne WJ, Cuthill IC, Emerson M, Altman DG. Improving bioscience research reporting: the ARRIVE guidelines for reporting animal research. Osteoarthr Cartil 2012;20:256–60. https://doi.org/10.1016/j.joca.2012.02.010.

[43] Qi L, Kogiso M, Du Y, Zhang H, Braun FK, Huang Y, et al. Impact of SCID mouse gender on

tumorigenicity, xenograft growth and drug-response in a large panel of orthotopic PDX models of pediatric brain tumors. Cancer Lett 2020;493:197–206. https://doi.org/https://doi.org/10.1016/j.canlet.2020.08.035.

[44] Committee for Medicinal Products for Human Use (CHMP). CHMP assessment report Lynparza. London: 2014.

[45] Su G, Qin L, Su X, Tao C, Wei Y. Gender-dependent pharmacokinetics of olaparib in rats determined by ultra-high performance liquid chromatography/electrospray ionization tandem mass spectrometry. Biomed Chromatogr 2020;34:e4791. https://doi.org/10.1002/bmc.4791.

[46] Spina R, Voss DM, Asnaghi L, Sloan A, Bar EE. Flow Cytometry-based Drug Screening System for the Identification of Small Molecules That Promote Cellular Differentiation of Glioblastoma Stem Cells. J Vis Exp 2018. https://doi.org/10.3791/56176.

[47] Niepel M, Hafner M, Chung M, Sorger PK. Measuring Cancer Drug Sensitivity and Resistance in Cultured Cells. Curr Protoc Chem Biol 2017;9:55–74. https://doi.org/10.1002/cpch.21.

[48] Franken NAP, Rodermond HM, Stap J, Haveman J, van Bree C. Clonogenic assay of cells in vitro. Nat Protoc 2006;1:2315–9. https://doi.org/10.1038/nprot.2006.339.

[49] Schneider CA, Rasband WS, Eliceiri KW. NIH Image to ImageJ: 25 years of image analysis. Nat Methods 2012;9:671–5. https://doi.org/10.1038/nmeth.2089.

[50] Haumann R, 't Hart E, Derieppe MPP, Besse HC, Kaspers GJL, Hoving E, et al. A High-Throughput Image-Guided Stereotactic Neuronavigation and Focused Ultrasound System for Blood-Brain Barrier Opening in Rodents. J Vis Exp 2020. https://doi.org/10.3791/61269.

[51] Greis C. Technology overview: SonoVue (Bracco, Milan). Eur Radiol 2004;14 Suppl 8:P11-5.

[52] Jansen MHA, Lagerweij T, Sewing ACP, Vugts DJ, van Vuurden DG, Molthoff CFM, et al. Bevacizumab targeting diffuse intrinsic pontine glioma: results of 89Zr-Bevacizumab PET imaging in brain tumor models. Mol Cancer Ther 2016;15:2166–74. https://doi.org/10.1158/1535-7163.MCT-15-0558.

[53] Nijenhuis CM, Lucas L, Rosing H, Schellens JHM, Beijnen JH. Development and validation of a high-performance liquid chromatography-tandem mass spectrometry assay quantifying olaparib in human plasma. J Chromatogr B, Anal Technol Biomed Life Sci 2013;940:121–5. https://doi.org/10.1016/j.jchromb.2013.09.020.

[54] European Medicines Agency (EMA). Guideline on bioanalytical method validation. https://www.ema.europa.eu/en/documents/scientific-guideline/guideline-bioanalytical-method-validation_en.pdf. n.d.

[55] (FDA) UF and DA. Guidance for industry: bioanalytical method validation guidance for industry bioanalytical method validation. http://www.fda.gov/Drugs/GuidanceComplianceRegulatoryInformation/Guidances/default.htm. n.d.

[56] Haumann R, Bianco JI, Waranecki PM, Gaillard PJ, Storm G, Ries M, et al. Imaged-guided focused ultrasound in combination with various formulations of doxorubicin for the treatment of diffuse intrinsic pontine glioma. Transl Med Commun 2022;7:8. https://doi.org/10.1186/s41231-022-00115-7.

[57] Lesueur P, Chevalier F, Austry J-B, Waissi W, Burckel H, Noël G, et al. Poly-(ADP-ribose)-polymerase inhibitors as radiosensitizers: a systematic review of pre-clinical and clinical human studies. Oncotarget 2017;8:69105–24. https://doi.org/10.18632/oncotarget.19079.

[58] Gandhi K, Barzegar-Fallah A, Banstola A, Rizwan SB, Reynolds JNJ. Ultrasound-Mediated

Blood-Brain Barrier Disruption for Drug Delivery: A Systematic Review of Protocols, Efficacy, and Safety Outcomes from Preclinical and Clinical Studies. Pharmaceutics 2022;14. https://doi.org/10.3390/pharmaceutics14040833.

[59] Ishida J, Alli S, Bondoc A, Golbourn B, Sabha N, Mikloska K, et al. MRI-guided focused ultrasound enhances drug delivery in experimental diffuse intrinsic pontine glioma. J Control Release 2021;330:1034–45. https://doi.org/10.1016/j.jconrel.2020.11.010.

[60] Ye D, Zhang X, Yue Y, Raliya R, Biswas P, Taylor S, et al. Focused ultrasound combined with microbubble-mediated intranasal delivery of gold nanoclusters to the brain. J Control Release 2018;286:145–53. https://doi.org/10.1016/j.jconrel.2018.07.020.

[61] Menezes MCS, Raheem F, Mina L, Ernst B, Batalini F. PARP Inhibitors for Breast Cancer: Germline BRCA1/2 and Beyond. Cancers (Basel) 2022;14. https://doi.org/10.3390/cancers14174332.

[62] Sun K, Mikule K, Wang Z, Poon G, Vaidyanathan A, Smith G, et al. A comparative pharmacokinetic study of PARP inhibitors demonstrates favorable properties for niraparib efficacy in preclinical tumor models. Oncotarget 2018;9:37080–96. https://doi.org/10.18632/oncotarget.26354.

[63] Xiong Y, Guo Y, Liu Y, Wang H, Gong W, Liu Y, et al. Pamiparib is a potent and selective PARP inhibitor with unique potential for the treatment of brain tumor. Neoplasia 2020;22:431–40. https://doi.org/10.1016/j.neo.2020.06.009.

[64] Rudolph J, Jung K, Luger K. Inhibitors of PARP: Number crunching and structure gazing. Proc Natl Acad Sci 2022;119:e2121979119. https://doi.org/10.1073/pnas.2121979119.

[65] Ferris AM, Duffy VB. Effect of olfactory deficits on nutritional status. Does age predict persons at risk? Ann N Y Acad Sci 1989;561:113–23. https://doi.org/10.1111/j.1749-6632.1989.tb20975.x.

[66] ’t Hart E, Bianco J, Besse HC, Chin Joe Kie LA, Cornet L, Eikelenboom KL, et al. Towards Standardisation of a Diffuse Midline Glioma Patient-Derived Xenograft Mouse Model Based on Suspension Matrices for Preclinical Research. Biomedicines 2023;11. https://doi.org/10.3390/biomedicines11020527.

Supplementary data

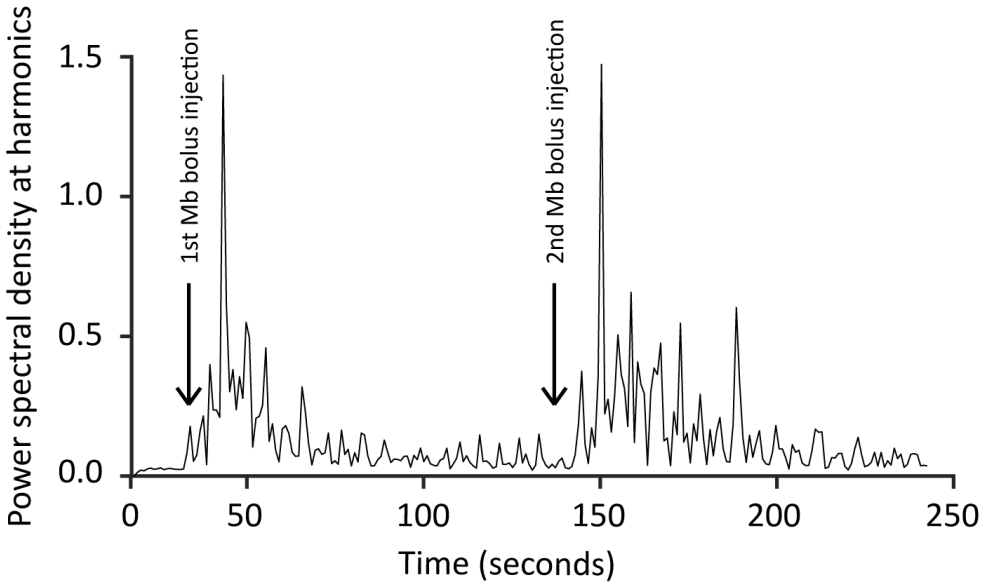

Supplementary figure 1: In vivo real time monitoring of microbubble cavitation based on the power spectral density at the harmonics. Enhanced signal immediately following each boli injection is indicated by arrows.

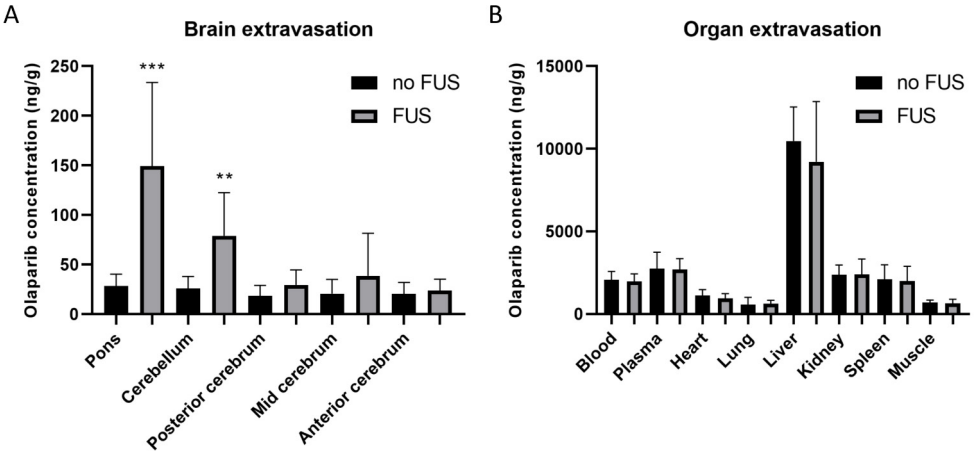

Supplementary figure 2: (A) 30min after FUS-BBBD a 5.23-fold (149.38ng/g ± 84.19 vs 28.54ng/g ± 11.87) increase in the pons, and 3.05-fold (79.01ng/g ± 43.58 vs 25.88ng/g ± 12.09) increase in the cerebellum were observed compared to no FUS treatment groups. (B), No changes of olaparib concentration in blood, plasma or organs were measured between mice with or without FUS-BBBD treatment. Data points are expressed as mean ± SD (n=7), **p<0.01, ***p<0.001

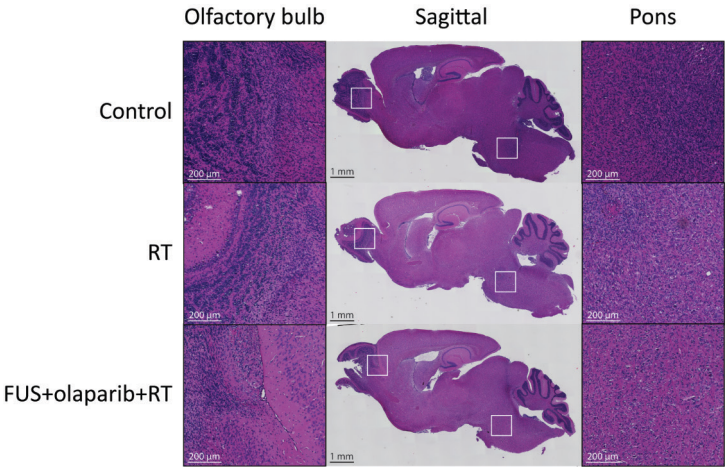

Supplementary figure 3: H&E tissue staining of control, radiated and olaparib treated animals. No apparent tissue damage was observed within the pons and olfactory bulb, which are the main locations for tumour growth as shown by human vimentin staining.


FOCUSED ULTRASOUND
DIFFUSE MIDLINE GLIOMA
RADIO-THERAPY
BLOOD BRAIN BARRIER
MOUSE MODEL
PhD
HELP

Chapter 6

General discussion and future prospects

Elvin ’t Hart[1]

1. Princess Máxima Center for Pediatric Oncology, Heidelberglaan 25, 3584 CS, Utrecht, The Netherlands

General discussion

Paediatric high-grade gliomas (pHGG), including their subtype diffuse midline gliomas H3K27-altered (DMG), are devastating brain tumours with a dismal survival [1,2]. DMG, previously also known as diffuse pontine gliomas (DIPG) when located in the pontine area, are paediatric brain tumours found in the midline regions of the brain (thalamus, spinal cord) and are predominantly seen in the pons [3]. Invasive growth of DMG into the pons impedes various vital functions resulting in severe clinical symptoms such as respiration and heart rate problems, disrupted eye movements, facial paresis, and impaired motor functions [4]. Despite the introduction of radiation and chemotherapeutic agents that has revolutionised treatment of other cancers, children's survival with DMG has only improved up to four months [5].

DMG is difficult to treat; surgery is practically impossible due to the unattainable location and invasive growth of the tumour, chemotherapy is limited due to intrinsic chemoresistance and the presence of the blood-brain barrier (BBB) and radiotherapy despite being the only treatment option is restricted by severe side-effects and the inevitable occurrence of resistance to radiotherapy[6,7]. However, with the introduction of microbubble mediated focused ultrasound BBB opening (FUS-BBBO) we now have means to improve drug delivery into the brain parenchyma and at the brain tumour site [8]. With this, better delivered medication that render cells more sensitive to radiation, in combination with radiotherapy might exert potentiating therapeutic effects beneficial to patients. Drugs that enhance the therapeutic effects of radiotherapy are also called radiosensitisers.

Although radiosensitization may be a promising therapeutic approach to synergize with radiotherapy, there is no conclusive evidence regarding its effectiveness for the treatment of DMG, therefore the aim of this thesis was to validate the treatment efficacy of radiosensitization by PARP inhibition in a DMG patient-derived xenograft (PDX) mouse model in combination with FUS-BBBO drug delivery. To answer this research question and since radiotherapy is still the current treatment modality for DMG, we first performed a systematic analysis of available literature to investigate the extent of BBBD properties of radiotherapy. Second, because FUS-BBBO creates the possibility for drug delivery in the pontine region, we investigated the safe usage of this technique in a mouse with various acoustic settings. Third, before examining the treatment efficacy of radiosensitization using FUS-BBBO, a DMG tumour model standardisation was performed of the commonly used HSJD-DIPG-007 PDX model elaborating the human disease progression. And finally, the possibility of drug delivery through FUS-BBBO and subsequent radiosensitization effectiveness in the DMG mouse model was examined.

Radiotherapy effects blood-brain barrier permeability

The current treatment regimen for children suffering of DMG is local fractionated radiotherapy which is often supplemented by concomitant and adjuvant administration of temozolomide, providing a temporary tumour reduction and clinical improvement, but with inevitable regrowth [9,10]. This tumour regrowth is a consequence of tumor cell survival after 54 Gy radiotherapy, likely partly caused by the upregulation of DNA-repair pathways

improving the survival of the cancerous cells, and the given radiation dose which is limited because of severe side-effects occurrence at higher cumulative doses. These radiation side-effects include cognitive deterioration, radiation necrosis but also BBB disruption [11,12]. The BBB, acting as a biological barrier in the blood vessels of the brain, tightly regulates the transport of substances into the brain parenchyma. Radiation-induced BBBD can cause increased permeability with unregulated exposure of the brain to medication, waste products and pathogens leading to neurological disorders [13–15]. Even though increased BBB permeability by radiotherapy is generally acknowledged, it remained unclear how and to what extent radiation schemes influenced it, which might be crucial for patients' safety and their treatment. Therefore in **chapter 2** a systematic review and meta-analysis of all available relevant pre-clinical and clinical studies was performed to investigate the effect of conventional photon radiation on BBB permeability [16]. Based on the qualitative analysis of clinical and preclinical studies an increase of BBB permeability upon radiotherapy was observed, which was significantly confirmed with a meta-analysis of the pre-clinical data. The differences observed between the clinical and preclinical studies regarding radiation increased BBB permeability can be partly explained by the used detection methods and study designs. More research is needed to ascertain acute and chronic BBB opening and the extent thereof, in patients and animal models during radiotherapy, using MR studies and/or PET-studies.

Increased BBB permeability may also have a clinical benefit due an increased drug concentration in the diseased part of the brain. This increase of chemotherapeutics can offer an alternative treatment option for DMG because radiation is restricted due to brain tissue sensitivity. However, to prevent adverse effects, it is important that the increase of drugs in the brain can be done locally and safely within a controlled environment to prevent neurotoxicity.

Focused ultrasound blood-brain barrier disruption

Different techniques are available to circumvent the BBB and deliver drugs into the brain such as intranasal delivery, intra-arterial delivery, nanoparticles, and convention enhanced delivery (CED) [22]. However, due to non-specificity, limitation of deliverable volumes and concentration, invasiveness by catheter insertion into brain tissue, , FUS-BBBO is an interesting approach for drug delivery into the brain, as it allows for non-invasive and dynamic, potentially repetitive targeting of different brain regions.

. With FUS-BBBO, intravenously injected microbubbles cavitate under the influence of locally applied ultrasound waves, causing a mechanical force on the blood vessel walls. This mechanical force causes the disruption of the tight junctions that connect the endothelial cells, resulting in an increased brain permeability. However, the increased brain permeability is temporary because the tight junctions between the endothelial cells recover overtime. Due to the temporary and local increased brain permeability, there is a clinical potential of FUS-BBBO. The clinical applicability of FUS-BBB may also apply for DMG, where it might increase the therapeutic efficiency [17,18]. Before the technique can be applied clinically, extensive preclinical research is required. In order to conduct this extensive preclinical research, we designed and described in **chapter 3** a stereotactic small animal FUS

platform [19]. With the use of this in-house designed top down stereotactic FUS platform, we achieved safe and local BBBO in the pontine region of mice. Local and safe BBBO was monitored in real-time by the detection of the microbubble cavitation with the integrated cavitation detector. Currently, in in vivo FUS-BBBO research, a variety of FUS-BBBO systems and designs are in use. Most preclinical FUS-BBBO systems are combined with MRI. The downside of MRI-image guided FUS-BBBO is that it is a time consuming and expensive technique with the need of experience personal [20,21]. Also, MRI systems are not always available for researchers, while extensive pre-clinical FUS-BBBO research is needed to investigate the clinical potential for the treatment of DMG or any other brain related disease. Because of this, we designed our stereotactic platform for use of X-ray or BLI for image targeting. Extensive, high throughput and cost-effective pre-clinical FUS-BBBO research is herewith possible. X-ray and BLI are low-cost image modalities and our FUS-BBBO system is adaptable and can be redesigned based on the research question and animal model of each study for relatively inexperienced researchers.

Besides the possibility for drug delivery in neuro-oncology, FUS-BBBO has shown treatment potential for various brain disorders, such as Alzheimer's disease, Parkinson's disease, and amyotrophic lateral sclerosis. Following up, various clinical trials involving these disorders have been performed confirming the safety of FUS-BBBO [23]. However, before FUS-BBBO can be used for clinical efficacy studies in delicate brain areas such as the pons, preclinical research is needed to determine treatment potency and toxicity of each individual drug candidate delivered by FUS-BBBO. To improve treatment potency translation of preclinical research, it is crucial to have animal DMG models reflecting accurately the human disease situation.

A diffuse midline glioma patient-derived xenograft mouse model standardisation

The development of DMG genetically engineered mouse models and PDXs reflecting the human disease situation enables research to explore the disease characteristics, progression and test new therapeutic options [24]. In vitro drug screenings for DMG have shown potential chemotherapeutics that can now be given and delivered into the brain parenchyma using FUS-BBBO. To preclinically test these chemotherapeutics in combination with FUS-BBBO, it is important to have an DMG animal model reflecting the human disease. The HSJD-DIPG-007 DMG PDX is commonly used animal model with an intact BBB and invasive growth mimicking the human pathology. However, the protocol to establish the HSJD-DIPG-007 DMG PDX model was not previously standardised complicating comparisons in between studies, thus potentiating different experimental outcomes. To characterise and standardise the HSJD-DIPG-007 DMG PDX model, we provided in **chapter 4** a literature overview of available protocols and performed intracranial tumour implantation with cells in two different suspension matrices to differentiate tumour growth [25]. Based on our literature review, we observed various protocols used to establish the HSJD-DIPG-007 DMG PDX model with diversities in cell suspension matrix, injection volume, injection of cell concentration and location. We observed that Matrigel as cell suspension matrix reduced metastases formation. Importantly, we also found individual tumour cells to be present at distant brain regions, as a 'contamination' following tumour cell inoculation. Despite the observation of metastatic occurrence, the disease progression and tumour growth of the

HSJD-DIPG-007 DMG PDX model is still clinical comparable due to the resemblance of brain parenchyma invasion and vascular proliferation

The clinical comparability of the HSJD-DIPG-007 DMG PDX, as well as any DMG mouse model is important for any clinical translation of potential future treatment modalities. Experimental outcome comparison and subsequent clinical translation is very complicated due to the use of diverse HSJD-DIPG-007 DMG PDX model establishment protocols. Because of this, protocol diversity, location and tumour growth may differ between studies. In addition, inter-study outcome comparability is furthermore compromised by treatment schedule variability, started between 0- and 80-days after different numbers of tumour cell inoculation. Our results indicate that in the time period between 0- and 80-days perivascular cell migration is present with consequently metastatic formations which can affect treatment outcome. Although, we do now suggest using Matrigel as cell suspension matrix and initiate treatment within 1-2 weeks after engraftment, further standardisation of the HSJD-DIPG-007 DMG PDX model needs to be performed regarding animal host, cell concentration and injection volume. With regards to the heterogenetic mutation diversity of DMG found in the clinic, the HSJD-DIPG-007 DMG PDX model is limited, as it only displays a H3.3 point mutation with mutations of PPMD1D, ACVR1 and PIK3CA, whereas in the clinic upt to 80% of all DMG cases harbour a TP53 mutation, among other common mutations such as PDGFRA, MYC and MAPK1 [26–28]. Besides the diverse mutation profiles of DMG between patients, multiple mutations are also commonly found within the tumour itself, complicating its treatment. This emphasises the need for multiple DMG models with different mutations profiles to test the efficacy of treatment modalities.

With exception for radiotherapy, no other treatment modality is currently as effective for the treatment of DMG. Because radiotherapy is effective and the standard treatment modality for DMG, it is worth to investigate to enhance its effect in the interest of the patients. It has subsequently been proven that radiotherapy can be more effective for multiple cancer types with the use of radiosensitizers [29]. Radiosensitizer effectivity for the treatment of DMG has not been shown yet due to the presence of the BBB and tumour location. However, FUS-BBBO can increase radiosensitizer concentration in the brain parenchyma, which might favour effective DMG treatment.

PARP1 inhibition for the radiosensitization of Diffuse Midline Glioma through Focused Ultrasound

Depending on the mechanism of action, radiosensitizers can be divided in multiple subtypes including the inhibition of DNA repair mechanisms. These DNA repair mechanisms are upregulated upon the induction of base damages, single stand breaks and double strand breaks of the DNA due to radiotherapy [30]. Single strand break repair relies on its detection by PARP1 and the synthesis of PAR, which in turn recruits DNA repair proteins [31]. If PARP1 and the synthesis of PAR is inhibited, cancerous cells are not able to repair their single strand breaks after radiotherapy properly, with possible cell death as consequence. PARP1 inhibition by olaparib in combination with radiotherapy has proven to be effective, because of its radiosensitization properties observed in vitro and in vivo studies with clinical application [32–37]. However, it is unknown whether PARP1 inhibition in combination with

radiotherapy has a therapeutic and clinical effect for the treatment of DMG, especially due to the presents of the BBB. To validate the radiosensitization properties of PARP1 inhibition for DMG treatment, we presented in **chapter 5** the pharmacological data of olaparib extravasation into the pons following FUS-BBBO and its therapeutic effects in vitro and in vivo with the HSJD-DIPG-007 DMG PDX mouse model [38]. We observed in vitro the radiosensitisation effects of olaparib by the inhibition of PARP1 activity and the reduction of cell viability, clonogenic capabilities and neurosphere growth of DMG cell lines. In vivo we observed that FUS-BBBO increases the concentration of olaparib in the pontine region of mice, but that no treatment efficacy could be achieved in combination with radiotherapy due to pharmacokinetic limitations of olaparib.. Further preclinical studies are needed to optimize pharmacokinetic properties of olaparib in the context of FUS-BBBO delivery to the brain, for therapeutic radiosensitization of DMG in combination with radiotherapy. This means that an optimal dose and timing needs to be found, that aligns with the opening of the BBB after FUS, to yield time- and dose-wise efficient local tissue drug concentrations of Olaparib or other radiosensitizers.

Although no survival benefit was observed, it has been proven through real-time microbubble cavitation monitoring, post-mortem Evans blue extravasation analyses and LC-MS/MS tissue analyses that FUS-BBBO enables successful olaparib delivery into the pontine region of mice. Drug delivery of olaparib upon FUS-BBBO is comparable to other drug studies that have evidenced increased extravasation of temozolomide, bevacizumab, carboplatin, etoposide, erlotinib and doxorubicin up to a fifty-fold compared to the control groups [39–44], although most studies focus on increase of tissue-Cmax and not tissue-AUC. Despite changing brain dynamics with the extravasation of 100 mg/kg olaparib upon FUS-BBBO and a 0.4 mechanical index , no unusual behaviour was observed confirming literature that stable cavitation has little to no side-effects with the reinstallation of the BBB [45,46]. FUS-BBBO causes brain dynamic changes through the disruption of the tight junction cohesion of the BBB, while ABC-transporters in the endothelial cells of the brain are still present and active. The activity of these ABC-transporters and subsequently affinity for each drug determine its degree of extravasation after FUS-BBBO [47]. Although olaparib is an ABC-transport substrate, FUS-BBBO causes sufficient permeabilisation for a significant, and temporal, concentration elevation in the pons of mice. Besides the extravasation of olaparib which has a molecular weight of 435.1 Da, FUS-BBBO also offers the opportunity for drug delivery with a substantial higher mass. Because of their high molecular mass and no ABC-transport affinity, these molecules can be extravasated through tight junction disruption by FUS-BBBO and remain in the brain parenchyma with potential beneficial effects. Bevacizumab is an anti-VEGF antibody with a molecular weight of 149 kDa which has proven to be able to extravasated with FUS-BBBO into the brain with observed treatment efficacy in a glioblastoma mouse model [42].

Although FUS-BBBO momentarily increases the concentration of olaparib in the pons, due to a short half-life it is no longer present in the mouse two hours after administration. This reduced exposure time, limited BBBD upon FUS, and competitive PARP1 binding of olaparib limits the possible synergetic effect with radiotherapy [48]. An additional variation is that these mice had a tumour implantation with PBS as suspension matrix with the control group having a median survival of 49 days, increasing the risk of metastases. Afterall in **chapter 4**

we observed metastases formation in the olfactory bulb and spine with a median free survival of 33 and 47 days. These metastases can decrease the condition of mice by less food intake and increased discomfort explaining the non-detected efficacy despite local tumour growth in the pontine region.

Future perspectives

Despite intensive research, there are still no good treatment methods available for DMG, resulting in a short-life expectancy of the patients. To ensure that the foundation for future FUS-BBBO and DMG treatment research laid out in this thesis can lead to an improved prognosis of patients, more preclinical research and subsequent validation is needed. Additional future research can emerge from the conclusions of each chapter, including the improvement of radiotherapy effectiveness, understanding the biological effects of FUS-BBBO, further standardisation of pre-clinical DMG model, and pharmacokinetics optimisation for improved treatment success and clinical translation.

(Epi)genetic alterations as targets to improve radiotherapy effectiveness

Radiotherapy remains the standard treatment option for DMG. Although radiotherapy initially reduces the tumour and temporarily stalls its progression, inevitable tumour growth will occur. There is evidence that re-irradiation of DMG can once again provide symptom relief with an improved survival, however the occurrence of radio necrosis as a severe side-effect highlights the importance of enhancing the effectiveness of the initial radiotherapy treatments [49]. The recurrence of the tumour is a consequence of a subset of cancer cells that manage to survive radiotherapy treatment. These cells either possess or have acquired unique genetic and epigenetic characteristics contributing to evade radiotherapy treatment [50]. Therefore, to develop therapies with higher efficacy, it is crucial to understand these differences.

To determine transcriptomic and epigenetic changes following radiotherapy that potentially induce radioresistance, comprehensive genomic and epigenomic analyses need to be performed. These will allow for comparison of the genetic and epigenetic profiles of DMG cells before, during and after radiotherapy. High-throughput sequencing will uncover genetic expression alterations, including the expression of additional genes [51]. Epigenetic modifications are revealed by investigating changes in DNA methylation and histone modifications [52]. In addition to genetic and epigenetics, further research can be conducted to identify variations in proteomics and metabolomics in DMG cells before, during and after radiotherapy. The integration of these molecular data can lead to the discovery of novel therapies for DMG and personalised treatment targeting these cancerous cells with potential improved clinical effectiveness.

Besides genetic alterations following radiotherapy, poor oxygenation of DMG tumours plays a crucial part in the occurrence of radioresistance. Poor oxygenation is a consequence of a diminished blood flow towards the DMG tumours [53]. Oxygen is crucial for the formation of free radicals, which play a vital role in damaging cancer cells following radiotherapy [54]. Contrarily, an hypoxic environment in DMG tumours promotes various tumour cell survival pathways adding to the radioresistance properties of these cancer cells [55]. Consequently,

the diminished treatment efficacy from oxygen deprivation highlights the need for strategies to overcome this limitation and improve the outcome of radiotherapy for DMG patients.

Alternative radiotherapy modalities

For now, the common method for radiotherapy for the treatment of brain cancer is conventional photon therapy. However as stated before the usage of the conventional photon radiotherapy has a limited due to the occurrence of severe side-effects since the brain is a delicate organ. An alternative of the current usage of conventional photon therapy is proton therapy. Proton therapy is characterized with the highest energy deposition at the region of interest without an exit dose, reducing radiation of healthy tissue reducing long term side effects [56]. However, more research is needed to determine the safety of proton for DMG usage. It is also important to determine whether proton therapy gives comparable radiosensitization effects with for example olaparib as conventional photon radiotherapy.

Brachytherapy as internal radiation instead of the conventional external radiation is another option for brain tumour treatment [57]. In case of brachytherapy, a radiation source is placed next to or in the tumour for local treatment [58]. Clinical studies concerning brain metastases and glioblastoma proved the effectiveness of brachytherapy with local control and improvement of quality of life, but further research is needed also because of the occurrence of radiation necrosis and the effectivity for treatment of DMG [59,60].

FUS-BBBO and circumventing ABC-transporters

Although radiotherapy is effective, treatment is limited. Therefore, it is important that initial radiotherapy treatments are as effective as possible. One of the options is to increase DMG treatment effectiveness is the use of simultaneously medication through FUS-BBBO. Even though FUS-BBBO can increase local drug concentrations, its extravasation effects can partly be negated by ABC-transporters activity. These ABC-transporters are normally involved in the efflux of small molecules and effectively render these agents inactive for the treatment of brain malignancies. To achieve a greater yield of drug extravasation with FUS-BBBO, a synergistic effect with the inhibition of these ABC-transporters could be considered. The only drawback is that ABC-transporters are present and active in the whole body and systemic administration of inhibitors can cause several side effects which are detriment for patients. One way to disable these ABC-transporters locally is by using anti-bubbles, which are microbubbles containing medication and can pop under the influence of FUS [61]. Just like with FUS-BBBO, ultrasound waves can be focused on the region of interest but adjusted with the settings suitable for the popping of these anti-bubbles. Due to the local popping ABC-transport inhibitors can be locally delivered without affecting the whole circulatory system.

Although ABC-transporters seem to be active at the time and immediately after FUS-BBBO, there are also some indications that the mechanical effects of microbubble cavitation and subsequent stress responses may lead to a reduced expression of these proteins up to 48 hours [62,63]. This reduced ABC-transporter expression could mean an increased BBB permeability for a longer time and increased drug extravasation without tight junctions'

disruption. However, these long-term effects of FUS-BBBO have not been studied well enough but are relevant enough to be investigated in the future to improve drug administration and exposure.

Tumour environment and Immune therapy treatment

FUS-BBBO and radiotherapy can also affect the immune system. Radiotherapy stressed cells release immune suppressive or stimulating substances, such as cytokines, chemokines and antigens [64]. These immune signals can consequently cause the activation of the innate and adaptive immune system, which can have a possible additional treatment effect by tumour recognition and subsequently control [65], and potentially further immune-induced BBB opening. Besides radiation also FUS-BBBO can induce an immune reaction by the mechanical stress on the tissue due to vibrating microbubbles. Studies involving FUS-BBBO observed changes in the RNA and protein expression with HSP70 and proinflammatory cytokines measured within 24 hours. Thereafter microglial activation and macrophages were found in the sonicated region after treatment [66]. In addition, the endothelial cells expressed an upregulation of chemokines and cytokines [67].

Although an immune response can be elicited by FUS-BBBO, the increased BBB permeability may allow cells to reach the brain parenchyma more easily. However, due to insufficient knowledge and research the beneficial effects for the treatment of cancer by the immune response are unknown. Not knowing the potential beneficial effects of immune activation highlights the importance of the development of mouse models with a functional immune system.

Standardisation and the development of preclinical diffuse midline glioma models

While several PDX DMG animal models have been developed, it is important to have a model for the different mutational profiles observed in DMG in order to test selected drugs and validate their treatment efficacy [24]. Following our research presented in chapter 4, it is important to standardise and validate various PDX mouse models with different mutational profiles. The use of PDX mouse models also has several disadvantages including the invasive character of inoculation of human DMG cells. This invasive insertion needs to be done carefully to avoid severe brain damage, but also with enough precision for correct local cell inoculation, avoiding contamination of other brain locations. In addition, to avoid graft rejection of tumour cells, mice models with a compromised immune system can only be used for intracranial inoculation injection of patient-derived DMG cells. Due to the use of these immune compromised mouse models clinical translation of any therapeutic effects have become more complicated since they don't display a natural tumour micro-environment that might have important mitigating effects on drug sensitivity.

In contrast to PDX mouse models, genetically engineered mouse models (GEMM) develop autologous tumours on by the induction of various mutations in their genetic code while still having a fully functioning immune system [68]. Various developed paediatric HGG/DMG GEMM models have revealed characteristic proliferation patterns while revealing unexpected drug vulnerabilities based on their mutation profiles [69]. Based on these new findings and the use of models which resemble more closely the human situation clinical

translation can be more straightforward, highlighting the necessity of proper mouse models for any future therapeutic studies. However, the real clinical situation of DMG is far more complex, since it is a heterogeneous disease in which treatment also has an effect as in case with PARP1 upregulation after radiotherapy [28,70].

Diffuse midline glioma heterogeneity and PARP1 inhibition

The most commonly observed alteration in DMG is the loss of the trimethylation of the chromatin due to point mutations at the histone H3 protein, combined with mutation variations such as at TP53, PPMD1D, PDGFRA and MYC [24,28,71,72]. However, despite this highly known diversity, radiosensitization susceptibility to PARP1 inhibition was demonstrated in two DMG cell lines that harbour mutations of ACVR1, PPMD1D, MYC and PIK3CA in chapter 4 [73]. More DMG cell lines with other genetic alterations need to be screened for radiosensitisation effectiveness of PARP1 inhibition by olaparib.

Although olaparib is one of the most studied PARP1 inhibitors, multiple other PARP1 inhibitors are available and have been investigated in various preclinical and clinical trials such as talazoparib, rucaparib, niraparib and veliparib. Of the wide selection of PARP1 inhibitors, talazoparib is one the most promising one due to its high binding affinity. Despite the wide selection of available PARP1 inhibitors, due to the lack of proper comparative studies, the activity difference between the various agents are still not known [74,75]. In addition to optimization of PARP1 inhibitor and FUS-BBBO pharmacokinetics, studies are needed to investigate if specific molecular subtypes of DMG respond differently to different PARP1 inhibitors.

Radiosensitiser screening and concomitant drug treatment

Although PARP1 inhibition still appears to be an effective and promising treatment modality for DMG, it is also important to investigate the effectiveness of other radiosensitisers. Several studies have already investigated the effectiveness of various radiosensitizers such as HDAC and RTK inhibitors for DMG and HGG treatment, but until now the focus has been on single agent therapy in combination with radiotherapy [76]. The more interesting it is to investigate the effectiveness of two or more agents in combination with radiation, especially because of the high mutation profiles between DMG patients and within the tumours [77]. The utilisation of multiple drugs simultaneously offers advantages such as synergistic effects and targeting of different pathways and mechanisms either involved in tumour growth invasion and angiogenesis.

In addition to alterations in H3K27M, one of the most commonly found mutations in DMG patients is the mutation of the TP53 gene. TP53 mutations cause resistance to apoptosis resulting in constant cell proliferation and reduced tumour suppression. This loss of function such as apoptosis is due to altered isoforms of the p53 protein, which is therefore not recognized or able to normally bind to apoptosis genes [78]. This potentially provides a treatment opportunity, in which research should be aimed to restore the function by stabilizing the p53 protein. The next step would then be to deliver a sufficient dose of such a TP53 modulating drug at the right location and for the right time

Pharmacokinetics are key for DMG treatment efficacy improvement

With FUS-BBBO we managed to increase the concentration of olaparib in the brain, but therapeutic efficacy was limited due to its low local drug concentration and exposure time. Consequently, due to the short half-life and the dynamic exchange of olaparib between blood and brain and, vice versa, brain and blood, local accumulation of the drug in the pontine region was hampered. A solution to overcome the problem of short drug exposure and therefore improve treatment efficacy is to increase the plasma AUC by longer infusions using osmotic minipumps in vivo. Depending on the research question, an osmotic minipump releases overtime a constant drug concentration causing a prolonged and constant concentration exposure. The osmotic minipump can be subcutaneously implanted in a mouse model and increase the AUC of a drug [79]. In the case of Olaparib, it is expected that with an increased AUC of olaparib and elongation of PARP1 inhibition, radiotherapy induced DNA damage will be more pronounced, leading to increase in cell death .

Osmotic minipumps make constant drug administration in animal models feasible, aligning it with FUS-BBBO that causes enhanced brain permeability for a specific time, dependent on several factors. The temporal enhanced brain permeability is due the repair of the tight junctions between the endothelial cells. Because of this repair, the gap between the endothelial cells reduces in size overtime, causing a shorter time window for large molecules to cross the BBB than smaller molecules. The difference of molecule weight therefore determines the extravasation time which can range between 4-24 hours [45,80]. Olaparib has a molecular weight of 435.08 Da and has proven to be extravasated upon FUS-BBBO treatment. However, it is unknown how long after FUS-BBBO the barrier is permeable enough for olaparib extravasation into the brain areas. By investigating the timespan of the BBB remaining permeable to olaparib, treatment can be adjusted resulting in a higher AUC which can be more clinically relevant. In addition, for clinical relevance and subsequent translation it is important to keep in mind that the half-life of olaparib can be up to 11.9 hours in humans, which is significantly longer than for example in mice [81]. Subsequently, a longer half-life leads to a longer olaparib exposure and greater AUC, with a possible better radiosensitisation treatment efficacy in the clinic.

Clinical translation of FUS-BBBO

Before any form of radiotherapy in combination with drug delivery by FUS-BBBO can be clinically applied further research is needed. Various clinical studies have demonstrated safe FUS-BBBO for the treatment of several neurological diseases, but improved drug delivery leading to improved outcome in patients has not yet been accomplished. Meanwhile, several clinical FUS systems with different applications, such as thermal ablation have been FDA approved [82], whereas other indications such as BBB permeabilization are still in early phase clinical trials. As stated earlier, it is important for clinical translation that preclinical DMG models reflect as accurate as possible the human disease situation. This is certainly due to prevent any severe side effects after the unnatural influx of medication into the human brain which is a very sensitive organ. Through in-depth research and screening, potential drug candidates can be selected which can be initially used to test the safe application of drug delivery by FUS-BBBO.

Due to the ethical side of clinical validation, the clinical FUS systems are more developed and advance than their preclinical counterparts. Thus, a clinical FUS system has several transducers at its disposal that from different angels can target more locally the region of interest. This advantage of multiple transducers does not apply to our own developed preclinical system, simply because of the smaller brain volumes of the mouse models to not allow for such a design. While FUS can help with drug delivery the indirect effect of immune system stimulation needs to be more investigated to determine their possible side effects. This is even though preclinical research in primates has shown that FUS can provoke an immune response but without any adverse responses [83].

Conclusion

DMG is a malignant paediatric brain tumour with a high lethality and limited therapeutic options. This thesis contributed to prove the radiosensitization efficacy of olaparib for the treatment of DMG in a PDX mouse model combined with FUS-BBBO using an in-house build high-throughput stereotactic platform. In chapter 2 we investigated and proved the effects of radiotherapy on BBB permeabilisation in both clinical and preclinical settings; In chapter 3 we developed a preclinical FUS-BBBO system and proved safe BBB opening; In chapter 4 we characterised the DMG PDX HSJD-DIPG-007 mouse model which is commonly used for preclinical research; Finally in chapter 5 we proved that olaparib, is a suitable DMG radiosensitizer suitable for extravasation into the brain parenchyma following FUS-BBBO. These results form the basis for further pharmacokinetics research of olaparib to optimize drug exposure. Besides the successful and safe usage of FUS-BBBO form the basis for the screening of more potential radiosensitizers specified for the heterogenic genetic background of DMG patients. The end goal is proper translational research for clinical usage of radiosensitizers combined with FUS-BBBO leading to treatment and possible cure of DMG.

References

[1] Hoffman LM, Veldhuijzen van Zanten SEM, Colditz N, Baugh J, Chaney B, Hoffmann M, et al. Clinical, radiologic, pathologic, and molecular characteristics of long-term survivors of diffuse intrinsic pontine glioma (DIPG): a collaborative report from the international and european society for pediatric oncology DIPG registries. J Clin Oncol 2018;36:1963–72. https://doi.org/10.1200/JCO.2017.75.9308.

[2] Jansen MH, Veldhuijzen van Zanten SE, Sanchez Aliaga E, Heymans MW, Warmuth-Metz M, Hargrave D, et al. Survival prediction model of children with diffuse intrinsic pontine glioma based on clinical and radiological criteria. Neuro Oncol 2015;17:160–6. https://doi.org/10.1093/neuonc/nou104.

[3] Louis DN, Perry A, Wesseling P, Brat DJ, Cree IA, Figarella-Branger D, et al. The 2021 WHO Classification of tumors of the central nervous system: a summary. Neuro Oncol 2021;23:1231–51. https://doi.org/10.1093/neuonc/noab106.

[4] Fisher PG, Breiter SN, Carson BS, Wharam MD, Williams JA, Weingart JD, et al. A clinicopathologic reappraisal of brain stem tumor classification. Identification of pilocystic astrocytoma and fibrillary astrocytoma as distinct entities. Cancer 2000;89:1569–76. https://doi.org/10.1002/1097-0142(20001001)89:7<1569::aid-cncr22>3.0.co;2-0.

[5] Lassman LP, Arjona VE. Pontine gliomas of childhood. Lancet (London, England) 1967;1:913–5. https://doi.org/10.1016/s0140-6736(67)91485-7.

[6] Stupp R, Hegi ME, Mason WP, van den Bent MJ, Taphoorn MJB, Janzer RC, et al. Effects of radiotherapy with concomitant and adjuvant temozolomide versus radiotherapy alone on survival in glioblastoma in a randomised phase III study: 5-year analysis of the EORTC-NCIC trial. Lancet Oncol 2009;10:459–66. https://doi.org/10.1016/S1470-2045(09)70025-7.

[7] Warren KE. Beyond the blood-brain barrier: the importance of central nervous system (CNS) pharmacokinetics for the treatment of CNS tumors, including diffuse intrinsic pontine glioma. Front Oncol 2018;8:239. https://doi.org/10.3389/fonc.2018.00239.

[8] Burgess A, Shah K, Hough O, Hynynen K. Focused ultrasound-mediated drug delivery through the blood-brain barrier. Expert Rev Neurother 2015;15:477–91. https://doi.org/10.1586/14737175.2015.1028369.

[9] Stupp R, Mason WP, van den Bent MJ, Weller M, Fisher B, Taphoorn MJB, et al. Radiotherapy plus concomitant and adjuvant temozolomide for glioblastoma. N Engl J Med 2005;352:987–96. https://doi.org/10.1056/NEJMoa043330.

[10] Biau J, Chautard E, Verrelle P, Dutreix M. Altering DNA Repair to Improve Radiation Therapy: Specific and Multiple Pathway Targeting. Front Oncol 2019;9:1009. https://doi.org/10.3389/fonc.2019.01009.

[11] Lawrence YR, Li XA, el Naqa I, Hahn CA, Marks LB, Merchant TE, et al. Radiation dose-volume effects in the brain. Int J Radiat Oncol Biol Phys 2010;76:S20-7. https://doi.org/10.1016/j.ijrobp.2009.02.091.

[12] Van Vulpen M, Kal HB, Taphoorn MJB, El Sharouni SY. Changes in blood-brain barrier permeability induced by radiotherapy: Implications for timing of chemotherapy? (Review). Oncol Rep 2002;9:683–8. https://doi.org/10.3892/or.9.4.683.

[13] Takata F, Nakagawa S, Matsumoto J, Dohgu S. Blood-Brain Barrier Dysfunction Amplifies the Development of Neuroinflammation: Understanding of Cellular Events in Brain Microvascular Endothelial Cells for Prevention and Treatment of BBB Dysfunction. Front Cell Neurosci 2021;15:661838. https://doi.org/10.3389/fncel.2021.661838.

[14] Erickson MA, Banks WA. Blood-brain barrier dysfunction as a cause and consequence of Alzheimer's disease. J Cereb Blood Flow Metab Off J Int Soc Cereb Blood Flow Metab 2013;33:1500–13. https://doi.org/10.1038/jcbfm.2013.135.

[15] Sweeney MD, Kisler K, Montagne A, Toga AW, Zlokovic B V. The role of brain vasculature in neurodegenerative disorders. Nat Neurosci 2018;21:1318–31. https://doi.org/10.1038/s41593-018-0234-x.

[16] Hart E, Odé Z, Derieppe MPP, Groenink L, Heymans MW, Otten R, et al. Blood-brain barrier permeability following conventional photon radiotherapy - A systematic review and meta-analysis of clinical and preclinical studies. Clin Transl Radiat Oncol 2022;35:44–55. https://doi.org/10.1016/j.ctro.2022.04.013.

[17] Obermeier B, Daneman R, Ransohoff RM. Development, maintenance and disruption of the blood-brain barrier. Nat Med 2013;19:1584–96. https://doi.org/10.1038/nm.3407.

[18] Pardridge WM. The blood-brain barrier: Bottleneck in brain drug development. NeuroRx 2005;2:3–14. https://doi.org/10.1602/neurorx.2.1.3.

[19] Haumann R, 't Hart E, Derieppe MPP, Besse HC, Kaspers GJL, Hoving E, et al. A High-Throughput Image-Guided Stereotactic Neuronavigation and Focused Ultrasound System for Blood-Brain Barrier Opening in Rodents. J Vis Exp 2020. https://doi.org/10.3791/61269.

[20] Chopra R, Curiel L, Staruch R, Morrison L, Hynynen K. An MRI-compatible system for focused ultrasound experiments in small animal models. Med Phys 2009;36:1867–74. https://doi.org/10.1118/1.3115680.

[21] Kinoshita M, McDannold N, Jolesz FA, Hynynen K. Targeted delivery of antibodies through the blood-brain barrier by MRI-guided focused ultrasound. Biochem Biophys Res Commun 2006;340:1085–90. https://doi.org/10.1016/j.bbrc.2005.12.112.

[22] Haumann R, Videira JC, Kaspers GJL, van Vuurden DG, Hulleman E. Overview of Current Drug Delivery Methods Across the Blood-Brain Barrier for the Treatment of Primary Brain Tumors. CNS Drugs 2020;34:1121–31. https://doi.org/10.1007/s40263-020-00766-w.

[23] Meng Y, Hynynen K, Lipsman N. Applications of focused ultrasound in the brain: from thermoablation to drug delivery. Nat Rev Neurol 2021;17:7–22. https://doi.org/10.1038/s41582-020-00418-z.

[24] Chen Z, Peng P, Zhang X, Mania-Farnell B, Xi G, Wan F. Advanced pediatric diffuse pontine glioma murine models pave the way towards precision medicine. Cancers (Basel) 2021;13. https://doi.org/10.3390/cancers13051114.

[25] 't Hart E, Bianco J, Besse HC, Chin Joe Kie LA, Cornet L, Eikelenboom KL, et al. Towards Standardisation of a Diffuse Midline Glioma Patient-Derived Xenograft Mouse Model Based on Suspension Matrices for Preclinical Research. Biomedicines 2023;11. https://doi.org/10.3390/biomedicines11020527.

[26] Xu C, Liu H, Pirozzi CJ, Chen LH, Greer PK, Diplas BH, et al. TP53 wild-type/PPM1D mutant diffuse intrinsic pontine gliomas are sensitive to a MDM2 antagonist. Acta Neuropathol Commun 2021;9:178. https://doi.org/10.1186/s40478-021-01270-y.

[27] Taylor KR, Mackay A, Truffaux N, Butterfield Y, Morozova O, Philippe C, et al. Recurrent activating ACVR1 mutations in diffuse intrinsic pontine glioma. Nat Genet 2014;46:457–61. https://doi.org/10.1038/ng.2925.

[28] Hoffman LM, DeWire M, Ryall S, Buczkowicz P, Leach J, Miles L, et al. Spatial genomic heterogeneity in diffuse intrinsic pontine and midline high-grade glioma: implications for diagnostic

biopsy and targeted therapeutics. Acta Neuropathol Commun 2016;4:1. https://doi.org/10.1186/s40478-015-0269-0.

[29] Gong L, Zhang Y, Liu C, Zhang M, Han S. Application of Radiosensitizers in Cancer Radiotherapy. Int J Nanomedicine 2021;16:1083–102. https://doi.org/10.2147/IJN.S290438.

[30] Foray N, Bourguignon M, Hamada N. Individual response to ionizing radiation. Mutat Res Rev Mutat Res 2016;770:369–86. https://doi.org/10.1016/j.mrrev.2016.09.001.

[31] Lesueur P, Chevalier F, Austry J-B, Waissi W, Burckel H, Noël G, et al. Poly-(ADP-ribose)-polymerase inhibitors as radiosensitizers: a systematic review of pre-clinical and clinical human studies. Oncotarget 2017;8:69105–24. https://doi.org/10.18632/oncotarget.19079.

[32] van Vuurden DG, Hulleman E, Meijer OLM, Wedekind LE, Kool M, Witt H, et al. PARP inhibition sensitizes childhood high grade glioma, medulloblastoma and ependymoma to radiation. Oncotarget 2011;2:984–96. https://doi.org/10.18632/oncotarget.362.

[33] Chornenkyy Y, Agnihotri S, Yu M, Buczkowicz P, Rakopoulos P, Golbourn B, et al. Poly-ADP-Ribose Polymerase as a Therapeutic Target in Pediatric Diffuse Intrinsic Pontine Glioma and Pediatric High-Grade Astrocytoma. Mol Cancer Ther 2015;14:2560–8. https://doi.org/10.1158/1535-7163.MCT-15-0282.

[34] Senra JM, Telfer BA, Cherry KE, McCrudden CM, Hirst DG, O'Connor MJ, et al. Inhibition of PARP-1 by olaparib (AZD2281) increases the radiosensitivity of a lung tumor xenograft. Mol Cancer Ther 2011;10:1949–58. https://doi.org/10.1158/1535-7163.MCT-11-0278.

[35] Jannetti SA, Carlucci G, Carney B, Kossatz S, Shenker L, Carter LM, et al. PARP-1-Targeted Radiotherapy in Mouse Models of Glioblastoma. J Nucl Med 2018;59:1225–33. https://doi.org/10.2967/jnumed.117.205054.

[36] Waissi W, Nicol A, Jung M, Rousseau M, Jarnet D, Noel G, et al. Radiosensitizing Pancreatic Cancer with PARP Inhibitor and Gemcitabine: An In Vivo and a Whole-Transcriptome Analysis after Proton or Photon Irradiation. Cancers (Basel) 2021;13. https://doi.org/10.3390/cancers13030527.

[37] Michmerhuizen AR, Pesch AM, Moubadder L, Chandler BC, Wilder-Romans K, Cameron M, et al. PARP1 Inhibition Radiosensitizes Models of Inflammatory Breast Cancer to Ionizing Radiation. Mol Cancer Ther 2019;18:2063–73. https://doi.org/10.1158/1535-7163.MCT-19-0520.

[38] 't Hart E, Bianco J, Bruin MAC, Derieppe M, Besse HC, Berkhout K, et al. Radiosensitisation by olaparib through focused ultrasound delivery in a diffuse midline glioma model. J Control Release 2023;357:287–98. https://doi.org/https://doi.org/10.1016/j.jconrel.2023.03.058.

[39] Alli S, Figueiredo CA, Golbourn B, Sabha N, Wu MY, Bondoc A, et al. Brainstem blood brain barrier disruption using focused ultrasound: A demonstration of feasibility and enhanced doxorubicin delivery. J Control Release 2018;281:29–41. https://doi.org/10.1016/j.jconrel.2018.05.005.

[40] Englander ZK, Wei H-J, Pouliopoulos AN, Bendau E, Upadhyayula P, Jan C-I, et al. Focused ultrasound mediated blood-brain barrier opening is safe and feasible in a murine pontine glioma model. Sci Rep 2021;11:6521. https://doi.org/10.1038/s41598-021-85180-y.

[41] Liu H-L, Huang C-Y, Chen J-Y, Wang H-YJ, Chen P-Y, Wei K-C. Pharmacodynamic and therapeutic investigation of focused ultrasound-induced blood-brain barrier opening for enhanced temozolomide delivery in glioma treatment. PLoS One 2014;9:e114311. https://doi.org/10.1371/journal.pone.0114311.

[42] Liu H-L, Hsu P-H, Lin C-Y, Huang C-W, Chai W-Y, Chu P-C, et al. Focused Ultrasound Enhances Central Nervous System Delivery of Bevacizumab for Malignant Glioma Treatment. Radiology 2016;281:99–108. https://doi.org/10.1148/radiol.2016152444.

[43] Dréan A, Lemaire N, Bouchoux G, Goldwirt L, Canney M, Goli L, et al. Temporary blood-brain barrier disruption by low intensity pulsed ultrasound increases carboplatin delivery and efficacy in preclinical models of glioblastoma. J Neurooncol 2019;144:33–41. https://doi.org/10.1007/s11060-019-03204-0.

[44] Ishida J, Alli S, Bondoc A, Golbourn B, Sabha N, Mikloska K, et al. MRI-guided focused ultrasound enhances drug delivery in experimental diffuse intrinsic pontine glioma. J Control Release 2021;330:1034–45. https://doi.org/10.1016/j.jconrel.2020.11.010.

[45] Todd N, Zhang Y, Arcaro M, Becerra L, Borsook D, Livingstone M, et al. Focused ultrasound induced opening of the blood-brain barrier disrupts inter-hemispheric resting state functional connectivity in the rat brain. Neuroimage 2018;178:414–22. https://doi.org/10.1016/j.neuroimage.2018.05.063.

[46] Park J, Zhang Y, Vykhodtseva N, Jolesz FA, McDannold NJ. The kinetics of blood brain barrier permeability and targeted doxorubicin delivery into brain induced by focused ultrasound. J Control Release Off J Control Release Soc 2012;162:134–42. https://doi.org/10.1016/j.jconrel.2012.06.012.

[47] Goutal S, Gerstenmayer M, Auvity S, Caillé F, Mériaux S, Buvat I, et al. Physical blood-brain barrier disruption induced by focused ultrasound does not overcome the transporter-mediated efflux of erlotinib. J Control Release 2018;292:210–20. https://doi.org/10.1016/j.jconrel.2018.11.009.

[48] Min A, Im S-A. PARP Inhibitors as Therapeutics: Beyond Modulation of PARylation. Cancers (Basel) 2020;12. https://doi.org/10.3390/cancers12020394.

[49] Janssens GO, Gandola L, Bolle S, Mandeville H, Ramos-Albiac M, van Beek K, et al. Survival benefit for patients with diffuse intrinsic pontine glioma (DIPG) undergoing re-irradiation at first progression: A matched-cohort analysis on behalf of the SIOP-E-HGG/DIPG working group. Eur J Cancer 2017;73:38–47. https://doi.org/10.1016/j.ejca.2016.12.007.

[50] Kelley K, Knisely J, Symons M, Ruggieri R. Radioresistance of Brain Tumors. Cancers (Basel) 2016;8. https://doi.org/10.3390/cancers8040042.

[51] Jia Q, Chu H, Jin Z, Long H, Zhu B. High-throughput single-cell sequencing in cancer research. Signal Transduct Target Ther 2022;7:145. https://doi.org/10.1038/s41392-022-00990-4.

[52] Zhao Z, Shilatifard A. Epigenetic modifications of histones in cancer. Genome Biol 2019;20:245. https://doi.org/10.1186/s13059-019-1870-5.

[53] Yeom KW, Lober RM, Nelson MDJ, Panigrahy A, Blüml S. Citrate concentrations increase with hypoperfusion in pediatric diffuse intrinsic pontine glioma. J Neurooncol 2015;122:383–9. https://doi.org/10.1007/s11060-015-1726-0.

[54] Shen H, Cook K, Gee HE, Hau E. Hypoxia, metabolism, and the circadian clock: new links to overcome radiation resistance in high-grade gliomas. J Exp Clin Cancer Res 2020;39:129. https://doi.org/10.1186/s13046-020-01639-2.

[55] Emami Nejad A, Najafgholian S, Rostami A, Sistani A, Shojaeifar S, Esparvarinha M, et al. The role of hypoxia in the tumor microenvironment and development of cancer stem cell: a novel approach to developing treatment. Cancer Cell Int 2021;21:62. https://doi.org/10.1186/s12935-020-01719-5.

[56] Kirsch DG, Tarbell NJ. New technologies in radiation therapy for pediatric brain tumors: the rationale for proton radiation therapy. Pediatr Blood Cancer 2004;42:461–4. https://doi.org/10.1002/pbc.10471.

[57] Bander ED, Knisely JPS, Schwartz TH. Brachytherapy for central nervous system tumors. J Neurooncol 2022;158:393–403. https://doi.org/10.1007/s11060-022-04026-3.

[58] Chargari C, Deutsch E, Blanchard P, Gouy S, Martelli H, Guérin F, et al. Brachytherapy: An overview for clinicians. CA Cancer J Clin 2019;69:386–401. https://doi.org/10.3322/caac.21578.

[59] Chitti B, Goyal S, Sherman JH, Caputy A, Sarfaraz M, Cifter G, et al. The role of brachytherapy in the management of brain metastases: a systematic review. J Contemp Brachytherapy 2020;12:67–83. https://doi.org/10.5114/jcb.2020.93543.

[60] Barbarite E, Sick JT, Berchmans E, Bregy A, Shah AH, Elsayyad N, et al. The role of brachytherapy in the treatment of glioblastoma multiforme. Neurosurg Rev 2017;40:195–211. https://doi.org/10.1007/s10143-016-0727-6.

[61] Kotopoulis S, Lam C, Haugse R, Snipstad S, Murvold E, Jouleh T, et al. Formulation and characterisation of drug-loaded antibubbles for image-guided and ultrasound-triggered drug delivery. Ultrason Sonochem 2022;85:105986. https://doi.org/https://doi.org/10.1016/j.ultsonch.2022.105986.

[62] Cho H, Lee H-Y, Han M, Choi J-R, Ahn S, Lee T, et al. Localized Down-regulation of P-glycoprotein by Focused Ultrasound and Microbubbles induced Blood-Brain Barrier Disruption in Rat Brain. Sci Rep 2016;6:31201. https://doi.org/10.1038/srep31201.

[63] Aryal M, Fischer K, Gentile C, Gitto S, Zhang Y-Z, McDannold N. Effects on P-Glycoprotein Expression after Blood-Brain Barrier Disruption Using Focused Ultrasound and Microbubbles. PLoS One 2017;12:e0166061. https://doi.org/10.1371/journal.pone.0166061.

[64] Carvalho H de A, Villar RC. Radiotherapy and immune response: the systemic effects of a local treatment. Clinics (Sao Paulo) 2018;73:e557s. https://doi.org/10.6061/clinics/2018/e557s.

[65] Reits EA, Hodge JW, Herberts CA, Groothuis TA, Chakraborty M, Wansley EK, et al. Radiation modulates the peptide repertoire, enhances MHC class I expression, and induces successful antitumor immunotherapy. J Exp Med 2006;203:1259–71. https://doi.org/10.1084/jem.20052494.

[66] Kovacs ZI, Burks SR, Frank JA. Focused ultrasound with microbubbles induces sterile inflammatory response proportional to the blood brain barrier opening: Attention to experimental conditions. Theranostics 2018;8:2245–8. https://doi.org/10.7150/thno.24181.

[67] Curley CT, Sheybani ND, Bullock TN, Price RJ. Focused Ultrasound Immunotherapy for Central Nervous System Pathologies: Challenges and Opportunities. Theranostics 2017;7:3608–23. https://doi.org/10.7150/thno.21225.

[68] Kersten K, de Visser KE, van Miltenburg MH, Jonkers J. Genetically engineered mouse models in oncology research and cancer medicine. EMBO Mol Med 2017;9:137–53. https://doi.org/10.15252/emmm.201606857.

[69] McNicholas M, De Cola A, Bashardanesh Z, Foss A, Lloyd CB, Hebert S, et al. A Compendium of Syngeneic, Transplantable Pediatric High-Grade Glioma Models Reveals Subtype-Specific Therapeutic Vulnerabilities. Cancer Discov 2023. https://doi.org/10.1158/2159-8290.CD-23-0004.

[70] Bugiani M, Veldhuijzen van Zanten SEM, Caretti V, Schellen P, Aronica E, Noske DP, et al. Deceptive morphologic and epigenetic heterogeneity in diffuse intrinsic pontine glioma. Oncotarget 2017;8:60447–52. https://doi.org/10.18632/oncotarget.19726.

[71] Khuong-Quang D-A, Buczkowicz P, Rakopoulos P, Liu X-Y, Fontebasso AM, Bouffet E, et al. K27M mutation in histone H3.3 defines clinically and biologically distinct subgroups of pediatric diffuse intrinsic pontine gliomas. Acta Neuropathol 2012;124:439–47. https://doi.org/10.1007/s00401-012-0998-0.

[72] Grill J, Puget S, Andreiuolo F, Philippe C, MacConaill L, Kieran MW. Critical oncogenic mutations in newly diagnosed pediatric diffuse intrinsic pontine glioma. Pediatr Blood Cancer

2012;58:489–91. https://doi.org/10.1002/pbc.24060.

[73] Carvalho DM, Temelso S, Mackay A, Pemberton HN, Rogers R, Kessler K, et al. Drug screening linked to molecular profiling identifies novel dependencies in patient-derived primary cultures of paediatric high grade glioma and DIPG. BioRxiv 2020:2020.12.29.424674. https://doi.org/10.1101/2020.12.29.424674.

[74] Rudolph J, Jung K, Luger K. Inhibitors of PARP: Number crunching and structure gazing. Proc Natl Acad Sci 2022;119:e2121979119. https://doi.org/10.1073/pnas.2121979119.

[75] Murthy P, Muggia F. PARP inhibitors: clinical development, emerging differences, and the current therapeutic issues. Cancer Drug Resist 2019;2:665–79. https://doi.org/10.20517/cdr.2019.002.

[76] Metselaar DS, du Chatinier A, Stuiver I, Kaspers GJL, Hulleman E. Radiosensitization in Pediatric High-Grade Glioma: Targets, Resistance and Developments. Front Oncol 2021;11:662209. https://doi.org/10.3389/fonc.2021.662209.

[77] Bayat Mokhtari R, Homayouni TS, Baluch N, Morgatskaya E, Kumar S, Das B, et al. Combination therapy in combating cancer. Oncotarget 2017;8:38022–43. https://doi.org/10.18632/oncotarget.16723.

[78] Olivier M, Hollstein M, Hainaut P. TP53 mutations in human cancers: origins, consequences, and clinical use. Cold Spring Harb Perspect Biol 2010;2:a001008. https://doi.org/10.1101/cshperspect.a001008.

[79] Keraliya RA, Patel C, Patel P, Keraliya V, Soni TG, Patel RC, et al. Osmotic drug delivery system as a part of modified release dosage form. ISRN Pharm 2012;2012:528079. https://doi.org/10.5402/2012/528079.

[80] Chen H, Konofagou EE. The size of blood-brain barrier opening induced by focused ultrasound is dictated by the acoustic pressure. J Cereb Blood Flow Metab Off J Int Soc Cereb Blood Flow Metab 2014;34:1197–204. https://doi.org/10.1038/jcbfm.2014.71.

[81] Chase DM, Patel S, Shields K. Profile of olaparib in the treatment of advanced ovarian cancer. Int J Womens Health 2016;8:125–9. https://doi.org/10.2147/IJWH.S55906.

[82] Baek H, Lockwood D, Mason EJ, Obusez E, Poturalski M, Rammo R, et al. Clinical Intervention Using Focused Ultrasound (FUS) Stimulation of the Brain in Diverse Neurological Disorders. Front Neurol 2022;13. https://doi.org/10.3389/fneur.2022.880814.

[83] Pouliopoulos AN, Kwon N, Jensen G, Meaney A, Niimi Y, Burgess MT, et al. Safety evaluation of a clinical focused ultrasound system for neuronavigation guided blood-brain barrier opening in non-human primates. Sci Rep 2021;11:15043. https://doi.org/10.1038/s41598-021-94188-3.

Addendum

English summary

Diffuse midline glioma (DMG), previously known as diffuse intrinsic pontine glioma when located in the pontine area, is a very aggressive paediatric brain tumour. After diagnosis, children with pontine DMG have a poor prognosis with a median survival of 11 months and a mortality rate of 95% within two years. Due to the location and invasive growth of the tumour, is DMG difficult to treat. Surgery is practically impossible, chemotherapy is limited due to the blood-brain barrier (BBB) and radiotherapy, which it is still the current treatment option, is restricted by severe side-effects and radio resistance occurrence. Microbubble and focused ultrasound-mediated BBB opening (FUS-BBBO) has made drug delivery into the brain parenchyma and potentially the tumour possible. Drug delivery of radiosensitisers, compounds that render tumour cells sensitive to radiation, by FUS-BBBO in combination with radiotherapy can have a beneficial effect for the patients. Although radiosensitization seems be a promising method for the treatment of DMG, there is no conclusive evidence regarding its effectiveness. The goal of this thesis was to validate the treatment effectiveness of radiosensitization through FUS-BBBO-mediated drug delivery in a DMG patient-derived xenograft (PDX) mouse model.

In **chapter 1** a general introduction is given to the most important topics discussed in this thesis. In **chapter 2**, a systematic review and meta-analysis were performed to determine the effects and extent of radiotherapy on BBB permeability. Clinical and pre-clinical studies were qualitatively and quantitatively analysed for essential parameters of radiotherapy induced BBB permeability. The quality of the included studies displayed a high heterogeneity, a high risk of bias and publication bias which limits the strength of any conclusions. Overall, qualitative analysis of the clinical and preclinical studies showed an increase of BBB permeability upon radiotherapy, which was significantly confirmed by a meta-analysis of the preclinical studies. Clinical studies showed an upward trend of BBB permeability at higher biological effective dose values. Based on the fractionation schedule, a correlation was observed between single-radiation dose and increased BBB permeability. Clinical studies showed mostly an increased radiation-induced BBB permeability effect after ≥6 months, which indicates a chronic effect caused by radio-necrosis. The difference between the clinical and preclinical studies regarding radiation increased BBB permeability can be partly explained by the used detection methods and study designs. It may be that the disease type, disease phase and medication usage of the patients can already affect the BBB, influencing the observation of radiation increased BBB permeability. Future studies need to be performed to determine the effects of radiotherapy on the BBB permeability during and right after treatment.

Although FUS-BBBO is a promising technique for drug delivery, current preclinical systems can be a time-consuming, expensive, and requiring experienced personal. Based on the necessity for high-throughput and cost-effective pre-clinical FUS-BBBO research, an in-house stereotactic FUS platform was developed and tested in **chapter 3** to determine local and safe BBBO. The stereotactic FUS platform is a top-down design where the transducer, coupled to a pulse generator and power amplifier, is placed on the mouse head. Microbubble oscillation induced by the transducer's ultrasound waves is monitored by an integrated cavitation detector. Ultrasound is locally applied based on X-ray or

bioluminescent (BLI) imagine targeting. Using this system, stable cavitation of the intravenously injected microbubbles after the generation of ultrasound waves was observed with a mechanical index of 0.4. Ultrasound waves with a higher mechanical index caused the increase of noise and the appearance of ultra- and subharmonics evidencing inertial cavitation. The high energy release due to inertial cavitation of the microbubbles led to tissue vacuolisation and haemorrhaging in the brain. Nevertheless, when FUS-BBBO was applied to lower mechanical index, an increase of BBB permeability in the pontine region of the brain was observed by the extravasation of Evans blue, without tissue damage.

Before radiosensitisation for the treatment of DMG in combination with FUS-BBBO can be tested in vivo, it is important to have a clinically relevant animal model with localized tumour growth in the pons. In **chapter 4**, different protocols to establish a DMG xenograft tumour model were examined. A literature review was performed to select protocols regarding the establishment of the HSJD-DIPG-007 DMG PDX animal model. Analysis of the protocols showed that mostly, athymic nude, nude BALB/c, NOD-SCID and NOD-SCID gamma nude mice were used as animal hosts in the adolescent stage of life. The location of tumour cell injection was mainly in the brainstem and more specifically in the pons and 4th ventricle of the animals with a total volume between 1 and 5 µl and a cell concentration between 1x105 and 7.5x105 suspended in PBS, Matrigel or growth medium. Based on the protocols available in literature we performed intracranial cell inoculation with HSJD-DIPG-007 cells suspended in PBS or Matrigel, but we did not observe any significant differences regarding weight, overall survival, and primary tumour growth. However, based on BLI signal, mice inoculated with cells suspended in PBS displayed earlier metastases in the olfactory bulb and spinal cord than mice injected with Matrigel-suspended cells. Histological analysis confirmed local tumour growth and metastatic formation following the intracranial injection of HSJD-DIPG-007 cells suspended in PBS or Matrigel. However, histological analysis also revealed that individual cells were already found in several distant brain structures immediately following intracranial injection, which explains the early metastatic occurrence due to individual cells. Despite the occurrence of metastases, progression and growth of the tumour of the HSJD-DIPG-007 DMG PDX model is clinically relevant due to the comparable brain parenchyma invasion and vascular proliferation. However, because DMG is characterised by different mutational profiles, it is important that further research is done to establish various relevant pre-clinical models.

In **chapter 5**, radiosensitisation by PARP1 inhibition was investigated, while exploring the drug delivery properties of FUS-BBBO and the potential beneficial effects of olaparib for the treatment of DMG. In vitro, radiosensitisation effects of olaparib were observed with inhibition of PARP1 activity and the reduction of cell viability and clonogenic capabilities upon treatment. After validating radiosensitization effects in vitro, FUS-BBBO enabled the extravasation of olaparib into the pons of mice with the establishment of its pharmacological profile. Subsequently, based on the pharmacological profile, an in vitro neurosphere growth assay showed radiosensitization. Knowing the in vitro effects of olaparib based on its pharmacological profile, the HSJD-DIPG-007 DMG PDX mouse model was used to investigate the survival and tumour growth following FUS-BBBO and olaparib extravasation combined with radiotherapy treatment. Although radiosensitisation effects were found in vitro, no additional survival benefit or tumour growth delay in vivo was

observed with the HSJD-DIPG-007 DMG PDX mouse model upon olaparib FUS-BBBO extravasation. Further research is needed to better understand the pharmacokinetics of olaparib extravasation in the pons in combination with FUS, so that can be applied to improve the treatment of DMG in mouse models.

Finally in **chapter 6**, a discussion is included explaining the most important aspects of each chapter. In addition, there is an elaboration of the future prospects of radiosensitizers, radiotherapy, the effects of FUS-BBBO and the importance of clinically relevant models based on genomic data of DMG patients. The data and results discussed in this thesis form the basis for further pharmacokinetics research of radiosensitisers in conjunction with FUS-BBBO. The end goal is proper translational research for clinical usage of radiosensitizers combined with FUS-BBBO leading to treatment and possible cure of DMG.

Nederlandse samenvatting

Difuus midlijn glioma (DMG), ook wel bekend als diffuus intrinsiek pons glioom, is een zeer agressieve hersentumor bij kinderen. Kinderen met een DMG gelokaliseerd in de pons hebben na diagnose een prognose met een mediane overlevingskans van maar 11 maanden en een sterftecijfer van 95% binnen twee jaar. De behandeling van DMG is complex door de locatie en invasieve tumorgroei. Chirurgie is praktisch onmogelijk, chemotherapie is beperkt vanwege de aanwezigheid van de bloed-hersenbarrière (BBB) en radiotherapie, wat de huidige behandelingsoptie is, is beperkt in effectiviteit als gevolg van ernstige bijwerkingen en resistentie tegen radiotherapie. De ontwikkeling van gefocust ultrageluid BBB-opening (FUS-BBBO) met behulp van microbellen heeft medicatie afgifte in het hersenparenchym en de tumor mogelijk gemaakt. Medicatie afgifte van de radiosensitieve medicijnen, die tumorcellen gevoeliger maken voor bestraling, in combinatie met FUS-BBBO en radiotherapie kan een gunstig gezondheid effect hebben voor patiënten. Hoewel radiosensitieve medicijnen een hoopvolle behandelingsmethode lijken te zijn voor de behandeling van DMG, is er nog geen sluitend bewijs. Het doel van dit proefschrift was het onderzoeken van de effectiviteit van radiosensitieve medicijnen met medicatie afgifte in de hersenen met behulp van FUS-BBBO in een DMG patiënt-afkomstig xenotransplantaat (PDX) muismodel.

In **hoofdstuk 1** wordt een algemene inleiding gegeven over de belangrijkste onderwerpen die in dit proefschrift worden besproken. In **hoofdstuk 2** wordt een systematische literatuuronderzoek en meta-analyse besproken om de effecten en mate van radiotherapie op de permeabiliteit van de BBB te bepalen. Klinische en preklinische studies zijn kwalitatief en kwantitatief geanalyseerd op essentiële parameters die radiotherapie-geïnduceerde BBB-permeabiliteit kunnen beïnvloeden. De kwaliteit van de geïncludeerde onderzoeken is beïnvloed door de hoge onderlinge heterogeniteit, hoge kans op vooringenomenheid en publicatie bevooroordeling, wat een nadelig effect heeft op conclusie betrouwbaarheid. Kwalitatieve analyse van de klinische en preklinische studies toonde aan dat er een verhoogde BBB-permeabiliteit is na behandeling met radiotherapie, wat significant is bevestigd met een meta-analyse van de preklinische studies. Klinische studies toonden aan dat er een verhoogde BBB-permeabiliteit wordt gemeten naar aanleiding van hogere biologische effectieve dosiswaarden. Als er gekeken wordt naar het fractioneringsschema dan is er een correlatie tussen een enkele bestraling en verhoogde BBB-permeabiliteit. Daarnaast toonden klinische studies aan dat meestal na ≥6 maanden een verhoogd BBB-permeabiliteit werd gemeten na radiotherapie behandeling, wat kan duiden op een chronisch effect veroorzaakt door radionecrose. Het verschil van BBB-permeabiliteit gemeten na behandeling met radiotherapie tussen de klinische en preklinische studies kan gedeeltelijk worden verklaard door het verschil in gebruikte detectiemethoden en het opstellen van het onderzoek. De ziekte, de fase en het gebruik van medicatie door patiënten kan ook een effect hebben op de BBB, wat de permeabiliteit naar aanleiding van radiotherapie kan beïnvloeden. Toekomstige studies zijn van belang om de effecten van radiotherapie op de BBB-permeabiliteit tijdens en direct na de behandeling te bepalen.

Hoewel FUS-BBBO een veelbelovende techniek is voor medicatie afgifte, zijn de huidige preklinische systemen tijdrovend, duur en ervaren personeel is nodig. Omdat er behoefte is

aan een goedkoper alternatief met een hoog onderzoek rendement wordt er in **hoofdstuk 3** een eigen ontworpen stereotactisch FUS-platform besproken om lokale en veilige BBBO vast te stellen. Het stereotactische FUS-platform is ontworpen waarbij de transducer, gekoppeld aan een pulsgenerator en versterker, boven op het hoofd van de muis kan worden geplaatst. Microbellen oscillatie veroorzaakt door de ultrageluidsgolven vanuit de transducer kunnen gemonitord worden doormiddel van geïntegreerde cavitatie detectie. Ultrageluidsgolven kunnen precies en lokaal worden toegepast met behulp van röntgen- of bioluminescente (BLI) foto's. Stabiele cavitatie van de intraveneus geïnjecteerde microbellen is waargenomen met ultrageluidsgolven met een mechanische index van 0.4. Ultrageluidsgolven met een hogere mechanische index veroorzaakten een toename van ruis, waarbij ook ultra- en subharmonisch golven werden waargenomen, wat wijst op instabiele cavitatie. Instabiele cavitatie van de microbellen en het daarbij vrijkomende energie kan vervolgens leiden tot weefsel vacuolisatie en uiteindelijk bloedingen in de hersenen. Als FUS-BBBO met verlaagde mechanische index veilig werd toegepast was een toename van de BBB-permeabiliteit in de pons waar te nemen doormiddel van de extravasatie van Evans-blauw zonder weefsel schade.

Voordat radiosensitieve medicijnen voor de behandeling van DMG in combinatie met FUS-BBBO in vivo kunnen worden getest, is het belangrijk om een klinisch relevant diermodel met lokale tumorgroet in te pons te hebben. In **hoofdstuk 4** worden verschillende protocollen besproken voor het tot stand brengen van een preklinisch tumormodel. Literatuuronderzoek is uitgevoerd om verschillende protocollen te vergelijken met betrekking totstandkoming van het HSJD-DIPG-007 DMG PDX-diermodel. De verschillende studies toonde aan dat voornamelijk adolescente athymische naakte, BALB/c-, NOD-SCID- en NOD-SCID-gamma muizen werden gebruikt als dierlijke gastheren. Tumorcellen werden voornamelijk geïnjecteerd in de hersenstam en specifiek in de pons en 4de ventrikel met een volume tussen 1 en 5 µl en een cel concentratie tussen 1x105 en 7,5x105 gesuspendeerd in PBS, Matrigel of groeimedium. Gebaseerd op de beschikbare protocollen in literatuur, is er intracraniale injectie uitgevoerd met HSJD-DIPG-007-cellen gesuspendeerd in PBS of Matrigel, Geen significante verschillen zijn waargenomen met betrekking tot gewicht, overleving en primaire tumorgroei. Op basis van het BLI-foto's bleek dat muizen met cellen gesuspendeerd in PBS eerder metastasen in de bulbus olfactorius en het ruggenmerg veroorzaakten dan muizen met cellen gesuspendeerd in Matrigel. Histologische analyse bevestigde lokale tumorgroei en metastatische vorming na intracraniale HSJD-DIPG-007 cel injectie gesuspendeerd in PBS of Matrigel. Daarnaast onthulde histologische analyse dat individuele tumorcellen al aanwezig waren in verschillende hersenstructuren onmiddellijk na intracraniale injectie, wat vroege metastasering kan verklaren. Ondanks de aanwezigheid van metastasen is de progressie en de groei van de tumor van het HSJD-DIPG-007 DMG PDX-model nog steeds klinisch relevant vanwege de vergelijkbare invasie van het hersenparenchym en vasculaire proliferatie. DMG wordt gekenmerkt door de vele verschillende mutatieprofielen dat het kan hebben, waardoor het belangrijk is om verschillende relevante preklinische modellen te ontwikkelen.

In **hoofdstuk 5** is radiosensitiviteit doormiddel van PARP1-remming met behulp van olaparib onderzocht voor de behandeling van DMG, tegelijkertijd met het vaststellen van de

medicatie afgifte eigenschappen van FUS-BBBO. In vitro zijn radiosensitiviteits effecten van olaparib gemeten, waaronder de remming van PARP1-activiteit en de vermindering van cel vitaliteit en klonogene vermogen na behandeling. Na radiosensitiviteits validatie in vitro, is er aangetoond dat FUS-BBBO extravasatie van olaparib in de pons van muizen mogelijk maakt, waarna een farmacologisch profiel kon worden opgesteld. Een in vitro neurosphere groei assay toonde aan dat gebaseerd op het farmacologisch profiel radiosensitiviteit kan worden bereikt. Het HSJD-DIPG-007 DMG PDX muismodel werd gebruikt om de overleving en tumorgroei te onderzoeken na behandeling van FUS-BBBO en extravasatie van olaparib gecombineerd met radiotherapiebehandeling. Hoewel radiosensitiviteit was aangetoond in vitro, is geen overlevingsvoordeel of tumorgroeivertraging in vivo waargenomen met het HSJD-DIPG-007 DMG PDX muismodel na olaparib FUS-BBBO extravasatie. Meer onderzoek is nodig om de farmacokinetiek van extravasatie van olaparib in de pons in combinatie met FUS-BBBO beter te begrijpen, voor een verbeterde toepassing van de behandeling van DMG in muismodellen.

Tenslotte in **hoofdstuk 6** worden de belangrijkste aspecten van elk hoofdstuk van dit proefschrift bediscussieert en verder uitgediept. Vervolgens wordt er ingegaan op de toekomstperspectieven van radiosensitieve medicijnen, radiotherapie, de effecten van FUS-BBBO en het belang van klinisch relevante modellen op basis van genetische gegevens van DMG-patiënten. De data en resultaten die in dit proefschrift zijn besproken, vormen de basis voor toekomstig farmacokinetische onderzoek van radiosensitieve medicijnen in combinatie met FUS-BBBO. Het einddoel is het ontwikkelen van translationeel onderzoek voor klinisch gebruik van radiosensitieve medicijnen in combinatie met FUS-BBBO, wat kan leiden tot de behandeling en mogelijke genezing van DMG.

List of publications

> **Elvin ‘t Hart***, Zelda Odé*, Marc Derieppe, Lucianne Groenink, Martijn Heymans, Rene Otten , Maarten Lequin, Geert Janssens, Eelco Hoving, Dannis van Vuurden. Blood-brain barrier permeability following conventional photon radiotherapy - A systematic review and meta-analysis of clinical and preclinical studies. Clinical Translational Radiation Oncology. 2022 May 4;35:44-55. doi: 10.1016/j.ctro.2022.04.013.

> Rianne Haumann*, **Elvin 't Hart***, Marc Derieppe, Helena Besse, Geert-Jan Kaspers, Eelco Hoving, Dannis van Vuurde, Esther Hulleman, Mario Ries. A Highk-Throughput Image-Guided Stereotactic Neuronavigation and Focused Ultrasound System for Blood-Brain Barrier Opening in Rodents. Journal of Visual Experiments. 2020 Jul 16;(161). doi: 10.3791/61269.

> **Elvin ’t Hart**, John Bianco, Helena Besse, Lois Chin Joe Kie, Lesley Cornet, Kimberly Eikelenboom, Thijs van den Broek, Marc Derieppe, Yan Su, Eelco Hoving, Mario Ries, Dannis van Vuurden. Diffuse Midline Glioma Patient-Derived Xenograft Mouse Model Based on Suspension Matrices for Preclinical Research. Biomedicines. 2023 Feb 11;11(2):527. doi: 10.3390/biomedicines11020527

> **Elvin ’t Hart**, John Bianco, Maaike Bruin, Marc Derieppe, Helena Besse, Kjelle-Lars Berkhout, Lois Chin Joe Kie, Yan Su, Eelco Hoving, Alwin Huitema, Mario Ries, Dannis van Vuurden. Radiosensitisation by olaparib through focused ultrasound delivery in a diffuse midline glioma model. Journal of Controlled Release. 2023 May;357:287-298. doi: 10.1016/j.jconrel.2023.03.058

Curriculum vitae

Elvin ‘t hart was born on the 12th of April 1991 in Bemmel as the third child in a family of four children. After four stress-free years as child, Elvin went to the primary school: de Regenboog in Bemmel. As a student, Elvin had a slow start and needed some extra care to learn how to read and write. Despite his slow start, Elvin had a big fascination for spiders and was able to tell the name of each spider. After eight years of learning the basic principles of the Dutch education system and some hard work, Elvin managed to get accepted at the Stedelijk Gymnasium Nijmegen for a high school education. Following his acceptance at the Stedelijk gymnasium Nijmegen and at an age of 12 years, Elvin had to bike every day from Bemmel to Nijmegen to attend his classes. During his high school education Elvin choose to follow courses within the major of “ Natuur en Gezondheid” and Latin. After some years of hard working Elvin managed to get his Gymnasium VWO certificate in 2010 and decided to pursue a new goal; getting a University degree.

In the summer of 2010, Elvin applied for the Bachelor Biology at the Radboud University in Nijmegen. While exploring the mysteries of life, Elvin choose to follow courses within the minor of Medical Biology and did a bachelor internship in the group of Marcel Verbeek at the Laboratory of Genetic, Endocrine and Metabolic Diseases at the Radboudumc in Nijmegen. The subject of his bachelor internship concerned “the Microglia activation and inflammatory reactions under influence of chronic amyloid-β”. After finishing his bachelor internship, Elvin obtained his bachelor certificate in 2014. Intrigued by the human physiology and diseases Elvin decided to do the master programme of Biomedical sciences at the Radboud University in Nijmegen. Elvin did two master internships, 1) at the department of Health protection at the National Institute for Public Health and the Environment (RIVM) in Bilthoven concerning the project “FutureNanoNeeds: in vitro toxicity of next generation Nanomaterials used in energy harvesting based on viability, IL-2 and ROS production in the human Tlymphocyte cell line Jurkat E6.1”, 2) in the group of Wilhelm Huck at the Department of Physical Organic Chemistry at the Radboud University in Nijmegen concerning the project: “Droplet-based microfluidics for isolation of B-cells producing antibodies against surface antigens of Bordetella pertussis”. In 2017 Elvin got his biomedical Sciences Master degree with specialisation in Human Toxicology and Infectious Diseases, while also following additional Neuroscience courses at the Donders Institute for Brain, Cognition and Behaviour in Nijmegen. The additional Neuroscience courses included 1) Neuroscience of sleep, 2) human neurobiology of (mal) adaptation and 3) Neurodevelopmental disorders.

After seeing the devastated effects of cancer in his personal life, Elvin decided to pursue a PhD within the scope of oncology and joined the team of Dannis van Vuurden at the Princess Maxima Center for pediatric oncology and Mario Ries of the UMC Utrecht within the project of “focused ultrasound-mediated blood-brain barrier opening for diffuse midline glioma radiosensitisation”. After four years and some extra months, Elvin managed to have four articles published within the scope of PhD, before he joined, the Dutch Research Council (NWO) as a program officer, within the High Tech Systems Team under supervision of Yvette Tuin. Within his tasks as programme officer, Elvin was involved in the application process of the NWO Open Technology Programme and the Summit grant 2023.

PhD portfolio

Naam: Elvin 't Hart
PhD period: Oktober 2018 – Oktober 2022
Research school: Cancer, Stem cells and Developmental biology, Utrecht University
Department: Neuro-oncology
Promotor: Prof. dr. E. Hoving
Co-promotors: Dr. D.G. van Vuurden, Dr. M. Ries

1. PhD training	**Year**	**ECTS**
Courses		
Introduction to the CS&D	2019	0.3
Introduction to Biomolecular Mass Spectrometry	2019	1.5
Digital pictures: Data integrity & display	2019	1
Concepts in Cancer Biology	2019	1.5
Cell Organisation in Health and Disease	2019	1.5
Being a Scientist: Integrity Issues in Practice	2019	0.2
Enabling technologies	2019	1.5
This Thing Called Science	2020	2
Mindfulness and stress reduction	2020	3
Research planning and time management	2020	0.4
Introductory Biostatistics for Researchers	2020	4.5
Seminars and workshops:		
Hands-on training in systematic reviews and meta-analysis of preclinical animal studies	2019	0.3
CSnD Masterclass	2019-2022	3
CSnD Retreat	2019-2022	3
2. Conferences and scientific meetings		
PMC symposium	2018	
BBB meeting, Leiden, the Netherlands	2019	
Therapy Ultrasound School, Les houches	2019	
BBB FUS, Rotterdam, the Netherlands - oral presentation	2020	
ISPNO, Karuizawa, Japan - online	2020	
3. Teaching activities		
Supervising Master student; Zelda Odé, 3 months	2018-2019	
Supervising HBO student: Kjelle Lars, 9 months	2021-2022	
Supervising Master student: Kimberely Eikelenboom 9 months	2022	
4. Committee activities		
CSnD PhD committee	2019-2021	3
Princes Maxima (PriMa) PhD committee	2020-2022	3

Acknowledgement

After my four years and some extra time, it is time to move on and complete my PhD. Although I might obtain a PhD and get my doctors title, this book is also a tribute to all the people and cats involved completing this story. Because in the end, researchers are storytellers.

Als eerste wil ik **Eelco** bedanken die gedurende de vier jaar mijn promotor is geweest. Hoewel het soms moeilijk was om elkaar te spreken door overvolle agenda's en natuurlijk de Covid pandemie, waren de gesprekken die we hadden meer dan waardevol. Ik dwaalde nog wel eens af van het rechte pad en verzonk in de onnodige details van het onderzoek. Jij leerde mij dat het soms niet ging om de details, maar om het geheel.

Als tweede wil ik mijn co-promotoren **Dannis** en **Mario** bedanken. **Dannis**, in de vier jaar dat ik in jouw groep werkzaam was, heb ik via jou meerdere kanten van onderzoek leren kennen. Hoewel het Prinses Maxima Centrum een geweldig plek is om te werken, was er ook een donkere keerzijde. Je vertelde immers hoe machteloos je soms als arts bent als je geen effectieve behandeling meer had voor de kinderen. Maar je toonde altijd aan dat je hart voor de zaak had. Je compassie en affectie die je voor de kinderen toonde maakte op mij diepe indruk. Je liet me de menselijk kant van het onderzoek zien en de reden waarom we dit moeten doen. **Mario**, die Frage, die du mir während meines Vorstellungsgesprächs gestellt hast: Was ist der Unterschied zwischen Radiologie und Strahlentherapie, ist eine Frage, auf die ich immer noch keine Antwort weiß. Zusätzlich zu unseren Gesprächen über deine wilden Dienstjahre in der Armee (mit vielen Explosionen), Dämonencore (wenn wir nur selbst einen hätten) und wie man einen Löffel benutzt (wobei ich jetzt sage, man muss die abgerundete Seite nach oben verwenden), weil man dann den Schallkopf besser verschmiert), hat man schon immer gesehen, wie engagiert Sie sich für die Forschung einsetzen. Sie haben mir beigebracht, dass eine Geschichte aus verschiedenen Perspektiven geschrieben werden kann und dass alles von der Geschichte abhängt, die Sie erzählen möchten.

Mijn paranimfen **Lisa** en **Kimberly**. Er is een reden waarom ik jullie twee heb uitgekozen als mijn paranimfen en niet omdat jullie tweede keuze waren. **Lisa**, we hebben beide een onvoorwaardelijke liefde voor onze katten en het beste advies dat ik je ooit heb kunnen geven is dat je een Litter-Robot moest aanschaffen. Jij noemde me elfje en ik wist nooit wat ik terug moest zeggen. Je besluit om een Master te gaan doen moedigde ik aan en binnenkort zul jij ook beginnen met een PhD. **Kimberly**, mijn laatste student en mede drug enthousiast. Een vent-diagram wat was dat ook alweer? Ik heb het idee dat ik meer van jou heb geleerd dan jij van mij. We hebben geworsteld met onze drug screening maar het heeft ook ons mooie momenten gebracht. Je bent nu zelf ook een PhD begonnen, waarvan ik vooral kan zeggen dat ik trots op je ben.

Marc, **Helen** en **John** mijn post-docs. **Marc** Je peux écrire des paragraphes, des chapitres et des livres (quand sort votre livre ?) sur notre temps et nos conversations en laboratoire, malheureusement je dois être bref. Nos plus beaux moments ont été les expériences sur les animaux à Amsterdam, où nous avons travaillé plusieurs jours d'affilée de 9 heures du matin

à 19 heures du soir. Et plus d'une fois, nous n'avons jamais vu le soleil ces jours-là. Tu sais combien je t'ai apprécié et nous avons développé une belle amitié grâce à cela. **Helen**, ik vind het nog steeds jammer dat het me niet is gelukt om je Dinaciclib verhaal uit te kunnen uitwerken. Zeker nadat je had aangetoond dat gezonde cellen met een kortere blootstelling eerder doodgingen dan de kankercellen. Jij had een compassie voor de dieren en stond er op dat een muis geen petrischaaltje op pootjes is. Samen met jou hebben we elke muisje zo goed en humaan mogelijk behandeld. G'day **John**, mate! You rocked up in the crew back when I kicked off my fourth year of the ol' PhD journey. Your entry injected the much-needed life and research mojo into the squad. In that short year and a bit, we smashed out all the crucial experiments, penned down and even chucked out a couple of articles. Despite you being a fair dinkum Aussie speaker (or maybe Bulgarian – who can tell?), you had this knack for giving our words and sentences a ripper natural flow. You copped the job of eyeballing my thesis intro (which we both reckoned was top-notch) and the discussion before the bigwigs took the reins. Remember that one time I accidentally dropped a "darling" on ya? Classic stuff, mate. Cheers, legend!

Zelda en **Kjelle**-**lars**, mijn andere twee studenten. **Zelda**, ik leerde je kennen net nadat ik zelf een maand of twee was begonnen met mijn PhD. Dannis zei dat we een review moeten schrijven en zo begon onze samenwerking. Samen hebben we dagenlang artikelen gelezen om een idee te creëren en om data te verzamelen. Het duurde eventjes maar na twee en een half jaar was het ons toch gelukt! **Kjelle**-**lars**, Kjelle, groeide en ontwikkelde je enorm als onderzoeker in de tijd dat jij mijn student was (en dat kwam natuurlijk door mij). Ik kon jouw hulp heel goed gebruiken, vooral met het tellen van kolonies. Waarschijnlijk zie je ze nog steeds voor je ogen voorbij drijven als je in bed legt. Maar jouw ontwikkeling is nog niet gestopt, want jij zal binnenkort onze eigen arts worden.

En nu de rest van de groep. **Lois**, jij en muizen dat is liefde op het eerste gezicht. Je was als student in onze groep begonnen, maar groeide door tot vaste kracht waar we niet zonder konden. Ik kon je blindelings vertrouwen als het om de muizen ging en jij wist ook wat er moest gebeuren. Sindsdien heb jij je alleen maar verder ontplooid en doe je de meest wonderbaarlijke chirurgische ingrepen waar ik alleen maar van kan dromen. **Yan**, you always was the happiest member of the whole group. Even though Mia kept you awake in the nights, you never lost your smile. I do hope you managed to make stamppot in the end, because you do not have to boil potatoes for forty minutes. **Rianne**, jij introduceerde mij in de praktische wereld van ons onderzoek. Jij leerde me hoe de naald in de staart van de muizen gestoken moest worden. Natuurlijk ons hoogtepunt was ons filmpje voor JoVE. **Josh**, we both struggled sometimes throughout our PhD and had grumpy times. You missed home, which I can understand, because the Netherlands is of course the better country. In the end, you are different than most of the Americans I have ever met (who always seem to scream when they are talking), because you were patient and calm. **Thijs**, als student vertrok je, maar je kwam ook weer terug. We hebben helaas te weinig tijd gehad om wetenschap te doen, want ik was heel erg geïnteresseerd in de Wess of Jess. **Raoul**, ook met jou heb ik toch net iets te weinig tijd doorgebracht omdat we op andere gebieden onderzoek deden. Ik denk wel dat ik veel over je inzichten had kunnen leren. **Lesley**, veel woorden kunnen je beschrijven, maar een paardengek is alles wat ik nodig heb.

Esther, onderzoek kan moeilijk en hard zijn met vele teleurstellingen die je tegen kan komen. Maar soms hoeft het helemaal niet zo moeilijk te zijn. Ik leerde van jou dat onderzoek ook makkelijk kan zijn, maar het ligt eraan hoe je er soms tegen aan kijkt. Helaas door uiteenlopende onderwerpen hebben we op het einde minder samen kunnen werken dan op het begin. **Claudia**, bisch scho uf dr Suach nach ewiger Jugend gstande? Du bisch vo all PI's, wo ich immer am härtschte gschafft han. Immer im Labor, um dini eigene Experimente z'mache, wie es sich für en echte Forscher ghört.

De Kuipers groep, Marc en ik waren jullie geadopteerde puppy's op het begin van mijn PhD. **Željko**, moj omiljeni srpski drug. Moja noć kod tebe će zauvek biti vrhunac u mom životu. Trebalo bi da bude inspiracija za priču iz perspektive čarobnog realizma. Neizreciva sila izazvala je fatalistički događaj koji me je naterao da završim na tvom kauču. A možda si ti bio samo još jedan od mojih mnogih sastanaka. Tvoja iskreno, PMC kurva. **Dilys**, ik zal me heel netjes houden en niet te veel van onze gekke gesprekken hier opschrijven. En dat is ook maar beter zo! **Nienke**, mijn CSnD commissielid opvolger. Ik zocht een waardige opvolger en die vond ik in jou. **Jette**, helaas moest ik je missen als mijn overbuurvrouw omdat we als groep van locatie gingen veranderen, gelukkig bleven we noodle eten. **Lionel**, Nunca tinha estado na monumental Câmara Municipal de Gouda antes, mas o seu casamento foi uma boa ocasião. Simon, ik kom je toch altijd weer ergens tegen. De rest van de groep die ik nu niet benoem, bedankt voor jullie aanwezigheid.

De **Tytgat** groep, onze gezellige zustergroep. **Yvette**, je was altijd gezellig en als een stuiterbal aan het rond springen. Altijd actief en niet te stoppen. **Astrid**, generatiegenoot, jij en ik konden het goed vinden omdat we simpelweg dezelfde smaak hadden in alles. **Marieke**, mijn buurvrouw die ik mis, want het is zo stil zonder jou aan mijn rechterzijde. **Nina**, het is me niet gelukt om mijn strandhout om te zetten tot een kunstwerk, maar ach we hebben ooit naar elkaar gezwaaid op het strand. **Atia**, ik weet heus wel dat jij mijn t-shirt wilde stelen, maar dat een schuldgevoel je uiteindelijk dwong om het terug te geven! **Carolina**, d deveríamos trazer da próxima vez um trenó maior. De rest van de groep, ik ben jullie ook niet vergeten, maar bedankt dat jullie er waren.

Leiah, ik weet even niet meer hoe we op het idee kwamen om noodles te gaan eten, maar dat was ons dingetje. Hoe pittiger hoe lekkerder het zou zijn dachten we, totdat ik koffiemelk kuipjes ging drinken tegen de bosbrand in mijn mond. Feestbeest tot quizmaster jij kan het allemaal. **Rachie**, ye had tae get yersel' settled doon at first in the Netherlands. Ye likely had tae gie up yer daily fix o' haggis an' Irn-Bru. Ye faced yer ain challenges an' of course, the Netherlands dinnae hae ony highlands, but ye pulled through in the end. An' ye even chose tae bide longer than needed! **Ziqin**, do not work too much and also think sometimes about yourself! **Winnie**, stress en nog heel veel meer stress is de kenmerk van een PhD. Wij beide hebben het ervaren. **Kimberly**, ik denk dat we toch beide een beetje prettig gestoord waren, want we genoten alle twee teveel van de foto's van je polsoperatie. Het waren gewoon hele mooie foto's. **Yvonne**, ik beloof dat ik nooit meer muisjes meeneem naar de ML-I. **Ivar**, namasté. **Eline**, tot het laatst proberen we nog naar de pubquiz te gaan, maar het mocht helaas niet meer baten. **Anne**, samen hebben we de lunch meetings mogen opzetten.

Mijn **CSnD** commissie met wie ik trots mag zeggen dat wij de langst zittende commissie van CSnD ooit zijn geweest. **Margit**, **Sanne**, **Eline**, **Anton**, **Louk** en waar is **Juri**? De vele voorbereidingen die we hadden getroffen om ons CSnD retreat te organiseren kon na het uitbreken van de pandemie de prullenbak in. En we wilde nog wel zo graag biggetjes gaan knuffelen als activiteit. Nog eventjes dan zijn we allemaal klaar!

De **PriMa** PhD commissie, ik heb toch een kleine twee jaar deel mogen nemen met het organiseren van allerlei activiteiten. Voor zei die ik nog niet had genoemd, bedankt!

Mijn platform mensen, **Jilbert**, **Marlinde** en **Gosia**, we hebben elkaar leren kennen toen we met zijn alle verhuisden naar ons nieuwe onderpand in Utrecht. Ik heb jullie mooi kunnen vertellen hoe ik mijn diertjes behandelde en dit kregen jullie te horen of jullie het wilden of niet. Jullie hebben me door dik en dun gesteund en mijn geklaag aan moeten horen. Jullie waren er en dat is voor mij de grootste steun die ik kon hebben.

Zonder familie ben je nergens. **Papa** het is zonde dat je er niet meer was toen ik begon met mijn PhD. Je had een lang ziekbed gehad en uiteindelijk een gevecht gevochten die je niet kon winnen. **Mama**, natuurlijk ben ik nog steeds je kleine jongen. Ik moest je helaas verlaten omdat ik naar Utrecht verhuizen om aan mijn PhD te werken. **Elmar**, mijn grote broer, de arts van de familie die ik maar toch telkens lastig viel als ik weer aan stresssymptomen leed of als ik even uit de put moest worden gehaald. **Elvira** mijn grote zus, zonder jouw grafische kennis en je kunsten had ik nooit dit boekje en enkele figuren kunnen maken. Ik weet dat ik met alles te laat begin en dan iedereen onnodig laat stressen. **Elsa**, mijn kleine zusje ik ben blij dat je ooit een hele kerstmiddag van het Prinses Maxima Centrum hebt kunnen genieten! **Daniel**, **Rachel** en **Rob**, ik kan nu een echte baan gaan zoeken! **Chloe**, **Yuki** en **Avy**, Kleine dreumels die jullie zijn. **Kritika**, In the years we have known each other, you have seen me being stressed about my research and my PhD. Nevertheless you always were there for me and supported me when needed. We made it, It is finally done!

Eigenlijk wil ik met jullie beginnen en ook eindigen, want jullie zijn mijn alles. **Yaquina**, **Zaya** en **Zarro**, jullie zijn ook alles wat iemand in het leven wil hebben. De liefde die jullie me hebben gegeven in de vele haren die ik elke dag naar werk mocht dragen. De slapeloze nachten omdat jullie maar al te graag onder de dekens wilde slapen en toch ook weer niet. Helaas **Zarro** jij bent er niet meer. Jij hebt je strijd tegen keel en maagkanker verloren. Je was zo dapper, zo sterk toen je een hormoon behandeling en chemotherapie kreeg, maar het mocht niet helpen. Je kon niet begrijpen wat er toch aan de hand was en waarom ik je elke week mee naar de dokter nam of met spoed naar het dierenziekenhuis nam. Een mens kan wellicht begrijpen dat hij of zij ziek is, maar jij kon alleen maar liefhebben en liefde geven. Je was de trots van je moeder en je zus en wij zullen je voor altijd missen.

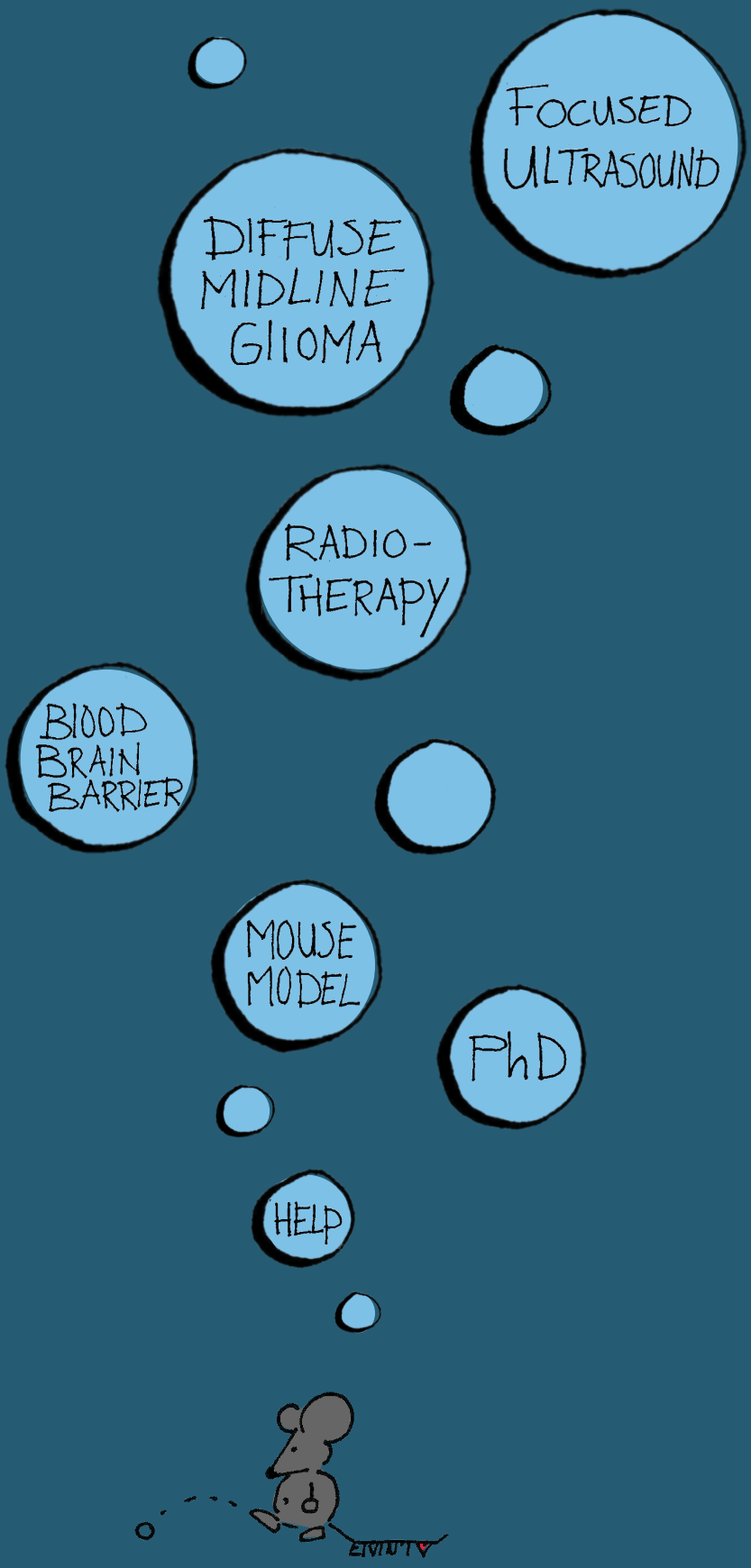
FOCUSED ULTRASOUND
DIFFUSE MIDLINE GLIOMA
RADIO-THERAPY
BLOOD BRAIN BARRIER
MOUSE MODEL
PhD
HELP